The interplay between retinal pigment epithelial cells and the C5b-9 complex

Apostolos Georgiannakis

This thesis is submitted to the University College of London for the degree of Doctor of Philosophy

October 2014

Cell Biology Department
UCL, Institute of Ophthalmology
11-43 Bath Street
EC1V 9EL
London
UK

Declaration

I, Apostolos Georgiannakis confirm that the work presented in this thesis is my own. Where information has been derived from other sources, I confirm that this has been indicated in the thesis.

Abstract

In age-related macular disease (AMD) accumulation of complement proteins in the sub-retinal space is believed to contribute to either the malfunction or apoptosis of retinal pigment epithelial (RPE) cells and ultimately the death of the associated photoreceptors. Here, the effects of basal formation of the terminal membrane attack complex, C5b-9, were examined using primary porcine RPE (pRPE) cells.

Immunohistochemical analysis showed that C5b-9 complex formation appeared to stabilise at 4 h on the basal surface of pRPE cells, after which it steadily decreased and was eliminated from the cell surface by 48 h. Within 1 h of C5b-9 formation there was a significant increase in trans-epithelial resistance (TER) when compared to untreated cells. Treatment with dynasore, an endocytosis inhibitor, suggested that pRPE cells may endocytose the C5b-9 complex, as this chemical reagent blocked the removal of C5b-9 from the cell surface. Surprisingly, treatment of pRPE cells with dynasore inhibited the C5b-9-mediated increase in TER. C5b-9 did not appear to have an effect on the expression of either the negative complement regulators CD59 and DAF, or the expression of the junctional protein ZO-1. However, immunofluorescence analysis demonstrated strong junctional staining for claudin-19 in C5b-9-treated pRPE cells when compared to control conditions. Also, the prolonged presence of C5b-9 appeared to reduce both mitochondria numbers and the localisation of Tim23, a trans-membrane mitochondrial channel. We also observed that basal assembly of C5b-9 slowed the binding of photoreceptor outer segments (POS) to the apical surface of pRPE cells. However, POS internalisation and the activation levels of MerTK, FAK and Src were not affected by the presence of C5b-9.

In conclusion, work in this thesis demonstrated that C5b-9 rapidly forms on the basal surface of pRPE cells, and that in doing so it modulates a number of RPE cell properties. RPE cells survive C5b-9 attack by endocytosing the complex, but when this process is blocked they exhibit signs of cellular stress. These studies provide mechanistic insight into some of the chronic cytotoxic effects of C5b-9 that could ultimately drive RPE cell loss and dysfunction in AMD.

Acknowledgments

First and foremost, I would like to thank Prof. Stephen E Moss for trusting me with this fascinating project. His guidance, support and kindness not only allowed me to successfully finish my project but also provided me with the opportunity to have a great time as a Ph.D. student. Additionally, I would like to thank my second supervisor, Prof. John Greenwood, for his guidance and for spending time with me to answer my questions and listen to my suggestions. I would also like to offer my special thanks to Fight for Sight for funding my research and for supporting this project altogether these three years.

I could not thank enough my new friends and colleagues (past and current) from Moss Lab: Jenny, Sterenn, Hui, Will, Katharina, Morgane, Vineeta, Dimitris and Jestin. I wish to specifically express my gratitude to Jenny, Katharina, Morgane and Vineeta for spending time with me in the lab, training me, supporting me and making my time there even more pleasant. Thank you Katharina for spending hours and hours with me dissecting eyes every single month. Jenny, thank you not only for helping me with the project during the first couple of months but also for being so caring and helpful all this time. Morgane, thank you for passing me on your knowledge in western blotting and for making me laugh in the lab most of the times. Vineeta, thank you for being there for me, answering my questions, being a friend and a colleague at the same time.

I also wish to thank people from Prof. Clare Futter's lab for their generous help through the entire duration of the project. I would like specifically to thank Matt for answering my questions regarding the immunofluorescence protocol and for fixing the microscope for me when it was broken down! I cannot thank enough Ingrid and Tom for their help with cell culture and immuno-electron microscopy, respectively. Ingrid, it was really a pleasure to work with you in the office, calming me down when I was panicking and for sharing your lovely shelf with the little treats that helped me to carry on! Tom, words really cannot describe how much helpful you were. Despite being busy with other projects, you were always willing to help me either in the lab or in the computer. You are simply a terrific colleague. Ingrid, Tom and Morgane I will never forget our frequent visits to the 'fountain of youth' just

across the street. It was always nice to occasionally relax with you guys after work. Other people I would like to thank for their support are: Claire Cox, Tim Levine, Karl Matter, Silene, Emily, Simon, Mohamed, Nick Burt, Maria Balda, Ahmed, Elisa and Peter Munro.

Last, but of course not least, I would like to thank my parents and my sister for their love and support. I would also like to thank the most generous in-laws in the whole world: Pavlos and Marie for supporting my aspirations in life and for always believing that I can do better. I also, wish to thank my lovely wife Xanthi for truly being on my side, being patient, for allowing me to share my dreams with her and for giving me, in a few days time, the best present of all times: my lovely daughter. Xanthi, thanks to you I am the happiest.

Thank you all.

Contents

List of Figures

List of Tables

List of abbreviations

AGE – Advanced glycation end-products
AMD – Age-related macular disease
AP – Alternative pathway
APOA1 – Apolipoprotein A-1
BM – Bruch's membrane
BRB – Blood-retinal barrier
C4BP – C4b-binding protein
CDKs – Cyclin-dependent kinases
CFB – C3b-Factor B
CFD – Complement Factor D
CFH – Complement factor H
CFHR1 – Complement Factor H-related protein 1
CFI – Complement factor I
CNV – Choroidal neovascularisation
CR – Complement receptor
CRALBP - Cellular retinaldehyde binding protein
CRBP – Cellular retinol binding protein
CRIg – Complement receptor of the immunoglobulin superfamily
Crry – Complement receptor 1-related protein/gene y
DAF – Decay-accelerating factor
DMEM – Dulbecco's Modified Eagle Medium
DMSO – Dimethylsulfoxide
DSS – Dextran sulphate sodium
DTT – Dithiothreitol
EC – Endothelial cell
EM – Electron microscopy
ER – Endoplasmic reticulum
ERK1 – Extracellular-regulated kinase 1
ETC – Electron transport chain
FAK – Focal adhesion kinase
FBS – Foetal Bovine Serum
FHL1 – Factor H-like protein 1
GA – Geographic atrophy
GEC – Glomerular epithelial cell
GPI – Glycophoshatidyl inositol
HESC-RPE – Human embryonic stem cell-derived retinal pigment epithelial cell
hfRPE – human foetal retinal pigment epithelial cells
hiPSC – human-derived pluripotent stem cell
HNE – Hydroxynonenal
IL-6 – Interleukin-6
$InsP_3$ Inositol tris-phosphate$_3$
iPS-RPE – induced pluripotent stem cell-derived retinal pigment epithelial cell
IRBP – Interstitial retinol binding protein
LCA – Leber's congenital amaurosis

LPS – Lipopolysaccharide
LRAT – Lecithin:retinol transferase
MAC – Membrane attack complex
MASPs – MBL-associated serine proteases
MBL – Mannan-binding lectin
MCP – Membrane cofactor protein
MCT1 – Monocarboxylate transporter 1
MerTK – Mer tyrosine kinase
MFG-E8 – Milk fat globule-EGF factor 8
MI – Membraneous in-foldings
MIRL – Membrane inhibitor of reactive lysis
mtDNA – mitochondrial DNA
MVB – Multi-vesicular bodies
N-CAM – Neural cell adhesion molecule
NADH – Nicotinamide adenine dinucleotide
nDNA – nuclear DNA
NF-κB – Nuclear factor kappa B
NHS – Normal human serum
NK – Natural killer
NLRP3 – NLR family, pyrin domain containing protein 3
OD – Optical density
ODN – Oligodeoxynucleotides
oxLDL – Oxidised low-density lipoproteins
P - Properdin
PAMPs – Pathogen-associated molecular patterns
PBS – Phosphate Buffered Saline
PBS-T – Phosphate buffered saline with Triton-X 100
PEDF – Pigment-epithelium growth factor
PFA – Paraformaldehyde
PI – Propidium iodide
PKC – Protein kinase C
PMA – Phorbol myristate acetate
PNH – Paroxysmal nocturnal haemoglobinuria
POS – Photoreceptor outer segments
PR – Retinal photoreceptors
pRPE – porcine retinal pigment epithelial cells
PVDF – Polyvinyl difluoride
RAGE – Receptor of advanced glycation end-products
RCA – Regulators of complement activation
RCS – Royal College of Surgeons
RDH5 – Retinol dehydrogenase 5
RGC – Retina ganglion cell
ROS – Reactive oxygen species
RP – Retinitis pigmentosa
RPE – Retinal pigment epithelial cells
SC5b-9 – Soluble C5b-9
SDS – Sodium dodecyl sulphate

SH3 – Src homology 3
siRNA – short interfering RNA
TBS – Tris-buffered saline
TBS-T – Tris-buffered saline with Tween-20
TCC – Terminal complement complex
TEC – Tubular epithelial cell
TER – Trans-epithelial resistance
VDCC – Voltage-dependent calcium channels
VEGF – Vascular endothelial growth factor
ZO – Zonula occludens
ZO-1 – Zonula occludens-1
ZONAB – ZO-1-associated nucleic acid binding protein

Introduction
(Chapter 1)

1.1 The retinal pigment epithelium

The retinal pigment epithelium (RPE) is a monolayer of cuboidal cells that forms the most anterior part of the blood-retinal barrier (BRB) (Ablonczy et al., 2011). It is vital that the RPE remains fully functional since its many roles (Figure 1) are required to maintain a healthy retina. These important roles include functions such as the transfer of various molecules (ions, metabolic end products, oxygen and water) from the neuro-retinal microenvironment to the choriocapillaris (Ablonczy et al., 2011). In addition, as the RPE is situated between the photoreceptors and the choroidal blood supply, it also transports glucose and fatty acids from the blood to supply the photoreceptors. Other specialised functions of the RPE include the absorption of scattered light, the secretion of growth factors and the sustainability of the visual cycle (Bandyopadhyay and Rohrer, 2012, McBee et al., 2001). The visual cycle is the biochemical transformation of all-*trans*-retinal to 11-*cis* retinal. Since photoreceptors are not able to transform retinal from the all-*trans* to the 11-*cis* state, to maintain their excitability, it is essential that retinal reaches the RPE (through phagocytosis and/or protein transportation), where it is re-isomerized. During visual cycle, all-*trans* retinal leaves the intradiscal space of photoreceptors to access their cytosol, where it will be converted to all-*trans* retinol by the all-retinol dehydrogenase, termed as RDH. From the cytosol of photoreceptors, all-*trans* retinol is then delivered to the RPE by binding to a carrier protein known as interstitial retinol binding protein (IRBP). Within the RPE, all-*trans* retinol binds to the cellular retinol binding protein (CRBP), which will in turn deliver all-*trans* retinol to a multi-protein complex, essential for the regeneration of 11-*cis* retinal. In more detail, this complex contains four essential proteins: RPE65, lecithin:retinol transferase (LRAT), cellular retinaldehyde binding protein (CRALBP) and the retinol dehydrogenase (RDH5). The first three proteins are required for the binding and conversion of all-*trans* retinol to 11-*cis* retinol, while RDH5 is responsible for the oxidation of 11-*cis* retinol to 11-*cis* retinal. Once recycling is complete, 11-*cis* retinal is delivered from the RPE to the sub-retinal space, from where it will return to the photoreceptors through binding to IRBP (Baehr et al., 2003, Sun and Nathans, 2001, Rattner et al., 2000, Gonzalez-Fernandez, 2003, Saari et al., 2002, Ruiz et al., 1999, Redmond et al., 1998, Jang et al., 2001, Saari et al., 2001).

In order for the RPE to carry out these specialised functions, polarisation of the epithelial cell is essential. The apical surface of RPE cells consists of elongated structures, known as microvilli, which surround the tips of the photoreceptor outer segments (POS). This physical interaction enables the RPE to sustain the survival of photoreceptors by phagocytosing shed outer segments (Nguyen-Legros and Hicks, 2000). In contrast the basal membrane of the RPE faces the Bruch's membrane which separates the choriocapillaris from the neuroretina (Gulcan et al., 1993).

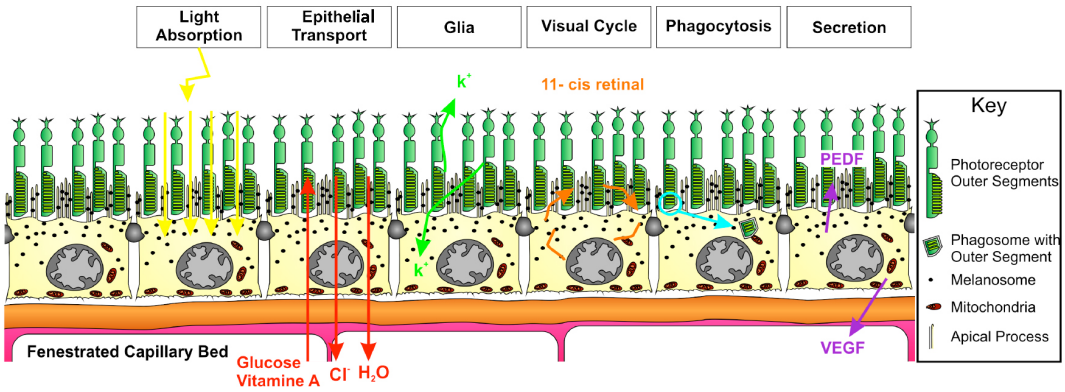

Figure 1. **Schematic representation of the main functions of RPE cells**. RPE cells perform a number of specialised functions including: scattered light absorption, transportation of glucose, vitamin A and ions from the blood to the photoreceptors and they sustain the visual cycle by recycling 11-*cis* retinal. They also maintain the survival of photoreceptors by phagocytosing shed outer segments and finally they produce and secrete growth factors, essential for the maintenance of a healthy retina: pigment-epithelium growth factor (PEDF) from the apical surface and vascular endothelial growth factor (VEGF) from their basal surface (Strauss, 2005).

1.2 Polarity of the RPE

The RPE develops an apical-to-basolateral polarity in terms of its unique structure, positioning of organelles, and the distribution of membrane proteins (Marmorstein, 2001). On the apical side, where melanosomes are also localised, microvilli enable RPE cells to perform physical interactions with POS, whilst the basal side, where mitochondria are concentrated, is characterized by membraneous in-foldings which increase the surface area for exchange with the choriocapillaris (Figure 2-A, -B) (Marmorstein, 2001). Several membrane proteins show a polarised distribution in order to carry out their specific functions at either the apical or basal surface (Rizzolo and Zhou, 1995). Such proteins include the Na/K-ATPase (an ion pump), (Rizzolo and Zhou, 1995), the αvß5 integrin (essential for binding of POS on the RPE cell membranes) (Nandrot et al., 2004), and neural cell adhesion molecule (N-CAM-

140), which is a morpho-regulator (Marmorstein et al., 1998). The aforementioned proteins have been demonstrated to localise on the apical surface of RPE cells. On the basal side, different proteins can be found such as monocarboxylate transporter 1 (MCT1) (associated with the controlled transportation of lactate and water from the RPE to the choroid) (Philp et al., 1998).

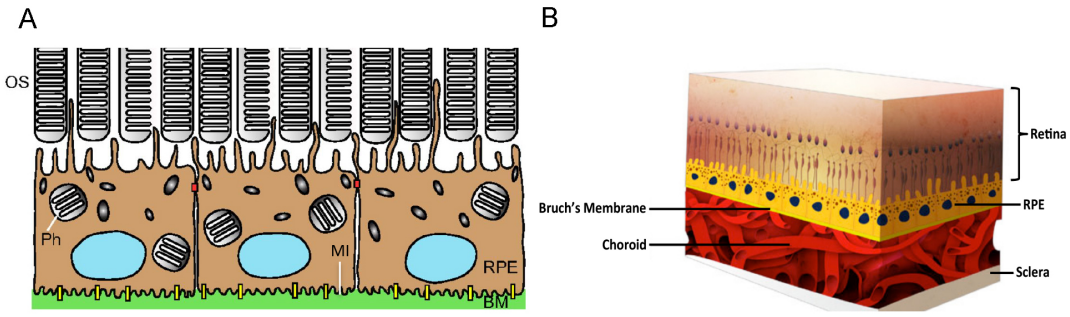

Figure 2. **Schematic representation of the retina.** (A) On the apical surface of RPE, microvilli allow cells to attach to outer segments (OS) in order to phagocytose photoreceptor outer segments (Ph). Membraneous in-foldings (MI) on the basal side increase the surface area with which RPE cells attach to bruch's membrane (BM). (B) 3D schematic representation of the retina and its underlying RPE monolayer. Sourced and adapted from: http://dev.ellex.com/2rt and http://dev.biologists.org/content/140/12/2576.figures-only.

1.3 Phagocytosis

Human vision depends on the presence of both, the melanopsin-expressing retina ganglion cells and the retinal photoreceptors (PR): the rods and cones. These ganglion cells are strongly activated by rods and cones and produce melanopsin, a photo-pigment molecule which helps to detect changes in light intensity. Gross changes in light intensity will therefore aid the functions of circadian rhythm and pupil constriction (Dacey et al., 2005). Rods are required for nocturnal vision due to their high light sensitivity (Rodieck and Rushton, 1976). In order for cones to be activated they need elevated light conditions, hence they are used for diurnal vision and are necessary for colour discrimination (Hestrin and Korenbrot, 1990). Both types need to be renewed by synthesising new membranes at the base of outer segments (OS) and by removing any aged membranes (Young and Bok, 1969). This renewal process is dependent on the underlying RPE monolayer, which is responsible for POS uptake and degradation (Young and Bok, 1969). In order for PR to maintain their excitability it is essential that POS phagocytosis from the RPE is regulated in a circadian manner (LaVail, 1976). Every morning, light conditions stimulate the phagocytic activity of RPE, which has been found to maintain a peak

for 1-2 h (Young and Droz, 1968). Within approximately 10 days, a whole length of a POS can be regenerated. Circadian regulation has been linked to various other cellular processes in the retina such as melatonin synthesis, ion channel sensitivity and visual pigment synthesis (Tosini, 2000, Ko et al., 2001, von Schantz et al., 1999).

The circadian phagocytosis of shed POS involves several stages, including the binding, internalisation, degradation and/or the recycling of constituents of the segments (Qin and Rodrigues, 2012). In order for RPE cells to carry out this process, they express a number of specific proteins such as αvβ5 integrin for binding (Nandrot et al., 2004), Mer tyrosine kinase (MerTK) (D'Cruz et al., 2000) and focal adhesion kinase (FAK), both necessary for internalization (Figure 3) (Finnemann, 2003).

Previous studies have demonstrated that the apically-expressed vitronectin receptor, αvβ5, is also essential for the attachment of POS to the surface of RPE cells, since blockade of αvβ5 with a neutralizing antibody impaired POS binding to the RPE but did not affect the internalisation of POS which were already bound to the cells (Finnemann et al., 1997). This integrin is required for the binding of POS, as beta5$^{-/-}$ RPE cells in culture failed to take up isolated POS (Nandrot et al., 2004).

The αvβ5 integrin, which mediates POS binding, activates a signaling cascade that leads to the re-organisation of the actin cytoskeleton in the RPE in order to allow the internalisation of bound POS (Finnemann et al., 1997). These signaling events involve activation of FAK, which is located at sites of integrin clustering on the apical side of the RPE cells (Finnemann, 2003).

Activated FAK in turn activates (through tyrosine phosphorylation) MerTK which translocates to the site of POS binding, which is also necessary for the engulfment of the POS (Feng et al., 2002, Finnemann, 2003). Studies showed that in the Royal College of Surgeons (RCS) rat that lacks MerTK, internalisation of the POS is severely compromised leading to rapid early onset photoreceptor degeneration (Chaitin and Hall, 1983). Ectopic expression of MerTK can rescue the RCS phenotype, demonstrating that this kinase plays a key role in the engulfment of outer segments (Feng et al., 2002).

The final stages of POS phagocytosis include digestion of these lipoproteinaceous bodies within RPE lysosomes (Deguchi et al., 1994). Since phagocytosis generates reactive oxygen species (ROS), and RPE cells perform this activity throughout a lifetime, RPE cells have developed mechanisms that protect them against photo-oxidation of lipids and proteins in order to mitigate the harmful effects of oxidative stress (Miceli et al., 1994). These mechanisms involve the production of large amounts of anti-oxidants, which remove ROS, filtration of light by the RPE in melanosomes and mechanisms to repair damaged nucleic acids, lipids and proteins (Kaemmerer et al., 2007).

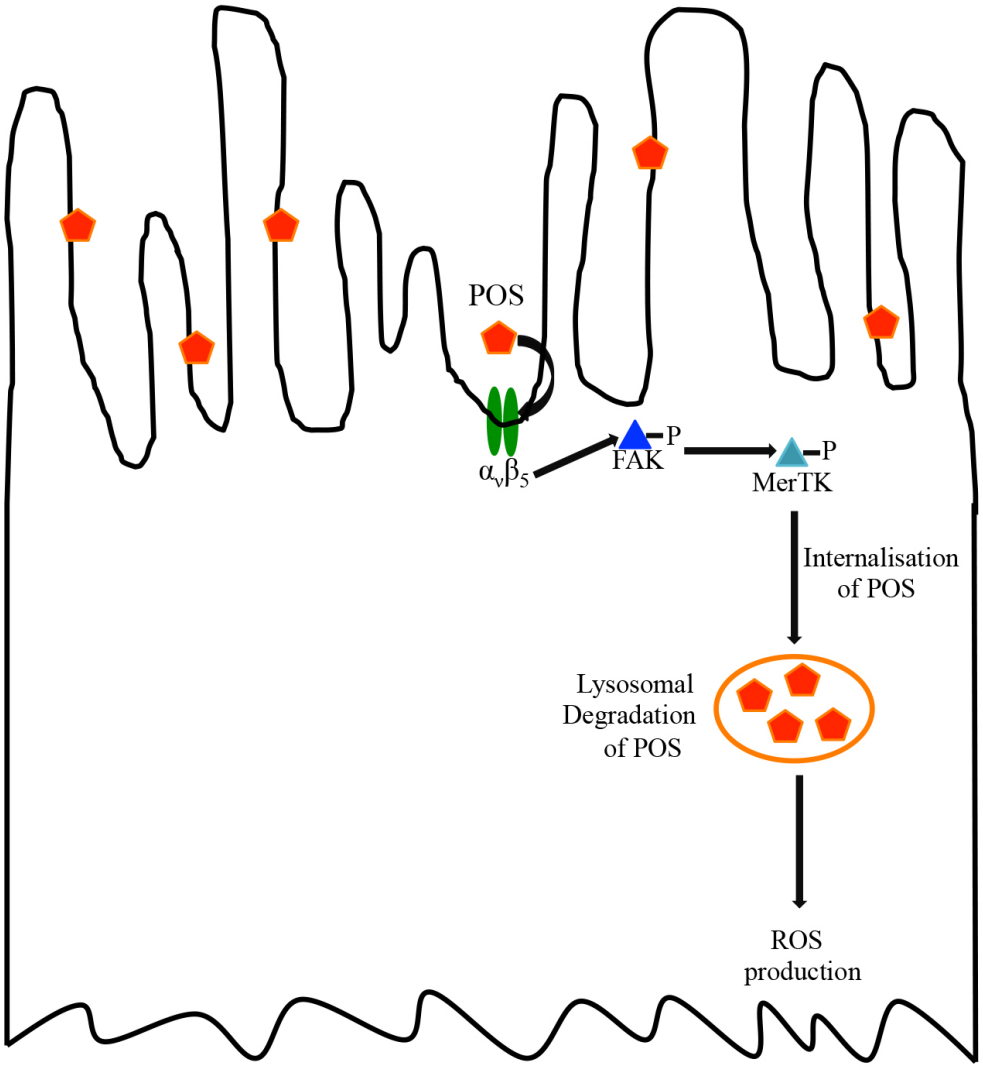

Figure 3. Schematic representation of RPE-specific POS phagocytosis. αvβ5 receptors are essential for the binding of POS on the apical surface of RPE cells. Successful binding of POS triggers the phosphorylation (activation) of FAK, which in turn phosphorylates (activates) its downstream target, MerTK, essential for the internalisation of POS. Internalised POS will

eventually be degraded in the lysosomes, a process known to cause production of reactive oxygen species (ROS) in RPE cells.

1.4 Secretory activity of the RPE

The RPE secretes a number of growth factors that are essential in maintaining the health of both the neuroretina and the choriocapillaris (Marneros et al., 2005). Two of the best-characterised growth factors secreted by the RPE are vascular endothelial growth factor (VEGF) and pigment-epithelium-derived factor (PEDF) (Sonoda et al., 2010). VEGF is required for choriocapillaris development and plays a major role in pathological neovascularisation in the eye (Marneros et al., 2005). The RPE is the main site of VEGF production in the posterior segment (Marneros et al., 2005), with secretion being necessary for the homeostasis of the extra-cellular space close to the Bruch's membrane, and modulation of endothelial cell fenestrations in the choriocapillaris (Roberts and Palade, 1995, Maminishkis et al., 2006).

PEDF is a member of the Serpin family of proteins with anti-angiogenic and neuro-protective actions, (Tombran-Tink et al., 1995). It is produced by RPE cells but unlike VEGF, PEDF is predominantly secreted from the apical side which is essential for preserving an anti-angiogenic environment in the outer retina (Maminishkis et al., 2006).

Previous work using cultured human fetal RPE (hfRPE cells) *in vitro*, suggested that a fine balance in the production and secretion of both VEGF and PEDF is essential for RPE cells to maintain their functionality (Sonoda et al., 2010). Thus, PEDF (either present in culture media or endogenously expressed from hfRPE cells) blocks the VEGF-derived disruption of trans-epithelial resistance (TER). Neutralisation of PEDF with an anti-PEDF antibody (added on the apical surface of cells for 1 h) leads to TER breakdown attributed to VEGF (Ablonczy et al., 2011).

1.5 The RPE and the blood-retinal barrier

Epithelial cells such as the RPE have a well-structured junctional complex to establish a barrier function. This complex includes tight junctions, adherens junctions, gap junctions and desmosomes (Denker and Nigam, 1998, Meyer et al., 2002). The major role of the tight junctions is to enable the RPE to regulate fluid flow between the neuroretina and the choriocapillaris (Turowski et al., 2004,

Rizzolo, 2014). The complexity of barrier function is exemplified by the fact that tight junctions involve the participation of approximately 40 different proteins including claudins, Zonula occludens-1 (ZO-1) and occludin (Gonzalez-Mariscal et al., 2003). Upon formation of the tight junctions, RPE cells are induced to express various essential molecules including glucose transporters, which are necessary for trans-epithelial glucose transport (Ban and Rizzolo, 2000).

The formation of fully structured tight junctions requires the association of three key different families of membrane proteins: occludins, claudins and zonula occludens (ZO) (Furuse et al., 1993, Jin et al., 2002). More importantly, ZO proteins have been identified as the backbone of tight junctions, with ZO-1 protein being described as the regulator of the degree of tightness of tight junctions (Mitic and Anderson, 1998, Wang et al., 2014). Cloning and sequencing of ZO proteins, demonstrated that they have three distinct PDZ domains, located on their N-termini, via which they can bind directly to the C-termini of claudins (Itoh et al., 1993, Itoh et al., 1999). This observation led to the hypothesis that ZO proteins could be the possible regulators of polymerisation of claudins at the site of tight junction formation in epithelial cells (Itoh et al., 1999). Knowing that the RPE is a claudin-19 dominant epithelium and that ZO-1 is an essential regulator of the tight junctional architecture, particularly close attention has been paid to these two junctional proteins in studies of RPE cell biology (Peng et al., 2011, Mitic and Anderson, 1998).

1.5.1 Zona Occludens-1, ZO-1

ZO-1, -2 and -3 are all members of the zonula occludens family of intracellular plaque proteins which have the capacity to interact with various barrier-forming, signaling and structural proteins, all being part of the tight junctional complex (Fanning et al., 2012). ZO-1, with a molecular mass of approximately 220 kDa, has the ability to directly interact with, via its Src homology 3 (SH3) domain, the ZO-1-associated nucleic acid binding protein (ZONAB) transcription factor, that regulates cell proliferation in epithelial cells (Balda et al., 2003, Balda and Matter, 2000, Stevenson et al., 1986). The more polarised epithelial cells become the more ZO-1 becomes enriched at junctions and therefore, via ZONAB, cell proliferation is arrested (Balda et al., 2003). Loss of ZO-1 leads to a delay in junction assembly as

was shown in polarised ZO-1$^{-/-}$ mouse epithelial cells (Umeda et al., 2004).

The ability of confluent ZO-1$^{-/-}$ mouse epithelial cells to form tight junctions was monitored once these cells were transferred back to normal Ca^{2+} medium (they were initially cultured in low Ca^{2+} medium containing 5μM Ca^{2+}). ZO-1 deficient cells even after 10 h of incubation in the normal Ca^{2+} medium demonstrated retarded recruitment of occludins and claudins, causing delays in tight junction assembly. This retardation in tight junction formation was completely rescued by exogenous expression of ZO-1, indicating the necessity of ZO-1 in the formation of tight junctions (Umeda et al., 2004).

1.5.2 Claudin-19

Currently 24 different claudin proteins have been characterised, each of which is believed to exert a unique influence on the selectivity and permeability of epithelial tight junctions (Peng et al., 2011). The claudins form a family of transmembrane proteins which function as either heterodimers or oligomers in epithelial cells (Peng et al., 2011).

Claudin-19 is encoded by the *CLDN19* gene and it has been found to be expressed at high levels in the kidney and the eye (Konrad et al., 2006). Claudin-19 is a necessary component of tight junctions in human RPE cells and in kidneys since individuals lacking its expression suffer from severe visual impairment and from a condition known as familial hypomagnesemia with hypercalciuria and nephrocalcinosis, which is a tubular disorder accompanied by excessive renal magnesium and Ca^{2+} excretion and chronic kidney failure (Konrad et al., 2006, Hou and Goodenough, 2010). These observations suggest a significant role for claudin-19 in paracellular ion re-absorption in the kidney and in the normal development of the retina, respectively (Konrad et al., 2006, Hou and Goodenough, 2010).

Further research indicated the necessity of claudin-19 in the assembly of tight junctions (Miyamoto et al., 2005). Examination of Schwann cells isolated from claudin-19-deficient mice showed that formation of tight junctions was arrested. This arrest was associated with claudin-19 deficiency and therefore it was hypothesised that claudin-19 is a crucial component of the tight junctions, via which Schwann

cells can perform their electrophysiological sealing function (Miyamoto et al., 2005).

1.6 RPE models of retinal disease

Despite the wealth of information about RPE and retinal diseases, which has been obtained from *in vivo* studies in mouse models, there are limitations within such models including limited availability of tissue, differences between mouse and human and long delivery times which can affect quality of the tissue and high variability amongst samples. This has led to the use of *in vitro* cultures of isolated RPE cells from different species as an alternative strategy (Maminishkis et al., 2006). However, it should be noted that *in vitro* models also have their limitations and in some cases mammalian RPE cell cultures fail to maintain key phenotypic characteristics such as polarity, pigmentation and phagocytic ability (Turowski et al., 2004).

1.7 RPE cell lines as tools for studying retinal physiology

A number of different cell culture models have been used in the past in order to examine RPE functionality *in vitro*, however every cell model has been demonstrated to have its advantages and limitations at the same time.

1.7.1 Human fetal RPE

Human fetal RPE cells (hfRPE) have been repeatedly used to unravel the molecular mechanisms of various RPE-related diseases. hfRPE cells can rapidly re-develop pigmentation once they are cultured *in vitro*, they can form well-organised RPE monolayers, with apical microvilli, express key proteins essential for RPE functionality and can retain their polarity with regards to the polarised expression of ion channels and transporters (Adijanto et al., 2012, Strunnikova et al., 2010, Maminishkis et al., 2006, Flannery et al., 1990, Castorino et al., 2011). In addition, they maintain their phagocytic activity, metabolise retinol, produce and secrete grown factors in a polarised fashion and they have the capacity to form strong tight junctions (Castorino et al., 2011, Flannery et al., 1990).

Although hfRPE cells represent an excellent RPE cell culture model, they have limitations. hfRPE cells are usually obtained in low numbers and they require several weeks of *in vitro* culture until they can reach a confluent state (Burke, 2008, Adijanto

et al., 2012). Also, hfRPE cells have to be seeded at a high density as cell-cell contact is crucial in order to control their ability to proliferate. Finally, hfRPE cells have a very limited number of divisions and therefore they can only be used until passage 2 as usually after that they tend to lose their capacity to re-differentiate (Burke, 2008).

1.7.2 ARPE-19

Although hfRPE cells form authentic RPE monolayers *in vivo* ARPE-19 cells are the most widely used *in vitro* model, as they can be manipulated to resemble diseased or aged RPE. ARPE-19 cells, which are an immortalised human cell line, are commercially available, very easy to maintain, and provide an unlimited number of cells (Ablonczy et al., 2011, Maminishkis et al., 2006, Dunn et al., 1996).

However, ARPE-19 cells have limitations as a model for RPE function *in vitro*. These cells are normally non-pigmented though they can regain melanosomes after many weeks of *in vitro* cell culture, they have variable cell shape (not hexagonal), they demonstrate low expression of RPE maturation markers such as RPE65 and they have relatively poor phagocytic capacity, most likely due to low level of expression of key regulators such as the avβ5 integrin and MerTK (Ablonczy et al., 2011).

1.7.3 Primary porcine RPE cells

Primary porcine cells are an excellent model for the *in vitro* study of RPE functionality as not only do they retain their pigmented phenotype but they also keep their hexagonal shape. In addition, they quickly develop tight junctions and establish a tight monolayer soon after plating. On the other hand, their isolation is time-consuming, they are generally obtained in small numbers and they have limited replicative potential which means they should be used before cell passage three.

1.7.4 Human-induced pluripotent stem cell-derived RPE cells

Human-induced pluripotent stem cell (hiPSC)-derived progenitors are increasing in popularity as they afford a means of obtaining many copies of progenitor cells which have a particular desired genetic profile as they originate from living patients (Gamm and Meyer, 2010). In the case of hiPSC-derived RPE cells, a large number of RPE

cells with a specific genetic profile linked to the retinal disease of interest could be obtained and maintained *in vitro* (Park et al., 2008). hiPSC from patients and generation of RPE cells allows the investigation of the cellular and molecular mechanisms of a given disease without the need to genetically manipulate the RPE cells. Moreover, hiPSC-derived RPE cells maintain an authentic RPE phenotype *in vitro* (Kokkinaki et al., 2011).

Although hiPSC-derived RPE cells could be a very promising tool for the investigation of several retinal conditions, the process of obtaining RPE cells from their progenitors is very long, expensive and all clones need to be screened before they can be used for any *in vitro* studies, in order to ensure that they have retained the desired genetic profile (Krohne et al., 2012).

1.7.5 RPE-J cell line

RPE-J cells are rat RPE cells which have been transfected with a temperature-sensitive mutant of the viral SV40 large T antigen. Transfection of these cells can only happen at a permissive temperature (33 ^{o}C) (Chou, 1989). At 33 ^{o}C RPE-J cells can be maintained indefinitely as an immortalised proliferative cell line, but upon transition to the non-permissive temperature (40^{o}C) they become highly differentiated and acquire their RPE phenotype (Jat and Sharp, 1989).

RPE-J cells develop strong tight junctions, as indicated by ZO-1 staining and acquired TER values, they have good polarity with long apical microvilli and pre-melanosomes accumulated towards their apical side (Nabi et al., 1993). Although RPE-Js become polarised, they demonstrate altered polarity of two essential proteins: the Na^{+}/K^{+}-ATPase ion pump and the N-CAM, which *in vivo* are exclusively located on the apical side of RPE (Nabi et al., 1993).

The use of RPE-Js overcomes the dependence of experiments on primary RPE cells, however the process of culturing RPE-J cells with good epithelial properties requires several rounds of cloning and selection, as well as dedicated incubators at the restrictive and permissive temperatures. Also, that fact that key proteins might lose their polarised expression *in vitro* might indicate that these cells could lose some of their RPE characteristics. Also, taking into account possible differences between

species, ARPE-19, hfRPE, hiPSC-derived RPE and porcine RPE cells could be more appropriate models than RPE-Js depending on the molecular events and biochemical pathways under investigation.

1.8 Diseases of the RPE

As previously mentioned the RPE performs a number of specialised functions, all necessary for the maintenance of a healthy neural retina. Gene mutations and/or disturbance of the RPE monolayer can lead to a number of hereditary retinopathies such as Leber's congenital amaurosis (LCA), Best's disease, retinitis pigmentosa (RP), choroideraemia and age-related macular degeneration (AMD), all of which have in common a dysfunctional and/or disrupted RPE monolayer (Musarella and Macdonald, 2011, Koirala et al., 2013, Bonilha, 2008, Triantafylla et al., 2014, Black et al., 2014).

1.9 Age-related macular degeneration (AMD):

AMD is the leading cause of blindness (in industrialised nations), in people aged over 65. As AMD progresses the central part of the retina, called the macula, degenerates (Figure 4). The macula is a particularly important part of the retina as it is essential for fine detail and image resolution. In other words, a decline in central vision, due to progressive AMD, prevents individuals from recognising objects and performing everyday activities. The rate of AMD progression is variable between individuals (Klein et al., 2010) in that it can either progress slowly so that patients notice little change in their vision or progress rapidly which in turn may lead to severe vision loss in just a few years.

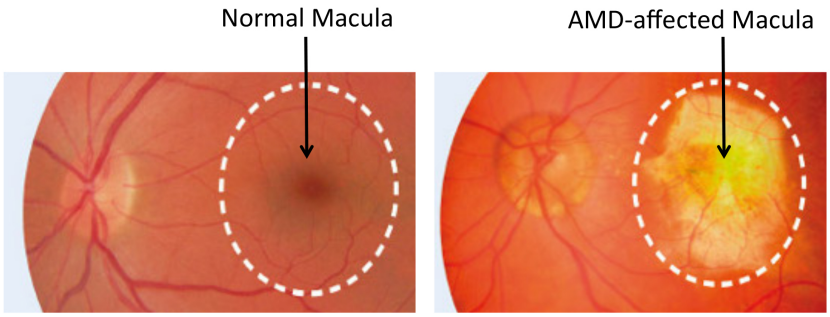

Figure 4. Demonstration of a healthy macula and of a wet AMD-affected macula. Color fundus photograph of a normal human retina (left) and of a wet AMD-affected human retina (right), where a large fibrovascular scar covers the macular region (black arrow, right). Sourced and adapted from www.eyesite.org.

1.10 Two forms of AMD

There are two main forms of AMD (Figure 5) which describe its clinical progression. The early form is known as 'atrophic' AMD (also known as non-exudative) and the more severe form which arises at a later stage in a minority of patients is 'neovascular' AMD (also known as exudative) (Anderson et al., 2002). Atrophic AMD generally progresses slowly and is mainly characterized by the formation of yellow extracellular insoluble lipoproteinaceous deposits, between the RPE and Bruch's membrane, termed drusen (Anderson et al., 2002). Enhanced development of drusen formation is associated with the later stage of atrophic AMD called geographic atrophy (GA), where blind spots develop within the macula due to areas of RPE cell loss and the death of overlying photoreceptors (Klein et al., 2008). Despite the fact that the exact mechanism of drusen formation is not fully understood previous research has demonstrated that these deposits are rich in a number of inflammatory proteins such as apolipoprotein E, amyloid P component, vitronectin and various complement proteins (e.g. C3b, C5 and C5b-9) (Anderson et al., 2002). Although there is no treatment available for the atrophic form, patients are given dietary supplements rich in antioxidants and zinc in an attempt to slow down the condition (Klein et al., 2008).

In contrast to the atrophic form of AMD, the neovascular type is more severe. Neovascular AMD, which occurs on a background of the atrophic form, accounts for approximately 10 % - 15 % of AMD and progresses rapidly (Guyer et al., 1986). There is evidence that unregulated RPE-driven VEGF production leads to choroidal neovascularisation (CNV), where new blood vessels start to emerge from the choroid, develop through Bruch's membrane and finally extend into the sub-retinal space where they may leak and haemorrhage (Lopez et al., 1996, Green and Enger, 2005).

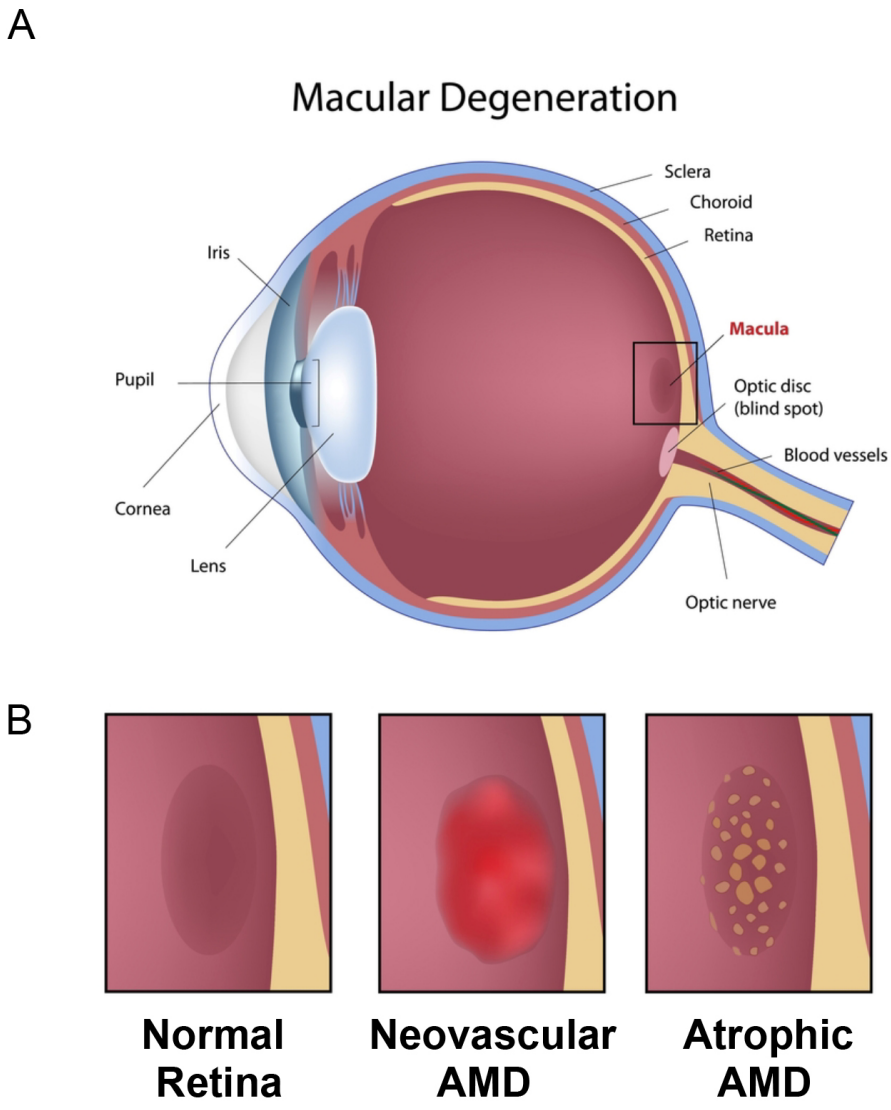

Figure 5. Comparison of the normal macula with a neovascular and an atrophic macula. (A) Schematic representation of the anatomy of a human eye, where the macula, the central part of the retina, is located at the back of the eye. (B) Comparison of a normal retina to an AMD-affected retina. In neovascular AMD blood vessels emerge from the choroid, expand through Bruch's membrane and finally extend into the sub-retinal space where they may induce haemorrhage. In atrophic AMD, a less severe form of AMD, yellow lipoproteinaceous deposits (drusen) develop between bruch's membrane and the RPE. Drusen might lead to apoptosis of the RPE and therefore compromise vision. Sourced and adapted from www.vision-and-eye-health.com.

1.11 AMD and the RPE

Age-related modifications of the RPE include a reduction in pigmentation (decrease in melanosomes), diminished cell density, decreased metabolic activity and enhanced secretion of pro-inflammatory cytokines (such as interleukin-6 and -8) (Mullins et al., 2000, Lueck et al., 2011). These changes are believed to be partly attributable to

the accumulative effects of oxidative stress.

1.12 Oxidative stress in AMD-affected RPE cells

The production of reactive oxygen species (ROS) in the RPE could stem from the phagocytosis of POS (RPE cells are known for their high phagocytic activity), the high oxygen consumption and the absorbance of scattered light (Tate et al., 1995, Sripathi et al., 2011). The inability of aged RPE cells to metabolise the ROS, produced from the above RPE functions, could result in ROS accumulation, which in turn can lead to oxidative stress and therefore RPE cell damage. This RPE degeneration has been shown to contribute towards AMD development (Sripathi et al., 2011).

Elevated oxidative stress leads to intracellular accumulation of lipofuscin, which is a non-degradable heterogeneous mixture of proteins and insoluble lipids that accumulate over the years within the RPE (Sparrow et al., 2010). Lipofuscin in the presence of light is able to induce further ROS formation which impairs several of the main functions of the RPE, including phagocytosis of POS and lysosomal degradation (Holz et al., 1999). In addition to lipofuscin, aged-RPE accumulate advanced glycation end-products (AGEs) which can also be found in drusen (Ishibashi et al., 1998). Once AGEs interact with their receptor (RAGE), which is expressed on RPE cells, in advanced AMD, the nuclear factor kappa B (NF-kB) is activated (Howes et al., 2004). Activation of this pro-inflammatory regulator may lead to the up-regulation of interleukin-6 (IL-6). IL-6 over-expression by RPE cells may in turn contribute to the development of CNV in neovascular AMD by autocrine stimulation of VEGF (Oskolkova et al., 2008, Paimela et al., 2007).

Furthermore, elevated intracellular levels of ROS can induce mitochondrial damage such as structural alterations in the mitochondrial membranes and mitochondrial DNA (mtDNA) damage resulting in insufficient ATP production. All these events can further enhance the accumulation of ROS and eventually lead to cell apoptosis (Tilleul et al., 2013, Wang et al., 2007).

1.13 Mitochondrial damage in AMD-affected RPE cells

Mitochondria are the main source of energy in eukaryotic cells, and as RPE cells are highly metabolically active their cytoplasm contains a large number of mitochondria (Jarrett et al., 2008). The inner and outer mitochondrial membranes consist of phospholipid bilayers with various integrated proteins. The inner membrane is organized into cristae, which provide the surface area sufficient for ATP production (Jarrett et al., 2008). In addition to supplying cellular energy, mitochondria are involved in a range of other processes, such as signalling, cell differentiation, cell death and control of the cell cycle (Nordgaard et al., 2008, Folmes et al., 2012). Mitochondria account for the mass production of ROS since approximately 90 % of the oxygen used by the cells is metabolised within these organelles via the electron transport chain (ETC) (Van Remmen and Richardson, 2001). This mitochondria-specific ROS production is the result of oxidative phosphorylation during which, mitochondria transfer electrons from nicotinamide adenine dinucleotide (NADH) to electron transporters so as to produce ATP (Van Remmen and Richardson, 2001).

In the event of electron leakage during this process O_2^- can accumulate which in turn can affect the integrity of mitochondrial lipids, proteins and mtDNA (Brand et al., 2004). Previous research has demonstrated the onset of mitochondrial dysfunction in AMD cases, where the matrix density and the overall number of mitochondria within RPE have been greatly reduced (Feher et al., 2006).

Furthermore, oxidative stress-induced mtDNA damage has previously been suggested to be one of the pathogenic mechanisms in AMD (Blasiak and Szaflik, 2011). mtDNA (approximately 16.5 kb) is organised into a specific structure, termed the nucleoid, which contains various maintenance and repair proteins such as DNA polymerase γ (Wang and Bogenhagen, 2006). mtDNA is especially vulnerable to oxidative damage because it lacks a number of histone and non-histone proteins and is an active site of ROS production (Wei, 1998). According to the mitochondrial theory of ageing, the co-localisation of ROS with the ETC during an organism's lifespan plays a fundamental role in mitochondrial dysfunction due to damage of the mtDNA (Miquel et al., 1980, Liang and Godley, 2003). This damage can include point mutations, deletions and rearrangements in mtDNA which may play a role retinal disease (Liang and Godley, 2003).

At this point it should be noted that in addition to ROS there are additional factors which increase oxidative stress in mitochondria including cigarette smoke, blue light and phagocytosis of photoreceptor outer segments (Figure 6) (Jarrett et al., 2008). All of these factors have the potential to challenge the integrity of mtDNA (increase mutagenesis), which is particularly vulnerable since mitochondrial repair mechanisms are believed to be less effective than nuclear DNA (nDNA) mechanisms (Yakes and Van Houten, 1997, Jin et al., 2001).

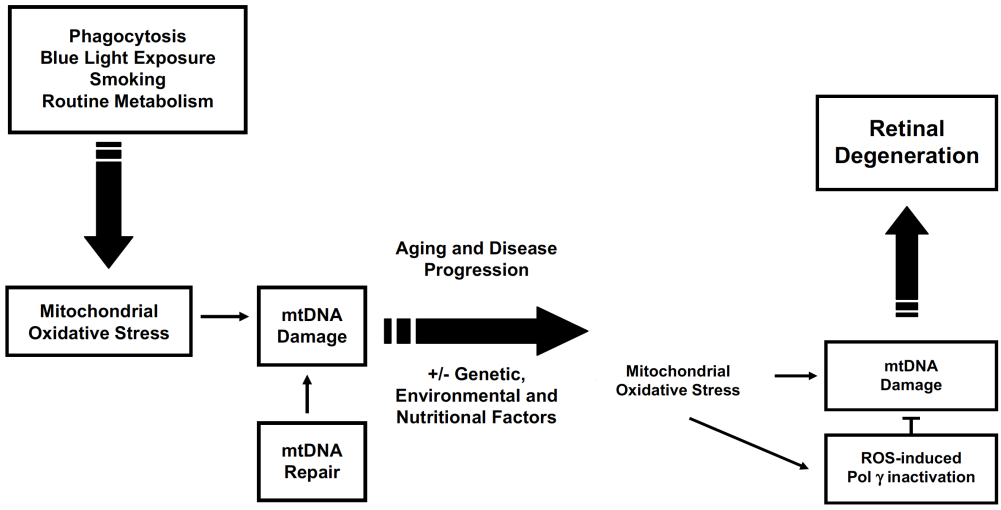

Figure 6. mtDNA damage and retinal degeneration. Once a certain threshold of mtDNA instability is breached, energy production levels drop in mitochondria and therefore cell functionality is impaired and mitochondria initiate apoptosis. This event will eventually contribute to the initiation of retinal degeneration. Sourced and adapted from (Jarrett et al., 2008).

1.14 The complement system

The complement system is part of the innate immune system consisting of more than 30 different proteins, which are present in blood plasma and on various cell surfaces (Krarup et al., 2008). The complement system not only provides immune defence by eliminating foreign particles and microorganisms but also plays a homeostatic role by regulating the degradation of damaged host cells such as apoptotic and necrotic cells (Krarup et al., 2008).

Complement proteins are primarily produced in the liver by hepatocytes, however

other cell types have been found to contribute to complement protein production including: endothelial, epithelial, and kidney cells (Morgan and Gasque, 1997). For instance it has previously been shown that apart from liver C2, C4 and factor B are produced in significant amounts in the human kidney as well (Feucht et al., 1989, Welch et al., 1996, Welch et al., 1993). However, circulation is not the only source of complement proteins. RT-PCR studies in the RPE/choroid (derived from C57BL/6 mice) demonstrated that specific components of the complement system can be produced locally in the retinal environment (Luo et al., 2011). The components identified by RT-PCR were: C1q, C1s, C1r, C2, C3, CFH and CFB, of which C3, upon cytokine treatment (interferon-γ), was up-regulated while, CFH was down-regulated (Luo et al., 2011). This finding, in combination with other studies could imply the significance of CFH to modulate local inflammation in the retina. In fact, it was previously reported that CFH expression levels in the retina were similar to CFH expression levels in the liver (Hageman et al., 2005). Several sequence variations in the CFH gene can lead to the onset of atypical hemolytic uremic syndrome and glomerulonephritis, both of them leading to kidney malfunction (Abrera-Abeleda et al., 2006, Remuzzi et al., 2002). There have been cases were individuals with atypical hemolytic uremic syndrome suffered from severe renal failure, indicating that mutated CFH protein levels can have an effect on retinal health as well (Remuzzi et al., 2002). Whether these amounts were stemming from circulation or produced locally in the retina remained to be addressed. Recently, it has been demonstrated that patients receiving a liver transplant for 5 years or more, develop AMD (Khandhadia et al., 2013). However, Khandhadia et al., 2013 reported that AMD development in liver transplant patients is only associated with recipient rather than donor amounts of CFH conferring the Y402H mutation. That said, presence of AMD does not depend on the hepatic expression of CFH but it depends on its local intraocular expression instead (Khandhadia et al., 2013).

1.15 Three activation pathways of the complement system

Three distinct pathways are able to activate the complement system: the classical, alternative and the lectin pathway (see Figure 7). Also, recently the coagulation system has been demonstrated to activate complement independently of the afore-mentioned pathways (Huber-Lang et al., 2006). Every pathway has its unique

mechanism to trigger its activation but all lead to the turnover, by enhanced enzymatic cleavage, of the most abundant complement protein, C3 into C3a and C3b (Kemper et al., 2008). C3b by attaching to target cell membranes tags the cell for either lysis by the assembly of lytic pores on the cell surface or for phagocytosis by immune cells (Kemper et al., 2008). In the case of target lysis the whole of the cascade must be activated. Target lysis is achieved through the assembly of membrane attack complex (MAC). MAC assembly begins with the cleavage of C5 molecules into C5a and C5b via C5 convertase. Then, C5b is associated with C6, C7, C8, and C9 complement proteins, to assemble the C5b-7, C5b-8, and finally MAC, C5b-9 complexes (Rus et al., 1996).

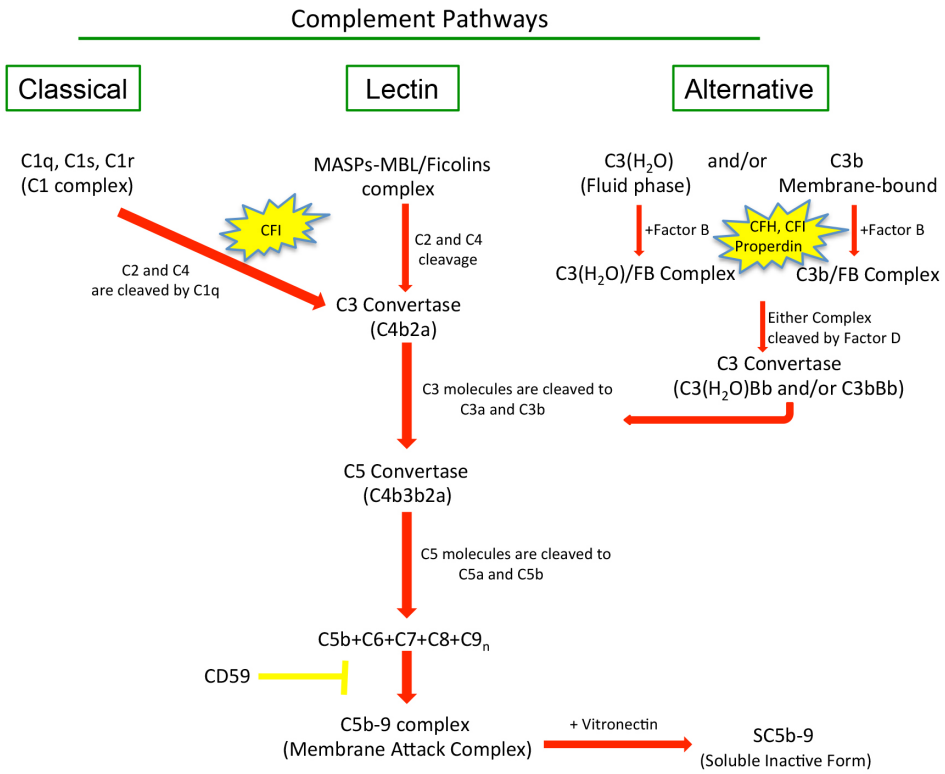

Figure 7. **The activation pathways of the complement system**. Each of the three pathways (classical, lectin and alternative) leads to the formation of the terminal membrane attack complex. MASPs, MBL-associated serine proteases; MBL, mannan-binding lectin; CFH, complement factor H; CFI, complement factor I; SC5b-9, soluble C5b-9.

1.16 The classical pathway

The classical pathway is initiated by the activation of the C1 complex, which is constituted of C1q protein and the two proteases C1r and C1s (Dodds et al., 1978). C1q recognises antibody-antigen aggregates and upon binding it activates the C1r

protease, which in turn cleaves and activates the two C1s molecules to form the active C1s serine protease (Dodds et al., 1978). This C1s molecule is able to cleave the C4 and C2 complement components in order to form the C3 convertase (C4b2a) which then cleaves soluble C3 protein into C3a and C3b. The C3b molecule plays an essential role within the complement cascade. It is an opsonin that marks either foreign particles or apoptotic cells to be phagocytosed. Free C3b molecules will either bind to target cells or to C4b to form the C5 convertase (C4b3b2a). C5 convertase will then cleave soluble C5 protein into C5a and C5b and the latter molecule may eventually drive MAC formation (Figure 8) (Wallis et al., 2010).

During activation of the classical pathway C3b production may be amplified through the alternative pathway due to the formation of a C3b-Factor B (CFB) complex (Farries et al., 1988). Once this complex is formed, an additional factor, Factor D (CFD), will contribute to the formation of another C3 convertase, C3bBb, by processing (cleavage) any C3Bb complexes. This amplification step can lead to the clustering of multiple C3b molecules on a target cell surface and therefore will enhance the opsonisation of the pathogen for phagocytic cells (Farries et al., 1988).

The classical pathway apart from its role in host defence could be involved in the pathogenesis of glaucoma, as immunohistochemical analysis of the glaucomatous retinas of mouse, monkey and humans, showed that C1q was significantly up-regulated (Stasi et al., 2006). This C1q up-regulation preceded the extensive death of retina ganglion cells (RGC), suggesting that the classical pathway could be directly associated with RGC degeneration in glaucoma (Ding et al., 2012, Stasi et al., 2006). Further research has demonstrated that C1q might be involved in the clearance of apoptotic cells from the retina. Thus, C1q was found to be gradually up-regulated in the retinas of mice lacking the rhodopsin gene (a model of RP) (Humphries et al., 2012). As the degeneration progressed, these higher levels of C1q in $Rho^{-/-}$ mice could have been part of a defence mechanism that favoured the clearance of apoptotic cells. Additionally, when C1q was eliminated in $Rho^{-/-}C1q^{-/-}$ mouse retinas, the viability and functionality of cone photoreceptors became severely compromised (Humphries et al., 2012). Further investigation of inflamed retinas (mice and human) identified the accumulation of C1q within ocular tissues adjacent to inflammatory sites (Murinello et al., 2014, Montalvo et al., 2007). In particular,

immunofluorescence analysis of human retinas derived from patients with early AMD, demonstrated the presence of C1q in the choriocapillaris but not in drusen deposits (Murinello et al., 2014).

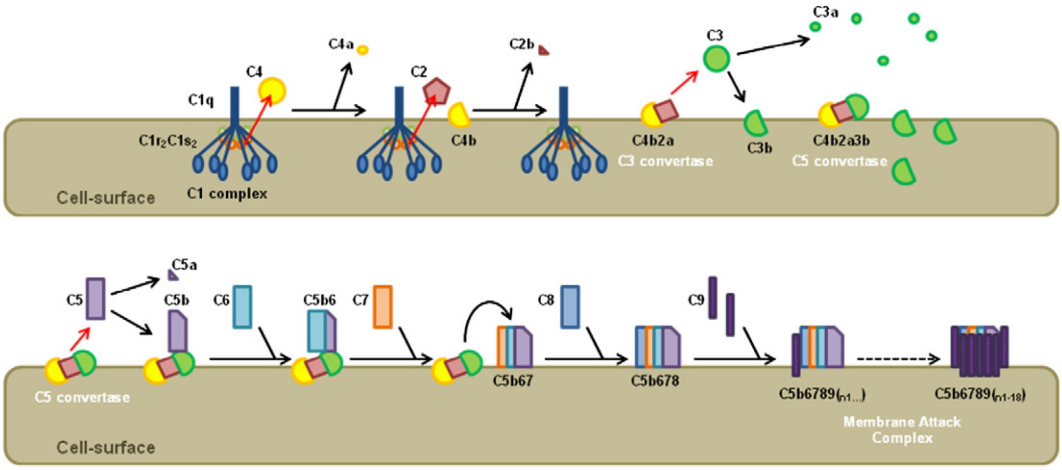

Figure 8. **Mechanism through which classical pathway activation leads to cell lysis**. When C1q (member of the C1q complex) binds to specific targets on a cell surface, C1s and C1r are activated. Then C1s contributes to the formation of C3 convertase (C4b2a) by cleaving C2 and C4 complement proteins. C3 convertase creates C3b (by cleaving C3), which in turn helps the assembly of C5 convertase. This convertase will finally cleave C5 to C5b, which will lead to the formation of the final complement complex (Carroll and Sim, 2011).

1.17 The lectin pathway

The lectin pathway is characterised by lower levels of activation than the classical pathway as its key protein mediators, L-, H-, and M-ficolins, mannan-binding lectin (MBL) and collectin, are found at lower levels in the blood compared to C1q. These mediators identify pathogen-associated molecular patterns (PAMPs) such as polysaccharides on the surface of pathogens (Krarup et al., 2008). Lectin pathway activation entails cleavage of MBL and ficolins by specific serine proteases termed: MBL-associated serine proteases (MASPs). These proteases form complexes with MBL or ficolins and once they bind to a cell surface, MASPs are auto-activated with the exception of MASP-3 (Zundel et al., 2004). Although much of the functionality of MASPs remains to be elucidated, it has been shown that the lectin pathway uses the same protein cascade to activate the complement system as the classical pathway, by forming the same C3 convertase C4b2a (Thiel et al., 1997).

1.18 The alternative pathway

As reviewed by (Thurman and Holers, 2006) one unique characteristic that

distinguishes the alternative pathway from the classical one, is that the alternative pathway is continuously activated (at low levels) as it depends on the constantly low levels of C3 hydrolysis in plasma to C3(H_2O) which is similar to the C3b molecule in terms of structure and functionality. C3(H_2O) is able to form, in a Mg^{2+}-dependent-manner, a complex with CFB which in turn is cleaved by CFD, leading to the formation of the fluid phase C3 convertase: C3(H_2O)Bb. This C3(H_2O)Bb protein complex, which is the equivalent of the classical pathway C3 convertase, cleaves C3 into C3a and C3b (as shown in Figure 9). These C3b molecules can be deposited on any available cell surface.

Additionally, CFB is able to bind to the previously produced C3b molecules and be cleaved by CFD to form an additional (but this time surface-bound) C3 convertase of the alternative pathway termed C3bBb. That way, the production of C3b molecules is enhanced and therefore leads to the so-called amplification loop of the alternative pathway.

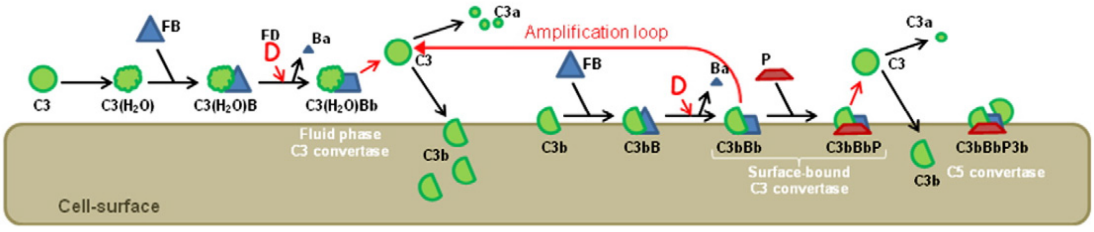

Figure 9. **Mechanism of alternative pathway activation.** During the alternative pathway activation two different forms of C3 convertases can be formed: the fluid phase C3 and the surface-bound one. Upon formation of the surface-bound C3 convertase, properdin (P) stabilises this convertase, maintaining the amplification loop. Cleaved C3 molecules (C3b) will contribute to the formation of C5 convertase (Carroll and Sim, 2011).

1.19 Regulators of the alternative pathway – Complement factor H

In order for the alternative pathway to be able to discriminate between host and pathogens it uses three major recognition proteins: Complement factor H (CFH), properdin and C3b (Pangburn et al., 2000).

CFH is a large soluble glycoprotein which is capable of interacting with molecular

patterns on host cell surfaces, which can either be polyanionic and/or membrane-bound C3b molecules (Jokiranta et al., 1996). These interactions allow CFH to suppress activation of the alternative pathway on host surfaces (Pangburn et al., 2000). In cases where any of the three C3b binding sites, located at the N-terminus of CFH, are mutated surface-bound C3b molecules start to aggregate and therefore they lead to enhanced alternative pathway (AP) activation (Sharma and Pangburn, 1996). In more detail, Sharma et al., 1996 demonstrated that mutated forms of CFH lacking any of the three C3b binding sites, conferred a 6- to 8-fold reduction in the ability of CFH to bind C3b on sheep erythrocytes, indicating that all three sites contribute to the regulation of complement activation on erythrocytes. That way the development of complement-mediated pathology can take place because the complement system targets cell surfaces of host cells which lack protection from CFH (Pangburn et al., 2000).

1.20 Regulators of the alternative pathway – Properdin

Properdin is a recently discovered pathogen recognition molecule. It has been shown to recognise bacteria and apoptotic human T-cells and promote complement activation via the alternative pathway (Kemper et al., 2008, Spitzer et al., 2007). Overall, properdin is believed to promote the alternative pathway in three ways: by binding to and providing stability to the AP C3 convertase C3bBb, by binding to multiple membrane-bound C3b molecules which enhances the production of the other C3 convertases (C3bBbP), and by interacting with complement-activated surfaces independently of C3b (Spitzer et al., 2007). People lacking properdin are more prone to developing bacterial infections (meningococcal septicaemia has been reported) showing that it has an essential role in the innate immune system (Sjoholm et al., 1982). Although C3b is not classified as a recognition molecule, it has strong binding preferences towards various carbohydrates and for specific amino acid hydroxyl groups localised on Threonine, Serine and Tyrosine residues of protein structures on cell surfaces (Sahu and Pangburn, 1995).

1.21 The terminal complement complexes – Formation of C5b-7

Once attachment of C6 to the alpha-chain of C5b takes place, C6 changes its conformation which enables it to bind to the hydrophobic area of the lipid membrane bilayer (formation of C5b-6) (Rus et al., 1996). After assembly of the C5b-6

complex, soluble C7 can bind to the alpha-chain of C5b (part of the C5b-6 complex) and this interaction allows the C5b-7 complex to minimally span the lipid bilayer, stabilising the nascent terminal complement complex (TCC) on the cell surface (Hu et al., 1981).

1.22 The terminal complement complexes – Formation of C5b-8 and C5b-9

Upon formation of the C5b-7 complex, C8 binds to the beta-chain of C5b, in order to form the C5b-8 complex (Stewart et al., 1987). Within C5b-8, the C8αβγ heterotrimeric protein initiates the insertion event of the first C9 molecule via its alpha-chain, thus assembling the C5b-9_1 complex (Stewart et al., 1987). In contrast to C5b-9, the less stable C5b-8 is less capable of lysing cells. Thus studies have demonstrated that hemolysis of erythrocytes requires the assembly of multiple C5b-8 complexes, because C5b-8 induces hemolysis at a slower rate than C5b-9 (Laine and Esser, 1989, Ramm et al., 1982).

During the attachment of the first C9 molecule of the C5b-9_1 complex, C9 unfolds into a tubular structure so as to allow the insertion of further C9 monomers (approximately 16-18 molecules) to form a poly-C9 lytic pore (C5b-9_n) via C9 polymerisation (Laine and Esser, 1989). The functional diameter of a C5b-9_n complex ranges from 1nm to approximately 11nm, where the pore size is dependent on the number of attached C9 molecules (Ramm et al., 1985). However, formation of a lytic pore is not always the final outcome of C5b-9 complex formation on the cell surface, with the exception of erythrocytes. Nucleated cells, including cases of RPE studies and K562 cells (erythroleukaemic cell line) have been shown to be more resistant towards complement-induced cell lysis (Anderson et al., 2002, Saar Ray et al., 2014).

1.23 Membrane attack complex, C5b-9

Activation of any of the three complement pathways leads to the formation of the final multi-protein complex capable of inducing cell lysis on erythrocytes: the membrane attack complex (MAC) or C5b-9 (Laine and Esser, 1989). Cleavage of C5 triggers the chain reaction described above that leads to the assembly of the final complex C5b-9 (as shown in Figure 10) (Rus et al., 1996). C5b-9 refers to the trans-membrane pores, on the cell surface, whose assembly requires prior sequential

formation of the rest of the TCC (Rus et al., 1996). Any soluble forms of the C5b-9 complex tend to bind to vitronectin (also known as S-protein), leading to formation of the SC5b-9 complex (Podack and Muller-Eberhard, 1980). Vitronectin is a soluble plasma glycoprotein which acts as a negative regulator of the complement system by inhibiting MAC-induced cell lysis (Podack and Muller-Eberhard, 1979).

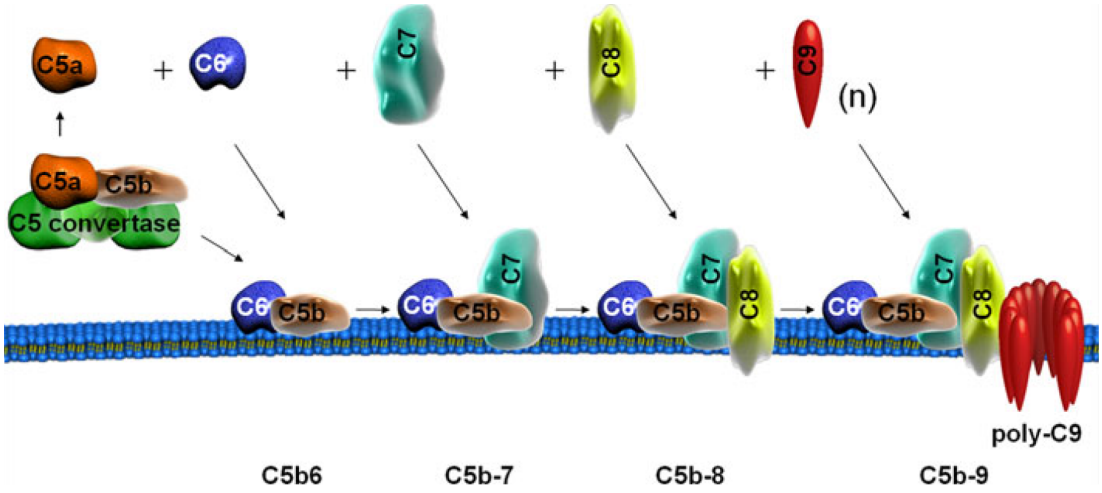

Figure 10. **Formation of the terminal membrane attack complex (MAC)**. Once C5 convertase forms, via activation of either of the three complement pathways, it cleaves C5 into C5a and C5b. C5b then binds to C6 and the C5b-6 complex is inserted in to the lipid bilayer of the cell membrane. Further binding of C7 and C8 will insert the newly formed C5b-8 complex deeper into the membrane. C8 acts as a binding site for the first C9 molecule, which in turn will attract more C9 molecules to form the multi-C9 sub-lytic pores (Tegla et al., 2011).

1.24 The dual role of the C5b-9 complex

Complement-mediated lysis is a 'multi-hit' process in which lysis of nucleated cells requires a large number of membrane-bound C5b-9 complexes (Koski et al., 1983). When there is limited complement present, C5b-9 can exert a protective effect on cells (Dashiell et al., 2000). Thus, these authors demonstrated that when complement C7 was added back to C7-depleted sera, a low level of C5b-9 complex formation promoted the proliferation of Schwann cells. Evidence suggests that the number of membrane-attached C5b-9 complexes determines whether the cellular response will be either lysis or survival and proliferation (Dashiell et al., 2000, Koski et al., 1983).

1.25 C5b-9 complex-mediated cell lysis

When C5b-9 complex formation increases, so that the rate of assembly exceeds the rate at which they can be removed from the cell surface, cell death is induced in

erythrocytes, regardless of cell-volume ratio (Koski et al., 1983). Originally it was believed that a single C5b-9 complex was able to lyse an erythrocyte through osmosis (Rommel and Mayer, 1973). However, most cells (nucleate and anucleate) need the localisation of multiple C5b-9 complexes on their cell surfaces to become lysed via complement (Koski et al., 1983). C5b-9-mediated lysis is driven largely by an increase in intracellular Ca^{2+} which in turn leads to mitochondrial dysfunction, which in turn causes loss of energy production (loss of ATP, ADP and AMP) (Papadimitriou et al., 1991).

1.26 Cell survival induced by C5b-9

Sub-lytic quantities of C5b-9 are able to promote cell cycle activation via activation of signalling cascades, which inhibit apoptosis/necrosis (Figure 11) (Dashiell et al., 2000). Research using various cell types (e.g. smooth muscle cells and Schwann cells), showed that cellular proliferation and protection from apoptosis is primarily based on signalling via heterotrimeric Gi proteins leading to downstream activation of phosphatidylinositol 3-kinase/Akt/FOXO1 (cell proliferation) and extracellular-regulated kinase 1 (ERK1) (Niculescu et al., 1999, Dashiell et al., 2000).

Additionally, the C5b-9 complex stimulates cellular proliferation by sequentially activating the cyclin-dependent kinases (CDKs), CDK4 and CDK2, which are vital for the transition from G1 to the S-phase of the cell cycle (Niculescu et al., 1999). This cell cycle progression, as reported in rat oligodendrocytes and endothelial cells, is further supported by the activation (via phosphorylation) of the RGC-32 kinase by Akt, which in turn forms a complex with cyclin B1-CDC (Fosbrink et al., 2009, Badea et al., 1998).

Evidence has also shown that sub-lytic doses of C5b-9 are able to prevent apoptosis by up-regulating FLIP, which leads to the inactivation of the pro-apoptotic proteins: Bad and caspase-8 (Cudrici et al., 2006). Taken together, these observations suggest that low level exposure to C5b-9 complex might favour cell survival and tissue homeostasis.

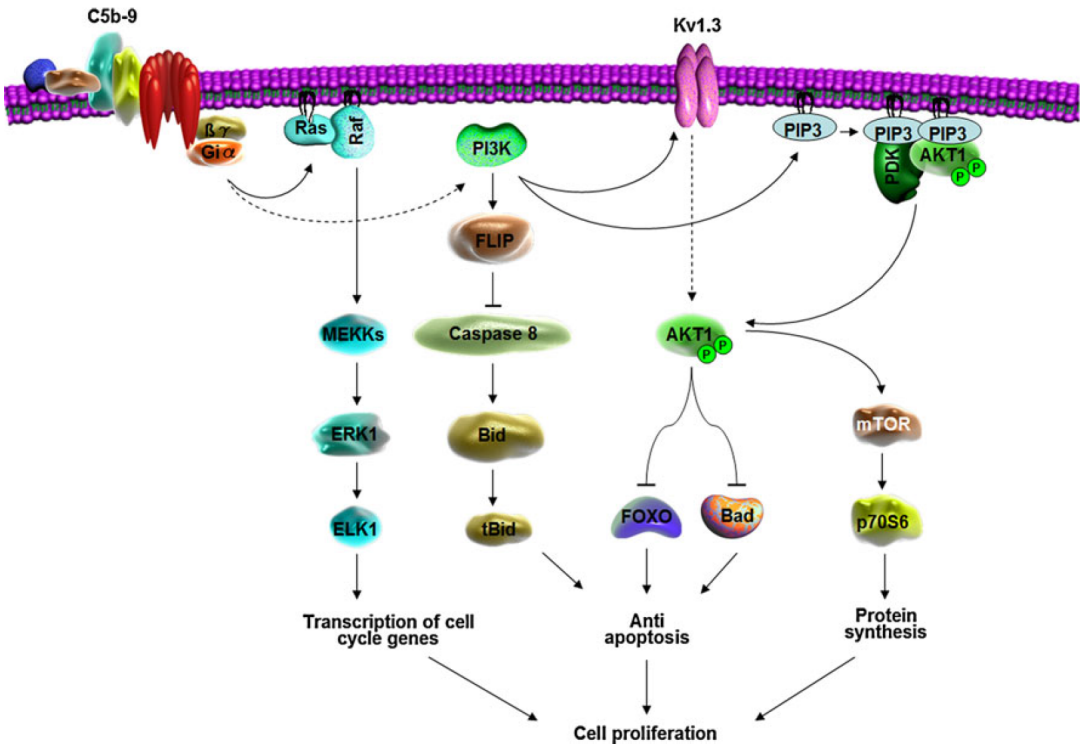

Figure 11. **Signaling from the C5b-9 complex promotes cell proliferation and prevents apoptosis**. Membrane-bound C5b-9 associates with membrane-bound Gi protein, activating Ras and Raf. Raf in turn, will activate MEK1 and ERK1. Additionally, C5b-9 activates PDK1 and AKT1 via PI3K. Activated PI3K up-regulates FLIP which inhibits activation of apoptosis-related caspase-8 and cleavage of Bid, while activated AKT1 prevents apoptosis by regulating FOXO and Bad. Sourced from Tegla et al., 2011.

1.27 Complement regulators

All three activation pathways of the complement system need to be tightly regulated to ensure that complement does not target healthy host cells. This can be achieved by both fluid-phase and membrane-bound regulatory proteins (Zipfel and Skerka, 2009) (full list of complement regulators is provided in Table 1). Currently, there are five known membrane-bound regulators: the C3b receptor (CD35), complement receptor of the immunoglobulin superfamily (CRIg), membrane cofactor protein (CD46), decay-accelerating factor (DAF, also known as CD55) and CD59, also known as membrane inhibitor of reactive lysis (MIRL) (Pangburn et al., 2000). While all the above regulators inhibit C3/C5 convertases, only CD59 inhibits the terminal stage of C5b-9 formation by inhibiting the binding of C9 proteins to C5b-8 complex (Rollins and Sims, 1990). For this reason, many studies on C5b-9 complex formation include a step in which CD59 is blocked using an appropriate antibody.

-	Additional Name	Stage of action	Ligand	Function
C1q - Heart, brain, eye (RPE)	N/A	C.P	IgM, IgG immune complexes	Activates classical pathway by binding to apoptotic surfaces
C1INH - Eye (RPE, choroid)	N/A	C.P and L.P	C1r, C1s and MASP2	Blocks serine proteases and is substrate for C1r, C1s, MASP2 and C3b proteins
C4BP - Eye (RPE)	N/A	C.P and L.P	C4	Cofactor for factor I
Carboxy-peptidase N - Erythroid progenitors, hepatocytes	Anaphylatoxin inactivator	C.P and L.P	C3a, C4a and C5a	Inactivates C3a and C5a
Factor H - Liver, cardiac veins, brain, eye (RPE), lungs, heart, spleen, kidney, pancreas and placenta	N/A	A.P	C3b and C3d	Cofactor for factor I
FHL1 - Plasma, eye (Bruch's membrane)	N/A	A.P	C3b	Cofactor for factor I
Properdin - Neutrophils, liver, endothelial cells, eye (RPE, choroid)	N/A	A.P	C3	Stabilises A.P convertases
CFHR1 - Plasma and eye (Bruch's membrane, RPE, choroid)	N/A	T.P	C5 Convertase, C5b-9 complex	Inhibits C5 convertase and formation of C5b-9 complex
Clusterin - Eye (RPE)	SP-40, apolipoprotein J	T.P	C7, C8β, C9 and C5b-9 complex	Transports cholesterol, HDL, APOA1 and lipids
Vitronectin - Eye (RPE)	S-protein	T.P	C5b-8 andC5b-9 complexes	Binds to soluble forms of C5b-7, -9 complexes and inactivates them
CD59 - Bone marrow, plasma, testis, urine, eye (RPE)	Protectin	C5b-9 complex	C8	Inhibits the assembly of C5b-9 complex
CD55 - Bone marrow, eye (RPE), T-cells, neutrophils and Natural-killer cells	DAF	C3	C4b2b and C3bBb	Accelates decay of C3 convertase
CD46 - Kidney, brain, eye (RPE)	MCP	C3	C3b and C4b	Cofactor for factors I & H
CR1 - Eryrthrocytes, leukocytes, dendritic , eye (RPE)	CD35	C3	C3b, iC3b, C4b and C1q	Regulates C3 breakdown to C3a and C3b
CR2 - B-cells and dendritic cells	CD21	C3	C3d and iC3b	Maintains any C3d-tagged immune complexes
CR3 - Leukocytes (Natural killer cells, monocytes and neutrophils)	αMβ2 integrin	C3	iC3b and factor H	Enhances, via iC3b, the contact of opsonised targets
CR4 - Leukocytes (monocytes/macrophages)	αXβ2 integrin	C3	Monocytes and macrophages	iC3b-mediated phagocytosis
CRIg - Macrophages	VSIG4	C3	C3b, iC3b	Inhibits the activation of A.P

Table 1. Summary of soluble (yellow-colored area) and of membrane-bound (blue-colored area) complement regulatory proteins. C1INH, C1 inhibitor; C4BP, C4b-binding protein; CFHR1, complement factor H-related protein 1; CR, complement receptor; CRIg, complement receptor of the immunoglobulin superfamily; DAF, complement decay-accelerating factor; FHL1, factor H-like protein 1; APOA1, apolipoprotein A-1; MASP2, mannan-binding lectin serine protease 2; MCP, membrane cofactor protein; C.P, complement pathway; A.P, alternative pathway; L.P, lectin pathway; N/A, not applicable. Sourced and adapted from Skerka et al., 2009.

1.28 Complement regulator CD59

CD59 (also known as protectin, p18 and MIRL) is structurally related to the leukocyte antigen 6 (Ly-6) family of proteins (Davies et al., 1989) and its human gene is located on chromosome 11p13 (Meri et al., 1991). It is an 18-kDa membrane glycoprotein that controls the formation of the C5b-9 complex on autologous tissue (Tomlinson, 2006). Thus, CD59 located on the cell surface of host cells, via its glycophosphatidyl inositol (GPI) anchor (Rudd et al., 1997), prevents the formation of the C5b-9 terminal complex by binding to the alpha-subunit of C8 in the C5b-8 multi-protein complex and/or to the C9b fragment of the final C5b-9 complex, blocking the input of further C9 proteins (Tomlinson, 2006, Rollins and Sims, 1990, Davies et al., 1989). Due to its crucial role, CD59 has a very wide expression profile and has been found to be present on most circulating blood cells, endothelial and epithelial cells, and spermatozoa (Davies et al., 1989). Additionally, CD59 can be present in a soluble form (either through direct release from the cell surface or due to enzymatic cleavage of the GPI anchor) where it is found in body fluids including urine and amniotic fluid (Qin et al., 2005).

CD59 serves several functions in addition to complement regulation. The identification of two forms of CD59 in the mouse has shown that this glycoprotein exerts complement-dependent (CD59a) and complement-independent functions (CD59b) (Qin et al., 2005). Lack of CD59a (one of the two forms found in the mouse) leads to haemolytic anaemia, in which mice develop a mild paroxysmal nocturnal haemoglobinuria (PNH)-like phenotype (Holt et al., 2001). A complement-independent function of CD59b (the second form found in the mouse) was found in the testis where studies demonstrated that in $CD59b^{-/-}$ mice, sperm viability and morphology were compromised (Qin et al., 2005). Although this phenotype was related to the absence of CD59b, it developed in a complement-independent fashion as there was no evidence for increased accumulation of C5b-9 complex, and also removal of C3 did not inhibit $CD59b^{-/-}$ mice from developing sperm abnormalities (Baalasubramanian et al., 2004). Other complement-independent activities of CD59 include signaling events within B-, T- and Natural Killer (NK)-cells, lipopolysaccharide (LPS) signaling and regulation of apoptosis (Sivasankar et al., 2007, Korty et al., 1991, Yamamoto et al., 2003, Marcenaro et al., 2003, Donev et

al., 2006).

The regulated expression of CD59 is of high importance since CD59 over-expression has been linked to tumour growth (Li et al., 2013). On the other hand its absence can lead to severe haemolytic anaemia (Motoyama et al., 1992). It is possible that exploring the multiple interactions between CD59 and its complement ligands will help enable the development of CD59-dependent therapeutics for treating inflammatory conditions such as PNH (Yamashina et al., 1990).

1.29 Decay-accelerating factor

Decay-accelerating factor (DAF), also known as CD55, is a 70-kDa glycophosphatidylinositol-anchored glycoprotein and is a member of the Regulators of Complement Activation (RCA) family of proteins (Nishikawa et al., 1998). As its name suggests, its primary role is to regulate the activity of C3 and C5 convertases (classical and alternative pathway, respectively), by accelerating their decay (Brodbeck et al., 2000). DAF is expressed by various cell types such as endothelial and epithelial cells (Post et al., 1990). DAF accelerates the decay of C3 convertases, C4b2a and C3bBb, by binding to C4b or C3b respectively (Medof et al., 1984). Individuals lacking DAF expression accumulate C3b molecules (as C3 convertase activity is not regulated) and develop PNH, which is a condition that leads to intravascular hemolysis and platelet activation. This suggests a primary role for DAF in protecting host-cells from complement activation (Hillmen et al., 1992).

1.30 Complement receptor 1-related protein/gene y

Complement receptor 1-related protein/gene y (Crry) is a key regulator of the complement system expressed exclusively on rodent (mouse, rat) cell membranes but not in human (Caragine et al., 2002). Crry is the structural and functional analog of DAF and the membrane cofactor protein (MCP) negative regulators of complement system (Caragine et al., 2002). MCP protein in humans has been found to exert a critical role in inhibiting complement-induced tissue injury as it can be significantly up-regulated in a number of diseases such as glomerulonephritis, ischemic acute kidney injury and acute renal allograft rejection (Endoh et al., 1993, Miao et al., 2014). Examination of Crry in rodents would help to elucidate the mechanisms of MCP action in humans (Miao et al., 2014).

Chronic kidney diseases have been correlated with deterioration of renal function due to structural damage in the tubulointerstitium (Schainuck et al., 1970). Blocked expression of Crry in rat mesangial cells via oligodeoxynucleotides (ODNs) led to enhanced complement-mediated cell lysis, while *in vivo,* Crry knockdown (ODN-mediated) in rats suffering from proteinuria, led to the enhanced accumulation of the C5b-9 complex and C3 protein (Hori et al., 1999). This observation indicated the importance of Crry in restricting complement activation and therefore inhibiting cell damage (Hori et al., 1999).

Further research re-confirmed the necessity for Crry expression on the basolateral surface of murine renal tubular epithelial cells (TECs) (Renner et al., 2010). Thus, exposure of the basolateral surface of TECs (derived from $Crry^{-/-}fB^{-/-}$ mice) to complement-component serum led to enhanced complement activation compared with TECs from wild-type mice (Renner et al., 2010).

1.31 Complement and AMD

Research has demonstrated the association of multiple risk factors with AMD, including family history, smoking, age, high blood pressure and inflammation. Specifically in recent years, genetic studies have revealed the role of the complement system in AMD (Smith et al., 2001) where polymorphisms in multiple complement genes either increase or decrease the risk of AMD development (Kunchithapautham et al., 2012).

Indeed, polymorphisms in complement activators such as CFB, complement inhibitors (complement factor H, complement 1 inhibitor C1) and other proteins of the complement cascade (complement factors 2 and 3) have all been shown to be related to AMD (Table 2) (Gold et al., 2006, Kunchithapautham et al., 2012).

The first genetic evidence for the complement system being associated with the development of AMD was the discovery of the Y402H polymorphism in the CFH gene. This causes tyrosine to be substituted for histidine at amino acid position 402 within the CFH protein and greatly increases the risk of AMD development (Haines et al., 2005, Hageman et al., 2005, Gold et al., 2006). Additionally, CFH is a member

of the RCA gene cluster and is therefore linked with other genes to create a haplotype that harbors polymorphisms that determine AMD susceptibility. For instance, deletion of the CFHR1 (Complement Factor H-related 1) and CFHR3 members of the above gene cluster reduces the risk of AMD development (Hageman et al., 2006).

AMD is a very complex genetic disease as other highly penetrant missense mutations have recently been identified in other loci, which may increase or decrease susceptibility (van de Ven et al., 2013). Genotyping of multiple samples derived from AMD patients led to the recognition of rare missense variants that increase the risk of advanced AMD. Such variants are substitution of Lysine to Glutamine at position 155 (Lys155Gln) in the C3 protein, substitution of Proline to Serine at position 167 (Pro167Ser) in C9, and substitution of Glycine to Arginine at position 119 (Gly119Arg) in complement factor I (CFI). Further investigation of some of the above variants showed that the allele of C3 encoding Lys155Gln increased resistance to proteolytic inactivation by CFH and CFI (Seddon et al., 2013). Therefore, this loss of C3 protein regulation led to the enhanced activation of the alternative pathway (Seddon et al., 2013). With regards to the allele of CFI encoding Gly119Arg, it has been demonstrated that the Gly119Arg mutant protein is expressed to a lesser extent than the wild-type protein and therefore C3b degradation was less evident in the plasma and sera of AMD patients carrying that mutation (van de Ven et al., 2013).

Complement factor (Gene)	Variants (Single nucleotide polymorphisms)	Risk of AMD development
Factor B / C2	L9H, R32Q (Factor B) and E318D, rs547154 SNP9 (C2)	All four polymorphisms are highly protective
C3	rs2230199 variant leads to R102G. Additional variant leads to Lys155Gln	Can increase AMD risk by three-fold.
Factor H	rs1061170 leads to Y402H, rs800292 leads to I162V, rs1061147 leads to A307A.	Y402H, can increase the risk by seven-fold
Complement factor H-related 1	rs10737680 and rs1061170 lead to Y402H, *CFHR1-3Δ*	Y402H, can increase the risk by seven-fold.*CFHR1-3Δ* protects against AMD
Complement factor H-related 3	*CFHR1-3Δ*	*CFHR1-3Δ* protects against AMD
C9	rs34882957 leads to Pro167Ser	Reduces the risk for AMD and CNV development.
C7	rs2876849	-
C5	Multiple variants	-
Factor I	rs13117504 and rs7675460 lead to Gly119Arg	Can increase the risk of AMD

Table 2. List of complement factors (genes) associated with increased and/or decreased risk of AMD development. R102G, substitution of arginine to glycine at position 102; Lys155Gln, substitution of lysine to glutamine at position 155; Y402H, exchange of tyrosine to histidine at position 402; I162V, exchange of isoleucine to valine at position 162; A307A, changes the codon but maintains alanine at position 307; Pro167Ser, substitutes proline to serine at position 167; Gly119Arg, substitute glycine to arginine at position 119. Sourced from Gold et al., 2006; Zipfel et al., 2010; Raychaudhuri et al., 2011; Seddon et al., 2013; Nishiguchi et al., 2011; van de Ven et al., 2013; Khandhadia et al., 2012.

1.32 Aims of the project

A strong association between the complement system and AMD has been established as mutations in genes encoding complement inhibitors/activators can promote or prevent the initiation of AMD. Also, it has been shown that C5b-9 is found in samples from AMD patients (mainly on the basal surface of RPE and/or drusen deposits). Therefore, it was essential to develop optimal conditions for the *in vitro* formation of C5b-9 on the basal surface of RPE cells in order to investigate whether this complex would induce any physiological changes to the RPE monolayer.

By determining which cell culture model is the most appropriate for our studies, it was desirable to investigate not only the elimination/formation rate of C5b-9 complex on the basal surface of RPE cells but also to examine the mechanism/s of its elimination. The next milestone of the project was to examine whether C5b-9 can induce any changes in the characteristics of RPE cells such as: TER, actin cytoskeleton, the expression of junctional proteins and the expression of some of the negative regulators of the complement system.

Since it has recently been suggested that complement activation could affect mitochondrial numbers and/or stability in a number of various cell lines including primary human lung epithelial cells and Ehrlich ascites tumor cells, it was intriguing to investigate whether the direct exposure of pRPE cells to basal amounts of C5b-9 would affect mitochondrial numbers and/or stability (Papadimitriou et al., 1991, Papadimitriou et al., 1994, Triantafilou et al., 2013). As Feher et al., 2006 demonstrated that RPE cells from patients with advanced AMD suffered from low mitochondrial numbers and altered mitochondrial structure, compared to control samples, it was hypothesized that complement could implement changes in mitochondria in the context of AMD.

The final aim of this project was to investigate whether C5b-9 would affect the process of POS phagocytosis by examining not only the binding and internalization of outer segments, but also by examining the activation levels of three phagocytosis-related kinases: p-MerTK, p-FAK and p-Src.

Materials & Methods (Chapter 2)

2. Materials and Methods

2.1 Cell lines

Two different cell lines were used to optimise and perform experiments in this project: ARPE-19 cells (an immortalised human cell line) and primary porcine retinal pigment epithelial cells (pRPE).

2.1.1 Cultivation of ARPE-19 cells

The ARPE-19 cell line (provided from ATCC, number CRL-2307) has been extensively used *in vitro*. ARPE-19 cells were cultured at 37 ºC with 5 % carbon dioxide (CO_2), using Dulbecco's Modified Eagle Medium (DMEM, Sigma-Aldrich, D5796) with 10 % foetal bovine serum (FBS, Gibco, 07F0423K) and 100 U/ml of penicillin/streptomycin (Gibco, 1469713). Media was changed twice per week.

At full confluence, cells were detached from their flasks by administering 0.02 % trypsin (Gibco, 15400-054). First, cells were washed twice with phosphate buffered saline (PBS), then trypsin was added and cells were incubated at 37 ºC for 3 min. Trypsinisation was stopped by adding FBS and cells were collected by centrifugation at 1,000 rpm for 3 min at room temperature.

2.1.2 Storing (freezing) and thawing of ARPE-19 cells

ARPE-19 cells were stored in cryo-tubes in 75 % of DMEM (10 % FBS, 100 U/ml of penicillin/streptomycin) and 25 % dimethylsulfoxide (DMSO, Sigma-Aldrich, 472301). Cells were initially frozen at -80 ºC overnight before being transferred to -196 ºC in liquid nitrogen tanks.

Thawing of cells was accomplished by rapidly warming the cryo-vials and then transferring the cells into 10 ml of pre-warmed DMEM (10 % FBS, 100 U/ml of penicillin/streptomycin). Cells were centrifuged at 1,000 rpm for 3 min at room temperature. The cell pellet was then re-suspended in fresh media and cells were plated in T25 flasks (Nunc flasks, Thermo Scientific, 178905) at 37 ºC with 5 % CO_2.

2.1.3 Collection of pRPE cells

Porcine eyes were freshly delivered from a slaughter house (via First Link, UK) and kept on ice, both during transportation and before processing in the lab. Once the bulbi were detached from the surrounding muscle tissue, they were disinfected using PBS and videne surgical scrub (Williams Medical Supplies, D748980). They were then placed at 4 ºC for 30 min in PBS and penicillin/streptomycin (1 mg/ml). Then the bulbi were cut underneath the ora serrata. The anterior part (including the lens and vitreous) was discarded, while the posterior part (neuroretina and RPE) was processed. Prior to the RPE isolation, the neuroretina was detached from the RPE monolayer, cut at the optic nerve and finally homogenised in 48 % sucrose solution, pH 7.0 and KCl buffer (0.3 M KCl, 10 mM HEPES, 0.5 mM $CaCl_2$ and 1 mM $MgCl_2$). Isolation of the RPE cells was performed by adding 10x trypsin-EDTA (Gibco, UK) for 20 min at 37 ºC to or into the posterior part of each eye. Then, RPE cells were detached and isolated by repetitive pipetting. Trypsinisation was stopped by the addition of DMEM and 10 % FBS. RPE cells were collected for *in vitro* culturing after centrifugation at 2,000 rpm for 3 min. The cell pellet was re-suspended in fresh DMEM containing 10 % FBS and 100 U/ml penicillin/ streptomycin. Finally, pRPE cells were placed in 6-well plates (Nunclon DeltaSurface, Thermo Scientific, 140675) at a cell density of approximately 1 x 10^5 cells/well.

2.1.4 Isolation and storage of photoreceptor outer segments (POS)

Neuroretinas were processed in order to extract the POS. Falcon tubes containing KCl buffer (0.3M KCl, 10 mM HEPES, 0.5 mM $CaCl_2$ and 1 mM $MgCl_2$) and 48 % sucrose at pH 7.0 were used to add and therefore homogenise the isolated neuroretinas. Falcon tubes containing the homogenised neuroretinas were shaken for 2 min and their contents were placed into 1.5 ml Eppendorf tubes. These tubes were then centrifuged at 7,000 rpm for 5 min. The supernatant, which contained the outer segments was filtered through sterile gauze (cheese cloth) and diluted 1:1 with KCl buffer (no sucrose). This mixture (buffer and POS) was centrifuged at 7,000 rpm for 7 min. Pellets were washed using 1 ml of PBS and centrifuged again at 7,000 rpm for 7 min. Pellets were re-suspended in serum-free DMEM with 100 U/ml penicillin/streptomycin. Aliquots of 200 µl were prepared and stored at -80 ºC.

2.1.5 *In vitro* culturing of pRPE cells

Upon isolation, pRPE cells were cultured in a separate incubator under the same conditions as specified in section **2.1.1**. Cells were washed once with sterile PBS before adding fresh media.

2.1.6 Cultivation of pRPE cells in trans-well inserts

In order to make both surfaces (apical and basolateral) of pRPE cells accessible to various treatments (binding of POS on the apical surface, C5b-9 complex assembly on the basal surface), pRPE cells were cultured on 12-well polyester trans-well inserts (Transwell® polyester membrane cell culture inserts, 12 mm Transwell, 0.4 μm pore polyester membrane insert, catalogue No. 734-1579, Corning, UK). Also, cultivation of pRPE cells in trans-wells allowed cells to polarise correctly and therefore mimic their morphology in the mammalian eye *in vivo*. Cells were grown using fresh DMEM containing 10 % FBS and 100 U/ml penicillin/streptomycin. Once they reached a confluent state, the amount of FBS was reduced to 1 %. As a general practise cells were maintained in trans-well inserts for 7 – 21 days prior to experimentation. To ensure the formation of a properly formed monolayer of pRPE cells within the trans-well plates, the TER was measured.

2.2 Measurement of TER

TER measurement allows the confirmation of a fully formed intact monolayer of pRPE cells grown in trans-well plates. When cells reach a confluent state and establish strong tight junctions, TER values increase correspondingly. Recording of stable TER measurement is therefore a good indication that an authentic monolayer of cells has formed (approximately two weeks after plating on trans-wells). Furthermore, a dense monolayer ensures that proteins and reagents added to one side will only be able to access the cell surface on that side. All TER values were corrected by subtracting the TER value obtained from a blank insert which did not contain any cells. Then, the corrected TER values were multiplied by the surface area of the insert to acquire the resistance of the entire area that cells occupy (Ω/cm^2) (Garcia-Diaz and Essig, 1985). All TER measurements were performed using an epithelial voltometer (Figure 12) (World Precision Instruments, Inc.).

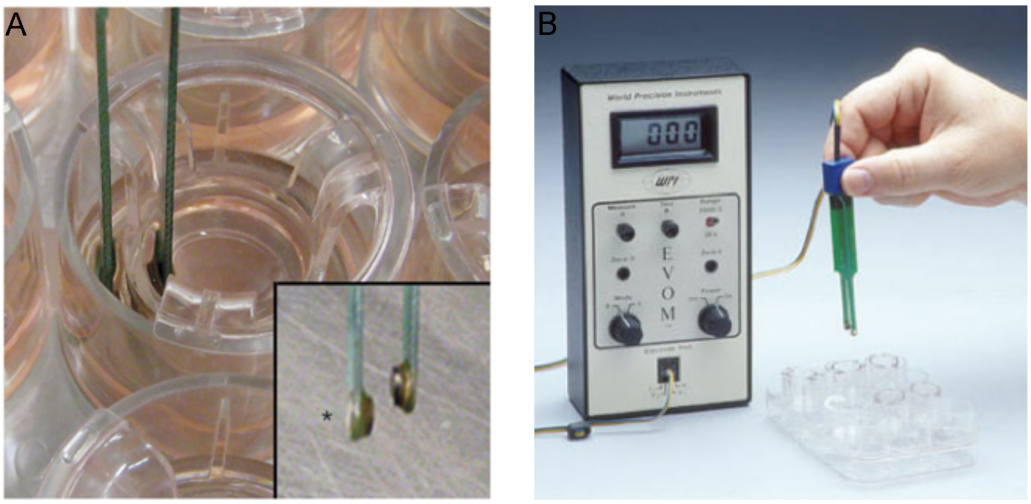

Figure 12. TER measurement in a 12-trans-well plate using an STX2 manual electrode. **A.** STX2 manual electrode. **B.** Epithelial voltometer (EVOM). Images acquired from (Sonoda et al., 2009) and www.pharmaceutical-int.com, respectively.

2.3 Permeability assay

In addition to TER measurements, permeability assays may be used to further monitor the integrity of pRPE cells grown in trans-well plates. Inserts were washed twice with sterile PBS, then 1 mg/ml of either low or high molecular weight (3-5 kDa and 70 kDa, respectively) dextran (fluorescein isothiocyanate-dextran, rhodamine B isothiocyanate-dextran, Sigma-Aldrich, FD4 and R9379, respectively) was added to the insert in DMEM (serum-free). At specified time points, 20 µl of media were collected from the outer well. The 20 µl aliquots were replaced with 20 µl of DMEM to prevent artificial effects of volume changes. The fluorescence intensity of the aspirated samples was measured at 520 nm (for fluorescein isothiocyanate-dextran) or at 590 nm (for rhodamine B isothiocyanate-dextran) with a Safire plate reader. The above protocol was adjusted from (Matter and Balda, 2003).

2.4 Cell viability assay

The viability of RPE cells (both ARPE-19 and pRPE) was examined using 3-(4,5-dimethylthiazol-2-yl)-2,5-diphenyltetrazolium bromide (MTT) in the MTT assay (Sigma-Aldrich, M2128) according to (Mosmann, 1983). In this assay, mitochondrial dehydrogenases of living cells cleave the tetrazolium ring of MTT and blue formazan crystals start to form. In contrast, dead cells do not develop formazan crystals as

mitochondrial dehydrogenases are not active. Formazan crystals were allowed to form by adding 180 µl of DMEM and 20 µl of MTT solution (5 mg thiazolyl blue / 1 ml PBS) at 37 ºC to cells plated on a 96-well micro-plate (Nunc Plates, Thermo Scientific, 167008). After 3 h crystals were dissolved by adding 100 µl of DMSO. The optical density (OD) of the supernatants was measured in a spectrophotometer at a wavelength of 490 nm. Every individual MTT cell viability assay included a positive control (untreated cells) and a negative control (cells treated with 1 % Triton-X 100 for 10 min, prior to the MTT assay).

2.5 *In vitro* formation of the C5b-9 multi-protein complex

To induce formation of the C5b-9 complex on the apical and/or basal surface of both cell types (ARPE-19 and / or pRPE cells) four different approaches were applied in order to achieve a uniform and reproducible pattern of C5b-9 complex formation. Each protocol is described here separately where they are referred to as methods A, B, C and D respectively. Method D_T refers to the *in vitro* formation of C5b-9 complex on the basal surface of pRPE cells, grown on trans-well plates.

Purified complement component proteins referenced below were purchased from Complement Technology, USA, unless stated otherwise. A summary of the different protocols is shown in Table 2.

2.5.1 Method A, C5b-9 complex induction with normal human serum

Studies of the C5b-9 complex frequently use normal human serum (NHS) as a source of complement proteins (Johnson et al., 2011, Lueck et al., 2011). To induce *in vitro* assembly of the C5b-9 complex using NHS, ARPE-19 cells (passage 26) were cultured on glass coverslips at 37 °C / 5 % CO_2, for approximately 10 days. Confluent cells were then washed twice with sterile PBS. To block one of the negative regulators of C5b-9 complex formation, cells were pre-incubated with a purified rabbit anti-human CD59 antibody (1.34 mg/ml, generous gift of Prof. M. P. Morgan, Cardiff University) for 1 h at 37 ^{o}C / 5 % CO_2 in DMEM. ARPE-19 cells were then washed once with sterile PBS and incubated in 20 % NHS in DMEM (Sigma-Aldrich, H4522) overnight at 37 ^{o}C / 5 % CO_2. As a control, ARPE-19 cells were treated as mentioned above except that the NHS was heat inactivated by incubation at 56 °C for 1 h (heat denatures complement proteins).

2.5.2 Method B, C5b-9 complex induction with C5-depleted human serum

ARPE-19 cells (passage 26) were cultured on glass coverslips for approximately 10 days after becoming confluent. Cells were washed twice with sterile PBS prior to incubation with the purified rabbit anti-human CD59 antibody for 1 h at 37 ^{o}C / 5 % CO_2 in DMEM. The cells were then washed once with sterile PBS and incubated overnight with 60 μg/ml of purified complement protein 5 (C5, A120) and 30 % C5-depleted human serum (A320) in DMEM at 37 ^{o}C / 5 % CO_2. As a control, ARPE-19 cells were pre-treated with the anti-CD59 antibody (as described above), washed once with PBS and treated with 30 % of C5-depleted human serum in DMEM overnight at 37 ^{o}C / 5 % CO_2.

Method B was also performed without blocking the CD59 negative regulator with the rabbit anti-human CD59 antibody.

2.5.3 Method C, C5b-9 complex induction with C5b-6, C7 proteins and C5-depleted human serum,

In order to increase the amount of C5b-9 complex formation *in vitro*, it was tested whether adding C5b-6 complex (A122) and C7 (A124) protein to C5-depleted human serum was able to enhance the levels of the C5b-9 complex. C5b-6 and C7 complement proteins are essential for the formation of the C5b-7 complex, which in turn allows the binding of C8 and C9 (Stewart et al., 1987).

ARPE-19 cells (passage 26) were cultured on glass coverslips for approximately 10 days. Once cells were confluent, they were washed twice with sterile PBS and incubated overnight with the C5b-6 complement complex (C5b-6, 0.2 mg/ml), complement protein 7 (C7, 60 μg/ml) and 30 % C5-depleted human serum in DMEM overnight at 37 ^{o}C / 5 % CO_2. As a control, ARPE-19 cells were incubated only with 30 % C5-depleted human serum and complement protein 7 (C7, 60 μg/ml) in DMEM overnight at 37 ^{o}C / 5 % CO_2.

Method C was also performed in the presence of 1 mg/ml propidium iodide (PI, Sigma Aldrich, UK). The addition of PI was to investigate whether the C5b-9 complex forms a functional pore on ARPE-19 cells.

It should be noted that at a later stage method C was also applied to pRPE cells grown on glass coverslips, as studies were progressing.

2.5.4 Method D, C5b-9 complex induction with purified complement proteins

Confluent pRPE cells (passage 1) grown on glass coverslips were incubated with 0.2 mg/ml of C5b-6 complex, 60 μg/ml of C7, 50 μg/ml of C8 (A125) and 60 μg/ml of C9 (A126) purified complement proteins in DMEM overnight at 37 ^{o}C / 5 % CO_2. This method of C5b-9 complex formation was initially tested on the apical surface of pRPE cells. As a control pRPE cells were incubated with C5b-6 complex (0.2 mg/ml), C7 (60 μg/ml) and C8 (50 μg/ml) purified complement proteins in DMEM overnight at 37 ^{o}C / 5 % CO_2.

2.5.4.1 Method D applied in trans-well inserts (method D_T)

As is discussed in the first results chapter (Section **3.7**), method D was judged to be the most efficient in inducing large and stable amounts of C5b-9 complex on the apical surface of pRPE cells, thus method D was selected as the method of choice for all future experiments. However, in order to more accurately reproduce the *in vivo* C5b-9 complex formation, it was necessary to modify the procedure to allow the complex to form on the basal surface of pRPE cells instead of the apical. For this reason, pRPE cells were allowed to form a confluent monolayer on trans-well inserts (as described in section **2.1.6** and shown schematically in Figure 13).

Cells were washed once with sterile PBS and incubated with 500 μl of DMEM on the apical surface. On the basal surface cells were treated with 500 μl of DMEM containing C5b-6 complex (0.2 mg/ml), C7 (60 μg/ml), C8 (50 μg/ml) and C9 (60 μg/ml) purified complement proteins (Figure 13). Cells were incubated for 1 h, 4 h, 8 h, 24 h and 48 h at 37 ^{o}C / 5 % CO_2, unless stated otherwise. As a control, C9 was omitted, thus cells were treated with C5b-6 complex (0.2 mg/ml), C7 (60 μg/ml) and C8 (50 μg/ml) purified complement proteins only.

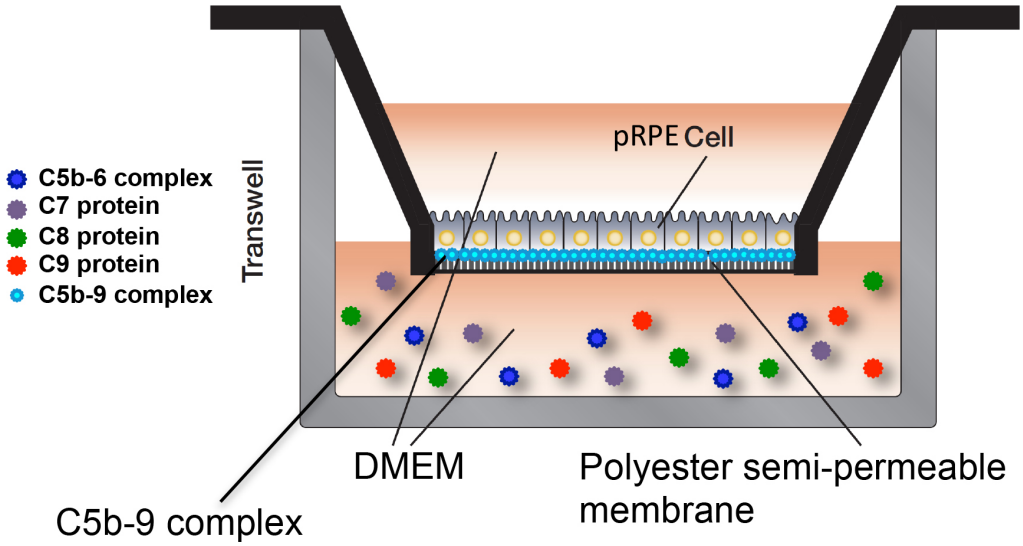

Figure 13. Schematic representation of complement studies in trans-well inserts. C5b-9 complex formation on the basal surface of pRPE cells at 37 ^{o}C / 5 % CO_2, for 1 h, 4 h, 8 h, 24 h and 48 h, unless stated otherwise.

Method	Treatment	Controls
A	Pre-treatment: α-CD59 antibody (1.34 mg/ml) in DMEM for 1 h. Then, 20 % NHS overnight.	Pre-treatment: α-CD59 antibody (1.34 mg/ml) in DMEM for 1 h. Then 20 % heat-inactivated NHS, overnight.
B	Pre-treatment: α-CD59 antibody (1.34 mg/ml) in DMEM for 1 h. Then, C5 (150 μg/ml) + 30 % C5-depleted human serum, overnight.	Pre-treatment: α-CD59 antibody (1.34 mg/ml) in DMEM for 1 h. Then, 30 % C5-depleted human serum, overnight.
C	C5b-6 complex (0.2 mg/ml) + C7 (60 μg/ml) + 30 % C5-depleted human serum, overnight	C7 (60 μg/ml) + 30 % C5-depleted human serum, overnight.
D	C5b-6 complex (0.2 mg/ml) + C7 (60 μg/ml) + C8 (50 μg/ml) + C9 (60 μg/ml) in DMEM, overnight.	C5b-6 complex (0.2 mg/ml) + C7 (60 μg/ml) + C8 (50 μg/ml) in DMEM, overnight.
D_T	Apical Chamber: DMEM (500 μl), overnight. Basal Chamber: C5b-6 complex (0.2 mg/ml) + C7 (60 μg/ml) + C8 (50 μg/ml) + C9 (60 μg/ml) in DMEM (500 μl), overnight.	Apical Chamber: DMEM (500 μl), overnight. Basal Chamber: C5b-6 complex (0.2 mg/ml) + C7 (60 μg/ml) + C8 (50 μg/ml), in DMEM (500 μl), overnight.

Table 2. **Summary of the protocols for the *in vitro* C5b-9 complex formation.**

2.6 Inhibition of C5b-9 endocytosis using dynasore

Basal C5b-9 complex was formed *in vitro* according to method D_T (Section **2.5.4.1**). In order to block the endocytosis of the C5b-9 complex, media was supplemented with 200 μg/ml of dynasore hydrate (Sigma-Aldrich, D7693) for 24 h (unless stated otherwise) at 37 ^{o}C / 5 % CO_2. The next day, cells were washed once with sterile

PBS and were either lysed for western blotting or fixed for immunofluorescence or electron microscopy.

2.7 Outer segment phagocytosis by C5b-9-treated pRPE cells

To investigate whether the C5b-9 complex influences retinal phagocytosis (binding, internalisation and/or degradation of POS), C5b-9 was assembled on the basal surface of pRPE cells (Method D_T) and at a later stage pRPE cells were fed with POS on their apical side according to the following protocol: POS were counted and used in a final concentration of 10^7 POS / ml. Then POS were sonicated for 10 min at room temperature and centrifuged at 13,000 rpm at room temperature for 1 min. The supernatant was discarded while the pellet was dissolved in 850 µl of 10 mM sodium phosphate buffer pH 7.2, 100 µl of 1 M sodium bicarbonate pH 9.0 and 5 µl (5 %) of alexa fluor 555 (Life Technologies, A-20009). The Eppendorf tube containing the POS was covered in foil and placed in the rotor for 1 h at room temperature. The outer segments were then centrifuged at 13,000 rpm for 1 min at room temperature, the supernatant was discarded and the pellet was re-suspended in 1 ml of DMEM. This washing step was repeated 3 times. After washing, POS were diluted in DMEM and 1 % FBS (500 µl) and added to the apical chamber of the trans-well insert of confluent pRPE cells for 1 h at 37 ^oC / 5 % CO_2, to allow the POS to bind to the apical cell surface. One hour prior to the addition of POS 500 µl of DMEM containing complement proteins (as described in Method D_T, Section **2.5.4.1**) was added to the basal compartment to allow basal formation of the C5b-9 complex. As a control, these conditions were replicated but with C9 omitted from the complement protein mix (Figure 14). One hour after the addition of POS the apical cell surface was washed 3 times with PBS to remove unbound POS. Then cells were either fixed with ice-cold methanol (100 %) and processed for immunofluorescence staining or returned to culture medium and incubated overnight at 37 ^oC / 5 % CO_2 (Section **2.9**).

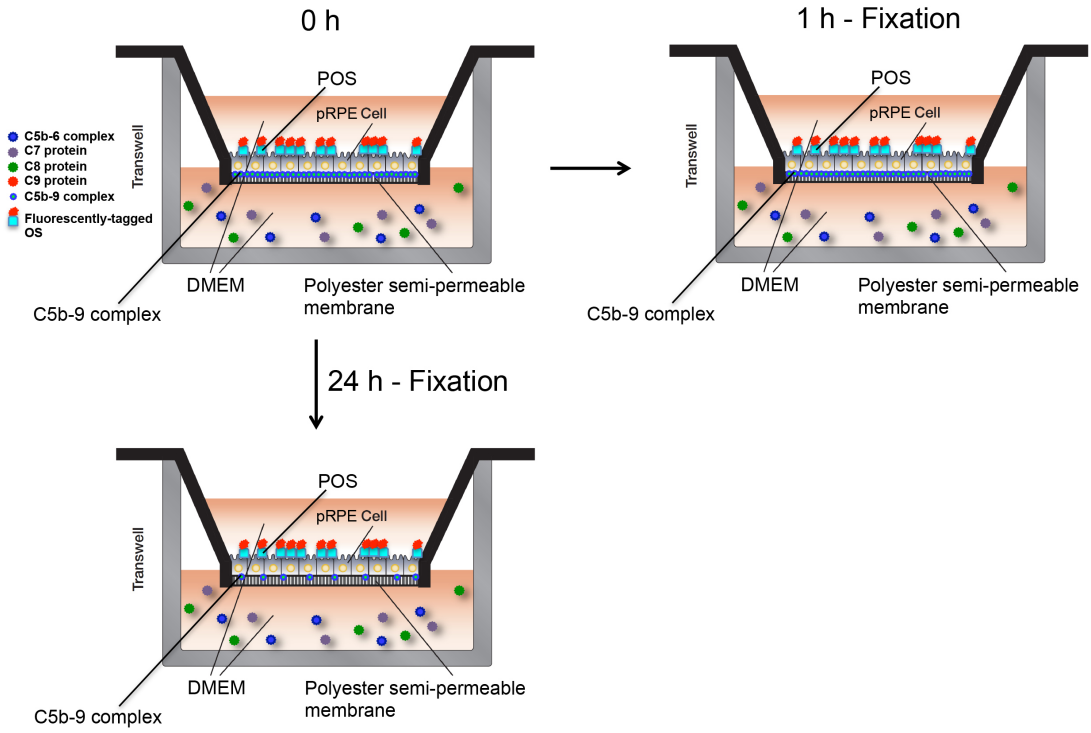

Figure 14 Schematic representation of phagocytosis in C5b-9-treated pRPE cells. At 0 h C5b-9-treated pRPE cells were fed apically with fluorescent POS for 1 h. After 1 h, cells were washed with sterile PBS and were fixed with pure ice-cold methanol. Alternatively, once cells were washed, at 1 h, were then maintained at 37 ^{o}C / 5 % CO_2 overnight. At 24 h most of the C5b-9 complex is absent from the basal surface of cells.

2.8.1 SDS – PAGE and western blotting

In order to investigate whether the C5b-9 complex affects the activation of the downstream effectors of POS phagocytosis, pRPE cells were exposed to POS according to the following protocol: one hour prior to the addition of POS on the apical surface of pRPE cells, 500 µl of DMEM containing complement proteins (as described in Method $D_{T,}$ Section **2.5.4.1**) was added to the basal compartment to allow formation of the C5b-9 complex. In the meantime, POS were prepared at a concentration of 10^7 / ml, sonicated for 10 min at room temperature and centrifuged at 13,000 rpm at room temperature for 1 min. After washing, POS were diluted in DMEM containing 1 % FBS. At 1 h after C5b-9 complex formation, 500 µl POS was added to the apical chamber (Figure 15). For control cells the same procedure was followed, however C9 protein was not included in the media on the basal chamber.

At the completion of each time point, cells were washed once with sterile PBS and then lysed in sample buffer, as described in Section **2.10.**

All primary and secondary antibodies used for the above studies are listed in Tables 3 and 4, respectively.

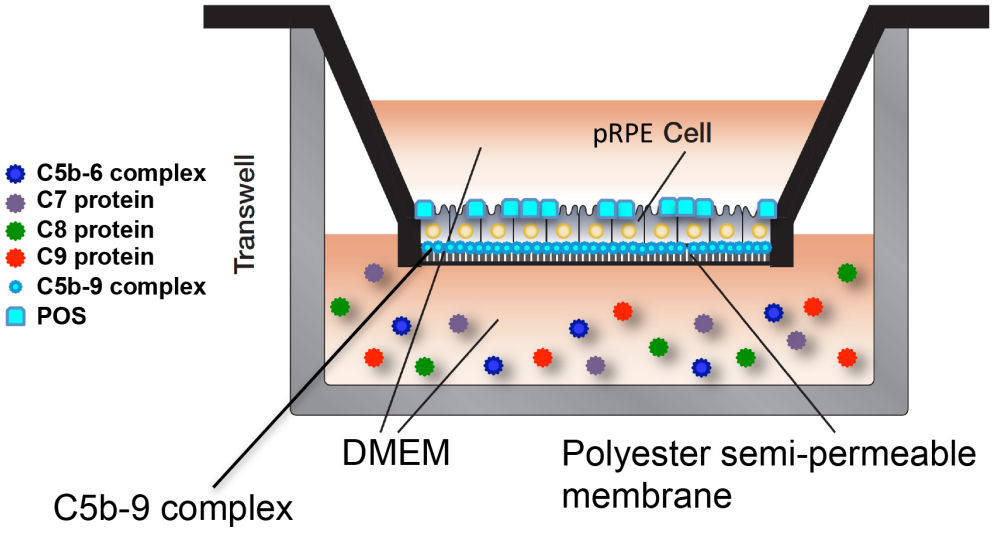

Figure 15. Schematic of the *in vitro* phagocytosis in complement-treated pRPE cells. C5b-9-treated cells were fed with POS apically at 37 ^{o}C / 5 % CO_2 for different time-points, and then lysed and processed for SDS-PAGE and western blotting.

Product Name	Company	Cat.Number	Clone/Isotype	Species	Reactivity	Dilution	Application
ZO-1	Invitrogen	33-9100	ZO1-1A12, IgG1 Kappa, mAb	Mouse	Human, Canine	1/50	IF
ZO-1	Abcam	ab59720	IgG, pAb	Rabbit	Mouse, Chicken, Dog, Human, Pig	1/1000	WB
Claudin-19	Novus Biologicals	H00149461-M02	2F2, IgG2a Kappa, mAb	Mouse	Human	1/50, 1/1000	IF, WB, respectively
GAPDH	Novus Biologicals	NB300-221	1D4, IgM Kappa, mAb	Mouse	Human, Mouse, Rat, Avian, Bovine, Chicken, Hamster, Primate, Oppossum, Porcine, Sheep, Zebrafish	1/1000	WB
Tim23	BD Transduction Laboratories	611222	32/Tim23, IgG2a, mAb	Mouse	Human, Rat	1/50, 1/1000	IF, WB, respectively
C5b-9	Dako Cytomation	M0777	aE11, IgG2a, Kappa, mAb	Mouse	Human	1/50	IF
Anti-MERTK (phospho Y749 + Y753 + Y754)	Abcam	ab14921	IgG, pAb	Rabbit	Human	1/1000	WB
Anti-MERTK [Y323]	Abcam	ab52968	Y323, IgG, mAb	Rabbit	Human	1/1000	WB
Phospho-FAK (Tyr397)	Cell Signaling	3283	pAb	Rabbit	Human, Mouse, Rat, Pig, Hamster	1/1000	WB
FAK	Cell Signaling	3285	pAb	Rabbit	Human, Mouse, Rat, Monkey, Bovine, Pig	1/1000	WB
Phospho-Src (Tyr416)	Cell Signaling	2101	pAb	Rabbit	Human, Mouse, Rat	1/1000	WB
Src	Cell Signaling	2109	IgG, mAb	Rabbit	Human, Mouse, Rat, Monkey, Bovine, Pig	1/1000	WB
DAF	Paul Morgan*	N/A	MD1, IgG1, mAb	Rat	Mouse	1/1000	WB

Table 3. Primary antibodies used in western blotting and immunofluorescence. Ig, Immunoglobulins ; mAb, Monoclonal antibody ; pAb, Polyclonal antiboby; IF, Immunofluorescence ; WB, Western Blot ; * Provided by Prof. M.P. Morgan, University of Cardiff.

Product Name	Company	Cat.Number	Clone/Isotype	Species	Reactivity	Dilution	Application
Goat Anti-Rat IgG Antibody, HRP conjugate	Merck Millipore	AP136P	IgG, pAb	Goat	Rat	1/1000	WB
Goat Anti-Rabbit Immunoglobulins /HRP	Dako Cytomation	P 0448	IgG, pAb	Goat	Rabbit	1/1000	WB
Goat Anti-Mouse Immunoglobulins /HRP	Dako Cytomation	P 0447	IgG, pAb	Goat	Mouse	1/1000	WB
Alexa Fluor® 488	Life Technologies	A-21202	IgG, pAb	Donkey	Mouse	1/100	IF
Alexa Fluor® 488	Life Technologies	A-21206	IgG, pAb	Donkey	Rabbit	1/100	IF
Alexa Fluor® 555	Life Technologies	A-31570	IgG, pAb	Donkey	Mouse	1/100	IF
Alexa Fluor® 555	Life Technologies	A-31572	IgG, pAb	Donkey	Rabbit	1/100	IF

Table 4. Secondary antibodies used in western blotting and immunofluorescence. Ig, Immunoglobulins ; pAb, Polyclonal antiboby; IF, Immunofluorescence ; WB, Western Blot.

2.8.2 Cell lysis

Upon completion of an individual treatment, the pRPE monolayer in 12-well trans-well inserts was washed once with sterile PBS and lysed with 200 µl of 2 % w/v sodium dodecyl sulfate (SDS), 25 % w/v glycerol, 0.5 M Tris, 154.52 g/mol dithiothreitol (DTT) and 0.2 % w/v bromophenol blue at room temperature.

2.8.3 Sodium dodecyl sulfate-polyAcrylamide gel electrophoresis (SDS)-PAGE

Following cell lysis, proteins were resolved by SDS-PAGE according to the method of (Laemmli, 1970). SDS denatures proteins and gives them all a negative charge. The ratio of mass and charge leads to protein separation according to the overall size of the protein. The DTT (one of the components of the sample buffer, described in section **2.10**) reduces the disulfide bonds of proteins so that they separate as monomers. The protein extract was loaded in the stacking gel (20 µl of protein extract was loaded per well per sample). Upon initiation of electrophoresis, proteins were separated within pre-cast gradient gels (NuPage® 4-12 % Bis-Tris gradient gels, Life Technologies, WG1402BX10). Electrophoresis was performed at 150 V for approximately 1.5 h at room temperature until the dye front reached the bottom of the gel.

2.8.4 Western blotting

Following SDS - PAGE, a blot sandwich was prepared to transfer the proteins from the gradient gel to a polyvinyl difluoride (PVDF) membrane (GE Healthcare, G3126136). The preparation of the sandwich blot was the following: sponge > two filter papers > gradient gel > PVDF membrane > two filter papers > sponge. It should be noted that, before the assembly of the sandwich blot, all parts were soaked with pure distilled H_20, 10x Tris-glycine (0.25M Tris and 1.92 M Glycine) pH 8.4 (GeneFlow, EC-880) and pure methanol. Transfer of the proteins from the gradient gel to the PVDF membrane was completed in a blotting chamber (XCell4 Surelock™ Midi-Cell) at 12 V overnight at 4 ^{o}C. The next day, the membranes were washed twice with 0.05 % Tween-20 (Sigma-Aldrich, P1379) in Tris-buffered saline (TBS) and blocked with 5 % milk powder in TBS-T (0.05 % Tween-20 + TBS) for 1 h at room temperature. Blocking with milk saturates any free binding sites on the membrane and therefore reduces background. After blocking, membranes were incubated with a primary antibody (Table 3, section **2.8.1**) (depending on the protein

of interest). Primary antibodies (1:1000 dilution, unless stated otherwise) were diluted in 5 % BSA in TBS-T at 4 ^{o}C overnight. Following the primary antibody incubation, membranes were washed 3 times with TBS-T (15 min each wash) and the secondary antibody was added (1:1000 dilution) in 5 % milk in TBS-T for 1 h at room temperature (Table 4, section **2.8.1**). After the one-hour incubation period, membranes were washed for at least 5 h with TBS-T. Finally, protein bands were visualised by chemiluminescence using ECL western blotting detection reagents (GE Healthcare, IRPN2209) at room temperature. Then, the membranes were transferred into cling-film and exposed to a Kodak Biomax XAR X-ray film in the dark room. All protein bands of interest were normalised to GAPDH, a house-keeping protein and quantified by densitometric analysis using ImageJ (NIH, freeware).

2.9 Confocal microscopy and image analysis

Cells were washed twice with sterile PBS and then fixed either with pure ice-cold methanol (5 min) or with 4 % paraformaldehyde (PFA, Sigma-Aldrich, 15,812-7) for 30 min at room temperature. Fixation was stopped by washing the cells thoroughly, three times with PBS at room temperature. Cells were then permeabilised with PBS containing 0.01 % Triton-X 100 (Sigma, T-8787) (PBS-T) for 15 min. To reduce background staining, the cells were blocked with 1 % bovine serum albumin (BSA, Sigma, A7906) in PBS-T for 1 h at room temperature. After blocking, cells were incubated with a primary antibody (depending on the protein of interest). All primary antibodies (Table 3, section **2.8.1**) were diluted 1:50 in 1 % BSA and PBS-T overnight at 4 ºC.

The next day, cells were washed three times with PBS at room temperature to remove non-bound primary antibody. Then a secondary antibody (Table 4, section **2.8.1**), FITC- or TRITC-conjugated, was applied at 1:100 dilution for 1 h at room temperature. When examination of the cytoskeleton (F-actin) was required, rhodamine phalloidin (1:2000 dilution, Life Technologies, R415) was added together with the secondary antibody. To stain cell nuclei, 10 min before the removal of the secondary antibody, DAPI (4', 6-diamidino-2-phenylindole) was added at 1 mg/ml. At this stage, it should be noted that all samples were protected from light as fluorophore-conjugated antibodies and DAPI are light sensitive. Excess secondary antibody was removed with three PBS washes at room temperature. Cells were

coated with mounting media (Mowiol) and analysed by confocal microscopy using a Leica SP2 confocal microscope. This approach allowed the acquisition of three-colour images and / or z-stacks via sequential scanning of the three main colour channels: DAPI (blue), FITC (green) and TRITC (red). Each channel covers different areas of the colour spectrum depending on the emission spectrum. DAPI's maximum emission wavelength is at 461 nm and therefore gives a blue colour. For the FITC channel a 488-green fluorescent dye was used with a maximum emission wavelength at 488 nm and for the FITC channel a 555-red fluorescent dye was used with an emission wavelength at 555 nm. These dyes, as mentioned above, were conjugated with the secondary antibody. To acquire 3D images of z-sections, data were processed using the Imaris® 3D reconstruction software.

2.10 Statistical Analysis

Data are shown as mean value and standard error. Student's t-test was performed to establish the significance of statistical differences between two groups.

2.11 Cryo-immunoelectron microscopy

Cryo-immunoelectron microscopy (Cryo-EM) was used to examine the subcellular localisation of the C5b-9 complex in pRPE cells, by gold particle-labelled anti-C5b-9 antibody, as described below.

Formation of the C5b-9 complex was performed on the basal surface of pRPE cells (Method D_T, section **2.5.4.1**) for 4 h and 24 h (± 200 μg/ml dynasore hydrate, as in Section **2.6**). As a control, C5b-8-treated pRPE cells were used (Method D_T, section **2.5.4.1**).

After the above treatments, pRPE cells were prepared for cryo-EM by incubating them in 4 % PFA in 0.1 M phosphate buffer pH 7.4 and then embedding them in 12 % gelatine. After infusion with 2.3 M sucrose, 90-nm sections were cut at -120 ^{o}C and collected in 1:1 2.3 M sucrose / 2 % methylcellulose. Sections were then immunolabelled by incubating them with the anti-C5b-9 antibody (Dako, UK) followed by 10 nm-gold-tagged protein A (UMC, Utrecht), as described ((Slot et al., 1991)). Analysis of the C5b-9 complex localisation in pRPE cells was performed using ImageJ. The number of gold particles counted was normalised to the

cytoplasmic area counted per cell, excluding the area covered by the nucleus. The cryo-EM studies were performed in collaboration with Dr. Thomas Burgoyne (UCL Institute of Ophthalmology, UK).

2.12 Electron-microscopy (EM) for mitochondrial analysis

In order to assess whether the basal C5b-9 complex affects mitochondrial integrity (by measuring mitochondrial number and morphology) the following samples were used: non-treated pRPE cells, cells incubated with DMEM + DMSO for 24 h (vehicle), DMEM with 200 μg/ml dynasore hydrate (24 h), C5b-8-treated cells (24 h), C5b-9-treated cells (24 h) and C5b-9-treated cells with 200 μg/ml dynasore hydrate (24 h). C5b-9 complex formation was performed according to Method D_T (Section **2.5.4.1**).

Upon completion of the treatments cells were fixed with 2 % w/v PFA / 2 % w/v glutaraldehyde for 2 h before incubating them in 1.5 % w/v osmium tetroxide / 1.5 % w/v potassium ferricyanide for 1 h. Cells were dehydrated using increasing concentrations of ethanol (70 %, 90 % and 100 % v/v ethanol) followed by propylene oxide before embedding in epon resin. 70 nm sections were cut using a Leica UC7 ultra-microtome and imaged on a JEOL 1010 transmission electron microscope. The EM studies were performed in collaboration with Dr. Thomas Burgoyne (UCL Institute of Ophthalmology, UK).

Mitochondria counting in pRPE cells was undertaken using ImageJ. The number of mitochondria counted was normalised to the cytoplasmic area per cell, excluding the area covered by the nucleus.

Chapter 3

3. Results

3.1 Membrane attack complex formation on ARPE-19 cells

The membrane attack complex (MAC), which is also referred to as C5b-9, is a multi-protein complex that is formed upon activation of the complement pathway (Laine and Esser, 1989). It can cause permeability of the target cell membrane and may therefore result in cell lysis (Laine and Esser, 1989). The aim of this part of the study was to determine if the formation of C5b-9 could be mimicked *in vitro* by treating ARPE-19 cells with normal human serum (NHS). To accomplish this, ARPE-19 cells (passage 26) were cultured on glass coverslips at 37 °C / 5 % CO_2, for approximately 10 days. Confluent monolayers were then washed twice with sterile PBS. In order to block the major negative regulator of C5b-9 formation, cells were first incubated with a purified rabbit anti-human CD59 antibody (1.34 mg/ml) for 1h. The cells were washed once with sterile PBS and incubated in 20 % NHS overnight (Table 2, Method A). To detect C5b-9, immunofluorescence staining was performed using an antibody that reacts with the poly-C9 neo-epitope of the C5b-9 complex. For controls, ARPE-19 cells were treated as described above, except that the NHS was heat inactivated (HI-NHS) by incubation at 58 °C for 1 h (Table 1, Method A) in order to denature the complement proteins.

C5b-9 complex formation was observed on ARPE-19 cells (Figure 16). However, it was not possible to analyse the precise location of the complex, with regard to whether it was on the cell surface or cytoplasmic. Furthermore, the pattern of C5b-9 complex formation was not uniform, some cells stained positively for C5b-9, while other cells showed weak or no C5b-9 staining. In control cells treated with HI-NHS no C5b-9 complex formation was observed, confirming that the heat denaturation of the serum complement proteins had been successful (Figure 16-B).

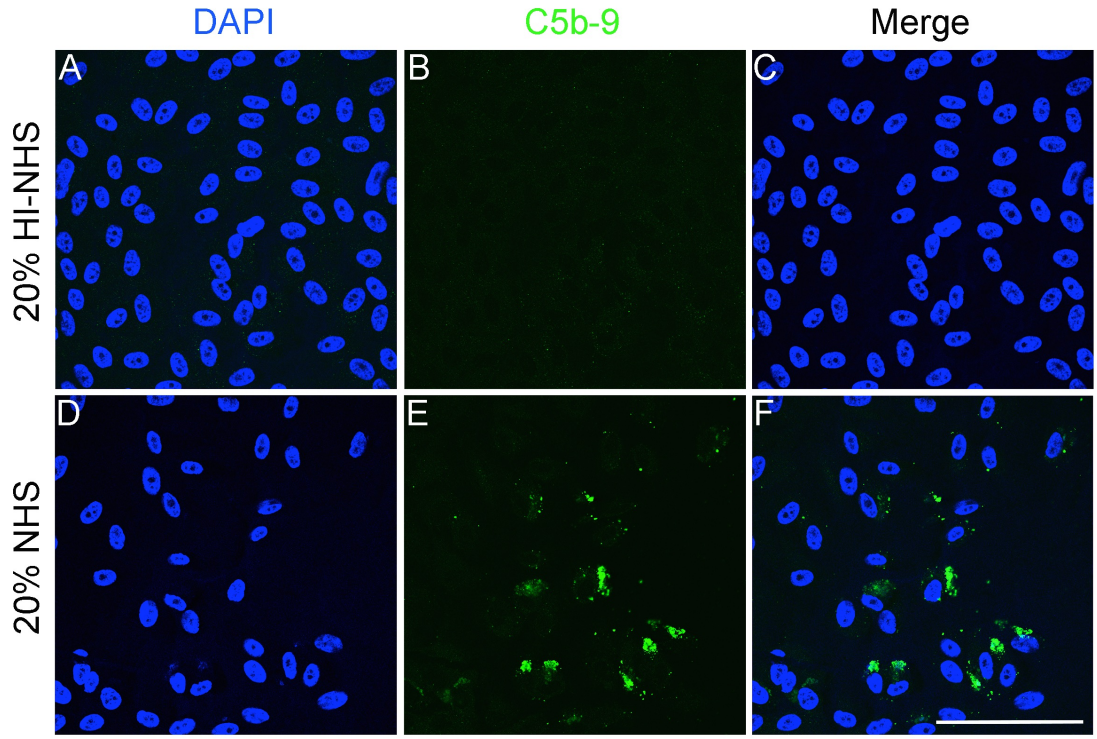

Figure 16. C5b-9 complex formation on ARPE-19 cells. (A-C) In control cells treated with HI-NHS, staining with C5b-9 antibody (green) showed that there was absence of C5b-9 complex. DAPI (blue) was used to observe cell nuclei. (D-F) ARPE-19 cells treated overnight with 20 % NHS. The C5b-9 staining (green) reveals patchy formation of the C5b-9 complex. Images A, B, C, D, E and F were derived from two independent experiments. Scale bar represents approximately 50 µm.

3.2 An alternative method to induce C5b-9 complex formation on ARPE-19 cells

In order to demonstrate that C5b-9 complex formation was indeed due to assembly of the individual C5b, C6, C7, C8 and C9 complement proteins, we next examined the effect of eliminating one of these five proteins (Hu et al., 1981, Stewart et al., 1987). To achieve this, as described in section **3.1**, ARPE-19 cells were cultured on glass coverslips for approximately 10 days. Cells were then washed twice with sterile PBS prior to incubation with the purified rabbit anti-human CD59 antibody (1.34 mg/ml), for 1 h in DMEM. The cells were then washed once with sterile PBS and incubated overnight either with 30 % C5-depleted NHS in DMEM supplemented with 150 µg/ml purified C5 protein, or with C5-depleted NHS in DMEM alone (control) (Table 2, Method B). To detect C5b-9 complex formation, immunofluorescence staining was performed using the anti-C5b-9 specific antibody (Section **3.1**). The results showed the presence of C5b-9 on the ARPE-19 cells but again it was not possible to define its precise location (cell surface or cytoplasmic), (Figure 17-A, C). Again, the pattern of C5b-9 formation was not uniform, as some

cells stained strongly for C5b-9, while other cells showed weak or no C5b-9 staining. In the case where C5 protein was depleted from the NHS, no C5b-9 staining was observed, confirming that the C5 protein is crucial for *in vitro* C5b-9 complex assembly (Figure 17-B).

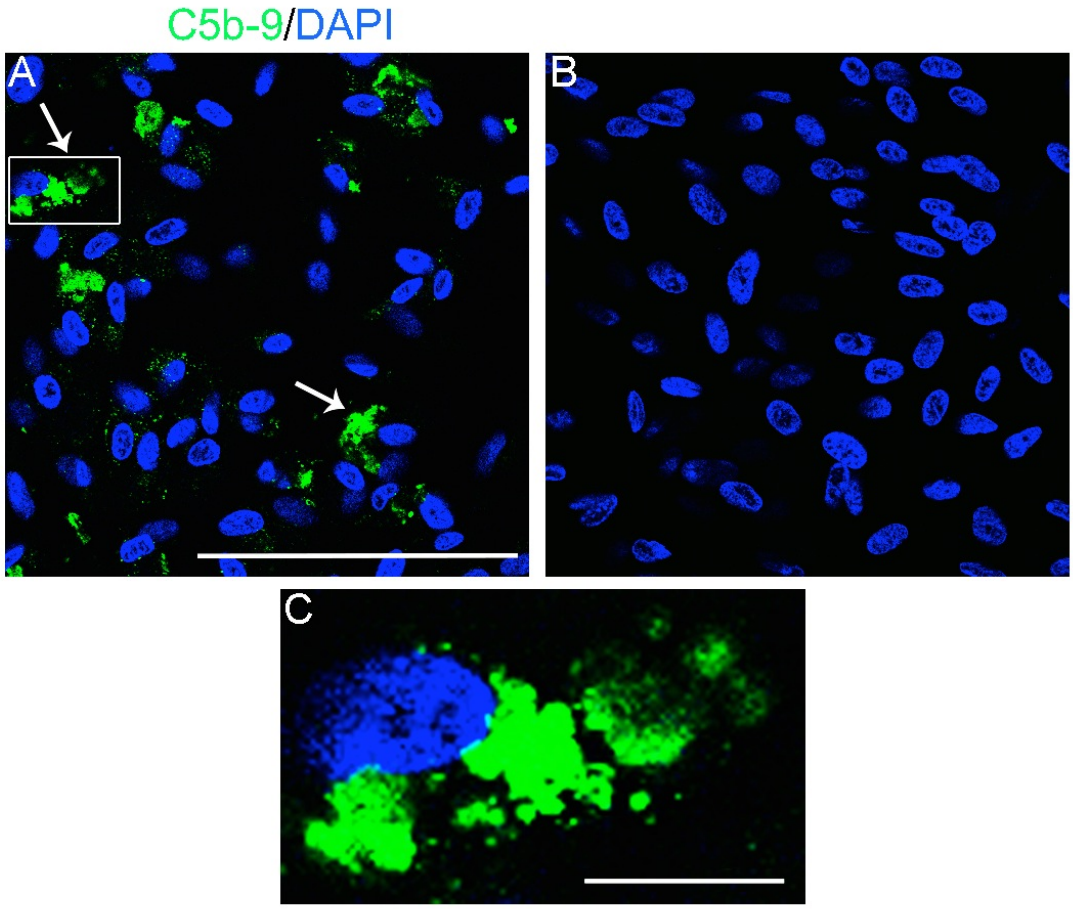

Figure 17. C5 is required for C5b-9 formation on ARPE-19 cells. (A) ARPE-19 cells were positive for C5b-9 (white arrows) when incubated overnight with 30 % C5-depleted NHS in DMEM supplemented with 150 µg/ml purified C5 protein. (B) Absence of C5b-9 staining on ARPE-19 cells incubated overnight with 30 % C5-depleted NHS in DMEM alone. (C) Higher magnification of an ARPE-19 cell stained positive for C5b-9 complex. Images A, B and C represent two independent experiments. Scale bars represent approximately 50µm (A and B) and 20µm (C), respectively.

To gain greater insight into the localisation of the C5b-9 in these experiments, we next performed 3D reconstructions of z-sections from a C5b-9-treated ARPE-19 monolayer, treated as described earlier (Table 2, Method B). Image stacks were obtained on a Leica SP2 confocal microscope. Using Imaris® for the 3D rendering, C5b-9-positive staining (green) was observed on the apical surface of the ARPE-19 cells (Figure 18-A, B), suggesting that the C5b-9-specific staining observed in Figures 16 and 17 was also on the apical cell surface. However, when compared to

the F-actin staining (Figure 18-A) it was still difficult to determine precisely whether or not some of the C5b-9 is cytoplasmic. It is possible that 10 days in culture is not sufficient to allow ARPE-19 cells to form a properly polarised, tightly-packed monolayer.

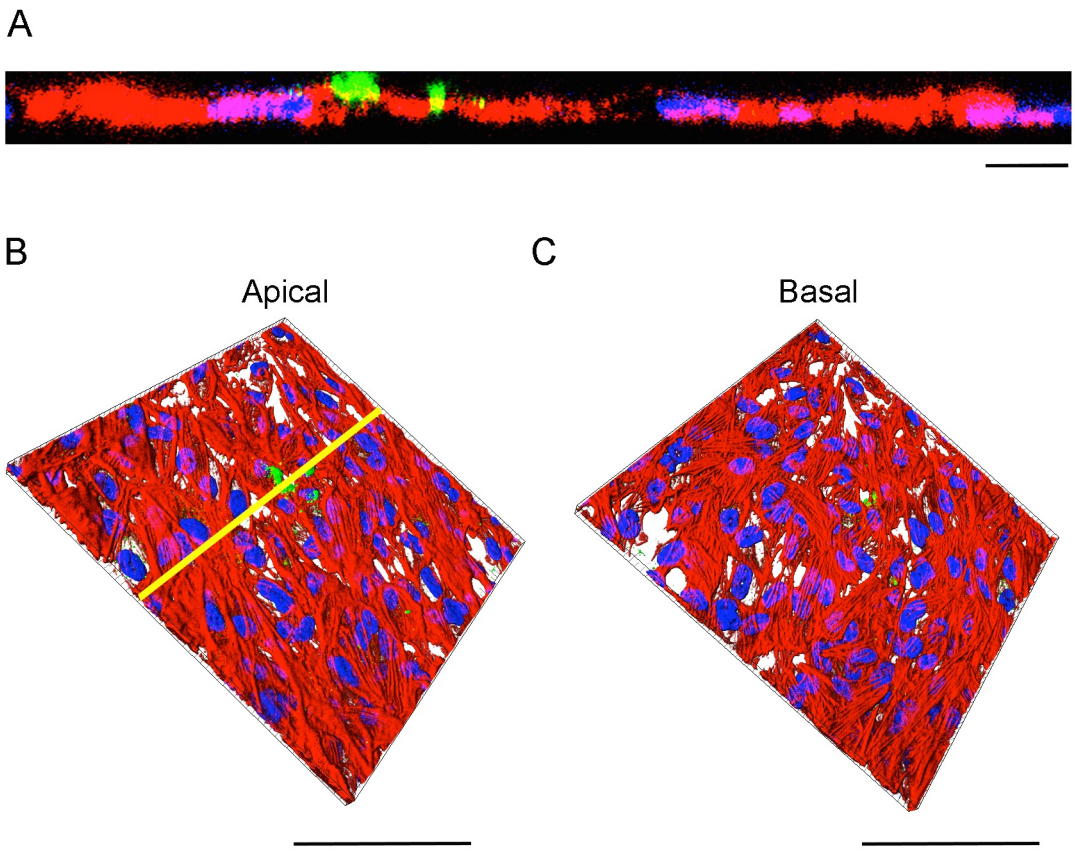

Figure 18. Cross-section of C5b-9-treated ARPE-19 cells cultured for 10 days. (A) C5b-9 staining (green) shows that C5b-9 is formed on the apical surface of ARPE-19 cells. (B) The yellow line indicates the location of the cross-section in (A). (A, B, C) F-actin (red) shows that stress fibres developed on both apical and basal sides. However, no C5b-9 staining was observed on the basal side of cells (C). Blue represents DAPI staining. Scale bars represent approximately 15µm (A) and 40µm (B, C). Images A, B and C were derived from two independent experiments. Image acquired using Imaris® software.

3.3 C5b-9 is formed on the apical surface of ARPE-19 cells

As previously discussed, ARPE-19 cells grown for 10 days were not suitable for the examination of C5b-9 complex localisation in detail, as cells within that amount of time did not form a sufficiently mature (with relation to pigment development), well-organised monolayer. To address this point and to determine the cellular

localisation of the C5b-9 complex in more detail, 3D reconstructions of z-sections were derived from ARPE-19 cells that were cultured for approximately 15 weeks instead of 10 days. This 15-week period enabled ARPE-19 cells to develop significantly greater depth that more closely resembled that seen in RPE cells *in vivo*, and which therefore provided a better insight into the localisation of the C5b-9 complex. ARPE-19 cells treated as in Method B were fixed and stained using the C5b-9 antibody. Volumetric rendering using Imaris® clearly revealed C5b-9 (Figure 19-A, B, green staining) on the apical surface of ARPE-19 cells, immediately adjacent to the F-actin staining (red). Interestingly the C5b-9 complex appeared to induce structural changes to the actin cytoskeleton (white arrow, Figure 19-A). It might be possible that this structural change is an early indication of C5b-9 endocytosis.

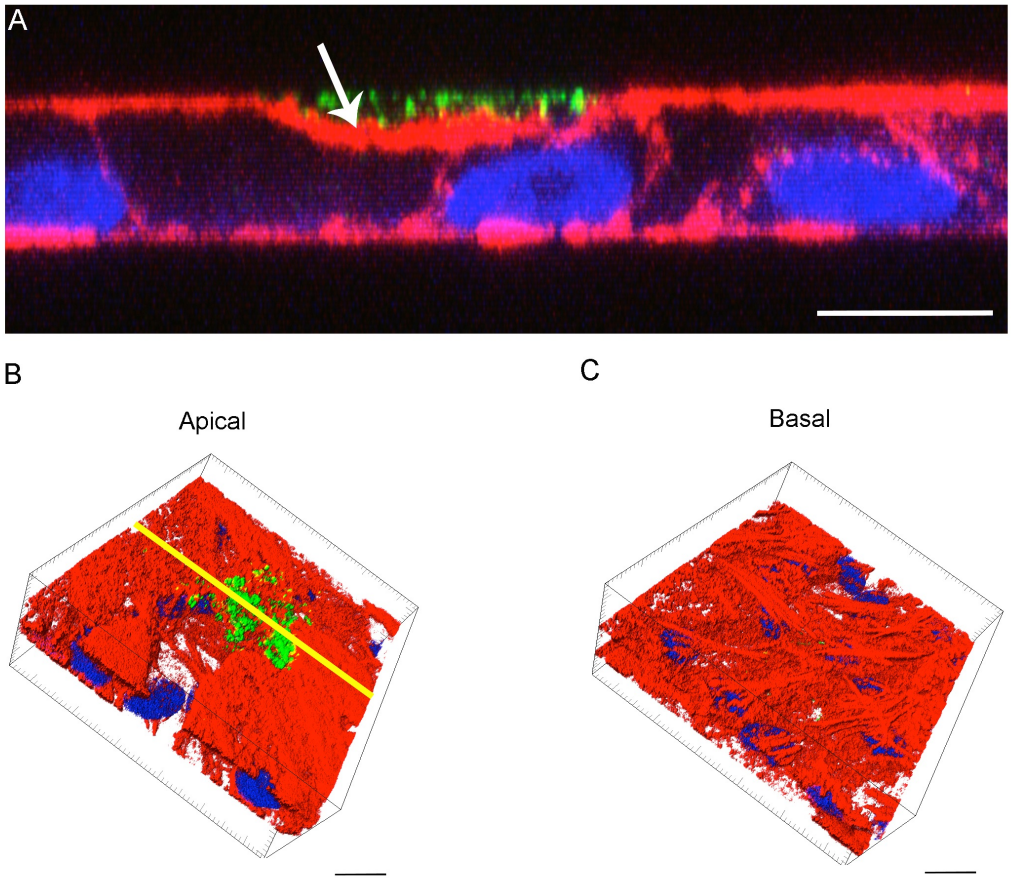

Figure 19. Cross-section of C5b-9-treated ARPE-19 cells cultured for 15 weeks. (A, B) The images show C5b-9 staining (green) on the apical surface of the cells in relation to the F-actin staining (red) and the position of nuclei (blue). C5b-9 complex formation seemed to distort the apical actin cytoskeleton (white arrow). The yellow line (B) indicates the location of the cross-section (A). (C) At the basal side of ARPE-19 cells abundant stress fibres are visible but no C5b-9 staining was observed, confirming that the complement proteins were unable to cross the monolayer. Scale bars represent approximately 10µm. Images A, B and C were derived from two independent experiments. Image acquired using Imaris® software.

3.4 C5b-9 complex formation without blocking CD59

Up to this point, prior to treatment with either NHS or C5 protein in C5-depleted human serum, ARPE-19 cells were incubated with a rabbit polyclonal anti-CD59 blocking antibody. The reason for performing this pre-treatment was to increase the formation of the C5b-9 complex *in vitro*, as CD59 is known to block the binding of C9 molecules to C5b-8 complex, thereby inhibiting the assembly of a fully formed C5b-9 complex, (Rollins and Sims, 1990, Davies et al., 1989, Tomlinson, 2006). Here it was investigated whether C5b-9 complex formation would occur in the absence of this pre-treatment stage. To this end, ARPE-19 cells were incubated (either pre-treated or non-treated with the anti-CD59 antibody), with 150 µg/ml C5 protein in 30 % C5-depleted human serum (Section **2.5.2**).

Immunofluorescence analysis showed that C5b-9 complex formation occurred without the need to block its negative regulator, CD59 (Figure 20). Additionally, comparison of the cells pre-treated with the anti-CD59 antibody (Figure 20-C) with cells that did not receive the pre-treatment (Figure 20-D), revealed that both samples developed qualitatively similar amounts of C5b-9 staining (green). As a control, ARPE-19 cells were incubated overnight only with 30 % C5-depleted human serum. No C5b-9-specific staining was observed in either sample (Figure 20-A, B). These results suggest that there was no need to use the anti-CD59 blocking antibody in these experiments, and therefore this step was eliminated from all future studies. One possible explanation for this observation might be that there is a threshold limit, above which, CD59 is not able to block the assembly of fully formed C5b-9 complex on the cell surface. It is possible that the concentration of complement proteins used in these applied methods of *in vitro* C5b-9 complex formation surpassed CD59's blocking activity.

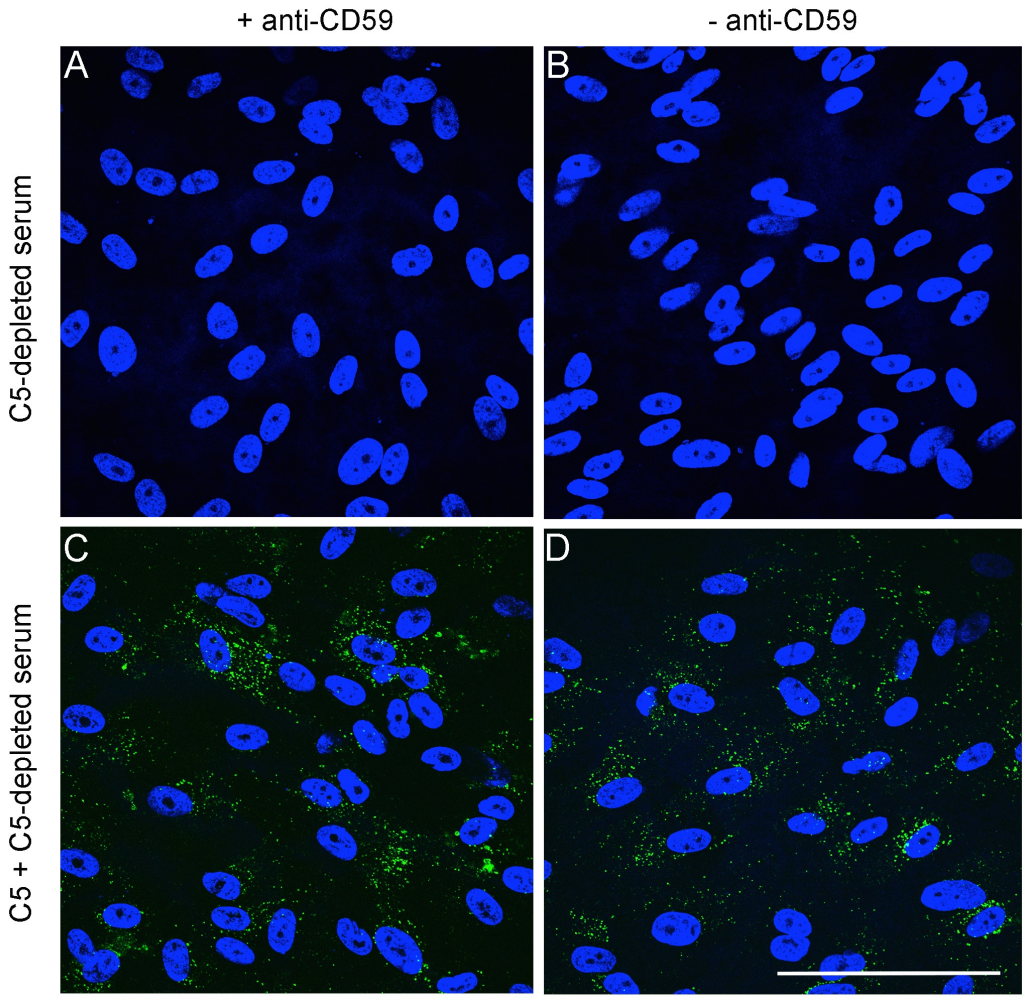

Figure 20. Induction of C5b-9 complex formation without blocking its negative regulator, CD59. (A, B) No C5b-9-positive staining (green) was detected in ARPE-19 cells incubated overnight only with 30 % C5-depleted human serum, regardless of whether they received the anti-CD59 pre-treatment or not, respectively. (C, D) C5b-9 staining (green) was observed in both experimental settings: ARPE-19 cells treated with the blocking antibody and ARPE-19 cells that did not receive the pre-treatment, respectively. C5b-9 was assembled by incubating the cells overnight with C5 protein and 30 % C5-depleted human serum. Images A, B, C and D were derived from one independent experiment. Scale bar represents approximately 50µm.

3.5 Assembled C5b-9 complex rarely induces cell permeability in ARPE-19 cells

Next we asked whether C5b-9 complex formation would have an effect on cell integrity by making the cells permeable. In bacterial cells and anucleate cells such as red blood cells, C5b-9 induces lysis by forming a pore in the cell membrane (Koski et al., 1983). In order to test cell permeability, ARPE-19 cells (passage 26) growing on glass coverslips for approximately 4 weeks, were treated overnight with C5b-6 complement complex, complement protein 7 (C7), 30 % C5-depleted human serum and propidium iodide (PI) (Table 2, Method C). PI is a small fluorescent molecule, able to access the cytoplasm and nucleus via permeabilised membranes. Once it

binds to the DNA of the target cell it can be observed by fluorescence microscopy. Here, a positive control was used where 0.01 % Triton-X 100 was administered to ARPE-19 cells for 5 min to induce permeability (Figure 21). Immunofluorescence analysis of C5b-9-treated and negative control cells (Figure 21) demonstrated that there was no staining for PI. Therefore, although C5b-9 complex has been extensively linked to cell lysis (Laine and Esser, 1989) this was not observed in these experiments in these cells. The rationale for using C5b-6 complexes and extra amounts of C7 purified protein (C7 is also present to the C5-depleted human serum) was to increase the possibility of obtaining higher amounts of *in vitro* C5b-9 complex. Furthermore, qualitative analysis of DAPI staining of control vs treated cells suggested that the cells were viable (Figure 21). Section **3.6** validates these findings via cell viability assays.

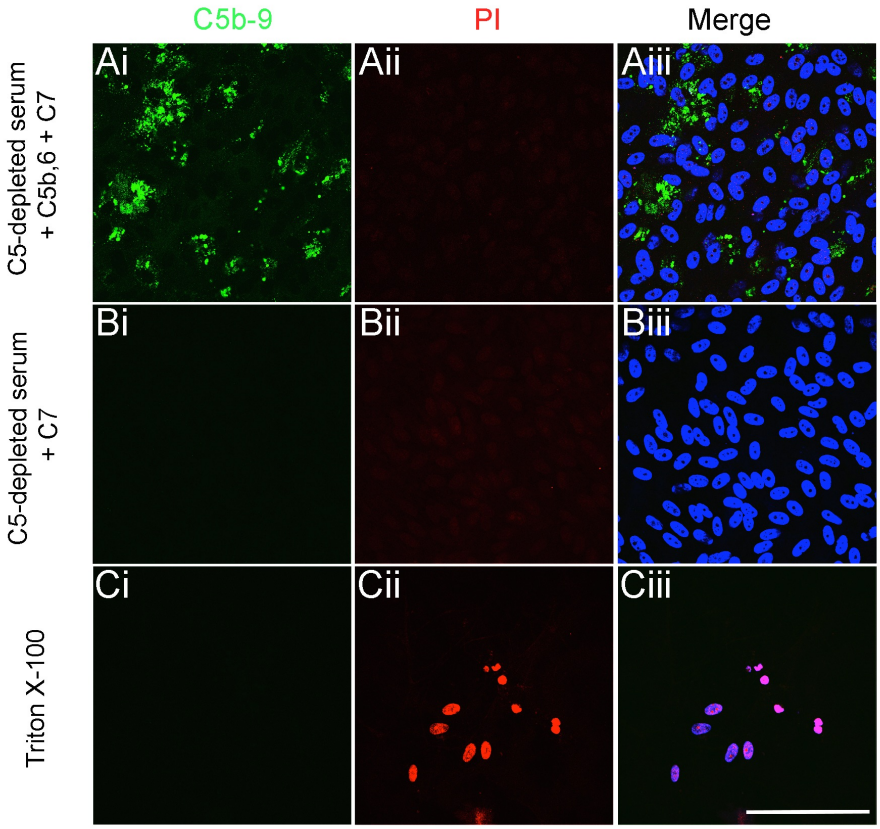

Figure 21. Effects of C5b-9 complex formation on permeability of ARPE-19 cells. C5b-9 complex formation was induced by treating ARPE-19 cells overnight with C5b-6 purified complement complex, C7 protein and C5-depleted human serum (A_{i-iii}). Control cells were incubated overnight with C7 protein and C5-depleted human serum (B_{i-iii}). Cells were treated with 0.01% Triton X-100 to induce cell permeability (red staining) (C_{i-iii}). While ARPE-19 cells showed positive staining for C5b-9 (green), there was an absence of PI staining (red), suggesting that C5b-9 complex formation does not form a pore in the cell membrane. Control cells showed an absence of PI staining as expected. Scale bar represents approximately 50µm. Images $A_{(i-iii)}$, $B_{(i-iii)}$ and $C_{(i-iii)}$ were derived from one independent experiment.

Although the results in Figure 21 demonstrate that C5b-9 does not appear to create functional pores in RPE cell membranes, permeability was observed in occasional cells (Figure 22). ARPE-19 cells positive for C5b-9 complex were also positive for PI and the cell nucleus also appeared to be smaller as compared to other cell nuclei, suggesting that in rare instances (approximately 4 ARPE-19 cells developed PI and C5b-9-specific staining within a population of 112 ARPE-19 cells, which only developed DAPI staining) C5b-9 formation may induce cell permeability and possibly apoptosis in ARPE-19 cells.

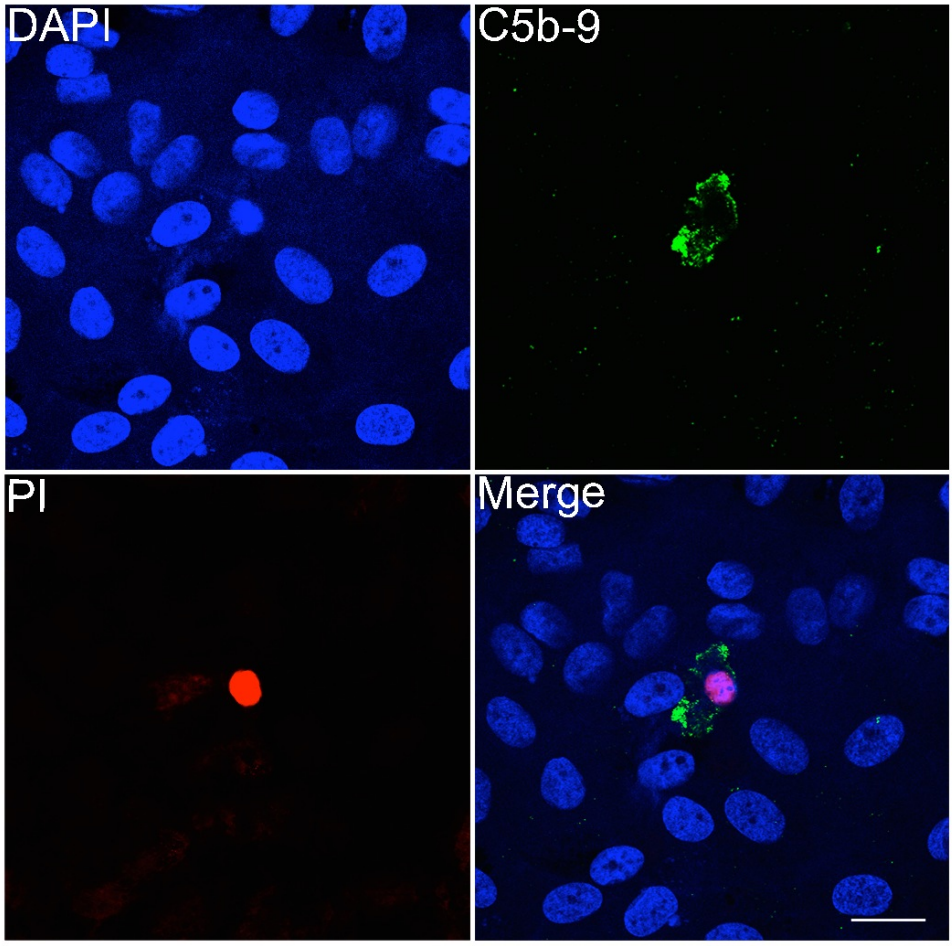

Figure 22. Cell permeability induced by the C5b-9 complex. Most ARPE-19 cells appear to be healthy as they develop normal nuclear staining (blue) with the exception of an occasional C5b-9-positive cell. Green staining represents the formation of C5b-9 on a single ARPE-19 cell after overnight incubation with C5b-6, C7 complement protein and 30 % C5-depleted human serum. The red nucleus depicts a permeabilised C5b-9-positive cell, stained positive for propidium iodide. Overall, the figure shows the contrast in cell integrity between a complement-affected cell and the surrounding unaffected ARPE-19 cells. These data represent one independent experiment. Scale bar represents 20µm.

3.6 C5b-9 does not affect RPE cell viability

C5b-9 complex formation is associated with lysis and therefore cell death in various cell types including erythrocytes (Rommel and Mayer, 1973, Koski et al., 1983). Therefore, the MTT cell viability assay was used to examine whether apical C5b-9 complex formation on ARPE-19 cells could lead to cell death. Also, the MTT assay was used as an alternative method to demonstrate that C5b-9 complex does not affect viability as previously shown by immunofluorescence analysis.

During this assay, cells were treated as described in Table 2, Method C. Three different controls were used: ARPE-19 cells treated with 1 % Triton X-100 to induce cell death (positive control), untreated ARPE-19 cells incubated in DMEM, and ARPE-19 cells incubated overnight with C7 protein and 30 % C5-depleted human serum (Table 2, Method C). Figure 23 reveals that C5b-9-treated cells have approximately the same levels of cell viability as the control and untreated samples. These data confirm that in this experimental model C5b-9 complex formation does not cause RPE cell death. Each bar represents the average absorbance measured at 490 nm, from three wells (triplicates) under the same condition. Data were expressed as mean ± SEM.

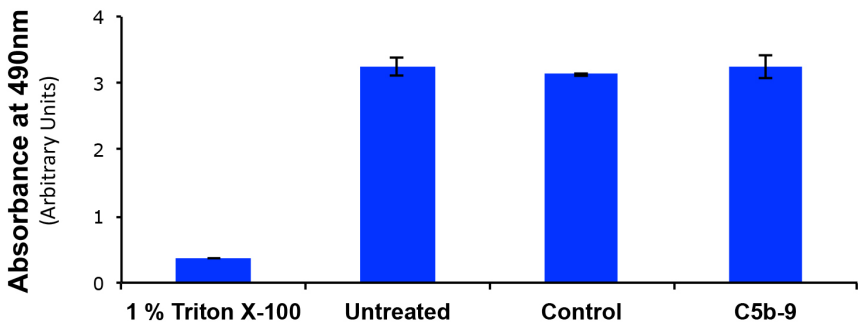

Figure 23. C5b-9 complex formation does not affect ARPE-19 cell survival. MTT cell viability assay measuring the levels of cell death on ARPE-19 cells treated overnight with C5b-6 and C7 complement proteins in 30 % C5-depleted human serum. Three different controls were used: ARPE-19 cells treated with 1 % Triton X-100 to induce cell death (positive control), untreated ARPE-19 cells incubated in DMEM, and ARPE-19 cells (control) incubated overnight with C7 protein and 30 % C5-depleted human serum. Each bar represents the average absorbance measured at 490 nm, from one independent experiment using three wells (triplicates) per condition. Data were expressed as mean ± SEM.

3.7 C5b-9 complex formation on primary porcine RPE cells

To exclude the possibility that the observations so far might be specific to ARPE-19 cells, primary porcine RPE cells (pRPE) were used as an alternative cell type to further investigate C5b-9 complex formation. In many ways pRPE cells are a better model to examine the effects of C5b-9 complex on the RPE *in vitro*, as these cells exhibit good retention of their epithelial phenotype following isolation from pig eyes.

Two methods were used to induce C5b-9 complex formation on confluent pRPE cells. In the first method (MAC-A) cells were incubated overnight with C5b-6 complex, C7 protein and 30 % C5-depleted human serum (Table 2, Method C). In the second method (MAC-B) cells were incubated overnight with C5b-6 complex, C7, C8 and C9 purified complement proteins in DMEM (Table 2, Method D). For this experiment two different negative controls were used: control-A and control-B. In control-A pRPE cells were incubated only with C7 protein and 30 % C5-depleted human serum, while in control-B, pRPE cells were incubated with C5b-6, C7 and C8 proteins in DMEM (Methods C and D, respectively).

As shown in Figure 24, these two methods yielded different effects with regard to C5b-9 complex formation. C5b-9 complex formation, when using the MAC-A method, was not uniform (Figure 24, $B_{i\text{-}iii}$). On the other hand, after performing the MAC-B method, C5b-9 complex formation was not only more evenly distributed but also relatively more C5b-9 complex was observed (Figure 24, $D_{i\text{-}iii}$). Moreover, immunofluorescence staining of F-actin (red) demonstrated the apparent development of abundant stress fibres upon application of the MAC-B method as compared to the MAC-A method (Figure 24, B_{ii}, D_{ii}, respectively).

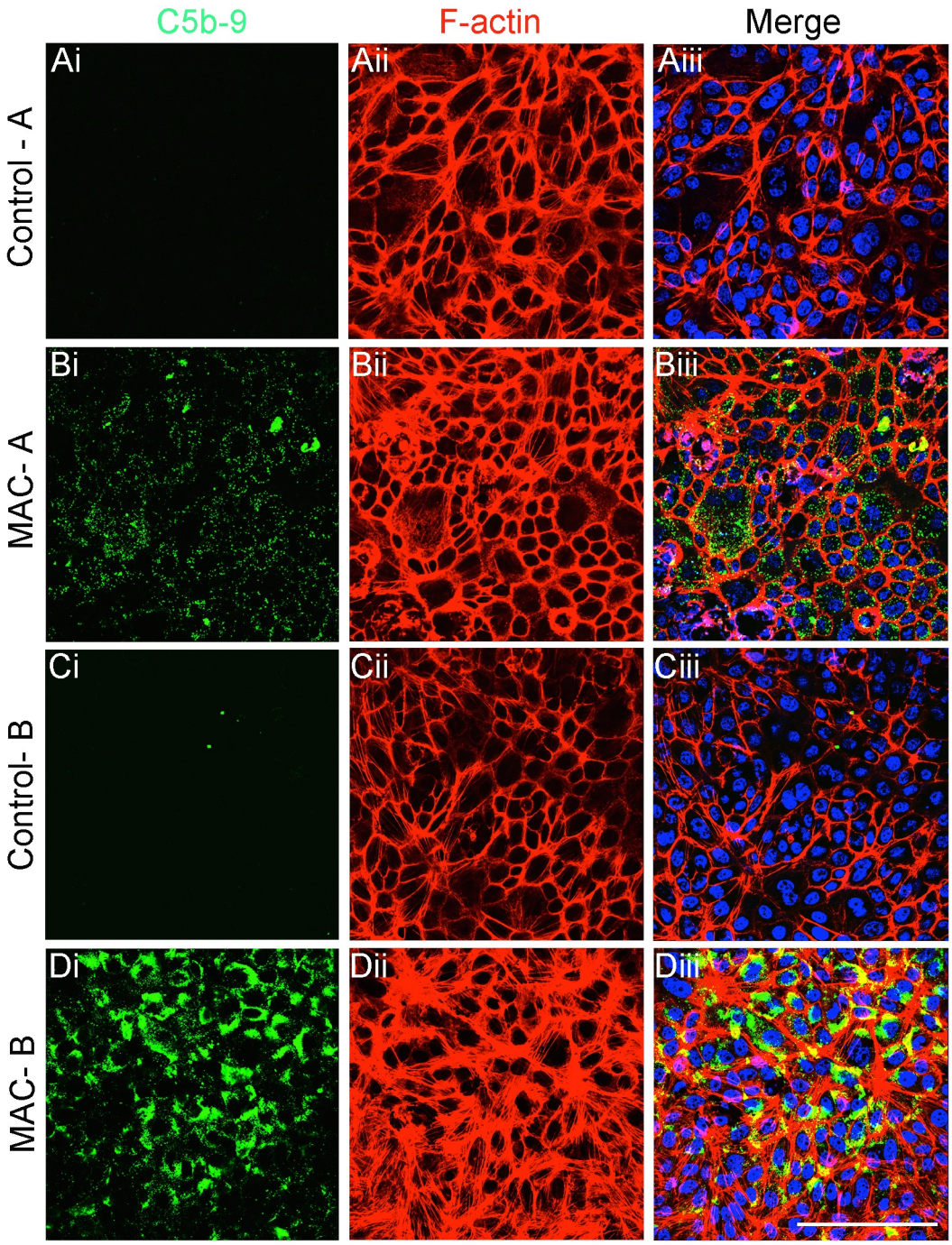

Figure 24. C5b-9 complex formation on the apical surface of porcine RPE cells using two methods. Method C (MAC-A) leads to a variable pattern of C5b-9 complex formation (B_i, B_{iii}, green staining), while method D (MAC-B) creates a more specific and intense staining specific for the C5b-9 complex (D_i, D_{iii}, green staining). The MAC-B method leads to the formation of abundant stress fibres (D_{ii}, D_{iii}, red staining), while actin filaments appear more circumferential in method MAC-A (B_{ii}, B_{iii}, red staining). Images $A_{(i\text{-}iii)}$, $B_{(i\text{-}iii)}$, $C_{(i\text{-}iii)}$ and $D_{(i\text{-}iii)}$ represent one independent experiment. Scale bar represents approximately 50µm.

3.8 C5b-9 complex formation on the basal aspect of pRPE cells

Thus far, the formation of the C5b-9 complex had only been investigated on the apical surface of ARPE-19 and pRPE cells, as both cell lines were growing on glass coverslips and therefore only the apical surface was accessible to complement proteins. But with the method of *in vitro* C5b-9 complex formation now optimised, further studies were carried out on pRPE cells grown on transwell cell culture plates, where both aspects (apical and basal) of pRPE cells were accessible to various treatments.

It is well established that *in vivo*, AMD patients develop C5b-9 complex formation on the basal surface of the retinal pigment epithelium and/or Bruch's membrane (Anderson et al., 2002). Therefore we decided to continue these studies using C5b-9 formation on the basal surface of pRPE cells, by using culture well inserts. pRPE cells were cultured (passage 1) in 12-transwell plates and after approximately two weeks when the RPE monolayer developed a stable trans-epithelial resistance, C5b-9 complex was assembled *in vitro* as described in Table 2, Method D_T. The C5b-6 complex, C7, C8 and C9 purified complement proteins were added in DMEM, to the basal chamber of the trans-well. As a control, only C5b-6, C7 and C8 proteins were added in DMEM, to the basal chamber of the trans-well. In the apical chamber (in all samples, including the control) only DMEM was added. In a first set of experiments three different time-points were used (1 h, 5 h and 24 h) for C5b-9 complex formation, in order to examine how rapidly C5b-9-positive staining developed as judged by immunofluorescence analysis. Imaris® software was used to examine both the apical and basal surface of cells. Immunofluorescence demonstrated the presence of substantial C5b-9 complex formation on the basal surface of pRPE cells within 1 h (Figure 25-B_{ii}). Basal levels of C5b-9 complex increased further by 5 h (Figure 25-C_{ii}), while at 24 h (Figure 25-D_{ii}) C5b-9 complex levels had decreased significantly. The pattern of basal C5b-9 complex accumulation was also quantified by measuring the fluorescence intensity specific to C5b-9 using Imaris®. The apical surface of pRPE cells (in all samples, including the control) remained negative for C5b-9 staining demonstrating the integrity of the monolayer throughout (Figure 25-A_i, B_i, C_i and D_i). Four different areas per sample were quantified. As described earlier in Section **3.7** on the 24 h sample (Figure 24-D_{ii}), abundant stress fibres developed as

observed by F-actin staining (red staining). This observation is in accordance with results in Figure 25, where C5b-9 complex was allowed to form for 24 h on the basal surface of pRPE cells (Figure 25-D_i, D_{ii}). The C5b-9 complex formation/elimination rate from the basal surface of pRPE cells over time will be examined in more detail in the next chapter.

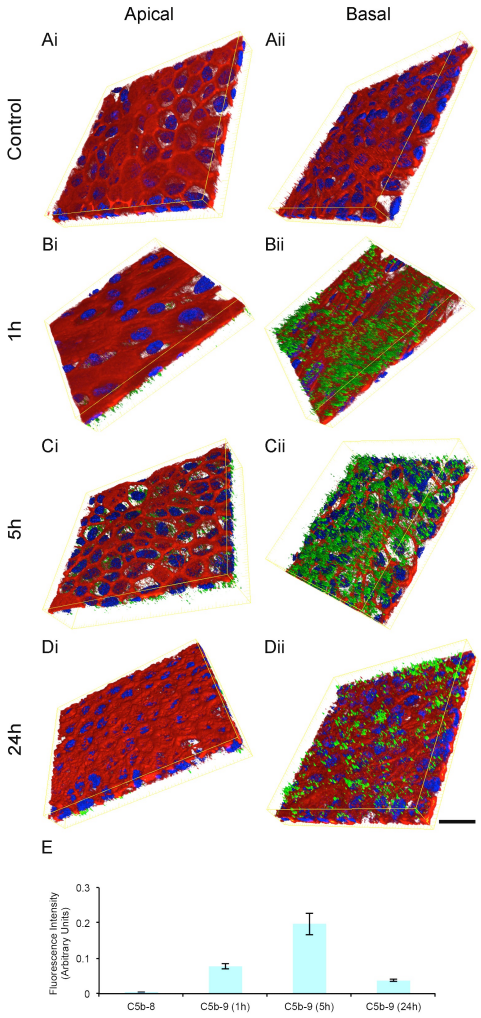

Figure 25. C5b-9 complex assembly on the basal surface of pRPE cells. C5b-9 (green staining) was detected via immunofluorescence when C5b-6, C7, C8 and C9 complement proteins were added in DMEM to the basal surface of pRPE for different time-points (B_{ii}, C_{ii} and D_{ii}). At 1 h (B_{ii}) C5b-9 complex was visible (green), and staining increased further at 5 h (C_{ii}), while at 24 h (D_{ii}) C5b-9-positive staining decreased significantly. Staining for F-actin (red) demonstrated the development of abundant stress fibres at 24 h (D_i and D_{ii}). The apical surface in all samples remained C5b-9-negative (A_i, B_i, C_i and D_i). As a control pRPE cells were used, where C5b-6, C7 and C8 proteins were added in DMEM on the basal surface for 24 h (A_{ii}). (E) Each bar represents the average of the C5b-9-related fluorescence intensity as measured from four independent areas per sample from one independent experiment, using Imaris® software. Data were expressed as mean ± SEM. Scale bar represents approximately 20μm.

3.9 C5b-9 complex formation does not affect the viability of pRPE cells

Overnight formation of C5b-9 (Table 2, method D) did not appear to induce the death of pRPE cells (Figure 26), as was observed previously for ARPE-19 cells (Figure 23). Again, for the MTT assay three different controls were used: cells treated with 1 % Triton X-100 (for 10 min) to induce cell death (positive control), untreated cells were pRPE cells incubated in DMEM, and negative control cells were cells that were incubated overnight with C5b-6, C7 and C8 purified complement proteins in DMEM.

The MTT cell viability assay demonstrated that C5b-9-treated pRPE cells (C5b-9 sample) had approximately the same levels of cell survival when compared to the untreated cells and the negative control.

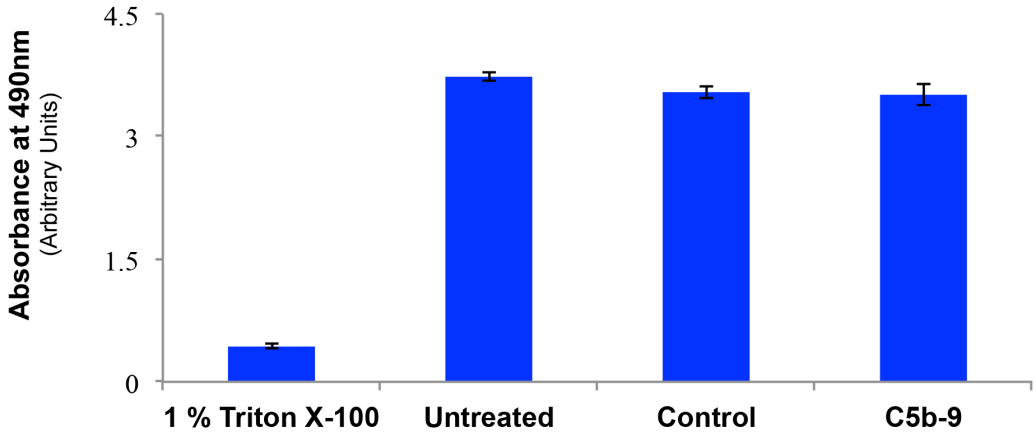

Figure 26. C5b-9 complex formation does not reduce the viability of primary porcine RPE cells. MTT cell viability assay was performed to measure survival of primary porcine RPE cells treated with C5b-6, C7, C8 and C9 complement proteins in DMEM, overnight at 37 ^{o}C / 5 % CO_2 (C5b-9). Three different controls were used: cells treated with 1 % Triton X-100 for 10 min to induce cell death (positive control), pRPE cells incubated in DMEM (untreated) and cells that were incubated overnight with C5b-6, C7 and C8 purified complement proteins in DMEM (control). Each bar represents the average absorbance measured at 490 nm, from one independent experiment using three wells (triplicates) per condition. Data were expressed as mean ± SEM.

3.10 Discussion

- **Assembling the C5b-9 complex *in vitro***

Optimising the conditions for the *in vitro* assembly of C5b-9 on the apical and/or the basal surface of RPE cells was an essential first step in defining a model in which to examine the interplay between the complement system and the retinal pigment epithelium. Testing and finally establishing method D_T (as shown in Table 2) as the optimal approach, allowed us to overcome potential inconsistencies in C5b-9 complex formation and to better control the *in vitro* conditions. Additional control was derived from the fact that a serum-free environment guaranteed that any effects observed were solely due to the presence of C5b-9 and not due to the presence of various other factors being present within human sera (NHS or C5-depleted serum).

The initial approach to inducing C5b-9 complex on the apical surface of ARPE-19 cells, by administering 20 % NHS overnight, did not yield consistent effects (Figure 16). The pattern of C5b-9 formation was not uniform, as some cells were stained positively for the C5b-9 complex, while others showed weak or no C5b-9-positive staining (Figure 16-F). Complement-competent NHS has previously been shown to be capable of inducing C5b-9 complex formation in two different cell models: hfRPE cells (Johnson et al., 2011) and ARPE-19 cells (Lueck et al., 2011). Johnson et al., (2011), demonstrated that 10 % NHS in serum-free media was capable of inducing uniform staining specific to C5b-9 on the basal surface of hfRPE cells. In addition, Lueck et al., (2011) by using ascending concentrations of NHS observed the *in vitro* formation of C5b-9 complex on the apical surface of ARPE-19 cells. This C5b-9 complex formation was accomplished by incubating ARPE-19 cells with 5-20 % NHS for 1 h. Therefore, in order to achieve high levels of C5b-9 complex formation, elements of the two different protocols described above, were combined by using 20% complement-competent NHS for 24 h instead of 1 h.

In combination with the above protocol, in order to investigate whether the prolonged use of NHS can induce complement activation and/or lysis, we performed a pilot experiment where ARPE-19 cells were treated with 20 % NHS for 1d, 2d, 5d and 7d. As a control ARPE-19 cells were incubated with 20 % HI-NHS, using the same timepoints. While low levels of C5b-9 formation were identified at 24 h, these

levels were significantly decreased by day 5, while at day 7, C5b-9 was not present any more. Similar results were observed when CNV was induced by laser-photocoagulation in C57BL/6 mice. Immunofluorescence analysis using flat mounts, demonstrated that C5b-9 formation was up-regulated on days 1 and 3 post-laser injury, however C5b-9 levels were significantly down-regulated on days 5 and 7 (Lyzogubov et al., 2010). Overall, Method A combined with the above pilot experiment indicated not only that ARPE-19 cells survived from the prolonged presence of complement but also it demonstrated once again that the NHS did not yield high levels of C5b-9 complex.

However, as this protocol did not yield useful results it was necessary to further refine the experimental conditions. To this end ARPE-19 cells were incubated with purified C5 protein and 30 % C5-depleted human serum (Figure 17-A). However, immunofluorescence analysis demonstrated a similar pattern of C5b-9 complex formation to that seen in Figure 16-F (where cells were treated only with 20 % NHS). C5-depleted human serum has previously been demonstrated to be capable of leading to C5b-9 complex assembly, when C5 protein was added back to the media (Johnson et al., 2011). C5 protein, essential for the assembly of C5b-9 complex, is synthesised primarily in the liver and its concentration in human plasma (derived from normal donors) ranges from 72 to 171 μg/ml (Gupta and Sarin, 1984, Sjoholm, 1975, Strunk et al., 1988). Therefore, in order to mimic the *in vivo* concentration of C5 protein in the circulation, C5 purified complement protein was used at 150 μg/ml. Examining the possibility Method B to sufficiently enable C5b-9 formation without compromising cell viability we performed a pilot study during which ARPE-19 cells were incubated with purified C5 protein and 30 % C5-depleted human serum on their apical cell surface for 1d, 3d, 5d and 7d. As a control, ARPE-19 cells were treated only with 30 % C5-depleted human serum on their apical cell surface for the same amount of time as above. Propidium iodide was present in the media at all times, in order to investigate whether the assembled C5b-9 could induce cell lysis or not. Immunofluorescence analysis demonstrated that Method B produced again low levels of C5b-9 on the apical surface of ARPE-19 cells at day 1, while most of the C5b-9-specific staining was absent by day 3. In addition to this observation, it should be noted that PI did not stain cell nuclei and therefore implicating that C5b-9 complex did not affect cell survival. Overall, Method B combined with the above

pilot experiment indicated the need to develop a more advanced protocol for the *in vitro* formation of C5b-9 complex.

Despite these refinements it was evident that neither of these methods (Method A and B, Table 2) was ideal for the *in vitro* formation of C5b-9 complex, as only minimal and patchy C5b-9-specific staining was observed. One explanation could be that the ARPE-19 cells, used in both conditions, were only grown *in vitro* for approximately 10 days, and therefore the cells did not have sufficient time to form a well-organised and more authentic RPE monolayer. Within this monolayer there may have been cells whose surface was less accessible to the complement proteins and serum in order for the C5b-9 complex to cover wider areas and therefore to develop a more uniform staining. The absence of a fully differentiated RPE phenotype was confirmed by 3D image reconstruction of ARPE-19 cells grown for 10 days *in vitro* (Figure 18). In particular, the F-actin staining indicated that cell height was not uniform (Figure 18-A). In general, ARPE-19 cells need longer periods to form a monolayer with RPE characteristics (Turowski et al., 2004). This is partly reflected by the fact that the ARPE-19 cell line is only able to reach low TER values of 30-45 Ω/cm^2. Even when ARPE-19 cells are grown *in vitro* for a longer period such as six months, there is usually little improvement in the TER (Luo et al., 2006).

Luo et al., (2006) and Ahmado et al., (2011) reported that in addition to exhibiting low TER values, F-actin appears to be far less organised in immature cultures of ARPE-19 cells compared to cells which have been grown for more than fifteen weeks (Ahmado et al., 2011). After approximately three months ARPE-19 cells develop a more epithelial-like phenotype where actin filaments appeared to be more circumferential. This observation was confirmed in this study where ARPE-19 cells, grown for approximately 15 weeks exhibited abundant basolateral stress fibres, and an apical layer of F-actin in the region where one would expect to observe microvilli *in vivo* (Figure 19).

Methods A and B demonstrated the need to use more mature ARPE-19 cells and therefore the optimisation of the conditions for C5b-9 complex formation was continued by using ARPE-19 cells grown on glass coverslips for 4 weeks instead of 10 days. These cells were treated with a mixture of purified complement proteins and serum in order to increase the amount of C5b-9 complex *in vitro*. Extra C7 was added as this is a crucial protein for the formation of the C5b-7 complex. It is mainly produced from the liver and bone marrow and its concentration varies from 50-70 μg/ml in human serum (Hammer et al., 1981, Naughton et al., 1996). Substitution of purified C5 from the C5b-6 complex eliminated the step where C5 protein in the media had to be cleaved to C5a and C5b molecules (Rawal and Pangburn, 1998). C5b production is the initial event in the formation of the C5b-9 complex (Silversmith and Nelsestuen, 1986). Although immunofluorescence analysis revealed the presence of stronger C5b-9-specific staining, again there was a sub-population of cells that did not develop C5b-9-positive staining at all (Figure 21-A_{iii}).

As 4-week-old ARPE-19 cells did not radically improve the end result of C5b-9 complex formation, pRPE cells were used instead, as these are known to retain their hexagonal phenotype and also to form a tight monolayer *in vitro*. The advantages of using pRPE as a cell model were discussed in more detail in Section **1.7.3**. Furthermore, as NHS and C5-depleted human serum contain a variety of growth factors and other growth modulating molecules, it was decided to develop a more reductionist version of the above protocol by omitting serum. Incubating pRPE cells with C5b-6 complex, C7, C8 and C9 purified complement proteins in DMEM led to a uniform staining pattern specific to C5b-9 across the apical surface of the pRPE monolayer (Figure 24-D_{iii}). Addition of purified C8 and C9 proteins in these *in vitro* conditions was essential. C8 is composed of three subunits (α, β and γ) which bind to the first C9 molecule on the C5b-8 complex. Its concentration in human plasma varies between 50-80 μg/ml (Manni and Muller-Eberhard, 1969, Schreck et al., 1998). C9 is the final component of the C5b-9 complex and its concentration in human serum ranges from 40 to 70 μg/ml (Hammer et al., 1981, Podack and Tschopp, 1982).

In addition, comparison of MAC-A method (also known as method C) with MAC-B method (also known as method D) showed that the latter protocol appeared to induce the formation of abundant F-actin stress fibres (Figure 24-B_{ii}, -D_{ii}, respectively). Stress fibres are needle-shaped bundles of actin filaments which contain various actin-associated proteins (Katoh et al., 1998). These F-actin stress fibres have previously been found to be regulated by RhoA, a member of the Rho family of small GTPases that mediate actin remodelling via activation of several signalling pathways (Zhang et al., 2007, Etienne-Manneville and Hall, 2002). Interestingly, the expression level of RhoA has previously been shown to be modulated by C5b-9 in rat glomerular epithelial cells (GECs) *in vitro* (Zhang et al., 2007). These authors showed that when rat GECs were cultured with NHS either for a short period (40 min) or for a long period (18 h), complement increased the activity of RhoA (GTP-bound form of RhoA protein levels were elevated compared to control samples). Further studies shown that this C5b-9-induced RhoA activation is partly attributed to the C5b-9-induced activation of the Erk pathway, upstream of RhoA (Mouawad et al., 2014).

Previous immunohistochemical studies from eyes derived from AMD donors had shown that *in vivo*, C5b-9 is localised at the basal surface of RPE cells (Johnson et al., 2000, Anderson et al., 2002). To attempt to reproduce this in culture pRPE cells were grown on trans-well plates in order to permit assembly of C5b-9 on the basal surface of these cells. Addition of the mix of purified complement proteins at the basal chamber led to the rapid formation of C5b-9 complex on the basal surface of pRPE cells. C5b-9 levels were increased at 5 h (Figure 25-C_{ii}) but were significantly reduced by 24 h (Figure 25-D_{ii}). These results show that pRPE cells have mechanisms that enable them to remove C5b-9, and the possible reasons for this observation will be addressed in the next chapter.

- **C5b-9 complex formation without blocking CD59**

The immunofluorescence analysis in Figure 20 demonstrated that is possible to assemble C5b-9 without the need to block its negative regulator, CD59. Comparison of the cells pre-treated with the anti-CD59 antibody (Figure 20-C) with cells that did

not receive the pre-treatment (Figure 20-D), showed that both developed similar amounts of C5b-9-positive staining.

CD59 is one of the membrane-bound negative complement regulators, which is expressed by several cell types including endothelial and epithelial cells (Nose et al., 1990, Meri et al., 1991). Its primary role is to inhibit the incorporation of multiple C9 molecules on the membrane-bound C5b-8 complex, by binding tightly to the C8 protein of this complex (Morgan, 1999). However, a single C9 protein may bind to C5b-8 even in the presence of CD59 and therefore permit the formation of small C5b-9 complexes in which C8 and C9 are in a ratio of 1:1.5 instead of 1:3.5 (Meri et al., 1990). Within these 'small' C5b-9 complexes CD59 is believed to mediate only a partial unfolding of the bound C9 protein and therefore, 'bigger' C5b-9 complexes ($C5b\text{-}9_{12}$) cannot be assembled. This reduces the possibility of cells suffering from ion leakage, which in turn is capable of inducing cell death (Rollins and Sims, 1990).

Despite the above observations that CD59 in principle inhibits the formation and therefore the lytic activity of C5b-9 there are cases of various neurodegenerative diseases where complement attack was believed to be responsible for the degeneration of neurons and glial cells, regardless of the presence of CD59 (as well as C1 inhibitor, clusterin, MCP and DAF) (Singhrao et al., 1999, Yasojima et al., 1999). It may therefore be that there is a threshold limit above which CD59 cannot inhibit the formation of multiple C5b-9 complexes. The results in Figure 20 are in line with this notion, as Method B clearly provides enough complement proteins to promote the assembly of C5b-9 complex on the ARPE-19 cells. The concentrations of the complement component proteins would therefore appear to overcome the inhibitory activity of CD59.

- **The C5b-9 complex does not affect cell viability**

Despite the presence of the terminal complex ARPE-19 cells remained viable, as judged by various criteria. Immunofluorescence analysis showed that PI was not able to access the nuclei, with only rare exceptions observed in these studies. In general, DAPI staining revealed a normal morphology of the nuclei for the majority of the ARPE-19 cells examined. It should be noted that the C5b-9 complex has an average

pore diameter of 90-100 Å, which is large enough to admit the passage of ions and is also large enough to enable PI to access the cytoplasm of ARPE-19 cells (Zalman and Muller-Eberhard, 1990). Cell viability was further confirmed by performing MTT assays on C5b-9-treated ARPE-19 and pRPE cells.

Decades ago it was demonstrated that C5b-9 can induce lysis of erythrocytes and lysis of various types of nucleated cells including cell lines such as Molt4 and U937, derived from human T lymphocytes and histiocytes, respectively (Koski et al., 1983). While initially it was believed that erythrocytes may be lysed by a single C5b-9 complex, this hypothesis ('one-hit' theory) was later challenged by the observation that approximately 850 C5b-9 complexes are required to lyse an erythrocyte. This number was derived from the measured number of C7 protein molecules required to induce cell lysis (Rommel and Mayer, 1973, Bauer and Valet, 1983). Perhaps lysis of nucleated cells such as RPE, requires an even higher number of C5b-9 complexes due to their bigger size, or perhaps nucleated cells have mechanisms to resist C5b-9 attack regardless of the amount of complex that forms. Normally red blood cells are approximately 6-8 μm in diameter while, RPE cells are approximately 15 μm (Aarts et al., 1983, Roorda et al., 2007).

The fact that complement-mediated cell lysis is not a simple process, as was previously thought, is supported by the observation that nucleated cells, upon immune attack, can increase lipid synthesis in their cell membranes to protect themselves from being permeabilised (Schlager et al., 1978). Currently, it is not known whether bound C5b-9 stimulates ARPE-19 cells to alter their metabolic activity in order to enrich their complement-attacked membranes with extra lipid molecules.

Overall, our data are consistent with the findings of Johnson et al., (2011) who showed that the presence of C5b-9 on the basal surface of hfRPE cells did not affect cell viability. The cells used here (ARPE-19 and pRPE) retained their viability, despite exposure to C5b-9, which is consistent with the observation that in AMD patients the RPE can remain viable for many years.

Chapter 4

4. RPE cell responses to C5b-9 complex assembly

4.1 C5b-9 formation/elimination from the basal surface of RPE cells

As shown in section **3.8**, C5b-9 is detectable on the basal surface of pRPE cells within 1 h of adding the purified proteins, while at 24 h levels of C5b-9 were significantly decreased. To acquire a better understanding of the formation/elimination of the C5b-9 complex and also to further validate the observations from Figure 25 the study was extended by including additional time points. pRPE cells were cultured in 12-well trans-well plates and once they had formed a confluent monolayer C5b-9 complex formation was developed as described in method $\mathbf{D_T}$ (section **2.5.4.1**). Thus, C5b-6, C7, C8 and C9 purified complement proteins were added in DMEM, on the basal chamber of the trans-well and incubated overnight. As a control C9 was omitted. Five different time points were applied (1 h, 4 h, 8 h, 24 h and 48 h) to study the formation/elimination of C5b-9 complex via immunofluorescence. High levels of C5b-9-positive staining were detected within 1 h on the basal RPE cell surface (Figure 27-B_{ii}). These high C5b-9 levels were maintained at 4 h (Figure 27-C_{ii}), but started to decline by 8 h (Figure 28-A_{ii}). The level of C5b-9-positive staining was further reduced at 24 h (Figure 28-B_{ii}) and by 48 h it was almost absent from the basal surface of the pRPE cells (Figure 28-C_{ii}). Control cells (cells treated with C5b-6 + C7 + C8 proteins) did not develop any staining specific to the α-C5b-9 antibody on their basal surface, as expected. To quantify these observations, the fluorescence intensity specific to C5b-9 was measured using Imaris® from three independent experiments (four different Z-sections per sample per experiment). The apical surface of all samples remained negative for C5b-9-specific staining (Figure 27-A_i, B_i, C_i and Figure 28-A_i, B_i and C_i) demonstrating the integrity of the monolayer throughout. These results show that RPE cells have mechanism(s) for eliminating C5b-9, probably to mitigate any harmful effects if C5b-9 were to remain at the cell surface. The next section examines the role of endocytosis in this process.

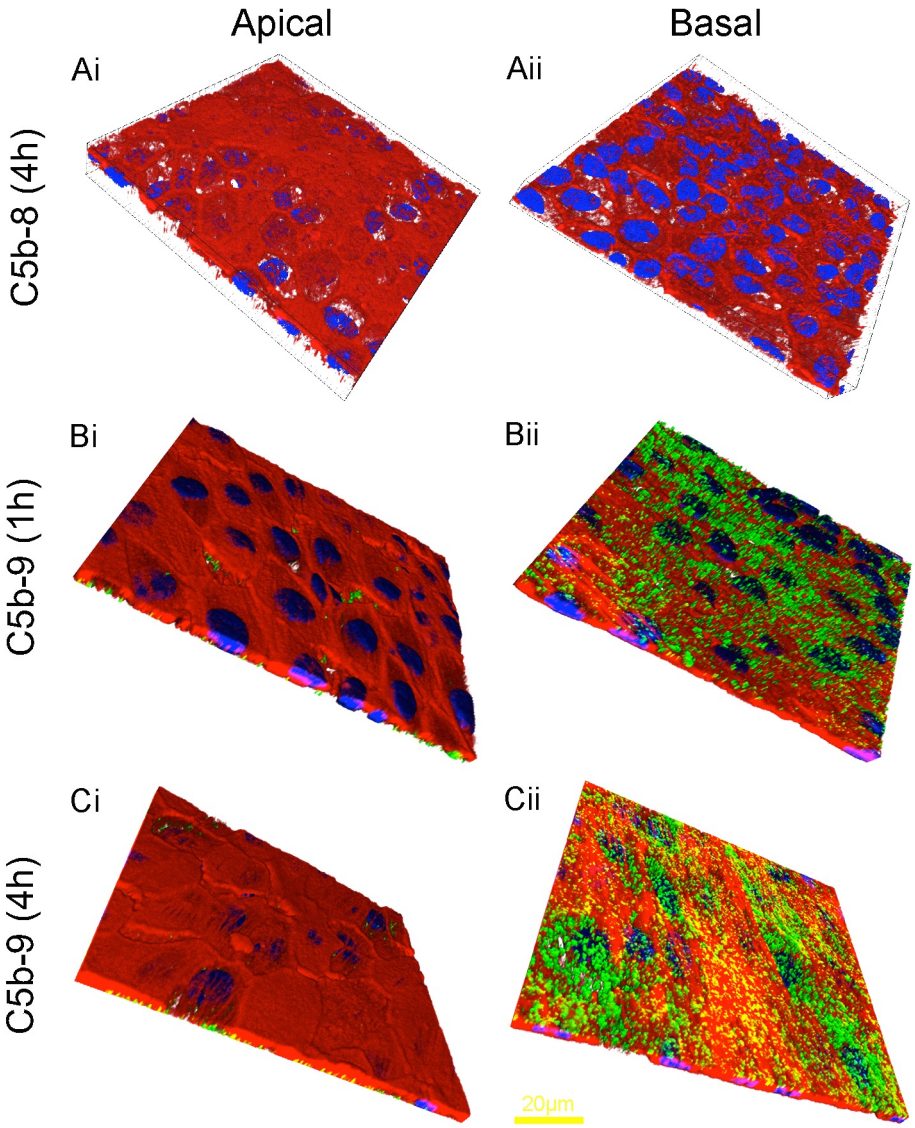

Figure 27. C5b-9 complex formation on the basal surface of pRPE cells. As a control, pRPE cells were incubated with DMEM apically (A_i) and with C5b-6, C7 and C8 proteins in DMEM basally, for 4 h (A_{ii}). pRPE cells were treated only with DMEM on their apical surface for 1 h and 4 h (B_i and C_i, respectively). C5b-6, C7, C8 and C9 purified complement proteins were added in DMEM media on the basal surface of pRPE cells for 1 h and 4 h (B_{ii} and C_{ii}, respectively). C5b-9 complex formation (green staining) was detected via immunofluorescence. High levels of C5b-9-positive staining were detected for both time points (1 h and 4 h) on the basal surface of the cells. The apical surfaces of all samples (including the control) were incubated with DMEM only and therefore they did not develop any C5b-9-positive staining (A_i, B_i and C_i). Red staining corresponds to F-actin, blue staining to DAPI. Scale bar represents approximately 20µm.

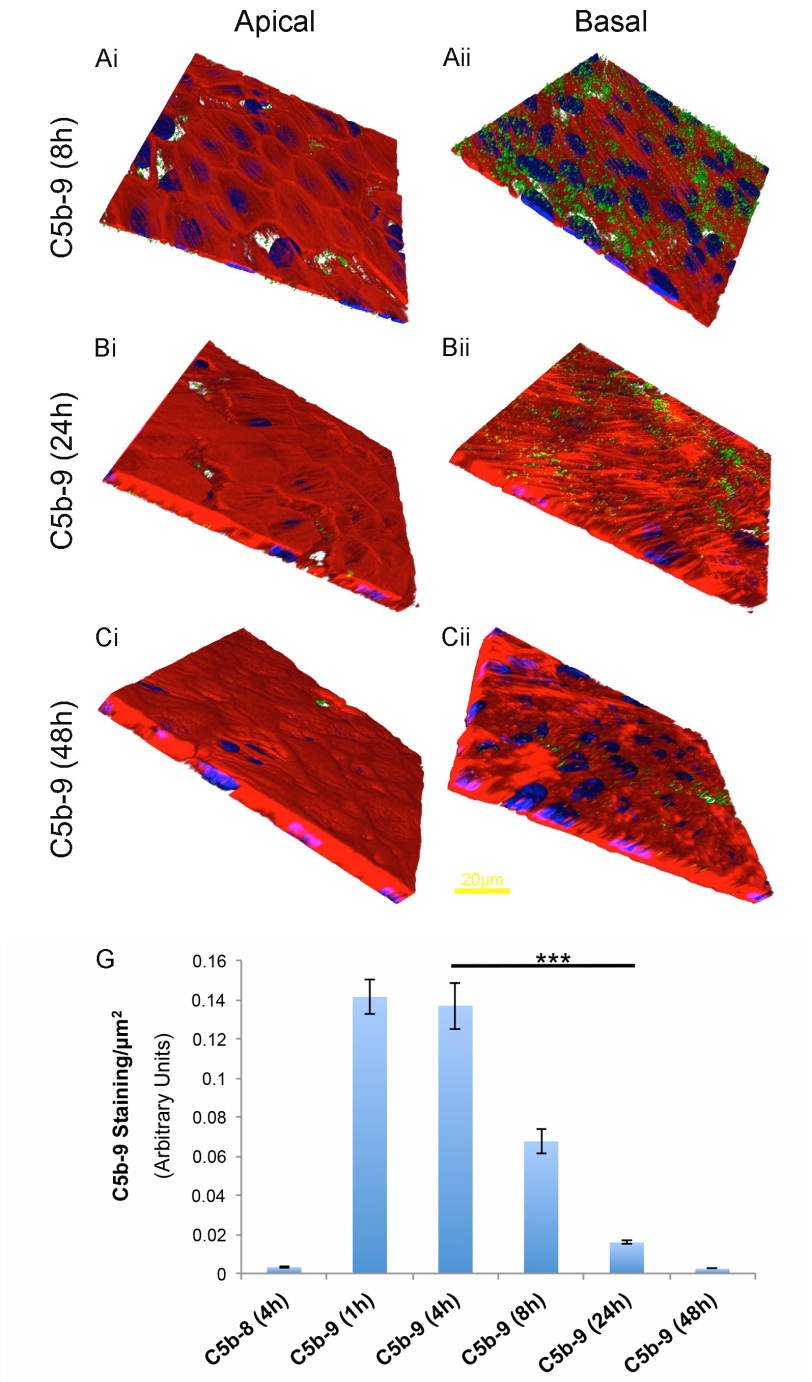

Figure 28. C5b-9 complex formation/elimination on the basal surface of pRPE cells. The images show a continuation of the experiment in Figure 26 at later time points. In combination with data from Figure 26, C5b-9 levels declined at 8 h on the basal surface of pRPE cells (A_{ii}) and a further reduction was observed at 24 h (B_{ii}). Hardly any C5b-9-positive staining was detected at 48 h (C_{ii}). The histogram (G) provides a quantitative readout of the staining intensity of the C5b-9 complex on the basal surface of pRPE cells as a function of time. Each bar represents the average of the C5b-9-related fluorescence intensity as measured from twelve independent areas stemming from three samples, from three independent experiments, using Imaris® software. Data expressed as mean ± SEM, ***P<0.001. Red staining corresponds to F-actin, blue staining to DAPI. Scale bar represents approximately 20µm.

4.2 Endocytosis of C5b-9 by RPE cells

To test whether the elimination of C5b-9 from the basal surface of pRPE cells could be attributed, at least partly, to endocytosis, dynasore monohydrate was used to block the endocytic pathway. Dynasore is able to block both types of endocytosis (clathrin-mediated and caveolae-mediated) as it acts as a non-competitive inhibitor of dynamins I, II and III by blocking their GTPase activity in a dose-dependent manner (Macia et al., 2006, Henley et al., 1998). More specifically, in clathrin-mediated endocytosis it has been shown that dynasore is capable of inhibiting endocytosis of transferrin in HeLa cells without interfering with membrane protein biosynthesis at the same time (Macia et al., 2006).

The aim of an initial pilot experiment was to demonstrate that dynasore blocks endocytosis of transferrin on the apical surface of pRPE cells. Transferrin is an 80-kDa glycoprotein essential for iron transportation from the bloodstream to various cells types, including RPE cells (Baudouin et al., 1992). The transferrin-iron complex binds to transferrin receptors on the surface of cells, gets internalised and therefore delivers iron to cells, essential for their growth and proliferation (Baudouin et al., 1992).

Confluent pRPE cells (passage 1) grown in 12-well trans-well plates were incubated with 200 μg/ml of dynasore monohydrate in DMEM on the apical chamber for 24 h. Prior to the completion of this incubation period, without changing the media, fluorescently tagged transferrin (5 mg/ml, Alexa Fluor® 555) was added to the apical chamber for 30 min. Cells were then methanol-fixed and stained (according to method **2.9**) with a mouse monoclonal anti-ezrin antibody, in order to label the apical surface of pRPE cells (Figure 29-A). Immunofluorescence staining of the apical cell surface provided a clear indication of whether transferrin became internalised or not. As a vehicle control, pRPE cells were incubated only with DMEM, containing 0.65 % DMSO that was used to dissolve dynasore on the previous sample. In both vehicle control and dynasore-treated cells DMEM was used in the basal chamber. Immunofluorescence analysis confirmed dynasore's ability to block the endocytosis of transferrin (red staining) on the apical surface (green staining) of pRPE cells (Figure 29-C_i). Transferrin levels were significantly lower on the apical surface of

the vehicle control (Figure 29-B_i), indicating that bound transferrin was successfully internalised. Figures 29-C_{ii} and B_{ii} show the same result from a basal perspective. Imaris® was used to quantify these observations by measuring the fluorescence volume specific to transferrin in treated and untreated cells (Figure 30). Analysis of the apical surfaces of both the vehicle control and the dynasore-treated cells was performed (Figure 30-A_i and B_i respectively), while Figures 30-A_{ii} and B_{ii} show the same apical surfaces viewed from their cytoplasmic sides. Figure 30-A_{iii} (vehicle) and Figure 30-B_{iii} (dynasore-treated cells) show optical sections proximal to the apical cell surface. Data from Figure 29 and 30 were derived from one independent experiment. This study shows that dynasore can be used as an effective endocytosis inhibitor in order to block endocytosis in pRPE cells.

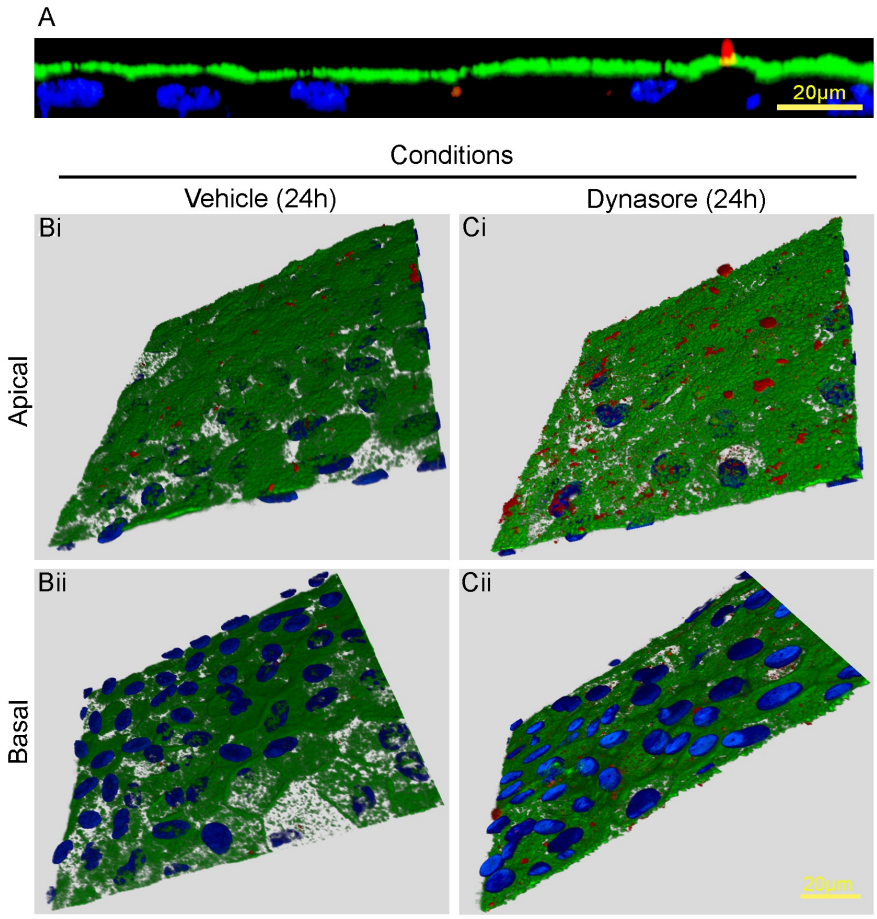

Figure 29. Dynasore blocks endocytosis of transferrin in pRPE cells. The apical surface of cells (green staining) was labelled using an antibody to ezrin. Red staining corresponds to fluorescently tagged transferrin Alexa Fluor® 555 (A). As vehicle control, cells were incubated with DMEM containing DMSO (B_i). The basal surface of cells was incubated only with DMEM (B_{ii}). On the apical surface of cells, 200 µg/ml of dynasore monohydrate was added in DMEM for 24 h. Before the end of this incubation period, transferrin was added for 30 min (C_i). The basal surface of cells was incubated only with DMEM for 24 h (C_{ii}). Comparison of dynasore-treated cells (C_i, C_{ii}) with vehicle control (B_i, B_{ii}) demonstrates dynasore's ability to block endocytosis of transferrin. Blue staining corresponds to DAPI. Scale bars represent approximately 20µm.

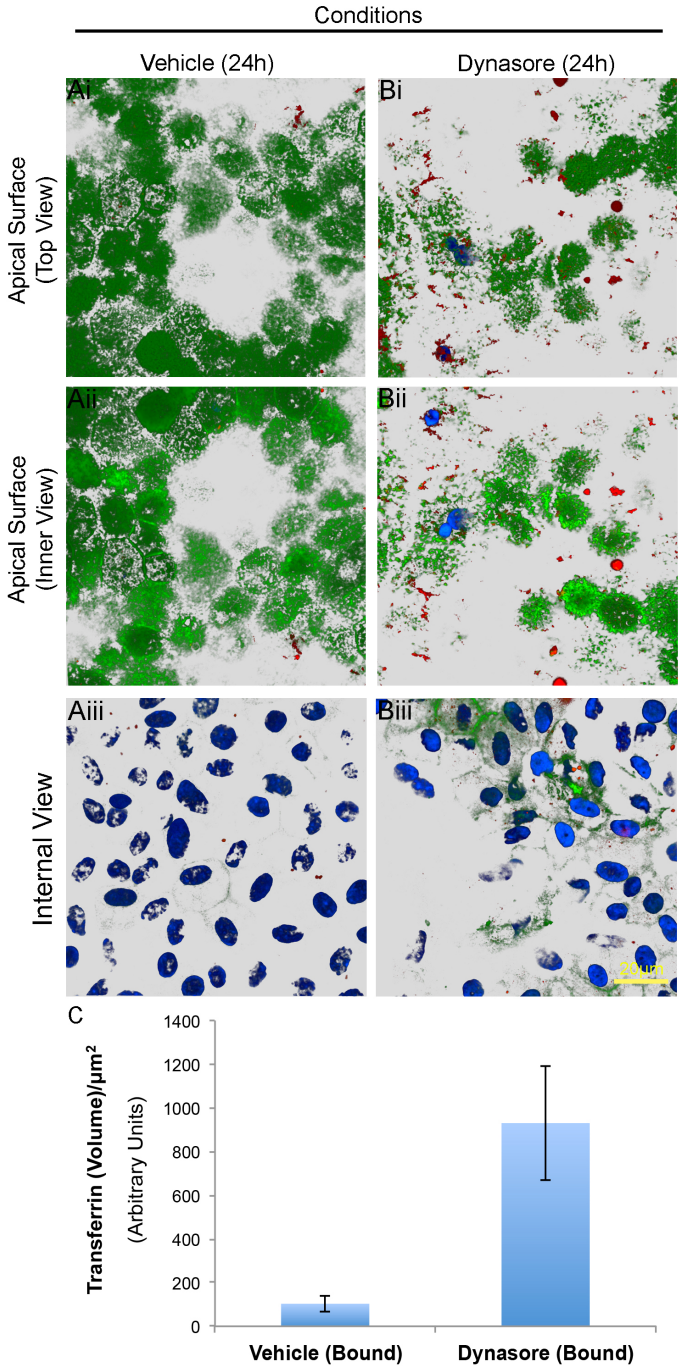

Figure 30. Quantification of transferrin endocytosis on the apical surface of pRPE cells. As vehicle control, cells were incubated with DMEM containing DMSO for 24 h ($A_{i\text{-}iii}$). The apical surface of all cells (green staining) was labeled using an antibody specific to ezrin. Top view of the apical surface of the vehicle control cells (A_i). A_{ii} provides an inner view of the apical surface of the vehicle control cells. A_{iii} depicts an optical section proximal to the apical surface. On the apical surface of cells, 200 µg/ml of dynasore monohydrate was added in DMEM for 24 h. Before the end of this incubation period, transferrin was added to the same media for 30 min ($B_{i\text{-}iii}$). B_i shows the top view of the apical surface of the dynasore-treated cells. B_{ii} provided an inner view of the apical surface of the dynasore-treated cells. B_{iii} depicts an optical section proximal to the apical surface. The histogram (C) demonstrates the blockage of transferrin internalisation in dynasore-treated pRPE cells. Each bar is derived from the measurement of fluorescence volume specific to transferrin derived from four independent z-sections per sample from one independent experiment using Imaris®. Data expressed as mean ± SEM. Blue staining corresponds to DAPI. Scale bar represents approximately 20µm.

4.3 The C5b-9 complex is eliminated via endocytosis

It has previously been shown that various cell types such as neutrophils, oligodendrocytes, platelets and tumour cells protect themselves from C5b-9-induced lysis via membrane vesiculation (Pilzer and Fishelson, 2005b). Membrane vesiculation involves the processes of exo-, ecto- and/or endo-cytosis (Pilzer et al., 2005a, Lakkaraju et al., 2014). Therefore, it was investigated whether the observed elimination of C5b-9 from the basal surface of pRPE cells was attributed, at least in part, to endocytosis.

pRPE cells were grown on 12-well trans-well plates and the C5b-9 complex was allowed to form *in vitro* as described in method $\mathbf{D_T}$ (section **2.5.4.1**) in the absence or presence of dynasore. As a control C5b-6, C7 and C8 proteins were added to the basal chamber of the trans-well, for 4 h. To the apical chamber (in all samples, including the control) only DMEM was added. Two time points (4 h, 24 h) were selected, as we had already shown (Section **4.1**) that at 4 h there were high levels of C5b-9 complex on the basal surface of pRPE cells while at 24 h these levels were significantly lower. Immunofluorescence was used to determine whether dynasore administration maintained C5b-9 levels at 24 h. Figure 31 demonstrates the accumulation of C5b-9 (green staining) on the basal surface of pRPE cells at 4 h, and its elimination at 24 h. However, in cells treated with the aforementioned complement proteins and dynasore for 24 h, C5b-9 staining remained at similar levels to those observed at 4 h (Figure 31-D_{iii}). C5b-8-treated cells did not develop staining for C5b-9. These studies show that dynasore inhibits the elimination of C5b-9, confirming that the major mechanism of C5b-9 complex removal in RPE cells is via endocytosis.

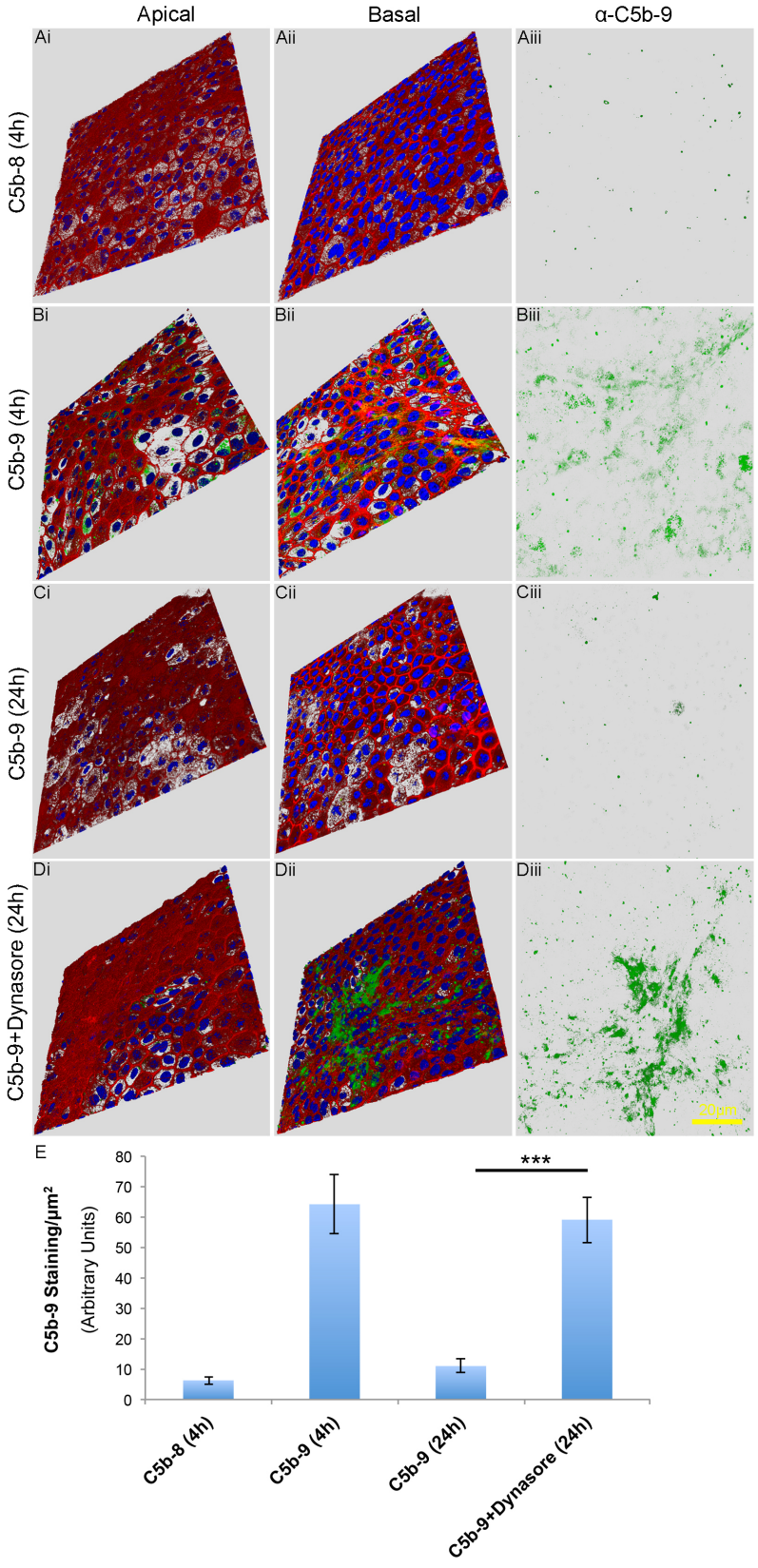

Figure 31. Dynasore blocks endocytosis of C5b-9 by pRPE cells. On the apical chamber of all samples (A_i, B_i, C_i and D_i) only DMEM was added. As a control C5b-6, C7 and C8 proteins were added in DMEM to the basal chamber of the trans-well, for 4 h (A_{ii}). C5b-6, C7, C8 and C9 purified complement proteins were added in DMEM to the basal chamber of the trans-well, for 4 h and 24 h (B_{ii} and C_{ii}, respectively). Also, pRPE cells were incubated (basal surface) with C5b-6 complex, C7, C8 and C9 purified complement proteins in DMEM with 200 µg/ml of dynasore, for 24 h (D_{ii}). Dynasore not only blocked endocytosis of the C5b-9 complex (green staining) at 24 h (D_{iii}) but also sustained C5b-9 levels similar to those seen at 4 h (B_{iii}). Without dynasore, the C5b-9 complex was endocytosed (C_{iii}). C5b-8 treated cells did not develop staining specific to the α-C5b-9 antibody (A_{iii}). The histogram (E) provides a quantitative readout of the above findings. Each bar represents the average of the C5b-9-related fluorescence intensity as measured from twelve independent areas from three samples, from three independent experiments, using Imaris®. Data expressed as mean ± SEM ***P<0.001. Red staining corresponds to F-actin, blue staining to DAPI. Scale bar represents approximately 20µm.

4.4 Cellular localisation of the C5b-9 complex in pRPE cells

To further investigate the processing of C5b-9 by RPE cells immuno-electron microscopy was used to examine the subcellular localisation of the C5b-9 complex in more detail.

The C5b-9 complex was allowed to form *in vitro* on confluent pRPE cells as described in method $\mathbf{D_T}$ (section **2.5.4.1**) in the presence or absence of dynasore for times indicated in the legend of Figure 32. At the end of the experiment cells were processed according to the cryo-EM method, described in Section **2.11**.

In cells treated for 4 h with C5b-9, gold particles indicated the presence of the C5b-9 complex (yellow arrows) on the basal surface of pRPE cells, possibly within basal in-foldings (Figure 32). At 24 h in C5b-9-treated cells, almost no gold particles were detected on the basal surface of the cells, however gold particles were identified in the cytoplasm of pRPE cells. This is an indication that most of the C5b-9 complex was already internalised and most likely degraded in lysosomes, as only a few gold particles were detected. However, when cells were treated with complement proteins and dynasore for 24 h, a plethora of gold particles was located at the basal surface of pRPE cells. This accumulation of gold particles at 24 h is consistent with the arrest of C5b-9 endocytosis due to the presence of dynasore. It should be noted that some low level background gold labeling was evident in the control sample (blue arrows). Figure 32 provides further evidence that dynasore maintains C5b-9 on the basal aspect of pRPE cells by blocking endocytosis. Figure 32 demonstrates that at 4 h despite the majority of the C5b-9 complex residing on the basal surface there is some already internalised, though this declines by 24 h. Each bar from both histograms (Figure 32) represents the average number of gold particles counted in pRPE cells from eight different sections, from one immuno-gold experiment. Counting of the gold particles was performed with ImageJ freeware.

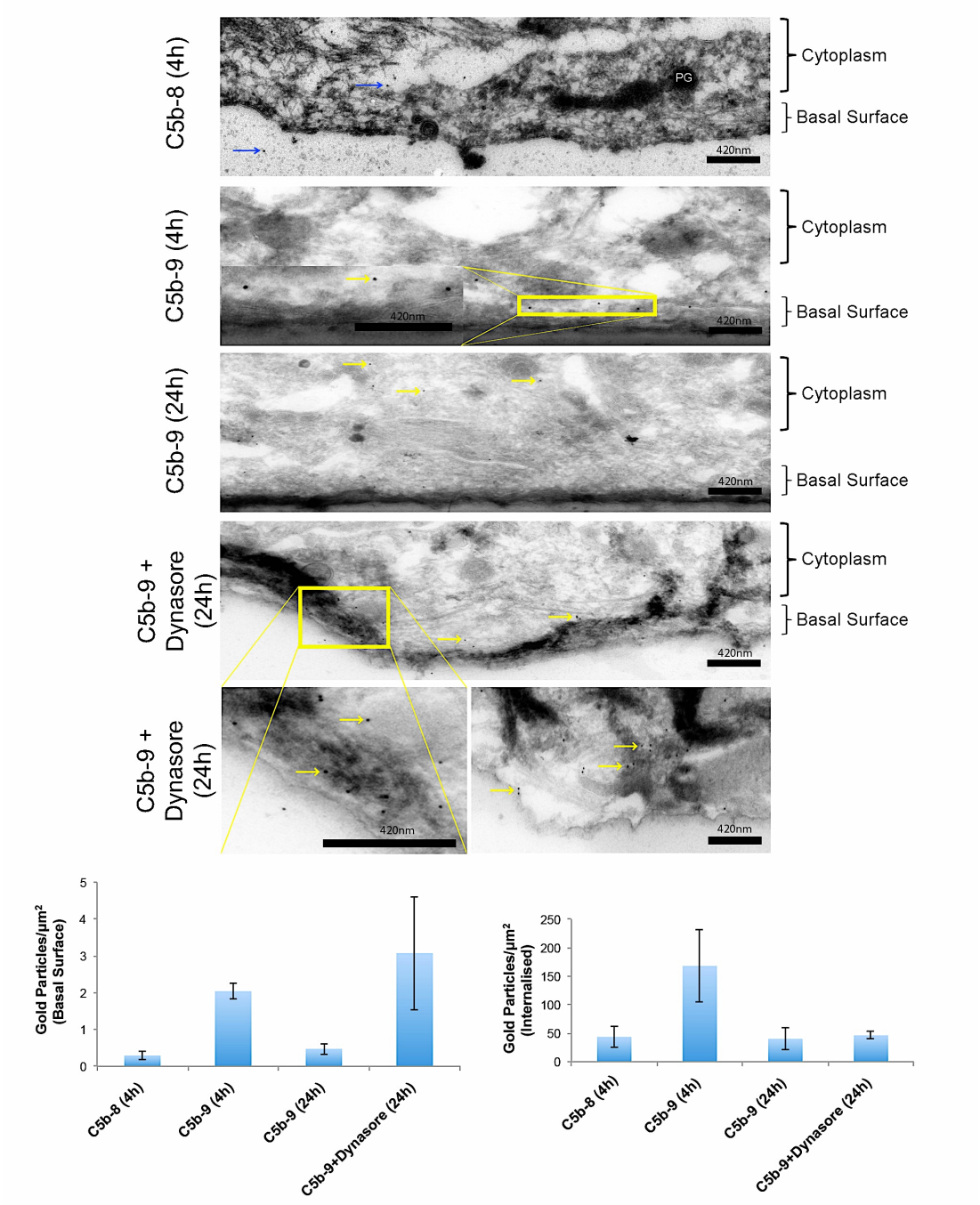

Figure 32. Localisation of C5b-9 in pRPE cells by immune-electron microscopy. As a control C5b-6, C7 and C8 proteins were added in DMEM, to the basal chamber of the trans-well, for 4 h. In test samples, C5b-6 complex, C7, C8 and C9 purified complement proteins were added in DMEM to the basal chamber of the trans-well ± 200 µg/ml dynasore for 24 h. At 4 h in C5b-9-treated cells, most gold particles (yellow arrows) resided on the basal surface of the cells. At 24 h, most of these gold particles were eliminated and only a few were identified as internalised due to their distant location from the basal surface. At 24 h, in cells treated with complement proteins and dynasore, many gold particles were located on the basal surface. The histograms show that no significant levels of internalised gold particles were detected apart from 4 h. Each bar from both quantification charts represents the average number of gold particles counted in pRPE cells from eight different sections, from one experiment. Counting of the gold particles was performed with ImageJ freeware. Data expressed as mean ± SEM. Scale bars represent approximately 420nm. The processing of samples for immune-electron microscopy was performed by Dr. Thomas Burgoyne, UCL Institute of Ophthalmology.

4.5 The effect of C5b-9 on trans-epithelial resistance in pRPE cells

These studies show that RPE cells tolerate C5b-9 remarkably well, with virtually no evidence of cell death, and that the complex is eliminated from the cell surface at least in part by endocytosis. Next we started to investigate whether the C5b-9 complex might affect any of the numerous functions of RPE cells. First we examined the barrier properties of the pRPE monolayer, since this is a key physiological feature of all mammalian epithelia. This was assessed by measuring the TER (Section **2.2**) and permeability of the pRPE monolayer with low and high molecular weight fluorescent markers (Section **2.3**).

4.5.1 TER measurements in C5b-9-treated pRPE cells

For this study confluent pRPE cells were grown in 12-well trans-well plates. C5b-9 was allowed to form on the basal surface of these cells as described previously for 1 h, 4 h, 8 h and 24 h and TER was measured at each time point using an EVOM with a STX2 manual electrode (section **2.2**). When pRPE cells were transferred from serum-containing media (1 % FBS in DMEM) to serum-free conditions (DMEM) TER increased slightly. Therefore, cells were incubated for 1 h in serum-free conditions in order to allow them to adjust to their new environment, and to allow the TER to stabilise as well. Two different controls were used: pRPE cells growing in DMEM (both apical and basal chambers) and C5b-8-treated cells. Basal C5b-9 complex formation led to a small but significant increase in TER at 1 h that remained stable until 24 h (Figure 33). Basal assembly of C5b-8 induced a similar effect on TER, however the magnitude of the increase was smaller. The results show that C5b-9 induced a significantly higher increase in TER (~90 Ω/cm^2 to ~130 Ω/cm^2, $p<0.001$) than either the switch to serum-free medium or C5b-8 ($p<0.05$). In Figure 32 each bar represents the average TER values obtained from twelve wells from three independent experiments.

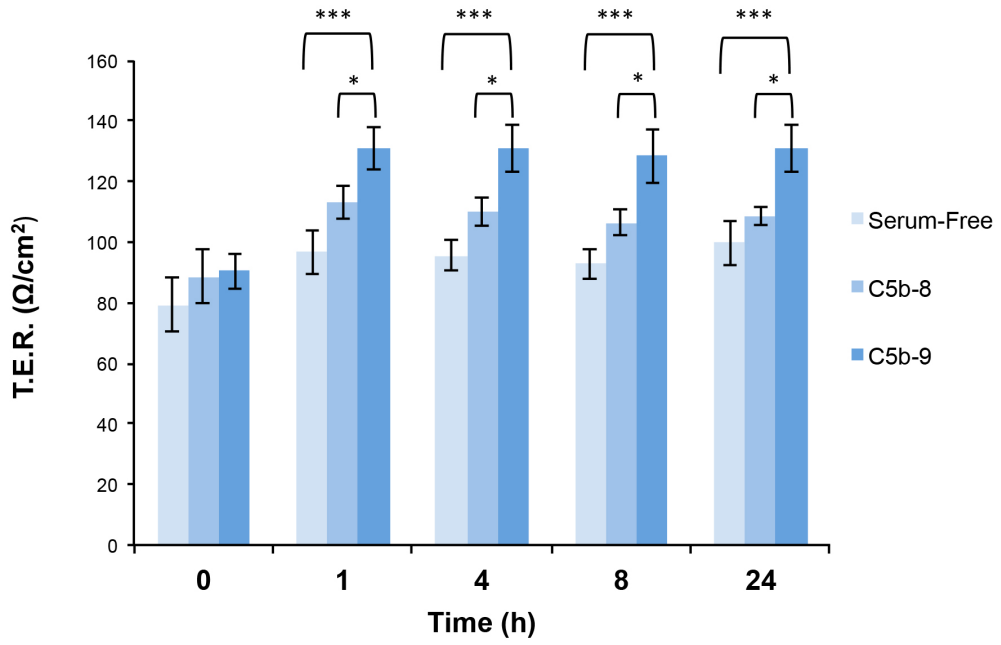

Figure 33. Basal C5b-9 complex assembly increases TER in pRPE cells. For C5b-8 formation, C5b-6 complex, C7 and C8 proteins were added in DMEM, to the basal chamber of the trans-well for 1 h, 4 h, 8 h and 24 h. C5b-9 complex was allowed to form on the basal surface of these cells by adding C5b-6 complex, C7, C8 and C9 purified complement proteins. The C5b-9 complex induced a higher TER increase than C5b-8 or DMEM alone. This effect was observed from 1 h through to 24 h. Each bar represents the average TER values obtained from twelve wells from three independent experiments. Data expressed as mean ± SEM, ***P<0.001, *P<0.05.

The same effects were observed when C5b-8 and C5b-9 complexes were formed on the apical surface of pRPE cells (Figure 34), and again, the increase was greater in C5b-9-treated cells than in DMEM-treated and C5b-8-treated cells. Each bar represents the average TER values obtained from four wells from one independent experiment.

Taken together, these experiments show that the *in vitro* assembly of the C5b-9 complex leads to an increase in the TER in pRPE cells, regardless of whether it forms on the apical or basal surface.

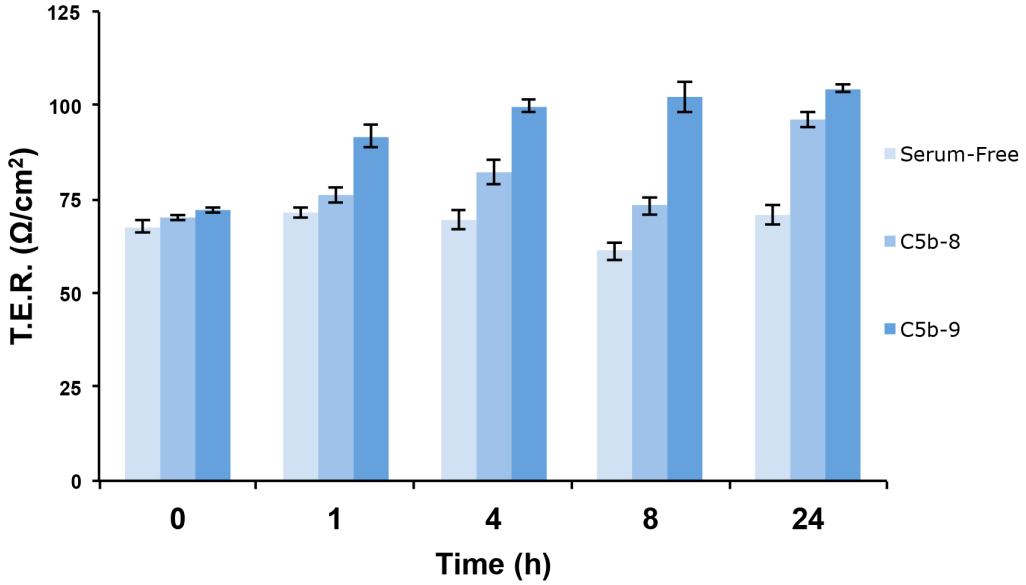

Figure 34. Apical C5b-9 complex formation increased TER in pRPE cells. C5b-8 and C5b-9 complexes were formed on the apical surfaces of pRPE cells as described in the legend of Figure 32. Apical C5b-9 complex induced higher TER increase than apical C5b-8 complex and serum-free alone. This effect was observed from 1 h until 24 h. Each bar represents the average TER values obtained from four wells from one independent experiment. Data expressed as mean ± SEM.

4.5.2 Effect of C5b-9 on permeability in pRPE cells

Results from the previous section (**4.5.1**) demonstrate that C5b-9 assembly on pRPE cells leads to an increase in TER. To investigate monolayer integrity using an alternative approach, low and high molecular weight dextrans were applied to the media (as described in Section **2.3**). Using both low and high molecular weight dextrans can provide insight into the extent of barrier permeability, since the low molecular weight dextran will penetrate smaller spaces more rapidly. In this study *in vitro* C5b-9 complex formation was applied only to the basal surface of pRPE cells.

When low molecular weight dextran (fluorescein dextran) was introduced to the system (Figure 35), no significant difference was detected in permeability between the C5b-8- and C5b-9-treated pRPE monolayers. At 4 h until 8 h, permeability in C5b-9-treated cells was slightly lower compared to the permeability of serum-free-treated cells, however this effect did not last until 24 h, where the system appeared to be saturated, as all samples (serum-free-, C5b-8- and C5b-9-treated cells)

demonstrated similar permeability to the empty well. Each bar represents the average value from four wells from one independent experiment.

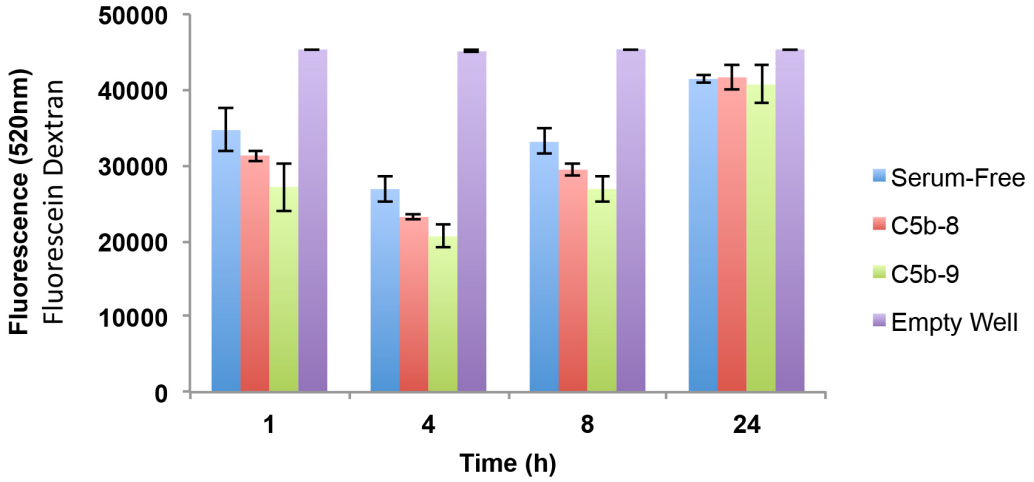

Figure 35. Permeability assessment of C5b-9-treated pRPE monolayers. C5b-9 was allowed to form on the basal cell surface by adding C5b-6 complex, C7, C8 and C9 purified complement proteins in DMEM for 1 h, 4 h, 8 h and 24 h. Permeability was monitored by adding 1 mg/ml of low molecular weight fluorescein dextran to the apical chamber. Sampling was taken from the basal chamber. No significant difference was detected in permeability between the C5b-8- and C5b-9-treated pRPE monolayers. At 4 h until 8 h, permeability in C5b-9-treated cells was slightly lower compared to the permeability of serum-free-treated cells, however this effect did not last until 24 h, where the system appeared to be saturated, as all samples (serum-free-, C5b-8-, C5b-9-treated cells) demonstrated similar permeability to the empty well. Each bar represents the average value from four wells from one independent experiment. Data expressed as mean ± SEM.

In order to confirm the findings from Figure 35, permeability was checked again with the low molecular weight dextran only at 4 h. As shown previously (Figure 27), between 1-4 h there is maximum basal C5b-9 complex deposition in pRPE cells. Therefore, it was tested whether fluorescein dextran will demonstrate lower or higher permeability of the C5b-9-treated monolayer (by 4 h there are high levels of C5b-9 basal deposition) compared with the permeability of the serum-free- and C5b-8-treated monolayers. Despite the increase in the TER in C5b-9-treated cells at 4 h (compared to serum-free-treated cells, Figure 36-A), fluorescein dextran failed to demonstrate similar results when permeability was checked at 4 h as well (Figure 36-B). Each bar represents the average value derived from four wells from one independent experiment (Figure 36-A, -B).

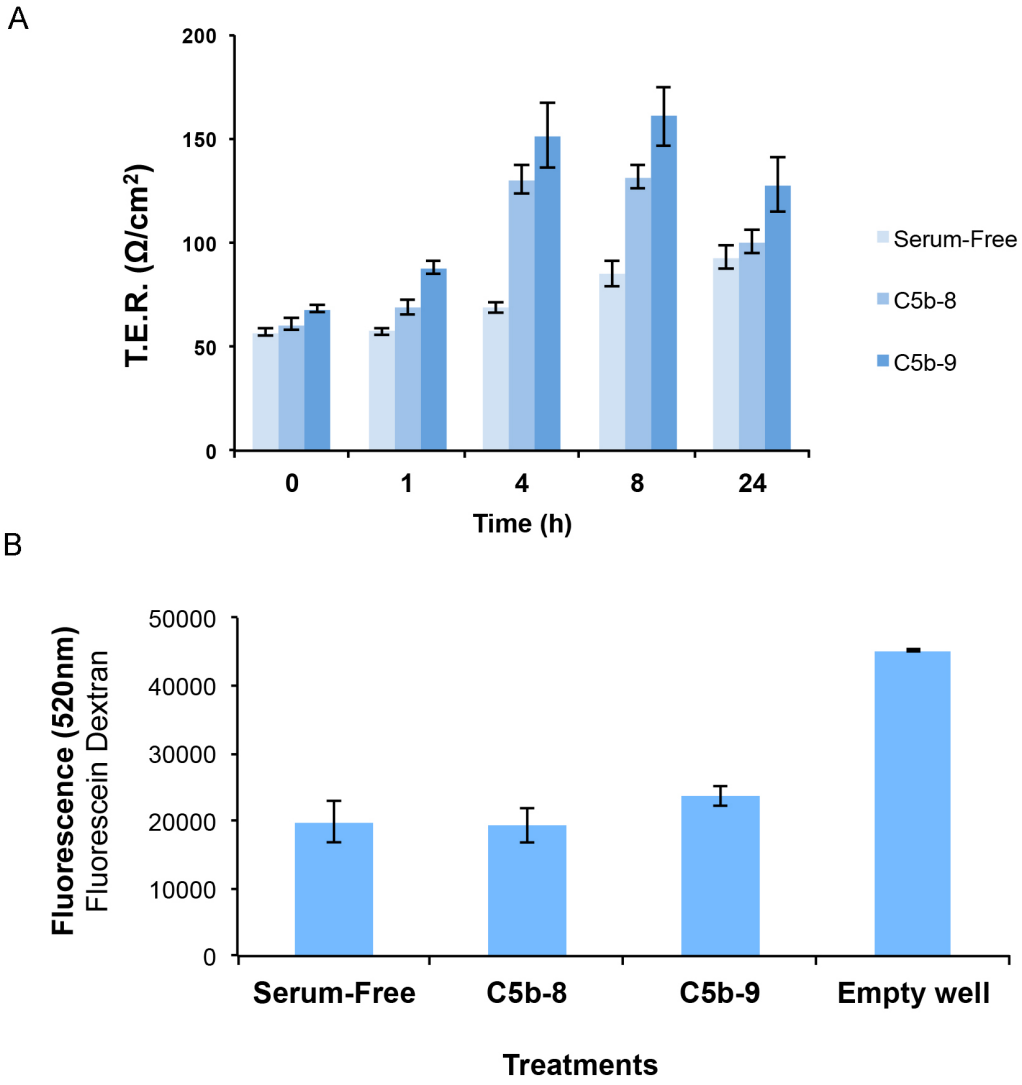

Figure 36. Simultaneous measurement of TER and permeability in pRPE cells. Before monitoring permeability of C5b-9-treated pRPE cells, TER was checked at 1 h, 4 h, 8 h and 24 h (A). Permeability was tested using a 3-5 kDa fluorescein dextran (administered to the apical chamber, that remained in the media until 4 h. Samples were taken from the basal compartment at 4 h (B). No difference was detected between serum-free-, C5b-8- and C5b-9-treated pRPE monolayers (B). Each bar represents the average value derived from four wells from one independent experiment. Data expressed as mean ± SEM.

Using low molecular weight dextrans provides a very sensitive method of detecting differences in permeability between the three different conditions applied. For comparison, higher molecular weight dextran was also used (rhodamine B-dextran, 70 kDa). Sampling of rhodamine B-dextran also demonstrated that the differently treated pRPE monolayers retained their integrity to a similar extent (Figure 37), with all test samples exhibiting much lower values than the empty well at all time points

examined. Despite recording lower values for the C5b-9-treated cells, which would be consistent with the data obtained using TER measurements, these did not reach statistical significance in this set of experiments. Each bar in Figure 37 represents the average value obtained from eight wells from two independent experiments.

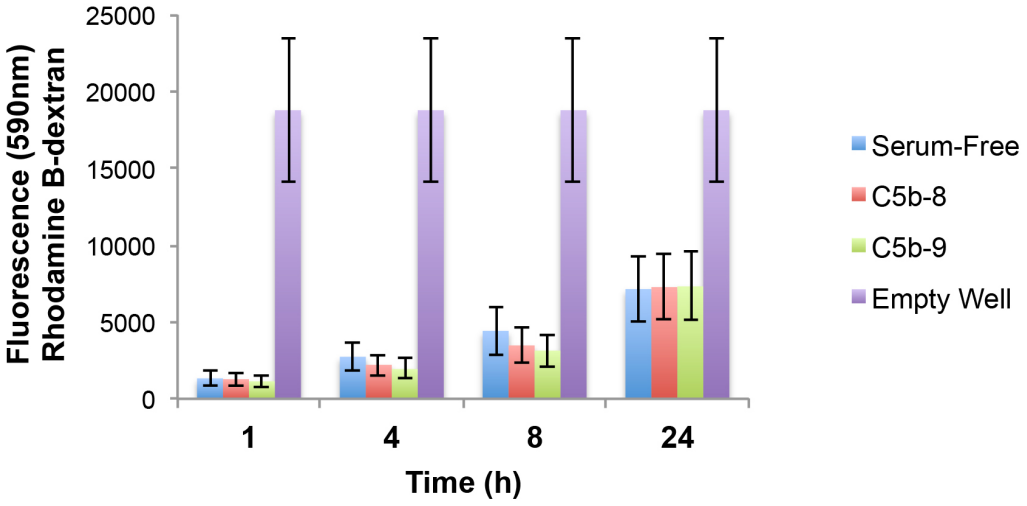

Figure 37. Permeability analysis of C5b-9-treated pRPE monolayers using high molecular weight dextran. C5b-9 was allowed to form on the basal cell surface by adding the C5b-6 complex, C7, C8 and C9 purified complement proteins in DMEM for 1 h, 4 h, 8 h and 24 h. Permeability was monitored by adding 1 mg/ml of high molecular weight rhodamine B dextran (70 kDa) to the apical chamber. Measurement of fluorescence in the lower chamber demonstrated that the differently treated pRPE monolayers retained their integrity, as the fluorescence values were much lower than those obtained from the empty well, at all time points examined. However, no significant differences in permeability were detected between serum-free-, C5b-8- and C5b-9-treated pRPE cells. Each bar represents the average values from eight wells from two independent experiments. Data expressed as mean ± SEM.

4.6 Does the C5b-9 complex affect levels of junctional proteins?

To further investigate possible causes for the aforementioned C5b-9-induced TER increase in pRPE cells, the expression of two abundant junctional proteins in RPE cells (claudin-19 and ZO-1) was examined. ZO-1, is part of the junctional complex, and by binding to ZONAB, can control proliferation in epithelial cells (Balda et al., 2003, Balda and Matter, 2000, Stevenson et al., 1986, Fanning et al., 2012). The better the monolayer RPE cells have formed the more ZO-1 becomes enriched at junctions and therefore cell proliferation is inhibited (Balda et al., 2003). Additionally, claudin-19 is a key component of the tight junctions in human RPE

cells and also in the kidney, having a crucial role in paracellular ion re-absoption in both tissues (Konrad et al., 2006, Hou and Goodenough, 2010).

The aim of this experiment was to find out whether C5b-9 assembly leads to an increase in expression of any key junctional proteins that would provide a mechanistic explanation for the rise in TER described earlier. However, western blot analysis did not reveal any significant changes in protein expression of either claudin-19 or ZO-1 (Figure 38) in any of the various conditions. Each bar in Figure 38 represents the average values derived from three wells from three independent experiments.

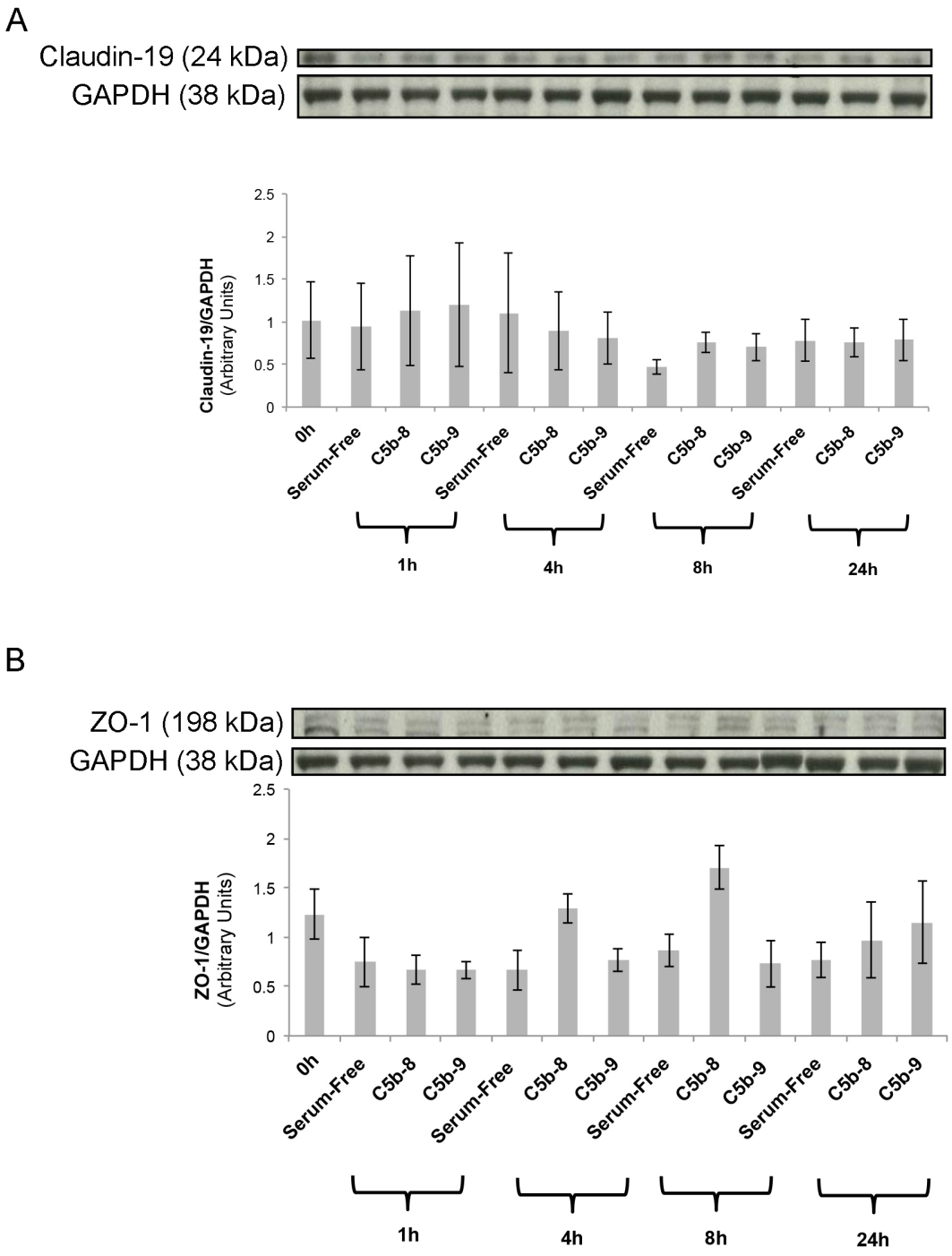

Figure 38. Exposure to C5b-9 does not alter expression of claudin-19 or ZO-1 in pRPE cells. The C5b-9 complex was allowed to form on the basal surface of pRPE cells by adding C5b-6, C7, C8 and C9 purified complement proteins in DMEM for 1 h, 4 h, 8 h and 24 h. Cells were extracted and whole cell lysates were analysed by SDS-PAGE and western blotting. Expression levels of both claudin-19 (A) and ZO-1 (B) remained relatively constant throughout. Blots were scanned and densitometric analysis yielded the respective histograms. Each bar represents the average values derived from three wells from three independent experiments. Data expressed as mean ± SEM.

4.7 Claudin-19 expression in C5b-9-treated pRPE cells

Although western blotting did not reveal any significant changes in protein levels of claudin-19 upon treatment of pRPE cells with C5b-9 (section **4.6**) it was possible that changes in the subcellular localisation of claudin-19 might be consistent with the effect on TER. To address this possibility immunofluorescence analysis was performed on pRPE cells exposed to basal C5b-9 for 1 h (Figure 39). The results show that there was no difference in the pattern of claudin-19 staining in serum-free- (Figure 39-B_i), C5b-8- (Figure 39-C_i) and C5b-9-treated cells (Figure 39-D_i). However, simply switching pRPE cells to serum-free medium has a striking effect on its own. Thus, under normal culture conditions, claudin-19 was mainly punctate and cytoplasmic with only faint staining at the cell junctions (Figure 39-A), whereas in serum-free conditions it became tightly localised to the cell junctions and almost undetectable in the cytoplasm. This observation is consistent with the small increase in TER observed in pRPE cells in serum-free medium (Figure 33) but cannot account for the more significant rise in TER in cells exposed to C5b-9. In Figure 39, this analysis was extended to cells at 4 h, 8 h and 24 h respectively. The images show that while there was little discernable change from 1-8 h, at 24 h there was a clear reappearance of punctate cytoplasmic staining for claudin-19, with a corresponding decrease in enrichment at the cell junctions. It should be mentioned however, that C5b-9-treated pRPE cells at 4 h developed stronger staining for claudin-19 compared to serum-free- and C5b-8-treated cells.

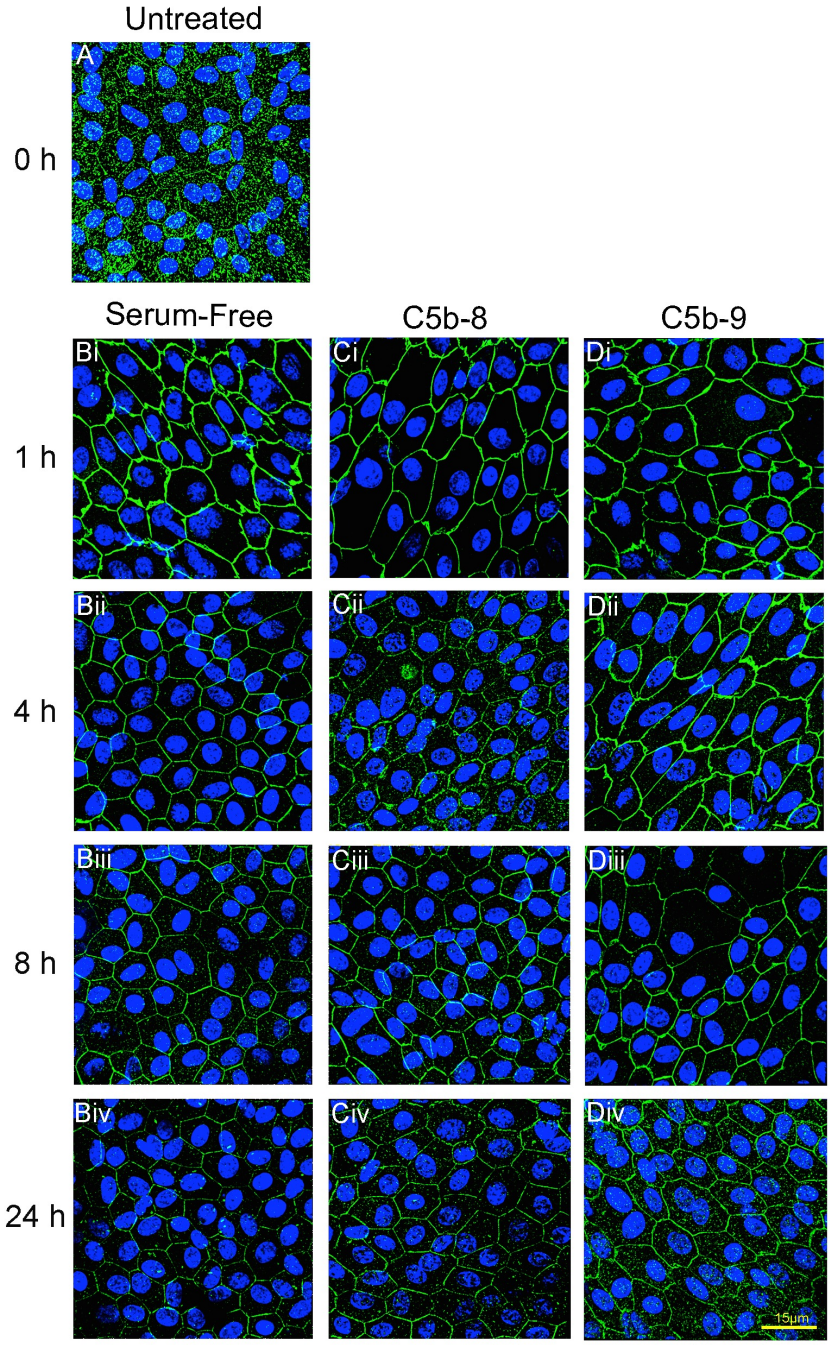

Figure 39. Immunofluorescence analysis of claudin-19 in C5b-9-treated pRPE cells. In the apical chamber of all samples only DMEM was added. Two different controls were used: pRPE cells growing with DMEM in both apical and basal chambers, and C5b-8-treated cells. For C5b-8 formation, C5b-6 complex, C7 and C8 proteins were added in DMEM, on the basal chamber of the trans-well, for 1 h, 4 h, 8 h and 24 h. C5b-9 complex was allowed to form on the basal surface of pRPE cells by adding C5b-6 complex, C7, C8 and C9 purified complement proteins in DMEM, for 1 h, 4 h, 8 h and 24 h. Untreated cells (A) were pRPE cells grown in 1 % FBS in DMEM. No changes in claudin-19 expression (green staining) between serum-free- (B_{i-iv}), C5b-8- (C_{i-iv}) and C5b-9-treated cells (D_{i-iv}) were observed. However, C5b-9-treated pRPE cells at 4 h (D_{ii}) developed stronger staining for claudin-19 compared to serum-free- (B_{ii}) and C5b-8-treated cells (C_{ii}). The transition from 1 % FBS to serum-free conditions seemed to affect expression of claudin-19. Blue staining represents DAPI. Scale bar represents approximately 15µm.

4.8 ZO-1 expression in C5b-9-treated pRPE cells

In a parallel study to that just described for claudin-19, the cellular expression of ZO-1 was examined in pRPE cells exposed to C5b-9, using immunofluorescence in conjunction with confocal microscopy (Figure 40). The results show that there was no difference in the pattern of ZO-1 staining in serum-free- (Figure 40-$B_{i\text{-}iv}$), C5b-8- (Figure 40-$C_{i\text{-}iv}$) and C5b-9-treated cells (Figure 40-$D_{i\text{-}iv}$). In contrast to findings presented in Figure 39, switching pRPE cells from 1 % FBS to serum-free conditions did not alter the pattern of ZO-1 staining.

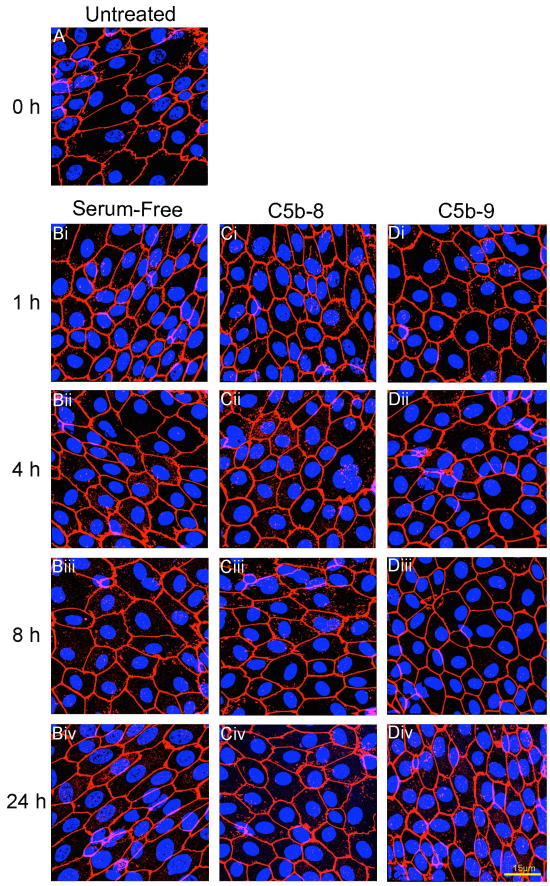

Figure 40. Immunofluorescence analysis of ZO-1 in C5b-9-treated pRPE cells. To the apical chamber of all samples only DMEM was added. Two different controls were used: pRPE cells growing in DMEM, on both apical and basal chambers and C5b-8-treated cells. For C5b-8 formation, C5b-6 complex, C7 and C8 proteins were added in DMEM, on the basal chamber of the trans-well, for 1 h, 4 h, 8 h and 24 h. C5b-9 complex was allowed to form on the basal surface of pRPE cells by adding C5b-6 complex, C7, C8 and C9 purified complement proteins in DMEM, for 1 h, 4 h, 8 h and 24 h. Untreated cells (A) were pRPE cells grown in 1 % FBS in DMEM. No changes in ZO-1 expression (red staining) between, untreated (A) serum-free- ($B_{i\text{-}iv}$), C5b-8- ($C_{i\text{-}iv}$) and C5b-9-treated cells ($D_{i\text{-}iv}$) were reported. Blue staining represents DAPI. Scale bar represents approximately 15µm.

4.9 C5b-9 endocytosis and TER in pRPE cells

Results in this chapter showed that dynasore arrests endocytosis of C5b-9 on the basal surface of pRPE cells (section **4.3**). Therefore, it was questioned whether the endocytosis and degradation of C5b-9 is important in linked in any way to the effects observed on TER. To answer this question, pRPE cells were incubated with complement proteins and dynasore monohydrate, simultaneously, for 1 h, 4 h, 8 h and 24 h. At the end of each incubation time, TER was measured according to method **2.2**.

As shown in Figure 41, basal C5b-9 complex deposition induced an increase in TER from 1 h until 24 h, as expected. However, when pRPE cells were incubated with complement proteins and dynasore, the TER remained unchanged, suggesting that endocytosis of C5b-9 from the cell surface might indeed mediate or contribute to the observed change in TER. Dynasore on its own did not affect TER values when pRPE cells were incubated with the reagent alone in DMEM.

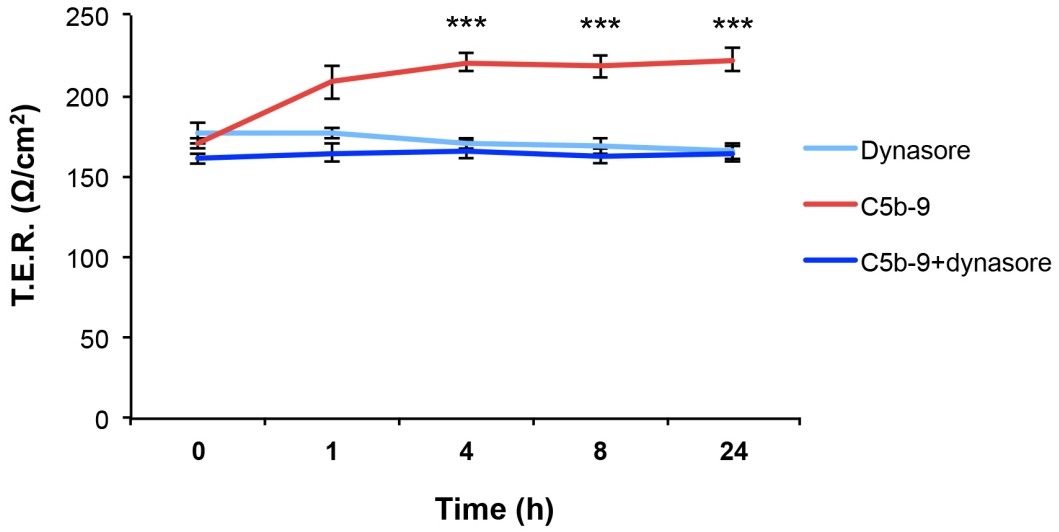

Figure 41. Maintenance of C5b-9 on the cell surface blocks the rise in TER. On the apical chamber of all samples only DMEM was added. As a control pRPE cells were incubated in DMEM with 200 µg/ml of dynasore (basal chamber) alone. Basal deposition of C5b-9 induced a TER increase from 1 h until 24 h. However, TER values remained unchanged when cells were treated with complement proteins and dynasore at the same time. Dynasore alone did not affect TER. Each data point represents the average value of twelve wells from three independent experiments. Data expressed as mean ± SEM, ***P<0.001.

4.10 Does inhibition of C5b-9 endocytosis affect expression levels of claudin-19 and ZO-1 junctional proteins?

Having shown that the prolonged presence of the C5b-9 complex on the basal surface of pRPE cells blocks the rise in TER, we next examined whether C5b-9 + dynasore down-regulates the expression of claudin-19 and ZO-1 (Figure 42).

Western blotting of whole cell lysates from control and C5b-9-treated cells ± dynasore revealed no significant changes in the protein levels of either claudin-19 or ZO-1.

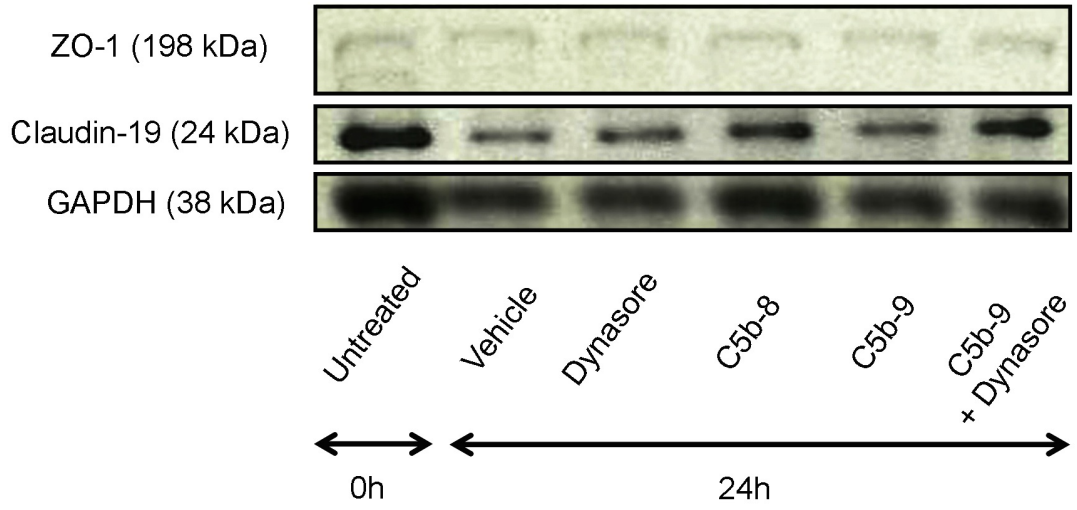

Figure 42. Prolonged presence of C5b-9 complex does not affect claudin-19 and ZO-1 protein levels in pRPE cells. To the apical chamber of all samples only DMEM was added. Four different controls were used: pRPE cells growing in 1 % FBS in DMEM media (Untreated), cells incubated with DMEM + DMSO (Vehicle), cells incubated with DMEM + 200 µg/ml of dynasore (Dynasore) and C5b-8-treated cells. For C5b-8 formation, C5b-6 complex, C7 and C8 proteins were added in DMEM, on the basal chamber of the trans-well. C5b-9 was formed on the basal surface of pRPE cells by adding C5b-6 complex, C7, C8 and C9 purified complement proteins in DMEM ± 200 µg/ml of dynasore. Cells were extracted and whole cell lysates were analysed by SDS-PAGE and western blotting. No changes were detected in the protein levels of claudin-19 and ZO-1 relative to GAPDH loading control.

4.11 Does inhibition of C5b-9 endocytosis affect the localisation of claudin-19?

Although western blotting showed that protein bands of claudin-19 and ZO-1 were unaffected by C5b-9, when endocytosis of the complex was blocked by dynasore, it was possible that these treatments could modulate junctional integrity by altering the

subcellular localisation of these proteins. To investigate this possibility immunofluorescence analysis was performed to cells treated with C5b-9 in the presence and absence of dynasore.

In untreated-cells (Figure 43-A_{i-ii}), vehicle control (Figure 43-B_{i-ii}), dynasore- (Figure 43-C_{i-ii}) and C5b-8-treated cells (Figure 43-D_{i-ii}) the pattern of claudin-19 protein expression was broadly similar. Cells treated with C5b-9 complex for 4 h (Figure 43-E_{i-ii}) demonstrated a much stronger and more specific staining for claudin-19 protein at the cell junctions. This observation is in line with results from Figure 39-D_{ii}, where cells treated with C5b-9 for 4 h, demonstrated a stronger and more specific pattern of claudin-19 staining. On the other hand, claudin-19 staining in C5b-9-treated cells for 24 h (Figure 43-F_{i-ii}) and C5b-9 + dynasore-treated cells for 24 h (Figure 43-G_{i-ii}) was similar to that in all four control samples.

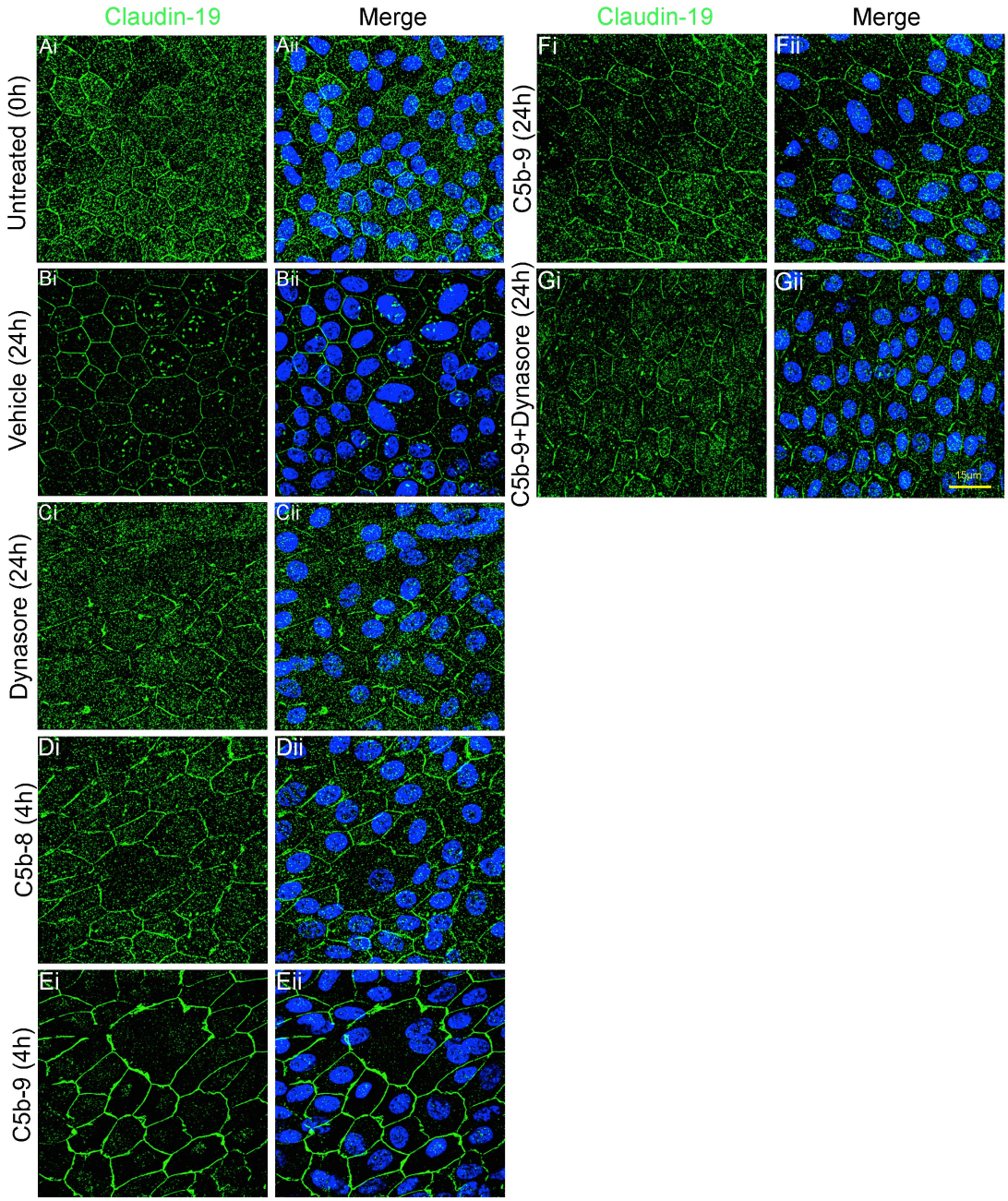

Figure 43. Claudin-19 expression in pRPE cells in which C5b-9 complex endocytosis has been arrested. To the apical chamber of all samples only DMEM was added. Four different controls were used: pRPE cells growing in 1 % FBS DMEM (A_{i-ii}), cells incubated with DMEM + DMSO (B_{i-ii}), cells incubated with DMEM + 200 µg/ml of dynasore (C_{i-ii}) and C5b-8-treated cells (D_{i-ii}). For C5b-8 formation, C5b-6 complex, C7 and C8 proteins were added in DMEM, on the basal chamber of the trans-well, for 4 h. In pRPE cells, C5b-9 complex was allowed to form on the basal surface by adding C5b-6 complex, C7, C8 and C9 purified complement proteins in DMEM for 4 h (E_{i-ii}). Also, pRPE cells were incubated with C5b-6 complex, C7, C8 and C9 purified complement proteins in DMEM ± 200 µg/ml of dynasore for 24 h (F_{i-ii} and G_{i-ii}, respectively). Claudin-19 protein levels (green staining) remained stable, except from C5b-9-treated cells for 4 h, where claudin-19-specific staining appeared to be stronger and more specific. Blue staining represents DAPI. Scale bar represents approximately 15µm.

4.12 Does C5b-9 complex formation influence expression of CD59 and DAF?

As CD59 and DAF are two well-characterised negative regulators of the complement system (Tomlinson, 2006, Brodbeck et al., 2000), it was examined whether expression of either of these two membrane-bound regulators is altered in response to the *in vitro* assembly of C5b-9 complex in pRPE cells. Western blot analysis revealed no significant changes in protein levels of DAF (Figure 44A) or CD59 (Figure 44B) in the various conditions.

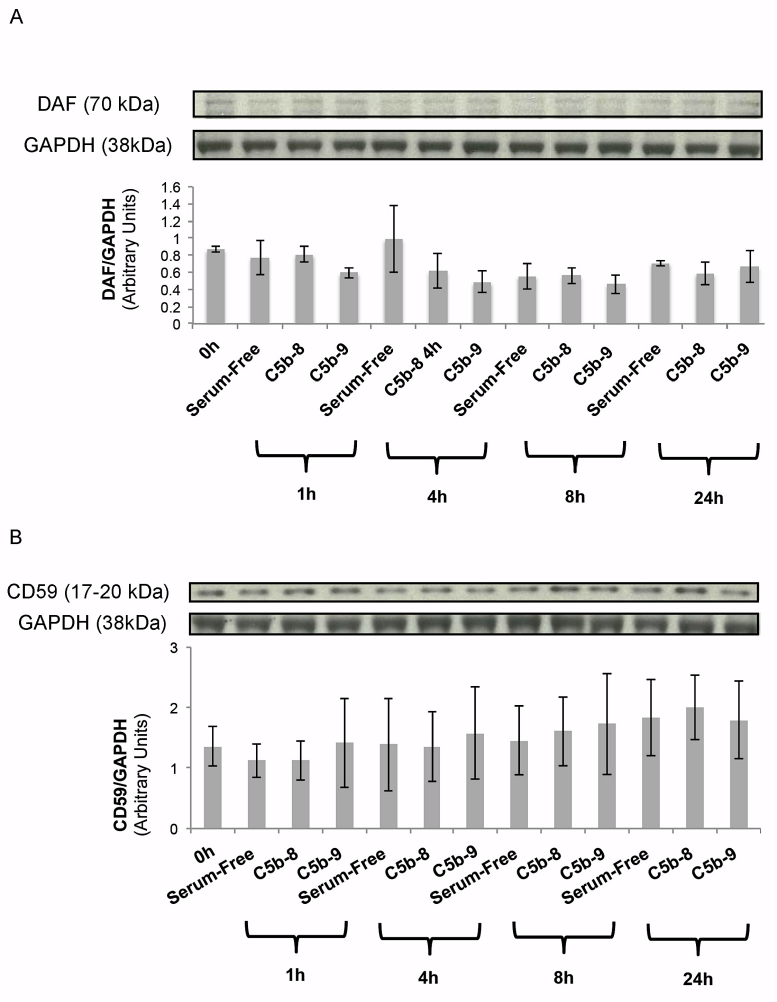

Figure 44. C5b-9 assembly does not affect protein expression of CD59 and DAF. On the apical chamber of all samples only DMEM was added. Two different controls were used: pRPE cells growing in DMEM (serum-free conditions) on both apical and basal chambers, and C5b-8-treated cells. For C5b-8 formation, C5b-6 complex, C7 and C8 proteins were added in DMEM, on the basal chamber of the trans-well, for 1 h, 4 h, 8 h and 24 h. C5b-9 was allowed to form on the basal surface of these cells by adding C5b-6 complex, C7, C8 and C9 purified complement proteins in DMEM, for 1 h, 4 h, 8 h and 24 h. Cells were extracted and whole cell lysates were analysed by SDS-PAGE and western blotting. Western blotting did not reveal any alteration in protein expression of both DAF (A) and CD59 (B) complement negative regulators between the different conditions relative to GAPDH loading control. Histograms of band intensities were generated by densitometric scanning of the western blots, with normalisation to the loading controls. Each bar represents the average values derived from three wells from three independent experiments. Data expressed as mean ± SEM.

4.13 Does prolonged presence of C5b-9 complex affect protein levels of DAF and CD59 complement negative regulators?

To extend the studies in Section **4.12** it was tested whether the combination of C5b-9 + dynasore would have any effect on the expression of DAF and CD59. Blot analysis revealed no alterations in the protein levels of both CD59 and DAF (Figure 45).

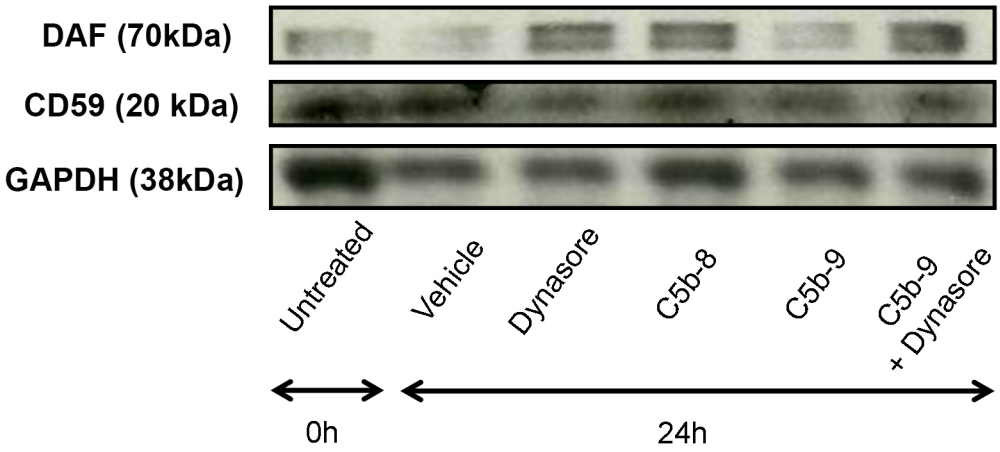

Figure 45. Prolonged presence of C5b-9 complex does not affect CD59 and DAF protein levels in pRPE cells. To the apical chamber of all samples only DMEM was added. Four different controls were used: pRPE cells growing in 1 % FBS DMEM media (Untreated), cells incubated with DMEM + DMSO (Vehicle), cells incubated with DMEM + 200 μg/ml of dynasore and C5b-8-treated cells. For C5b-8 formation, C5b-6 complex, C7 and C8 proteins were added in DMEM to the basal chamber of the trans-well for 24 h. C5b-9 was formed on the basal surface of pRPE cells by adding C5b-6, C7, C8 and C9 purified complement proteins in DMEM ± 200 μg/ml of dynasore for 24 h. Cells were extracted and whole cell lysates were analysed by SDS-PAGE and western blotting. No changes were detected in the protein levels of CD59 and DAF relative to GAPDH loading control.

4.14 Effect of the C5b-9 complex on pRPE cell mitochondria

RPE cells are highly metabolically active and in order to function properly it is essential that their cytoplasm is rich in mitochondria (Jarrett et al., 2008). Mitochondrial dysfunction has been linked to AMD, as previous research demonstrated that mitochondria derived from RPE cells from AMD patients are reduced in numbers, suffer from mtDNA mutations, have altered morphology and have changes in their content of proteins essential for protein trafficking (Feher et al., 2006, Nordgaard et al., 2008).

The aim of this experiment was to investigate whether C5b-9 affects mitochondria in pRPE cells. For the purpose of this experiment Mitotracker® Red CMXRos was administered. Mitotracker® labels mitochondria within live cells (Chazotte, 2011). On the basal surface of confluent pRPE cells grown in 12-well trans-well plates, C5b-9 complex was allowed to form in the presence and absence of dynasore for 24 h. On the apical chamber of all samples, where only DMEM was added, Mitotracker® Red CMXRos was added in the media for 30 min. Then cells were washed with sterile PBS, fixed with 4 % PFA and processed for immunofluorescence (Section **2.9**).

Fluorescence analysis of the Mitotracker®-specific staining (red staining), in Figure 46, demonstrated that C5b-9 complex alone at 24 h (Figure 46-$D_{i,iii}$) did not cause any discernable changes to gross mitochondria-associated fluorescence, when compared with either of the control samples (Figure 46-$A_{i,iii}$, -$B_{i,iii}$, -$C_{i-,iii}$). However, when endocytosis of C5b-9 complex was blocked with dynasore for 24 h (Figure 46-$E_{i,iii}$) the Mitotracker®-specific staining was greatly reduced. The histogram quantifies (Figure 46-F) the Mitotracker® staining from one independent experiment (three different Z-sections per sample per experiment). This observation suggests that the prolonged presence of C5b-9 complex on the basal surface of pRPE cells reduces either mitochondrial numbers and/or mitochondrial integrity.

However, the precise mechanism of how Mitotracker® accesses the cytoplasm of live RPE cells and how it recognises metabolically active mitochondria is currently not well understood. Therefore, in order to validate findings from Figure 46 the same studies were performed, but this time using a marker for an integral mitochondrial protein.

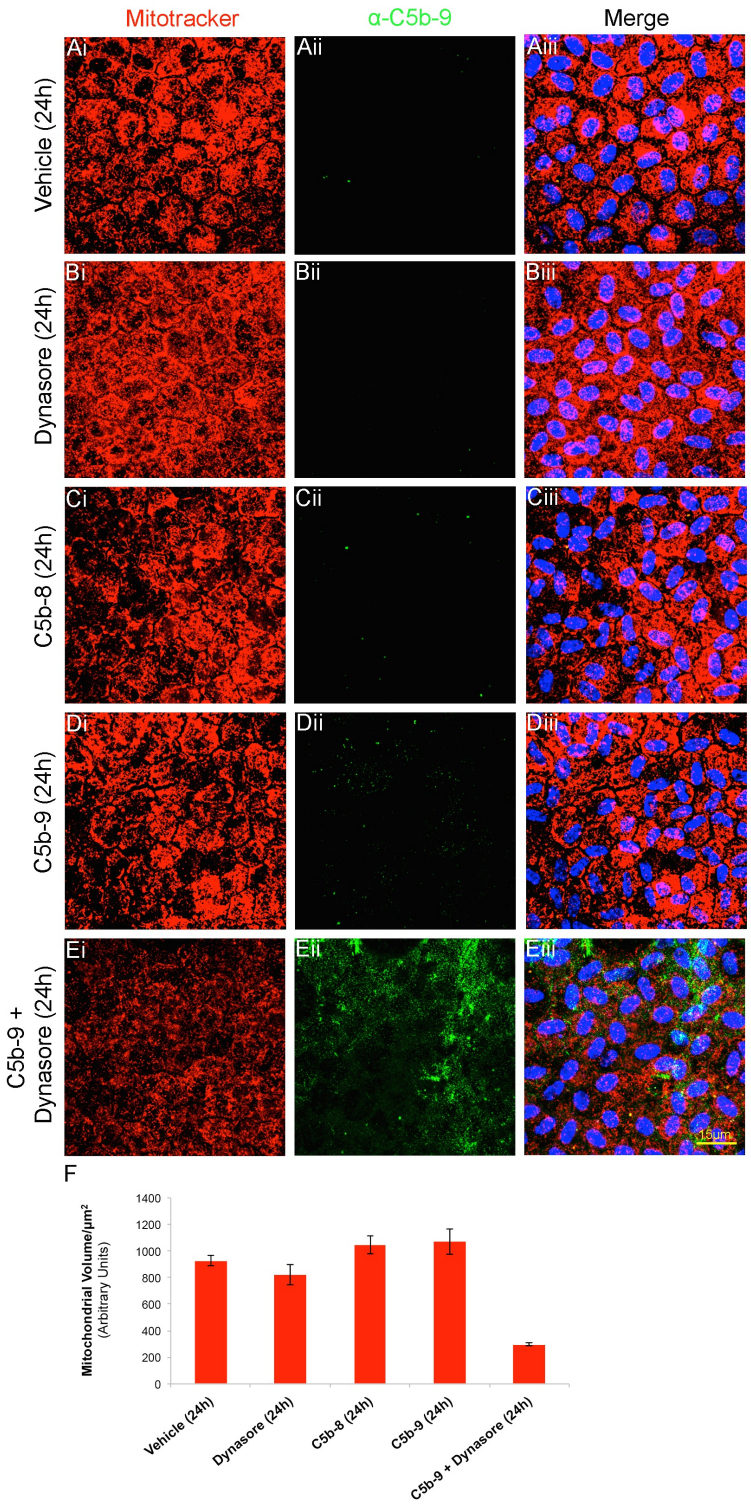

Figure 46. Prolonged presence of C5b-9 reduces Mitotracker® staining in pRPE cells. To the apical chamber of all samples only DMEM was added. Three different controls were used: pRPE cells incubated with DMEM + DMSO (A_{i-iii}), cells incubated with DMEM + 200 µg/ml of dynasore (B_{i-iii}) and C5b-8-treated cells (C_{i-iii}). For C5b-8 formation, C5b-6 complex, C7 and C8 proteins were added in DMEM, on the basal chamber of the trans-well for 24 h. In pRPE cells, C5b-9 complex was allowed to form on the basal surface by adding C5b-6 complex, C7, C8 and C9 purified complement proteins in DMEM for 24 h (D_{i-iii}). Also, pRPE cells were incubated with C5b-6 complex, C7, C8 and C9 purified complement proteins in DMEM + 200 µg ml of dynasore for 24 h (E_{i-iii}). Mitotracker® Red CMXRos (red staining) was added in the media of all samples, 30 min before cells were fixed. C5b-9 complex formation at 24 h ($D_{i,iii}$) did not affect mitochondrial staining when compared to any of the control samples ($A_{i,iii}$, $B_{i,iii}$, and $C_{i,iii}$) according to the Mitotracker® staining. However, when endocytosis of C5b-9 complex was arrested, mitochondrial staining was greatly reduced ($E_{i,iii}$). The histogram (F) quantifies the above observations. Each bar represents the average fluorescence volume specific to the Mitotracker® staining derived from three z-sections per sample from one independent experiment. Data expressed as mean ± SEM. Blue staining represents DAPI. Scale bar represents approximately 15µm.

4.15 C5b-9 complex reduces Tim23 staining in pRPE cells

The aim of this study was to validate the findings from Section **4.14**. The interplay between C5b-9 complex formation and mitochondrial integrity was examined by staining mitochondria for Tim23. Tim23 is a mitochondrial translocase, a member of the TIM23 complex, essential for protein import in mitochondria (Donzeau et al., 2000). Tim23 spans the inner and outer mitochondrial membranes in order to function and therefore its stability in mitochondria makes Tim23 an ideal protein for these studies (Donzeau et al., 2000).

To perform these studies, confluent pRPE cells (passage 1) were used. In untreated cells (Figure 47-A_{i-ii}), vehicle control (Figure 47-B_{i-ii}), dynasore- (Figure 47-C_{i-ii}) and C5b-8-treated cells (Figure 47-D_{i-ii}) Tim23 staining remained constant. Cells treated with C5b-9 for 24 h (Figure 47-E_{i-ii}) also demonstrated similar intensity of Tim23-staining to the above controls. On the other hand, Tim23 staining in C5b-9 + dynasore-treated cells (Figure 47-F_{i-ii}) was greatly reduced, consistent with the Mitotracker® staining in Figure 46. Quantification (Figure 47-G) of these images confirms that blocking endocytosis of C5b-9 leads to a significant (P<0.001) reduction in Tim23 staining. Each bar represents the fluorescence specific to the Tim23 staining from three independent experiments (four different Z-sections per sample per experiment).

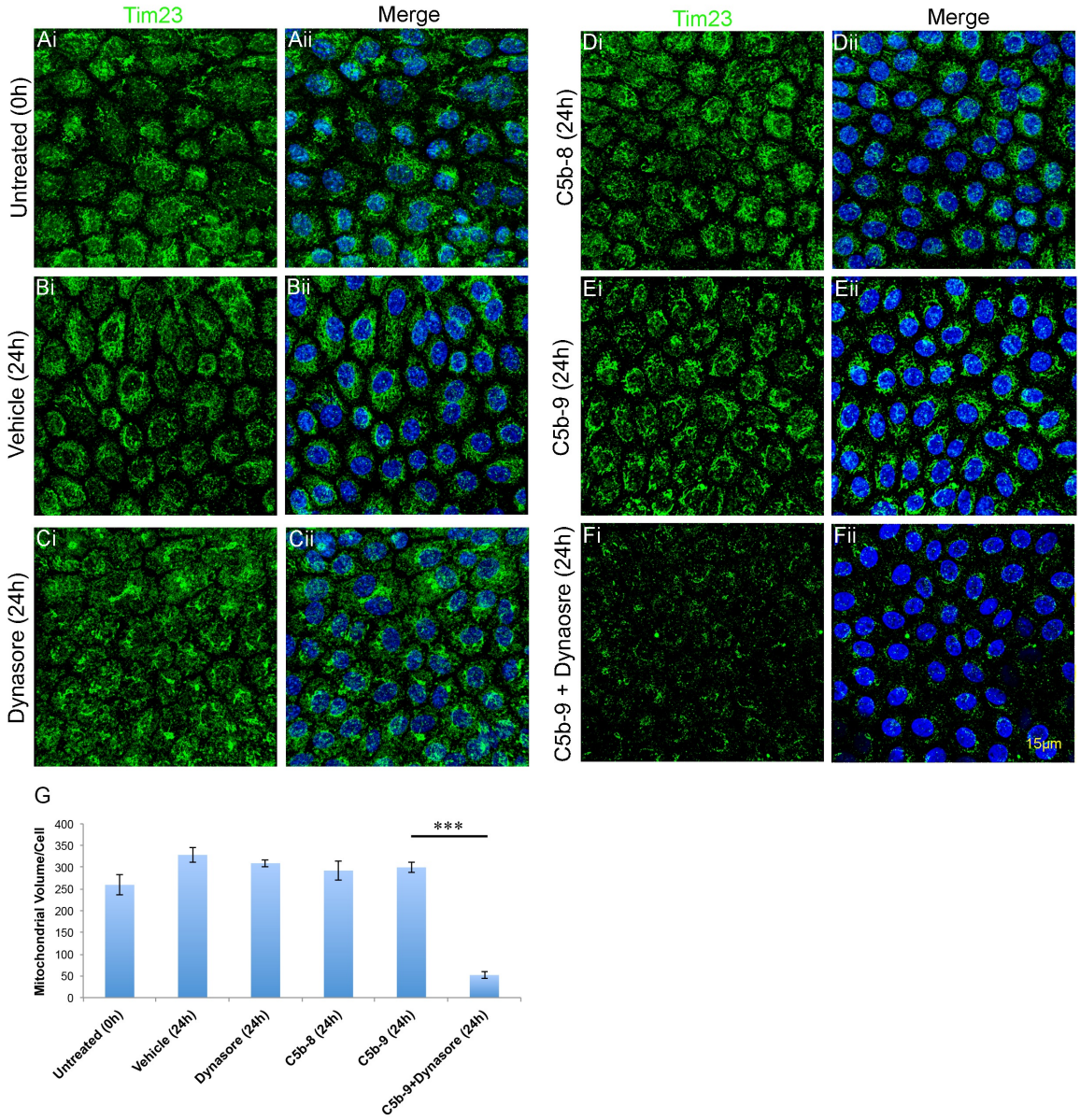

Figure 47. C5b-9 complex reduces Tim23 staining in pRPE cells. To the apical chamber of all samples only DMEM was added. Four different controls were used: pRPE cells growing in 1 % FBS DMEM (A_{i-ii}), cells incubated with DMEM + DMSO (B_{i-ii}), cells incubated with DMEM + 200 µg/ml of dynasore (C_{i-ii}) and, C5b-8-treated cells (D_{i-ii}). For C5b-8 formation, C5b-6 complex, C7 and C8 proteins were added in DMEM, on the basal chamber of the trans-well for 24 h. pRPE cells were incubated with C5b-6 complex, C7, C8 and C9 purified complement proteins in DMEM ± 200 µg/ml of dynasore for 24 h (E_{i-ii} and F_{i-ii}, respectively). Tim23 protein levels (green staining) were similar in all samples, except for C5b-9 + dynasore-treated cells (F_{i-ii}), where Tim23-specific staining was greatly reduced. The histogram quantifies these observations (G). Each bar represents the fluorescence specific to the Tim23 staining from three independent experiments (four different Z-sections per sample per experiment). Data expressed as mean ± SEM, ***P<0.001. Blue staining corresponds to DAPI. Scale bar represents approximately 15µm.

4.16 The C5b-9 complex reduces mitochondria numbers in pRPE cells

Although immunofluorescence analysis of Tim23 and Mitotracker® staining suggests that the prolonged presence of the C5b-9 complex (induced by dynasore) decreases the mitochondrial content of pRPE cells, these studies do not give any information about actual mitochondria numbers.

To investigate whether the C5b-9 complex on the basal surface of pRPE cells affects the number of mitochondria, electron microscopy (EM) was performed (Section **2.12**) in order to permit mitochondria counting.

EM analysis provided ultra-structural information about general RPE cell morphology and mitochondria numbers (Figure 48, 49). Overall, pRPE cells under all control conditions retained a normal phenotype. However, pRPE cells treated with complement proteins and dynasore for 24 h demonstrated clear abnormalities, with cells containing large vacuolar structures and fewer mitochondria. Quantification of mitochondria in these samples confirmed a reduction in mitochondria number in cells treated with C5b-9 + dynasore, and also in cells treated with C5b-9 alone (Figure 50).

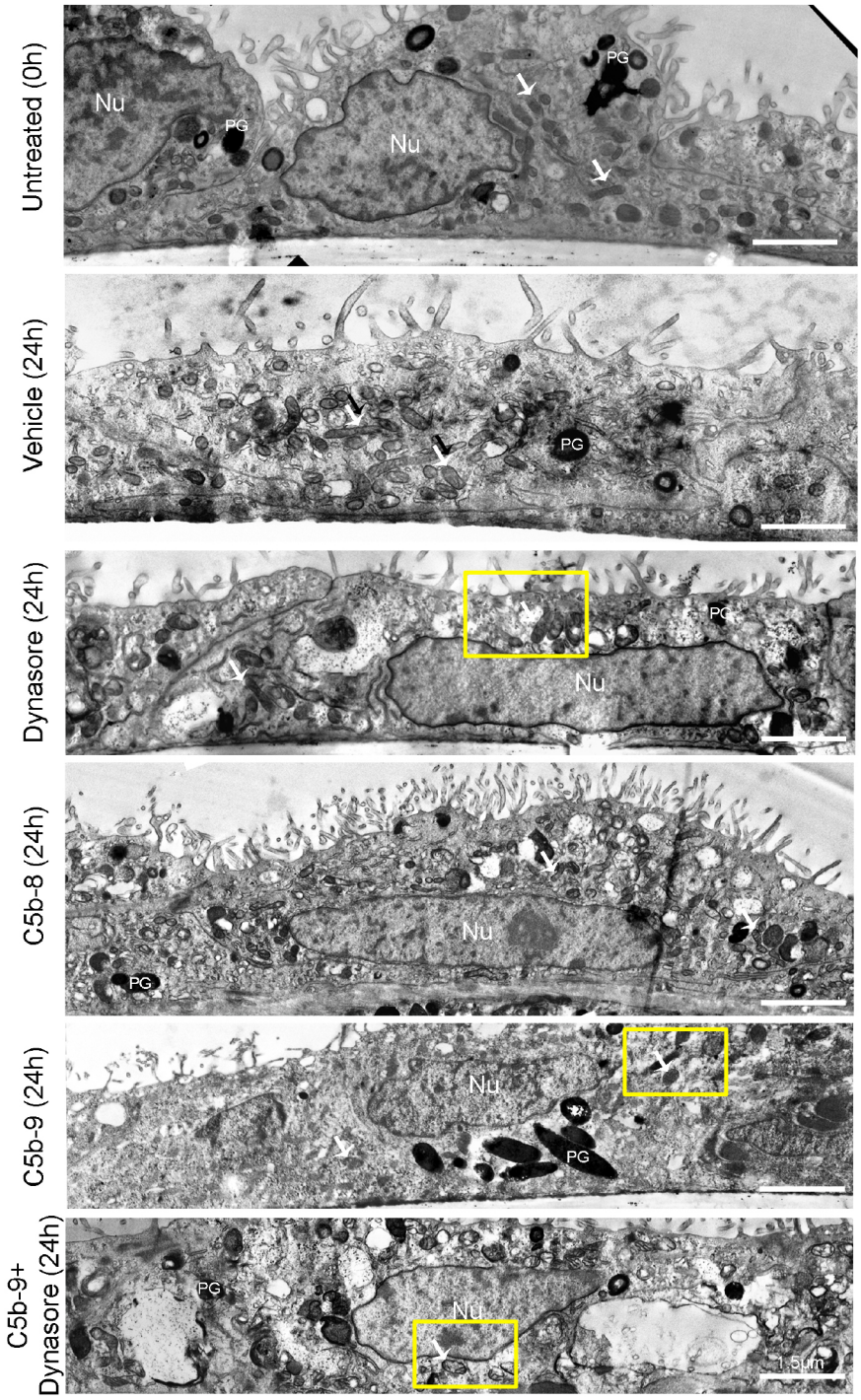

Figure 48. Effect of C5b-9 on mitochondria numbers in pRPE cells. To the apical chamber of all samples only DMEM was added. Four different controls were used: pRPE cells growing in 1 % FBS DMEM media, cells incubated with DMEM + DMSO, cells incubated with DMEM + 200 µg/ml of dynasore and C5b-8-treated cells. For C5b-8 formation, C5b-6 complex, C7 and C8 proteins were added in DMEM, on the basal chamber of the trans-well for 24 h. pRPE cells were incubated with C5b-6 complex, C7, C8 and C9 purified complement proteins in DMEM ± 200 µg/ml of dynasore for 24 h. C5b-9 + dynasore-treated cells developed a less healthier phenotype. C5b-9- and C5b-9 + dynasore-treated cells displayed a decline in mitochondria numbers. Scale bars represent approximately 1.5µm. Nu, Nucleus ; PG, Pigment Granule. Yellow boxes refer to high power images in Figure 48. Sample processing for EM was performed by Dr. Thomas Burgoyne, UCL Institute of Ophthalmology.

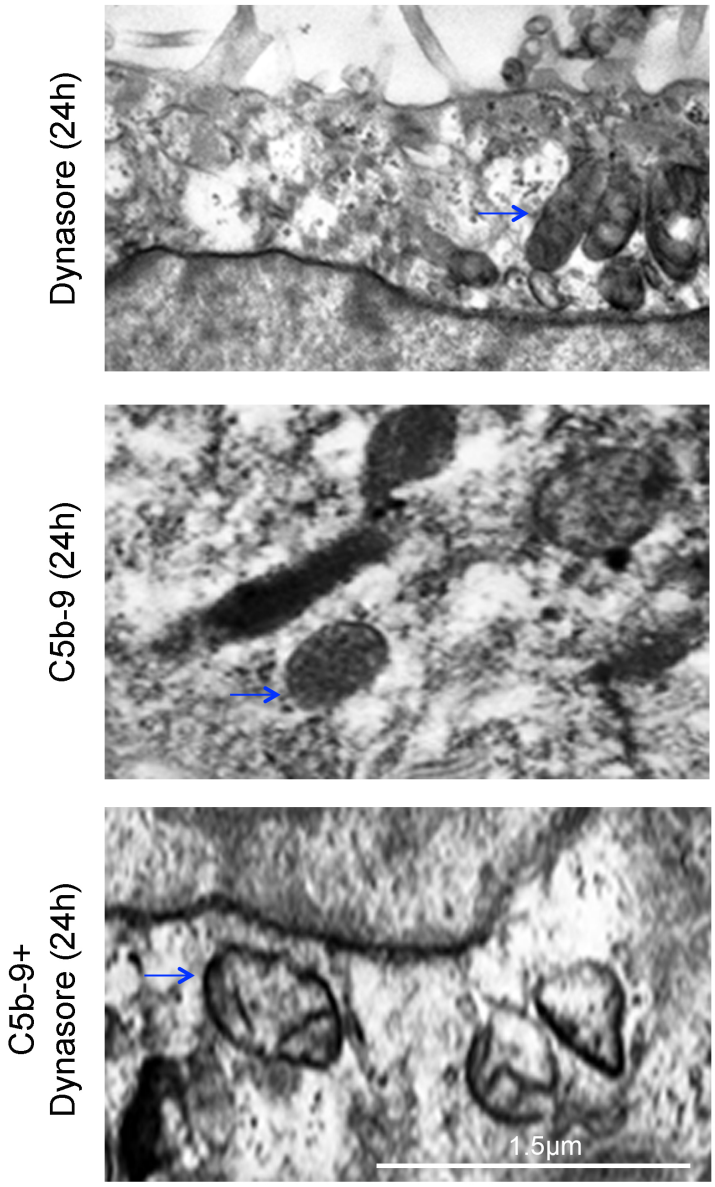

Figure 49. High power images of mitochondria from pRPE cells. High power images of mitochondria from pRPE cells treated with DMEM ± 200 µg/ml of dynasore alone, C5b-9 and C5b-9 + dynasore for 24 h, as described in detail in the legend of Figure 47. The structure of mitochondria (blue arrow) appeared to be adversely affected from the simultaneous presence of C5b-9 + dynasore when compared to mitochondria structure of pRPE cells treated either with C5b-9 or dynasore alone. Scale bars represent approximately 1.5µm. Nu, Nucleus; PG, Pigment Granule. Sample processing for EM was performed by Dr. Thomas Burgoyne, UCL Institute of Ophthalmology.

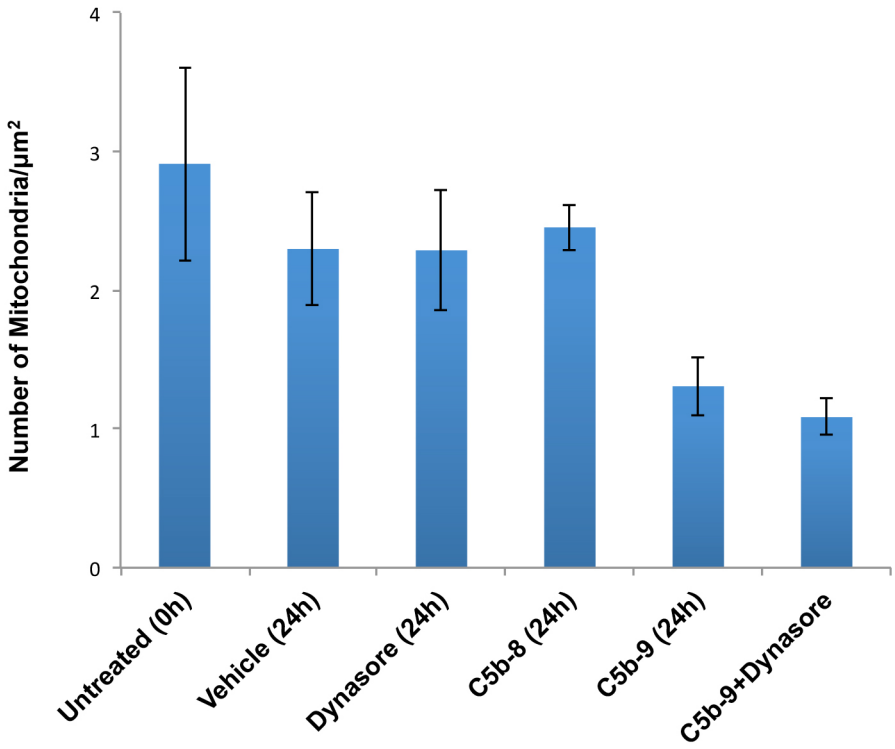

Figure 50. C5b-9 reduces mitochondria numbers in pRPE cells. The histogram provides quantitative analysis of the images in Figure 47. C5b-9- and C5b-9 + dynasore-treated cells reported a decline in mitochondria numbers. Each bar in the histogram represents the average number of mitochondria counted in pRPE cells from five different sections, from one independent experiment. Data expressed as mean ± SEM. Counting of mitochondria was performed with ImageJ freeware.

4.17 Western blot analysis of Tim23 and cytochrome C in C5b-9-treated pRPE cells

Immunofluorescence analysis (Section **4.15**) of Tim23 protein suggested that C5b-9 reduces expression of this protein in the presence of dynasore. To investigate this further, the protein levels of Tim23 and cytochrome C were examined by western blotting in pRPE cells exposed to C5b-9 + dynasore. Cytochrome C is attached to the inner membrane of mitochondria where it promotes electron transfer (Sanghera and Pinheiro, 2000). Its release from mitochondria indicates the initiation of apoptosis, during which, permeability of the outer and inner membranes increases and therefore leads to mitochondrial swelling and rupture (Ott et al., 2002).

Western blot analysis did not reveal any significant expression changes either in Tim23 or cytochrome C protein levels (Figure 51). These results suggest that whilst C5b-9 in the presence of dynasore causes loss of mitochondrial enrichment of Tim23, the protein is still present at normal levels in the RPE cells.

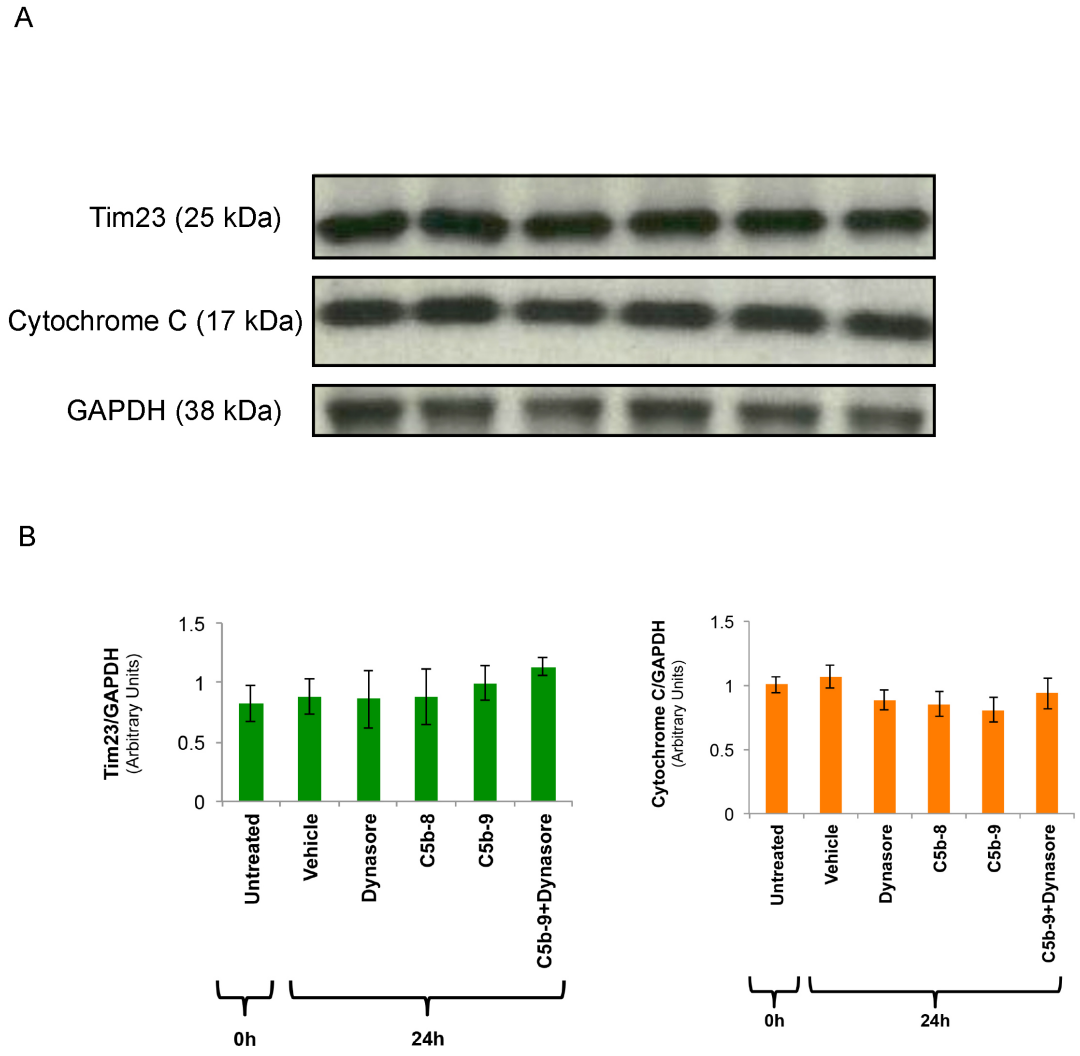

Figure 51. Western blot analysis of Tim23 and cytochrome C in C5b-9-treated pRPE cells. To the apical chamber of all samples only DMEM was added. Four different controls were used: pRPE cells growing in 1 % FBS DMEM (Untreated), cells incubated with DMEM + DMSO (Vehicle), cells incubated with DMEM + 200 µg/ml of dynasore and C5b-8-treated cells. For C5b-8 formation, C5b-6 complex, C7 and C8 proteins were added in DMEM, on the basal chamber of the trans-well for 24 h. pRPE cells were incubated with C5b-6 complex, C7, C8 and C9 purified complement proteins in DMEM ± 200 µg/ml of dynasore for 24 h. Cells were extracted and whole cell lysates were analysed by SDS-PAGE and western blotting (A). Blots were scanned and densitometric analysis yielded the respective histograms (B). No significant changes either in Tim23 or cytochrome C protein levels were observed. GAPDH was used as a loading control. Results were derived from three independent experiments. Data expressed as mean ± SEM. Blots were quantified by using Image J freeware.

4.18 - Discussion

- **Elimination of the C5b-9 complex by endocytosis**

Work in this chapter shows that when C5b-9 was allowed to form on the basal surface of pRPE cells it did so rapidly, being evident at 1 h, and almost absent again by 24 h (Figure 27, 28, respectively). These studies formed the starting point for a detailed examination of the formation and elimination of C5b-9 on the basal surface of pRPE cells. Administration of dynasore led to retention of the C5b-9 complex on the basal surface of pRPE cells at 24 h (Figure 31), showing that C5b-9 complex elimination from the basal surface can be largely attributed to endocytosis.

Endocytosis is one of several mechanisms that cells use to remove C5b-9. Previous research has demonstrated that some cell types survive C5b-9 attack by membrane vesiculation, a process that could involve exo-, ecto- and/or endo-cytosis (Figure 52) (Pilzer et al., 2005a, Lakkaraju et al., 2014). Thus, when Pilzer et al., (2005a) incubated K562 cells, a human erythroleukemic cell line, with 50 % complement-competent NHS, C5b-8 and C5b-9 complexes were expelled to the extracellular space via membrane vesiculation. Western blot and ELISA analysis demonstrated that even after 5 min exposure to complement-competent media, mortalin, known for its ability to bind C8 and C9 proteins, was released to cell media (Saar Ray et al., 2014). Other pore-forming molecules, such as streptolysin O did not induce release of mortalin, indicating the specificity of this protein for C8 and C9. This mortalin-dependent mechanism aids the clearance of the cell membranes from complement attack. When K562 cells were treated with anti-mortalin antibodies, prior to the addition of NHS, they lysed due to the insufficient clearance of C5b-9 complex.

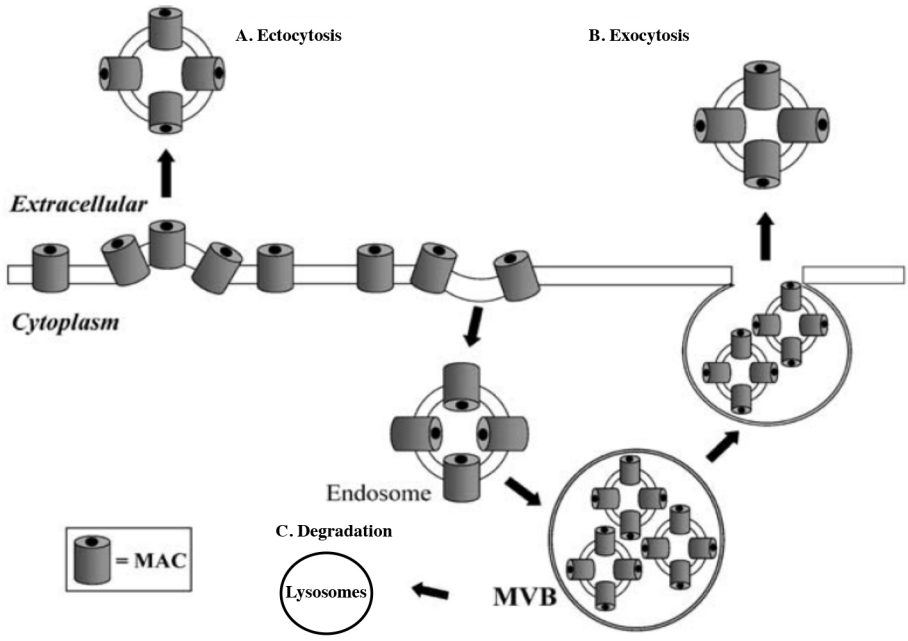

Figure 52. Schematic representation of the mechanism(s) of C5b-9 elimination. Some cell types, including RPE cells, use the process of membrane vesiculation to remove C5b-9 complex. Membrane vesiculation includes the processes of ecto-, exo- and/or endocytosis. Ectocytosis involves the removal of the membrane-bound C5b-9 to the extracellular space, whereas endocytosed C5b-9 can either return to the cell surface, from which becomes expelled (exocytosis) or gets degraded in lysosomes following its fusion with multi-vesicular bodies (MVB), in the cytoplasm. Image adapted from Pilzer et al., (2005a).

Live cell imaging and immunofluorescence analysis of C5b-9-treated cells shed more light on the membrane trafficking of the C5b-9 complex. Upon treatment of K562 cells with C9-deficient human sera and fluorescently-tagged C9 protein the C5b-9 complex was expelled from the cell surface via outward vesiculation. Simultaneously, C5b-9 complex was found in the perinuclear bodies along with fluorescently-tagged transferrin, as a result of inward vesiculation (Moskovich and Fishelson, 2007). The process of inward vesiculation was further examined by Moskovich et al., (2012), who demonstrated that endocytosis of C5b-9 complex is a dynamin-2 and caveolin-1 dependent process. Incubation of K562 cells with 60 or 80 μM dynasore for 30 min at 37 ^{o}C, inhibited the endocytosis of C5b-9 complex (Moskovich et al., 2012).

If it is assumed that outward vesiculation would be unaffected by dynasore, the results suggest that endocytosis is the major mechanism by which pRPE cells dispose of C5b-9. The quantitative immunofluorescence studies were further validated by immuno-gold labeling specific to C5b-9 (Figure 32). At 4 h most gold particles

specific to the α-C5b-9 antibody were enriched at the basal surface of pRPE cells (Figure 32). By 24 h these gold particles were almost all localised within the cytoplasm of pRPE cells, however their precise location, for instance lysosomes, could not be identified. Upon dynasore administration, C5b-9 did not become endocytosed but accumulated on the basal surface instead. Perhaps direct conjugation of gold particles to purified C9, instead of the α-C5b-9 antibody, could provide a better insight into the cellular trafficking of the C5b-9 complex. However, in the event of rapid lysosomal degradation of C5b-9 within pRPE cells, this method may also have limited sensitivity in identifying the fate of internalised C5b-9 complexes.

Overall, the above K562-related studies are in accordance with these pRPE studies. C5b-9 may assemble rapidly on the cell surface and it appears to be eliminated, primarily by endocytosis. It is worth noting in our studies that only a relatively high concentration of dynasore (200 μM) was able to inhibit the elimination of C5b-9 complex from the basal surface of cells (Figure 31). In pRPE cells lower concentrations of dynasore (80 μM) that are typically used in other cell types, did not inhibit endocytosis of C5b-9.

- **The C5b-9 complex and trans-epithelial resistance**

One striking and highly reproducible observation was that the C5b-9 complex increases TER in pRPE cells (Figure 33). Basal assembly of C5b-8 conferred the same effect on TER, however the magnitude of the increase was significantly lower than that observed with C5b-9. It was observed that apical C5b-9 complex formation also increased the TER (Figure 34) demonstrating that the effect of C5b-9 did not depend on its formation site.

Despite the consistency of our observations, they are at odds with what has previously been shown. TER measurements derived from both hfRPE and ARPE-19 cells incubated with hydrogen peroxide and complement-sufficient sera were reported to be significantly lower than TER measurements acquired from control cells (Bandyopadhyay and Rohrer, 2012, Thurman et al., 2009, Joseph et al., 2013). These studies led the authors to conclude that C5b-9 can disrupt monolayer integrity.

However, this C5b-9-induced decline in TER only occurred when ARPE-19 cells were first sensitised with hydrogen peroxide and then treated with complement proteins. Other studies have shown that C5b-9 on its own does not compromise TER in RPE cells (Lueck et al., 2012). These authors reported that when ARPE-19 cells grown on trans-well plates, were treated either with 2 % or 4 % complement-competent human sera at the basolateral surface for 24 h, TER remained stable.

One reported case in which TER was increased, was when ARPE-19 cells were exposed to endoplasmic reticulum (ER) stress, using either tunicamycin or thapsigargin (Yoshikawa et al., 2011). Although this study examined ER stress alone and did not consider complement or C5b-9, other studies in glomerular epithelial cells have shown that the C5b-9 complex has the capacity to induce ER stress. Here, C5b-9 increased the expression of two well-known ER-stress-related proteins: bip and grp94 (Cybulsky et al., 2002). The increase in TER observed in our studies in C5b-9-treated pRPE cells could therefore be a consequence of ER stress. However, to further support this notion, western blot and RT-PCR studies would need to be performed in order to examine the expression of ER-stress-related proteins and mRNA, respectively.

The above TER studies were combined with permeability assays using fluorescent dextrans to further investigate the integrity of the C5b-9-treated pRPE monolayer. Although using low and high molecular weight dextrans to detect changes in monolayer permeability is an established method (Balda et al., 1996, Phillips et al., 2008), in these studies, the method seemed to be less sensitive and yielded variable results.

To further examine the mechanism/s behind the C5b-9-induced TER increase, as observed in Figures 33 and 34, the expression of two junctional proteins was examined: claudin-19 and ZO-1. Claudin-19 is the most abundant junctional protein of the claudin family in RPE cells, therefore its expression was examined via western blotting and immunofluorescence in C5b-9-treated pRPE cells (Peng et al., 2011, Peng et al., 2012). Despite the failure of western blotting to demonstrate any differences in claudin-19 expression, immunofluorescence analysis detected a much stronger staining for claudin-19 at the cell junctions in C5b-9-treated cells at 4 h

(Figure 39). While no differences in claudin-19-specific staining were observed at 1 h, 8 h and 24 h, at 4 h claudin-19 staining appeared to be more specific in C5b-9-treated cells compared to the controls. As the increase in TER in C5b-9-treated pRPE cells is sustained from 1 h until 24 h (Figure 33) it is unclear whether this increase can be exclusively attributed to claudin-19, as western blotting did not detect any significant up-regulation of this protein at any of the timepoints examined. However, the fact that stronger junctional staining for claudin-19 was a reproducible result is noteworthy and could be in line with the findings of Yoshikawa et al., (2011) who showed that increased TER, due to ER stress, in ARPE-19 cells can be accompanied with an increase in the expression of several junctional proteins including ZO-1, occludin and claudin-1. Perhaps claudin-19 expression can be affected as well. Furthermore, the link between claudin-19 expression and a stable TER was established by Peng et al., (2011) who demonstrated that when claudin-19 was knocked down via small-interfering RNA (siRNA), in hfRPE cells, TER was greatly reduced. siRNAs for other claudins had only minor effects on the TER.

In combination with the claudin-19 studies, expression of ZO-1 was examined by western blotting and immunofluorescence. ZO-1 is essential for the homeostasis of the RPE monolayer, as its down-regulation may result in RPE dysfunction and monolayer breaks (Georgiadis et al., 2010). Therefore, it was a good candidate protein for a role in regulating TER in pRPE cells. However, western blotting (Figure 38-B) and immunofluorescence data (Figure 40) failed to identify any changes in ZO-1 expression that could account for the increased TER in C5b-9-treated pRPE cells.

Immunofluorescence analysis of samples obtained from AMD patients has previously shown the co-existence of human RPE cells with C5b-9, as this complex accumulates in drusen deposits, which are located between the RPE monolayer and the underlying Bruch's membrane (Anderson et al., 2002, Mullins et al., 2014). As not much is currently known about how RPE cells would respond to the sustained presence of C5b-9, the TER of pRPE cells was measured, whilst simultaneously blocking the endocytosis of C5b-9. The results in Figure 41 show that when dynasore is used to inhibit the internalisation of C5b-9 from the basal surface of pRPE cells, no C5b-9-induced TER increase was observed. These results show that it is the

endocytosis of C5b-9 that is linked to the change in TER rather than simply the assembly of C5b-9 on the basal cell surface. This is consistent with our further observation that C5b-9 assembly on the apical cell surface had the same effect on TER. Additionally, an increase in TER was observed during the formation and endocytosis of C5b-8 (regardless of its formation site), but to a lesser extent compared to C5b-9-treated pRPE cells, in both Figures 33 and 34. This finding suggests that the accumulation and therefore endocytosis of C5b-8 could influence TER as well, but C9 is the key protein to increase TER even further. The etiology for this observation is currently unknown and needs to be further investigated.

In summary, C5b-8 and C5b-9 both increased the TER of the RPE monolayer. However, whilst western blotting did not reveal any up-regulation of either ZO-1 and/or claudin-19 in C5b-9-treated cells, claudin-19 immunostaining appeared more aligned with cell junctions. C5b-9 might enhance the *de novo* synthesis of other proteins, whose expression was not examined during this project, or as C5b-9 has previously been shown to up-regulate ER-stress proteins, these proteins could in turn regulate TER via modulation of other factors.

- **Expression of DAF and CD59 in C5b-9-treated pRPE cells**

CD59 and DAF are widely expressed membrane-bound glycoproteins, that have been shown in ARPE-19 cells to be located on the apical and basolateral surfaces, and have the ability to prevent C5b-9-induced cell damage (Ma et al., 2010, Davies et al., 1994, Thurman et al., 2009). CD59 is a 17-20 kDa glycoprotein that prevents the assembly of C5b-9 complexes by binding either to the alpha-subunit of C8 in the C5b-8 complex and/or to the beta-subunit of C9 in C5b-9 (Tomlinson, 2006, Davies et al., 1989, Watson et al., 2014). It can be found either as a membrane-bound protein in several cell types and/or as a soluble protein in body fluids (Qin et al., 2005). CD59 expression needs to be regulated as its over-expression may lead to tumour development, while its absence can lead to severe anemias (Li et al., 2013, Motoyama et al., 1992). DAF is a 70 kDa glycoprotein responsible for the accelerated decay of the C5 and C3 convertases, C4b2a and C3bBb, by attaching either to the C4b or C3b units respectively (Nishikawa et al., 1998, Medof et al., 1984). Its depletion can lead to intravascular haemolysis and platelet activation in humans (Martinez-Hervas et al., 2014).

We therefore hypothesised that the C5b-9 complex would up-regulate the expression of these complement negative regulators in pRPE cells, possibly as part of a defense mechanism against a potentially harmful insult. However, our studies failed to identify any significant change in expression of CD59 or DAF in response to C5b-9, and although the expression of these proteins on RPE cells is well-documented, there is limited information about how these negative regulators are affected by C5b-9. It has previously been shown that when endothelial cells (ECs) were treated with 2.5 % NHS, DAF was significantly up-regulated (Mason et al., 1999). Sensitisation of ECs with a cytokine cocktail prior to the addition of the NHS, increased protein levels of DAF even further. However, it is unknown whether the complement system has a direct effect on the expression of DAF and/or CD59 in the RPE. Pro-inflammatory cytokines are able to up-regulate CD59, DAF and CD46 in human and mouse RPE cells and human hepatoma cells (Yang et al., 2009, Spiller et al., 2000). On the other hand, Lueck et al., (2011) showed that incubation of ARPE-19 cells with 5 % NHS for 1 h triggered the production and release of several pro-inflammatory cytokines (IL-6 and IL-8), VEGF and MCP-1. Therefore there could be a regulatory loop in which C5b-9 increases the production and release of pro-inflammatory cytokines and growth factors, which in turn up-regulate the complement negative regulators.

- **C5b-9-induced mitochondrial stress**

Modifications in mitochondrial number, size, cristae architecture, matrix density and mitochondrial membrane integrity have been observed, via electron microscopy, in the RPE derived from AMD patients (Feher et al., 2006). These findings are supported by studies in aging RPE cells (RPE cells from 62-year-old individuals), in which mitochondrial dysfunction was associated with impaired ATP production and the down-regulation of mitochondrial proteins (He and Tombran-Tink, 2010). Further evidence supporting the link between mitochondrial damage and AMD emerged from analysis of aging retinas from AMD patients that revealed high levels of large mtDNA deletions and rearrangements in the AMD-affected RPE (Barreau et al., 1996, Udar et al., 2009, Kenney et al., 2010). In fact, it was reported that AMD patients not only have mtDNA damage to a much larger extent than age-matched controls but they also have changes in proteins associated with mitochondrial

translation, nuclear transport and adenosine triphosphate synthase activity, in their RPE (Karunadharma et al., 2010).

Although AMD pathogenesis is linked with mitochondrial alterations in the aged RPE, it is currently unknown whether C5b-9 (a constituent of drusen) has an immediate effect on mitochondrial integrity and/or mitochondrial numbers. A single previous study reported that in C5b-9-treated Ehrlich ascites tumor cells, the inner mitochondrial membrane potential ($\Delta\Psi_m$) was compromised soon after C5b-9 complex assembly (Papadimitriou et al., 1994). However, the direct effect of C5b-9 complex on mitochondria in RPE cells remains to be elucidated.

In the initial experiments, Mitotracker® CMX Red was used to stain the mitochondria of RPE cells while endocytosis of C5b-9 was arrested with dynasore (Figure 46). While the C5b-9 complex did not seem to have a direct effect on mitochondria, under control conditions its prolonged presence greatly reduced the Mitotracker®-specific fluorescence staining suggesting that maintenance of C5b-9 at the cell surface might have an effect on mitochondrial number and/or integrity.

Mitotracker® is a mitochondrial-specific fluorescent dye, commonly used in confocal microscopy. It has been used in the past to demonstrate mitochondrial fragmentation after the treatment of human RPE cells (derived from 62-76-year-old donors) with hydrogen peroxide (He et al., 2010). It has the capacity to covalently bind to mitochondrial proteins once it accumulates in the mitochondrial matrix (Presley et al., 2003). This covalent bond occurs via any free thiol groups of cysteine residues within mitochondrial proteins. Therefore, proteins that do not possess free thiol groups will not react with Mitotracker®, potentially causing a reduction of fluorescence.

To address this possible concern the experiment was repeated but this time staining mitochondria with a Tim23 antibody (Figure 47). As previously discussed (Section **4.15**), Tim23 is an essential member of a large channel-forming complex, responsible for protein transportation inside mitochondria (Pareek et al., 2013). It spans the outer and inner mitochondrial membranes and therefore its stability in mitochondria established this protein as a good target to examine mitochondrial

integrity (Donzeau et al., 2000). Tim23 staining demonstrated similar results to those obtained with Mitotracker®, as it was markedly reduced when endocytosis of C5b-9 was blocked.

Proteomic analysis of the human RPE, isolated from AMD patients, revealed that aged RPE cells, compared to control samples, were characterised by alterations in their protein content (Nordgaard et al., 2008). More specifically, several key mitochondrial proteins, essential for mitochondrial translation (Factor Tu), import of nuclear-encoded proteins (Hsp70) and ATP synthesis (α-, β- and δ-subunits of ATP synthase) were down-regulated. With regards to Tim23, it has previously been shown that in HeLa cells, when Tim23 was depleted with siRNA, cell proliferation and long-term cell survival were inhibited (Goemans et al., 2008). Depletion of Tim23 led to mitochondrial self-destruction and therefore it was hypothesised that this protein is necessary for mitochondrial biogenesis and therefore cell viability. Although C5b-9 did not cause cell death in pRPE cells (as discussed in chapter 3), down-regulating Tim23 expression in mitochondria, might be a sign of cell stress due to the constant presence of complement.

As the data in Figures 46 and 47 did not provide any information about mitochondria numbers between control and C5b-9-treated cells, electron microscopy (EM) studies were performed. Data from Figures 48, 49 and 50 show that C5b-9-treated pRPE cells (either treated with dynasore or not) appear to have fewer mitochondria. Also, the cell morphology of C5b-9 + dynasore-treated cells exhibited a number of abnormal ultra-structural features that were not observed in dynasore-treated cells, confirming that the prolonged presence of C5b-9 may stress pRPE cells. Unfortunately, EM studies did not permit the clear examination of intra-mitochondrial structures (integrity of mitochondrial membranes, matrix and cristae), however the observed reduction in mitochondrial numbers is in accordance with findings from Feher at el., (2006) who demonstrated that RPE cells derived from AMD patients had reduced numbers of mitochondria.

To extend these studies, the expression levels of Tim23 and cytochrome C in C5b-9-treated pRPE cells (Figure 51) were investigated by western blotting. Cytochrome C is located in mitochondria and is responsible for electron transport between the outer

and inner mitochondrial membranes (Goodsell, 2004). No differences in the expression levels either of Tim23 or cytochrome C were detected between control and C5b-9-treated pRPE cells. The lack of correlation between the Tim23 western blot data (Figure 51) and the Tim23 immunofluorescence data (Figure 47) might indicate that Tim23 is released from or not targeted to mitochondria, yet remains in the cell cytosol. Any differences in exposure of the antigen binding sites on Tim23 between the two different methods may also contribute to different results.

With regards to cytochrome C, immunofluorescence analysis and confocal microscopy may have been a more efficient method of detecting any expression and localisation changes in pRPE cells. It has previously been demonstrated that induction of cell apoptosis in RPE cells (ARPE-19s and human RPE cells), via chemical reagents, resulted in the release of cytochrome C in the cytoplasm (Zhang et al., 2003, Jin et al., 2005). In the event of cytochrome C release in C5b-9-treated pRPE cells, perhaps immunofluorescence would have been able to demonstrate the re-location of cytochrome C within pRPE cells. A possible re-location of cytochrome C due to the presence of complement, (as a sign of cell apoptosis) would not necessarily be expected to be accompanied by changes in protein expression levels. Staining of cytochrome C, via immunofluorescence, was performed in this study however, the available antibodies that were tested at the time did not yield specific staining.

Chapter 5

5. C5b-9 and retinal phagocytosis

5.1 Preliminary phagocytosis studies in C5b-9-treated pRPE cells

One of the specialised functions of RPE cells is the maintenance of the visual cycle, during which, all-*trans*-retinal is converted back to 11-*cis* retinal (McBee et al., 2001). This biochemical process ensures that photoreceptors preserve their excitability and this can only be accomplished via phagocytosis of the POS from the underlying RPE monolayer (Lamb and Pugh, 2004). Once the re-isomerisation of retinal occurs, 11-*cis* retinal returns back to the photoreceptors (Baehr et al., 2003).

It has previously been shown, in C5b-9-treated glomerular epithelial cells (GECs), that the C5b-9 complex has the capacity to regulate the actin cytoskeleton by up-regulating RhoA, a small GTPase, necessary for actin organisation (Zhang et al., 2007, Sit and Manser, 2011). Knowing that the binding and internalisation of POS from the RPE requires actin remodelling we asked here whether C5b-9 can affect the process of POS phagocytosis (Hayes et al., 2009, Law et al., 2009, Anderson et al., 2002).

To investigate this, C5b-9-treated pRPE cells were incubated with fluorescently-tagged POS. One advantage of the experimental model developed in chapters 3 and 4 is that it allows assembly of C5b-9 on the basal RPE cell surface, with simultaneous delivery of POS to the apical surface, thus replicating the compartmentalisation of activities encountered by RPE cells *in vivo*. In more detail, in confluent pRPE cells, C5b-9 was allowed to form *in vitro* as described earlier in method $\mathbf{D_T}$ (section **2.5.4.1**) 1 h prior to the addition of POS. In the meantime, fluorescently-tagged POS were prepared and used as described in section **2.7**, however at this stage the sonication and the washing steps were eliminated. Therefore POS were conjugated to the fluorophore and added to the apical surface of pRPE cells for 24 h without being fragmented into smaller sizes, and without removing any unbound POS after 1 h.

Immunofluorescence analysis demonstrated that non-sonicated POS were poorly phagocytosed by pRPE cells (Figure 53). Untreated- (Figure 53-A_i), C5b-8- (Figure 53-A_{ii}) and C5b-9-treated cells (Figure 53-A_{iii}) retained the majority of POS (red staining) on their apical surface (green staining), an observation that may have two

explanations: the large size of the POS used and the fact that POS were incubated with the cells for 24 h (without removing any unbound POS after 1 h). This 24 h incubation period could have induced saturation of the system, as RPE cells may have a threshold level above which are not able to phagocytose POS continuously. Whatever the explanation, we did not observe any C5b-9-induced changes (if any) in the binding, internalisation and/or degradation of POS *in vitro* (Figure 53-$A_{iii,}$ -B_{iii} and –C_{iii}).

Therefore, improvement of the *in vitro* conditions was essential in order to further investigate the interplay between outer segment phagocytosis and assembly of the C5b-9 complex. These improvements included the sonication of the POS, to reduce their size, and additionally, incubation of pRPE cells with POS only for 1 h, not for 24 h, with a wash to remove any unbound POS from the medium. Examination of the phagocytosis rate of these cultured pRPE cells was performed in the presence of 1 % FBS.

Before engaging in a detailed analysis of POS phagocytosis it was critical to determine the timepoint at which POS became attached to the apical surface of pRPE cells and the timepoint by which they were completely phagocytosed. In turn, these timepoints could be used in subsequent immunofluorescence and western blot studies (Section **5.3** and **5.4**, respectively).

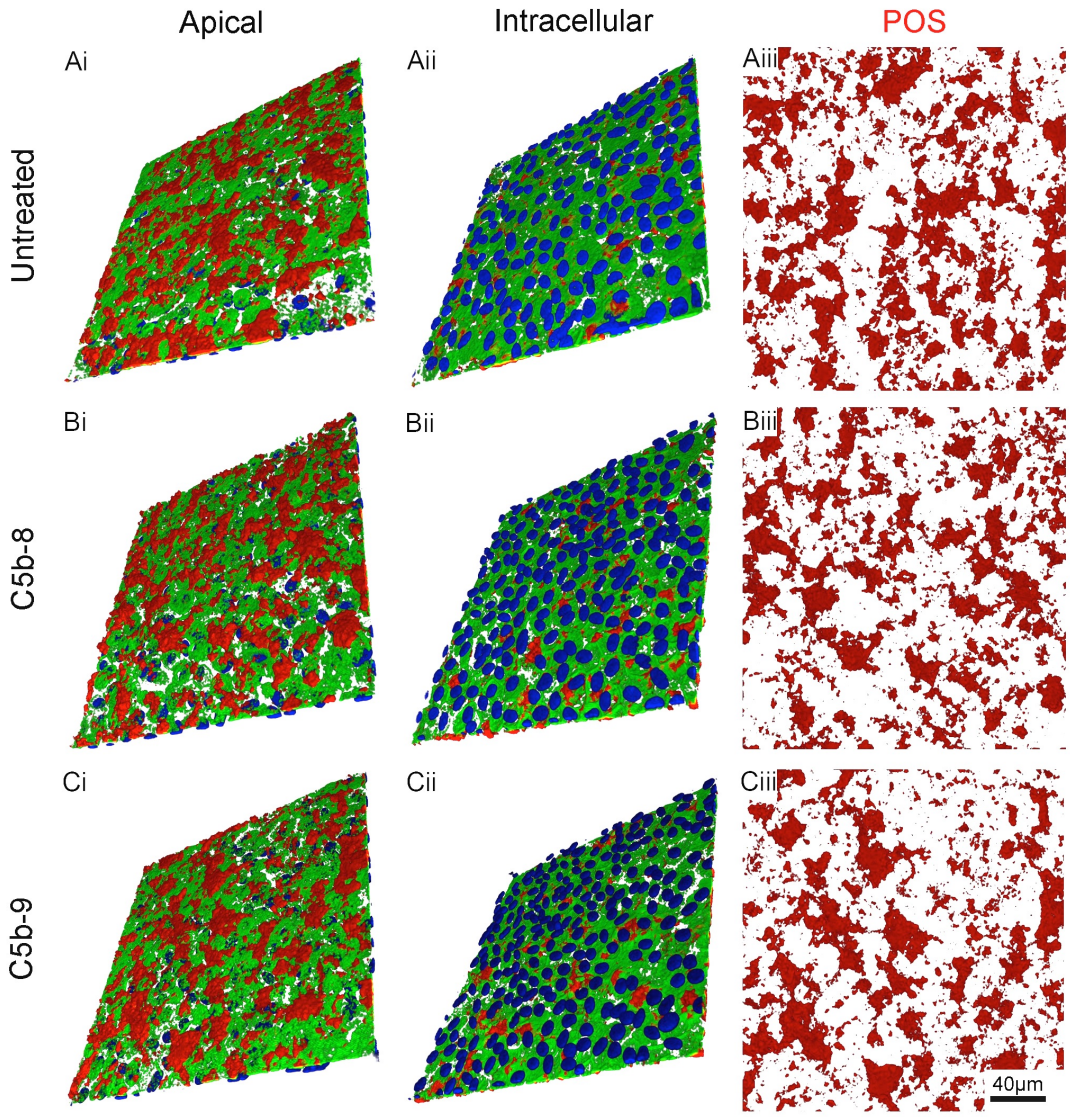

Figure 53. Phagocytosis of non-sonicated POS by pRPE cells. Two different controls were used: Untreated pRPE cells ($A_{i\text{-}iii}$ – 1 % FBS DMEM, apically and DMEM basally) and C5b-8-treated cells ($B_{i\text{-}iii}$). For C5b-8 and C5b-9 complex formation ($B_{i\text{-}iii}$ and $C_{i\text{-}iii}$ respectively), the necessary complement proteins were added in DMEM at 37 ^{o}C / 5 % CO_2 for 1 h (method D_T, section **2.5.4.1**). After 1 h incubation with the complement proteins, POS (red) were added to the apical surface for 24 h. No changes were observed in the binding, internalisation and/or degradation of POS between untreated- ($A_{i\text{-}iii}$), C5b-8- ($B_{i\text{-}iii}$) and C5b-9-treated cells ($C_{i\text{-}iii}$). Green staining represents ezrin (an apical surface marker) and blue staining corresponds to DAPI. Scale bar represents approximately 40µm.

5.2 Phagocytosis of POS in cultured pRPE cells

Having designed improvements to the *in vitro* phagocytosis conditions (as discussed in section **5.1**), we examined the binding and internalisation of POS by pRPE cells.

These experiments were undertaken to optimise the key timepoints to be used later on, in studies aimed at investigating whether C5b-9 affects POS phagocytosis.

To perform this study, confluent pRPE cells were allowed to phagocytose POS for 1 h, 5 h, and 24 h (section **2.7**). At the end of each time point cells were fixed with pure ice-cold methanol and stained as described in section **2.9**.

Figure 54 demonstrates that POS bound to the apical surface of pRPE cells within 1 h (Figure 54-A). No internalised POS were visible at this stage, as can be seen in the z-sections (Figure 54-A_c). On the other hand, by 5 h most of the POS had been internalised, as the apical surface (green staining) had much less bound POS (Figure 54-B), and internalised POS were clearly observable in the z-section (Figure 54-B_c). At 24 h (Figure 54-C) there were no POS visible on the apical cell surface and only a few were detectable within the cells (Figure 54-C_c).

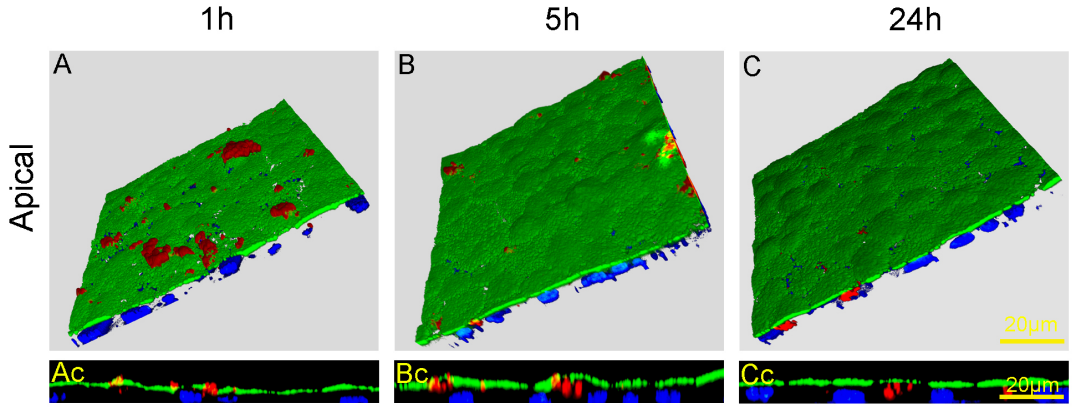

Figure 54. Binding and internalisation of POS by pRPE cells. Confluent pRPE cells were incubated with 10^7 POS / ml in DMEM containing 1 % FBS for 1 h. After 1 h, cells were washed with sterile PBS, which was then replaced with DMEM containing 1 % FBS, after which cells were allowed to phagocytose bound POS for 1 h, 5 h and 24 h. At 1 h the binding of POS (red staining) is evident on the apical cell surface (green staining) (A). No internalisation of POS was observed at that stage (A_c). At 5 h there was a mixture of bound and internalised POS, with the majority of POS internalised (B, B_c). At 24 h all POS were internalised (C, C_c). Blue staining corresponds to DAPI. Scale bar represents approximately 20µm.

Overall, this study provides insight into the kinetics of POS phagocytosis, that were exploited in the next experiment. Thus, for the immunofluorescence studies, the effects of C5b-9 on the binding, internalisation and/or degradation of POS, were examined at 1 h and 24 h. On the other hand, the effects of C5b-9 on POS-driven intracellular signalling was tested at 30 min, 1 h and 5 h. Signalling cascades may be

activated / de-activated rapidly and therefore 30 min was chosen as the starting point of these studies and 5 h the end point, as it is known that mediators such as MerTK and FAK are activated rapidly upon POS binding (Finnemann, 2003, Finnemann and Nandrot, 2006).

5.3 The effect of C5b-9 on POS binding to pRPE cells

Phagocytosis of POS involves the sequential binding, internalisation and degradation, with each step driven by a different molecular machinery (Nandrot et al., 2004). To examine whether C5b-9 interferes with the above processes or not, C5b-9-treated pRPE cells were fed with POS and examined by confocal microscopy.

Briefly, in confluent pRPE cells, C5b-9 was allowed to form on the basal surface, (as described in method $\mathbf{D_T}$ (section **2.5.4.1**), 1 h prior to the addition of POS (see relevant section **2.7**). Two different controls were used: untreated pRPE cells (growing in 1 % FBS DMEM in the upper chamber, and DMEM in the lower chamber) and C5b-8-treated cells. C5b-8 complex formation was accomplished according to method $\mathbf{D_T}$ (section **2.5.4.1**). Cells were allowed to phagocytose POS for 1 h and 24 h (POS incubation according to section **2.7**) and at the end of each time point cells were fixed with pure ice-cold methanol and stained as described in section **2.9**.

Optical slicing on the confocal microscope enabled us to capture images of the apical surfaces of untreated-, C5b-8- and C5b-9-treated cells, viewed from both the extra-cellular and intra-cellular aspect. The images reveal that both C5b-8- and C5b-9-treated cells appeared to have reduced binding of POS at 1 h, when compared to the apical surface of untreated cells (Figure 55-$B_{i\text{-}ii}$, -$C_{i\text{-}ii}$ and -$A_{i\text{-}ii}$, respectively). These observations are supported by quantitative analysis of surface bound fluorescence in the different samples (Figure 55-D). Each bar on the histogram represents the fluorescence volume specific to the POS (red staining) from three independent experiments (three different Z-sections per sample per experiment). However, by 24 h the amount of surface-bound POS was equivalent under all three conditions.

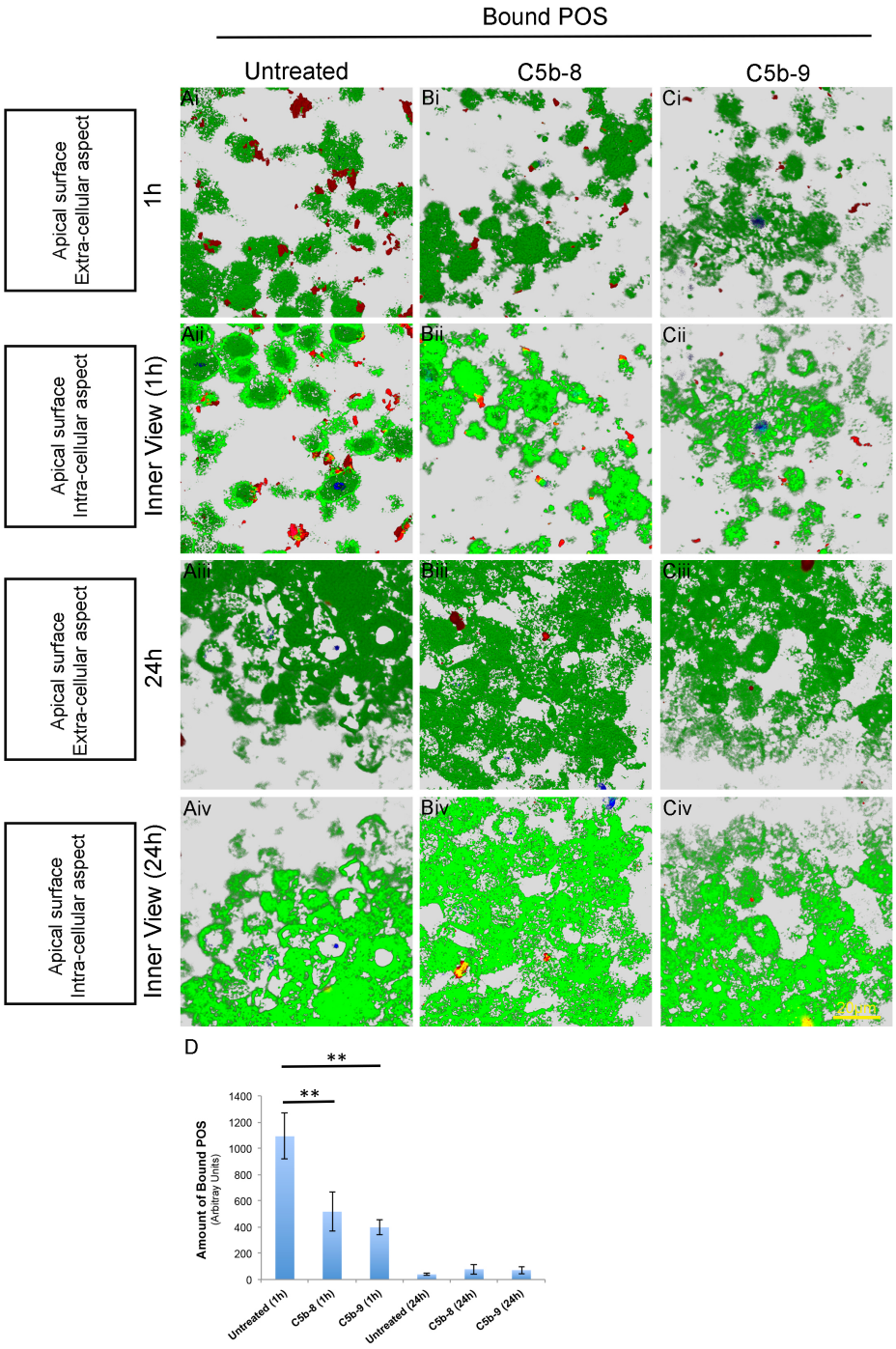

Figure 55. C5b-8 and C5b-9 reduce POS binding to pRPE cells. Two different controls were used: untreated pRPE cells ($A_{i\text{-}iv}$) and C5b-8-treated cells ($B_{i\text{-}iv}$). For C5b-8 and C5b-9 complex formation ($B_{i\text{-}iv}$ and $C_{i\text{-}iv}$ respectively), all necessary complement proteins were added in DMEM, on the basal chamber of the trans-well, for 1 h (method D_T, section **2.5.4.1**). On the apical chamber of all samples only 1 % FBS DMEM was added. After 1 h of incubation with the complement proteins, POS (red staining) were added on the apical surface for 1 h after which, any non-bound POS were removed and replaced by fresh 1 % FBS DMEM. Cells were allowed to phagocytose for 1 h and 24 h. Optical slicing showed that both C5b-8- and C5b-9-treated cells appeared to have reduced binding of POS at 1 h, however by 24 h the amount of surface-bound POS was equivalent under all three conditions. Each bar on the histogram (D) represents the fluorescence volume specific to the POS (red staining) from three independent experiments (three different Z-sections per sample per experiment). Green staining represents ezrin (an apical surface marker) and blue staining corresponds to DAPI. Scale bar represents approximately 20µm. Data expressed as mean ± SEM, $^{**}P<0.05$.

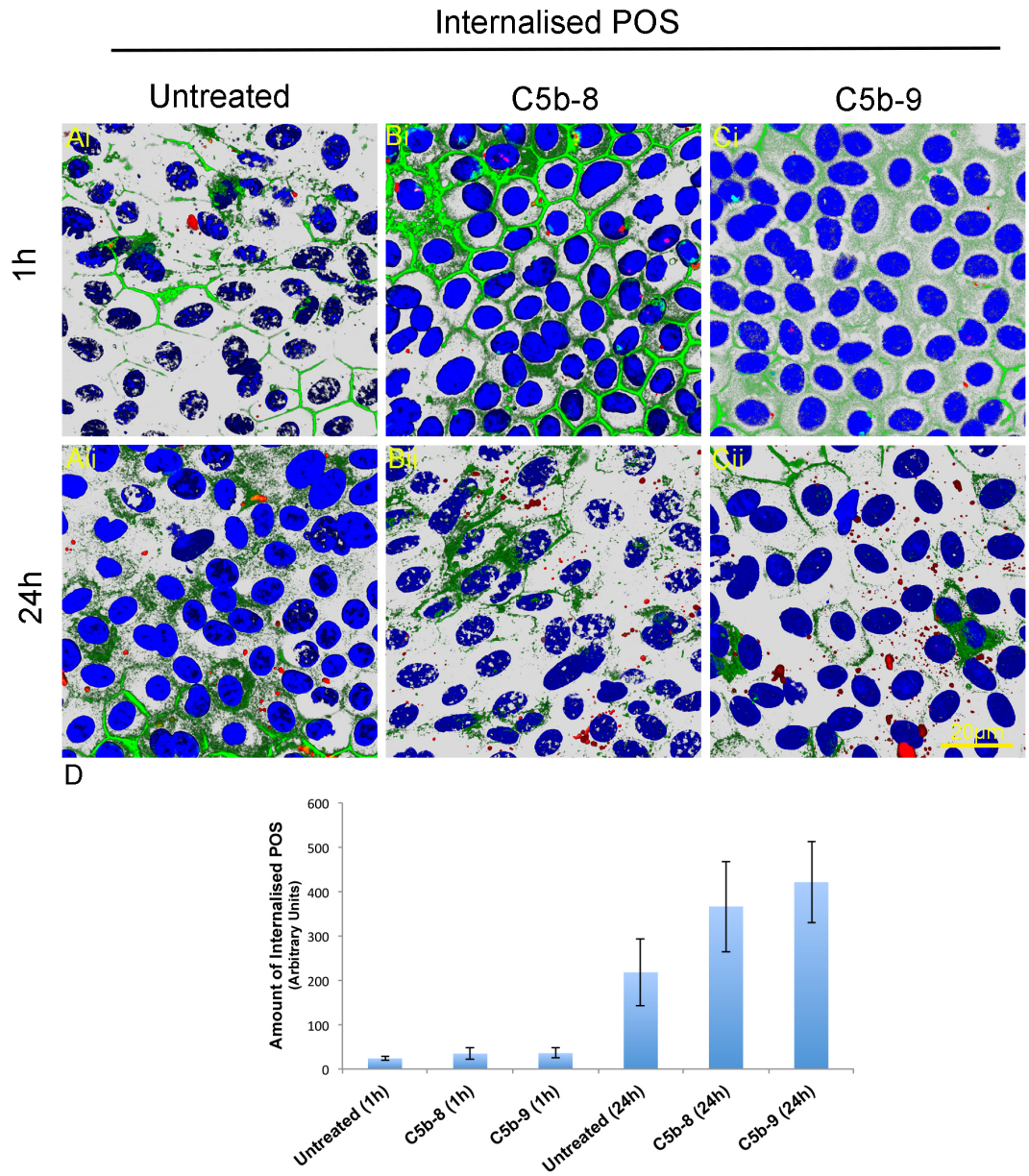

Figure 56. C5b-9 and the internalisation of POS by pRPE cells. The control (A_{i-ii}) and test samples (B_{i-ii} and C_{i-ii}) were exactly as described in the legend of Figure 54. Optical slices were obtained by confocal microscopy at approximately the mid point between the apical and basal cell membranes. POS are stained red, ezrin is green and nuclei are stained with DAPI (blue). The histogram shows quantification of internalised POS identified within the cytoplasm of untreated, C5b-8- and C5b-9-treated pRPE cells at 1 h and at 24 h (D). Each bar on the histogram (D) represents the fluorescence volume specific to the POS (red staining) from three independent experiments (three different Z-sections per sample per experiment). Data expressed as mean ± SEM. Scale bar represents approximately 20µm.

To further investigate the internalisation of POS in pRPE cells exposed to C5b-9, we performed a similar quantitative analysis of images representing optical sections taken through the middle of the nuclei, i.e approximately midway between the apical and basal membranes (Figure 56). At 1 h post-feeding of POS, internalised material was virtually undetectable in any of the samples, whereas at 24 h internalised POS were present throughout. Note that although the differences in the amount of internalised POS were not statistically significant, the fact that there were equivalent levels of POS in cells treated with C5b-8 and C5b-9, compared to control, despite these cells having bound less POS at 1 h, suggests that exposure to these complement complexes may delay the degradation of POS once they are internalised.

5.4 Does C5b-9 complex affect POS-dependent signal transduction in RPE cells?

Phagocytosis of POS by RPE cells requires the concerted activities of a large number of specific proteins (Finnemann and Nandrot, 2006). While the initial step of POS binding on the apical surface of the RPE requires the expression of the αvβ5 integrin, the successful internalisation of POS is established by activation (phosphorylation) of FAK (Finnemann, 2003). Tyrosine phosphorylated-FAK will in turn phosphorylate MerTK that is required for the engulfment of POS as well (Feng et al., 2002). In the following studies phosphorylation of the Src tyrosine kinase was also examined, as FAK is a well-defined substrate for Src (Bellagamba et al., 1997).

The aim of the experiments here was to investigate whether basal formation of C5b-9 influences the activation of any of the afore-mentioned kinases. Confluent C5b-9-treated pRPE cells, (C5b-9 complex formation is described in method $\mathbf{D_T}$ (section **2.5.4.1**)), were allowed to phagocytose POS for 30 min, 1 h and 5 h (section **2.8.1**). Two different controls were used: untreated pRPE cells and C5b-8-treated cells. At the end of each timepoint cells were prepared for western blotting as described in sections **2.8.2**, **2.8.3** and **2.8.4**.

Western blot analysis did not reveal any significant changes in the phosphorylation of MerTK (Figure 57-A), FAK (Figure 57-B) and Src kinases (Figure 57-C) in untreated, C5b-8- and C5b-9-treated pRPE cells. Each bar in the accompanying histograms represents the average value of three wells from three independent experiments.

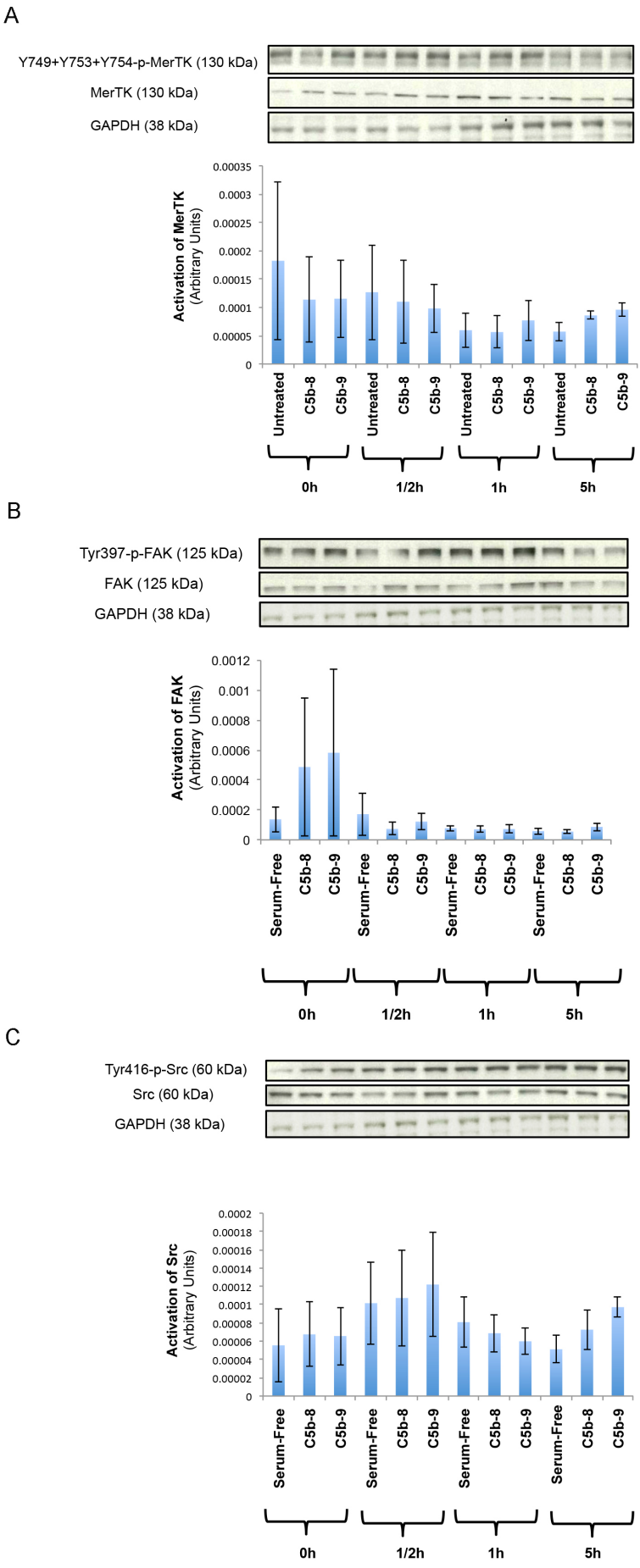

Figure 57. Phosphorylation of MerTK, FAK and Src kinases in C5b-9-treated pRPE cells. Two different controls were used: untreated pRPE cells (1 % FBS in DMEM, apically and DMEM basally) and C5b-8-treated cells. For C5b-8 and C5b-9 formation, all relevant complement proteins were added in DMEM, on the basal chamber of the trans-well for 1 h. (method D_T, section **2.5.4.1**). After 1 h of incubation with the complement proteins, POS were added to the apical surface for 1 h after which any non-bound POS were washed and replaced with fresh 1 % FBS in DMEM (section **2.7**). Cells were allowed to phagocytose for 30 min, 1 h and 5 h. Each bar in the histograms, represents the average value of three wells from three independent experiments. Data expressed as mean ± SEM. Cell extracts were resolved by SDS-PAGE, and western blotted using antibodies against p-MerTK, total MerTK (A), p-FAK, total FAK (B), p-Src and total Src (C) and GAPDH, as a loading control. Blots were quantified by densitometry and bands were normalised against GAPDH.

5.5 Discussion

- **Phagocytic activity of C5b-9-treated pRPE cells**

The renewal of retinal photoreceptors (PR) (rods and cones), in order to maintain nocturnal and diurnal vision respectively, is dependent on the phagocytosis of OS from the underlying RPE monolayer (Rodieck and Rushton, 1976, Hestrin and Korenbrot, 1990). Renewal of these photoreceptors requires the efficient binding, internalisation, degradation and recycling of POS from the RPE in a synchronised fashion (circadian regulation) (Young and Droz, 1968, LaVail, 1976, Qin and Rodrigues, 2012). Circadian control ensures that every morning light can stimulate the phagocytic activity of RPE cells for approximately 1-2 h. In addition, this circadian rhythm has been found to be capable of regulating other cellular functions as well, including melatonin synthesis, ion channel sensitivity and pigment synthesis (Young and Droz, 1968, Ko et al., 2001, Goldman et al., 1980).

Since RPE cell lines (such as ARPE-19 cells) and primary pRPE cells share much of the same phagocytic machinery, we investigated not only how efficiently but also how rapidly pRPE cells would perform synchronised phagocytosis of POS *in vitro* (Mao and Finnemann, 2013). It should be noted here that the isolated POS and the RPE cells used in this thesis were both of porcine origin. Although it is known that RPE cells from different species such as human, porcine, bovine and rat maintain their phagocytic activity when feeding them with POS from different species, by using POS and RPE cells from the same species (pig), we aimed to maximise the phagocytosis rate (Finnemann et al., 1997, Turowski et al., 2004, Mao and Finnemann, 2013).

The results in Figure 54 show that POS bind to pRPE cells in our experimental model and that by 5 h the majority of POS were internalised (Figure 54-B, -B_c). At 24 h no POS were identified on the apical cell surface of pRPE cells (Figure 54-C, -C_c). These findings are in agreement with previous *in vitro* phagocytosis experiments based on various types of RPE cells. When human embryonic stem cell-derived RPE cells (HESC-RPE) were fed with FITC-conjugated POS for 0.5 h, 1 h, 4 h and 20 h, confocal microscopy revealed that by 4 h there were already significant levels of internalised POS, but not at 1 h. At 20 h levels of phagocytosed POS were even

higher (Carr et al., 2009). Further studies in which pRPE cells were fed with FITC-labelled latex beads (opsonised with POS fragments) for various timepoints (0.5 h, 2 h, 4 h, 6 h and 8 h), revealed that only between 6 h to 8 h there was maximum POS internalisation (Klettner et al., 2011). In support of the above studies, Westenskow et al., (2012), recently demonstrated that POS binding and internalisation levels in both hfRPE cells and in induced pluripotent stem cell-derived RPE cells (iPS-RPE) are slightly lower than in ARPE-19 cells. Thus, in hfRPE cells maximum binding levels were observed at 3 h while internalisation was reported at 5 h. Maximum levels of POS binding using iPSC-derived RPE cells were recorded at 4 h and internalisation at 5 h (Westenskow et al., 2012).

Overall, these studies suggest that RPE cell lines might have a greater capacity for POS phagocytosis than primary and iPS-derived RPE cells, however the timeframe for POS binding and internalisation remained approximately the same between HESC-RPE, pRPE, iPS-RPE and ARPE-19 cells. In the studies here we found that 1 h and 24 h were suitable timepoints at which to measure POS binding and internalisation respectively, and are broadly in line with the studies mentioned above.

It is currently unknown whether the C5b-9 complex has the capacity to impair POS phagocytosis or not. Only until recently the interplay of complement with POS phagocytosis was examined in ARPE-19 cells (Lueck et al., 2012). These authors demonstrated that when ARPE-19 cells were fed apically with POS and basally with 4 % competent-human sera for 24 h, levels of IL-6, IL-8, MCP-1 and VEGF were significantly up-regulated when compared to cells only treated with POS. These results suggested that C5b-9 complex might have the ability to cause an inflammatory response in RPE cells that are undergoing phagocytosis. However, it still is uncertain to what extent the C5b-9 complex might affect this process *in vitro*.

Recent studies demonstrated that C5b-9 also has the capacity to trigger inflammasome activation (the set of cytosolic multi-molecular protein complexes responsible for regulating pro-apoptotic and pro-inflammatory events), and in turn that the activated inflammasome may impair POS phagocytosis (Triantafilou et al., 2013, Kaarniranta et al., 2013). In more detail, Triantafilou et al., (2013) demonstrated that C5b-9 assembly in confluent primary human lung epithelial cells

leads to Ca^{2+} influx and increased cytosolic Ca^{2+} activation. Release of Ca^{2+} in turn triggered the activation of several proteins including IL-1β, caspase-1 and more importantly NLRP3 (NLR family, pyrin domain containing protein 3), the main indicator of inflammasome activation. On the other hand, Kaarniranta et al., (2012) showed that incubation of ARPE-19 cells with the peroxidation end product 4-hydroxynonenal (HNE) can induce oxidative stress, which further provokes inflammasome activation which has the capacity to impair both autophagy (removal of damaged organelles and proteins) and POS phagocytosis in RPE cells (Kaarniranta et al., 2013, Kauppinen et al., 2012). Therefore, there could be a link between C5b-9 and impaired POS phagocytosis through Ca^{2+}-dependent inflammasome activation.

It has previously been reported that phagocytosis requires the co-operation of the cytoskeleton, as actin needs to be re-organised (May and Machesky, 2001). Once POS recognise and bind to the apically-expressed $\alpha_v\beta_5$ receptor of RPE cells, actin has to be remodelled in order for the nascent phagocytic cups to close (Hayes et al., 2009, Finnemann and Rodriguez-Boulan, 1999). The C5b-9 complex might either have an effect on actin remodelling and/or might affect the expression levels of $\alpha_v\beta_5$ receptor.

C5b-9 complex formation was previously shown to be capable of increasing the number of stress fibers on pRPE cells grown either on glass coverslips and/or on trans-wells. This enhanced appearance of stress fibers might indicate that C5b-9 inteferes with actin re-organisation. Perhaps when pRPE cells (Figures 55 and 56) were treated simultaneously with POS (apical surface) and C5b-9, (basal surface) a conflict between the phagocytic and endocytic pathways was induced. Both pathways have been shown to depend on actin remodelling. As C5b-9 endocytosis is a caveolin-1 dependent process and POS phagocytosis requires actin to close the phagocytic cups on the apical cell surface, it could be possible that cells favour C5b-9 endocytosis and delay POS phagocytosis in order to deal with both processes (Moskovich et al., 2012). One possible explanation as to why pRPE cells could prioritise C5b-9 endocytosis, is the size of the assembled C5b-9 complexes. Caveolin-1 endocytosis only requires particules to have an approximate size of 50 nm (Parton and Simons, 2007). C5b-9 complex is approximately 11 nm, significanlty

smaller than outer segments which reside on the apical cell surface (Finnemann and Rodriguez-Boulan, 1999, Ramm et al., 1985). In fact, as discussed in chapter 3, C5b-9 has previously been associated with actin remodelling as it can regulate the actin cytoskeleton via RhoA activation (Zhang et al., 2007). This mediator of actin remodelling becomes up-regulated upon activation of Erk1/2, in C5b-9-treated GECs (Etienne-Manneville and Hall, 2002, Mouawad et al., 2014). Should both phagocytosis and C5b-9 formation force actin to re-organise, then perhaps the actin cytoskeleton would be compromised in its ability to respond to these two distinct stimuli. At 24 h (Figure 55) no difference in the amount of bound POS was detected between untreated, C5b-8- and C5b-9-treated cells. It has been shown that the C5b-9 complex by 24 h is mostly endocytosed and/or expelled from pRPE cells. Therefore, after 1 h pRPE cells can perform phagocytosis with no further delays, once they start to degrade (degradation pathway) or expell C5b-9 to the extra-cellular space (ecto-/exo-cytosis).

It is also possible that C5b-9 has the ability to regulate surface organisation of the $\alpha_v\beta_5$ receptor by inducing a Ca^{2+} influx in pRPE cells. In support of this theory, it was previously shown that in human MG-63 osteosarcoma cells that the extracellular presence of Ca^{2+} led to the localisation of $\alpha_v\beta_5$ in focal contacts (Stuiver et al., 1996). As there are numerous studies that have demonstrated the ability of C5b-9 to change Ca^{2+} levels, therefore it could be suggested that C5b-9 assembly on the basal cell surface of pRPE cells might induce re-distribution of the $\alpha_v\beta_5$ receptor (Cybulsky et al., 1989, Papadimitriou et al., 1994, Wiedmer and Sims, 1991, Triantafilou et al., 2013). This event in turn could, for a certain amount of time, impair the binding of POS to the apical cell surface. Therefore, immunofluorescence studies using an antibody against $\alpha_v\beta_5$ could reveal whether $\alpha_v\beta_5$ becomes re-distributed on the apical cell surface due to the presence of C5b-9 in pRPE cells.

Although the $\alpha_v\beta_5$ receptor is essential for POS binding to the apical cell surface of RPE cells, it does not bind substrate directly (Hanayama et al., 2002). Instead, the $\alpha_v\beta_5$ receptor needs to be ligated with milk fat globule-EGF-factor 8 (MFG-E8) in order to increase POS binding (Hanayama et al., 2002). MFG-E8 is a heavily glycosylated protein whose diurnal expression has been found to peak soon after light onset in mouse RPE cells *in vitro* (Nandrot et al., 2007). MFG-$E8^{-/-}$ mice

develop a similar phenotype to $\beta5^{-/-}$ mice, which suffer from loss of synchronised daily phagocytosis due to failure to activate MerTK kinase, essential for the engulfment of POS (Nandrot et al., 2006, Nandrot et al., 2004, Nandrot et al., 2007). Despite this loss, MFG-E8 deficient mice still maintain a low level of ongoing phagocytosis, indicating that MFG-E8 under normal conditions promotes phagocytosis. It has previously been reported that MFG-E8 integrin becomes up-regulated in mice gut epithelial cells (Chogle et al., 2011). Treatment of MFG-$E8^{-/-}$ C57BL/6 mice with dextran sulfate sodium (DSS)-induced colitis led to the up-regulation of this integrin, indicating its protective role in inflammatory bowel disease (Chogle et al., 2011). From these observations it might be inferred that upon inflammasome activation, due to cytosolic Ca^{2+} increase, C5b-9 might lead to the up-regulation of MFG-E8 in pRPE cells. If this is the case then we can speculate that the C5b-9-induced up-regulation of MFG-E8 enhances POS binding on the apical cell surface of pRPE cells and therefore compensates for the delayed POS binding, which is only observed at 1 h in C5b-9-treated pRPE cells (Figure 54).

Another candidate protein that could act against a C5b-9-induced delay in POS binding is CD36. CD36 is a class B scavenger receptor, expressed in several cell types including RPE cells (Ryeom et al., 1996). It is involved in various biological processes such as angiogenesis, atherosclerosis, inflammation, lipid metabolism and phagocytosis of photoreceptor outer segments (Febbraio et al., 2001). CD36 has been shown to aid the binding and internalisation of POS since blockage of this receptor in RPE-J cells with CD36-specific antibodies, decreased the process of phagocytosis (Finnemann and Silverstein, 2001). Furthermore, CD36 has previously been shown to prevent the accumulation of age-dependent retinal laminar deposits such as oxidised low-density lipoproteins (oxLDL) (Picard et al., 2010). Laminal and drusen deposits are common features of AMD. CD36 is responsible for the uptake of oxLDL in RPE both *in vitro* and *in vivo* and its protective role in AMD can be inferred from the observation that $CD36^{-/-}$ mice accumulate oxLDL and develop sub-retinal thickening (Picard et al., 2010). Should the elimination of C5b-9 from the basal cell surface of pRPE cells be partly dependent on CD36, then this could be another candidate protein that not only shields POS phagocytosis from the presence of C5b-9 but at the same time helps RPE cells to deal with C5b-9.

Figure 56 demonstrates that although the differences in the amount of internalised POS were not statistically significant, the fact that there were equivalent levels of POS in cells treated with C5b-8 and C5b-9, compared to control, despite these cells having bound less POS at 1 h, suggests that exposure to C5b-9 may delay the degradation of POS once they are internalised. In order for RPE cells to successfully digest any bound POS, they have developed a maturation process which includes several fusion steps (Herman and Steinberg, 1982b). Internalised POS become fused with early endosomes, then with late endosomes which finally become fused with lysosomes where POS are degraded (Herman and Steinberg, 1982a). Each step is accompanied by the production and release of reactive oxygen species (ROS). POS phagocytosis is a polarised process, during which apically-bound POS become internalised and organised in phagosomes (fusion with endosomes) which in turn transit towards the basal membrane of RPE cells, where they become degraded in lysosomes (Herman and Steinberg, 1982b, Gibbs et al., 2003). Mutations in the gene encoding the motor protein myosin VIIa, essential for the transportation of phagosomes, lead to Usher Syndrome 1B in humans, during which POS phagocytosis in the RPE is arrested and therefore the underlying photoreceptors degenerate (Gibbs et al., 2003). One of the best-studied lysosomal enzymes, found in many cell types including the RPE, is cathepsin D, which is essential for the lysosomal degradation of outer segments (Benes et al., 2008, Deguchi et al., 1994). Cathepsin D is an intra-cellular aspartic protease of the pepsin superfamily involved in several biological processes such as protein degradation, autophagy and apoptosis (Benes et al., 2008). It has also been associated in the past with several pathological conditions such as cancer and Altzheimer's disease (Vetvicka et al., 1994, Zhou et al., 2006). Intracellular trafficking of cathepsin D to lysosomes is essential for its normal proteolytic function (Benes et al., 2008). Translocation and increased secretion of this enzyme to the extracellular space by cancer cells enhances the invasive and metastatic ability of these cells, as cathepsin D will act in an autocrine and/or paracrine manner (Koblinski et al., 2000).

Recent studies demonstrated that mtDNA damage and therefore mitochondrial instability has the potential to decrease the expression of cathepsin D in the RPE *in vitro* (Wang et al., 2009). Thus, when ARPE-19 cells were incubated with rotenone, proteins levels of cathepsin D were significantly decreased due to the induction of

mtDNA damage (Wang et al., 2009). Rotenone increases mitochondrial ROS production, by inhibiting mitochondrial complex I, and therefore induces mtDNA damage (Indo et al., 2007, Li et al., 2003). Decreased protein levels of cathepsin D were consistent with a decrease in this enzyme's activity. However, the mechanism by which mtDNA damage leads to decreased cathepsin D levels needs to be addressed.

Since we previously demonstrated that C5b-9 (either with the presence of dynasore or not) has the ability to decrease mitochondrial numbers, and perhaps to a certain extent induce mitochondrial instability, it is possible that the basal deposition of C5b-9 in pRPE cells can lead to insufficient POS degradation due to reduced cathepsin D levels or availability of ATP. Additionally, in the event of C5b-9-induced cytoplasmic Ca^{2+} release in the pRPE cells, C5b-9 might at 1 h slow down the ingestion of POS due to failure to properly activate protein kinase C (PKC). PKC activation has previously been demonstrated to be Ca^{2+} dependent and it terminates POS phagocytosis in RPE-J cells (Heth and Marescalchi, 1994, Hall et al., 1991). Overall, additional experiments such as Ca^{2+} imaging, western blotting using antibodies against PKC and cathepsin D should provide more information as to whether the complement system has the ability to interfere with POS phagocytosis in the RPE.

- **C5b-9 does not activate MerTK, FAK and Src kinases**

The process of POS internalisation requires the activation of a signalling cascade in order for RPE cells to re-organise their actin cytoskeleton which in turn will allow the internalisation and therefore the processing of outer segments (Finnemann et al., 1997). Thus, once αvβ5 integrin binds to POS on the apical cell surface, it triggers the re-location of FAK, which is a non-receptor tyrosine kinase, to the apical cell surface where it becomes activated, via auto-phosphorylation (Finnemann, 2003). FAK is localised at areas of integrin clustering, termed focal adhesions, and is essential for the engulfment of POS. Phosphorylated FAK (p-FAK) will in turn phosphorylate the tyrosine kinase MerTK (Finnemann, 2003). Activation of MerTK is a crucial part of POS engulfment since RCS rats lacking MerTK developed severe impairment of POS internalisation, an event that leads to an early onset photoreceptor degeneration *in vivo* (D'Cruz et al., 2000, Gal et al., 2000). Ectopic

expression of MerTK in RCS RPE cells by a recombinant adenovirus, can rescue the RCS phenotype (Feng et al., 2002, Hall et al., 2005). MerTK is believed to accomplish its role with the help of ligands such as Gas6 and Protein S, both members of a family of K^+-dependent proteins known for their post-translational γ-carboxylation of their glutamic acid residues (Hall et al., 2005, Hall et al., 2001). These residues aid the binding of POS. However, it is still under investigation how Gas6 and Protein S function precisely. For instance, it is currently uncertain to what extent Gas6 is needed for the MerTK-dependent internalisation of POS in the RPE, as in gas6 deficient mice RPE cells did not show any signs of POS phagocytosis disruption (Hall et al., 2005). Activation of MerTK leads to increased levels of inositol tris-phosphate ($InsP_3$) and activates the tyrosine kinase Src (Heth and Marescalchi, 1994). $InsP_3$ stimulates the release of Ca^{2+} from intracellular stores, which in turn will activate PKC (Heth and Marescalchi, 1994). PKC has the capacity to terminate POS phagocytosis as was demonstrated in rat RPE cells *in vitro* (Hall et al., 1991). Thus, when these cells were incubated with phorbol myristate acetate (PMA) PKC activity was increased and the phagocytosis of outer segments was rapidly brought into a halt. Although the ingestion of the outer segments was stopped, PKC activation did not inhibit the binding of outer segments to the apical cell surface of RPE cells (Hall et al., 1991).

Figure 57 shows that C5b-9 complex did not alter the phosphorylation levels of any of the three phagocytosis-related kinases: MerTK, FAK and Src, respectively. However, it should be noted that in the pRPE cells at 0 h, p-MerTK, p-FAK and p-Src were all detectable. Therefore it might be concluded either that pRPE cells have an endogenous level of constitutively activated MerTK, FAK and Src, or that a more rigorous serum starvation protocol should be applied in order to fully deactivate these kinases.

It was expected that any differences observed (between untreated, C5b-8- and C5b-9-treated pRPE cells) in POS uptake would be reflected by differences in the activation levels of MerTK, FAK and/or Src. Since we did not observe any differences in the phosphorylation of the above kinases, in future studies it might be worth performing this experiment using antibodies that recognise different phosphorylation sites on p-FAK, p-MerTK and p-Src. For instance in Figure 57 we only used an antibody

against Tyr397-p-FAK. In contrast, Finnemann et al. (2003) used two additional antibodies in order to detect activated FAK during POS phagocytosis in RPE-J cells: Tyr576-p-FAK and Tyr861-p-FAK. Using alternative antibodies not only could reveal a possible response of the phagocytosis-related signalling cascade but it could also provide an insight as to whether complement interferes with the activation of any of the above kinases.

While currently no direct association has been reported between C5b-9 complex formation and MerTK and/or FAK kinases in the RPE, it has recently been proposed that complement enhances the activation of Src (phospho-Src) (Kunchithapautham et al., 2012, Rohrer et al., 2014). These authors showed that when ARPE-19 cells were incubated with 0.5 mM H_2O_2 and 25 % NHS for 5 min, 10 min, 20 min, 30 min and 60 min p-Src levels were significantly increased from 5 min until 60 min. ARPE-19 cells treated only with 0.5 mM H_2O_2 for the same timepoints as above, did not active Src kinase. Kunchithapautham et al., (2012) suggested that C5b-9 formation on RPE cells increases the influx of Ca^{2+} and Na^{+} ions, which in turn depolarise the cell membrane. This membrane depolarisation activates voltage-dependent calcium channels (VDCC) that further increase the influx of Ca^{2+} ions. This enhanced Ca^{2+} influx is proposed to trigger the activation of Src. The Src pathway can also crosstalk with the Ras/Erk pathway, which is essential for VEGF secretion. Therefore one can envisage a model in which C5b-9, by increasing the influx of Ca^{2+} ions, can activate Src kinase, which in turn indirectly drives the release of VEGF. A similar association between complement-induced Ca^{2+} influx, inflammation and therefore kinase phosphorylation could exist for FAK and MerTK.

Conclusions & Future Perspectives (Chapter 6)

6.1 Summary and conclusions

The aim of this thesis was to investigate the *in vitro* interaction of the retinal pigment epithelium with the terminal product of the complement system: the C5b-9 complex. To achieve this, initially the *in vitro* conditions of C5b-9 complex assembly had to be optimised. A range of C5b-9 complex assembly conditions were tested in ARPE-19 cells and once the C5b-9 complex formation protocol was established, ARPE-19 cells were replaced with primary porcine RPE cells.

The initial studies demonstrated the necessity of using cells with authentic RPE-like phenotypic characteristics, in order to investigate the effects of C5b-9 complex deposition on the RPE monolayer. Usage of ARPE-19 cells that were only cultured *in vitro* for 10 days did not permit thorough examination of the precise cellular localisation of the assembled C5b-9 complex. As the ARPE-19-derived monolayer of cells was relatively immature it was not possible to distinguish whether the C5b-9 complex was on the apical surface and/or inside the cytoplasm of cells. This problem was overcome when ARPE-19 cells were incubated for 15 weeks before being used. These highly differentiated cells developed a well-organised monolayer, where it was easy to identify the apical deposition of C5b-9 complex via immunofluorescence. However, this was an impractical solution for a long-term study, and it could not be relied on as there were instances where monolayers would inexplicably detach from the substratum, so an alternative model system was required.

Four different protocols were tested with the aim of efficiently forming significant levels of C5b-9 complex. Previous publications showed that C5b-9 complex could be induced by incubating cells either with various amounts of complement-competent human sera and/or with C5 + C5-depleted human sera (Johnson et al., 2011, Lueck et al., 2011). The final protocol which we used to induce uniform levels of C5b-9 complex on the apical surface of pRPE cells was C5b,6 complex + C7 + C8 + C9 purified complement proteins in DMEM. This reductionist approach increased the simplicity of the *in vitro* system, as it eliminated the presence of various proteins and growth factors that are normally present in human serum. Also, the switch to pRPE cells, known for their ability to retain their phenotype *in vitro*, along with cultivation of these cells on trans-well plates, permitted formation of C5b-9 complex on the

basal surface of cells. We reasoned that basal complement deposition would mimic the *in vivo* deposition of C5b-9 complex (component of drusen deposits) on the RPE monolayer of AMD patients (Anderson et al., 2002).

C5b-9 complex assembly in both ARPE-19 and pRPE cells did not affect cell survival, according to the MTT assays, consistent with propidium iodide studies in ARPE-19 cells demonstrating that, with only rare exceptions, C5b-9 did not make cell membranes permeable. Although C5b-9-treated pRPE cells remained viable, it was observed that by 24 h these cells developed abundant stress fibres indicating that C5b-9 can interfere with actin dynamics and induce actin remodelling.

Having establishment of an *in vitro* model using pRPE cells we examined the kinetics of C5b-9 complex formation. Our studies demonstrated that C5b-9 forms rapidly on the basal surface of pRPE cells, remaining stable for several hours, followed by gradual elimination until after 24 h the complex is no longer detectable. While it has previously been reported that C5b-9 can be eliminated from cells via membrane vesiculation, Moskovich and Fishelson (2007) demonstrated in K562 cells that C5b-9 complex could be removed either via exocytosis and/or be sequestered in perinuclear bodies via endocytosis as well. Here we showed that incubation of C5b-9-treated pRPE cells with dynasore led to the sustained presence of the complex on pRPE cells, demonstrating the endocytosis is a major route for C5b-9 elimination in these cells. Immuno-electron microscopy studies supported this conclusion.

Interestingly, the C5b-9 and C5b-8 complexes both increased TER, however higher values were obtained from C5b-9-treated cells. In contrast, the prolonged presence of C5b-9 (dynasore studies) on the basal surface of pRPE cells did not lead to an increase in TER and the mechanism for this observation is unknown. Only a few previous studies examined the effects of C5b-9 on TER. One report, using a different experimental approach in RPE cells showed that TER values were unaffected (Lueck et al., 2012), whereas TERs were reported to decrease when cells were treated first with hydrogen peroxide and then with complement-competent human sera (Bandyopadhyay and Rohrer, 2012, Thurman et al., 2009, Joseph et al., 2013).

Western blotting and immunofluorescence analysis of two highly expressed junctional proteins (ZO-1 and claudin-19) failed to demonstrate any signs of up-regulation at the protein level. However, confocal microscopy revealed that staining for claudin-19 was more tightly aligned with cell junctions in C5b-9-treated pRPE cells than in serum-free- and C5b-8-treated cells. This observation provides evidence that the C5b-9 complex has an effect on claudin-19 (the predominant junction protein in pRPE cells) that may at least partly explain the C5b-9-induced TER increase. One previous report showed that TER increased in ARPE-19 cells in response to ER stress (Yoshikawa et al., 2011). This may be relevant since the C5b-9 complex has previously been shown to be capable of inducing ER stress in glomerular epithelial cells (GECs) (Cybulsky et al., 2002). In future work it would be interesting to perform western blotting and RT-PCR in C5b-9-treated pRPE cells for ER-stress-related proteins and mRNA respectively.

Previous studies have shown that AMD is associated with modifications in mitochondrial architecture and/or mitochondria numbers. As it is currently unknown whether C5b-9 has the potential to affect mitochondrial integrity and/or mitochondria numbers in RPE cells, immunofluorescence and electron microscopy were performed in C5b-9-treated pRPE cells. Both immunofluorescence for Tim23 (essential for protein transportation in mitochondria) and Mitotracker® (a mitochondrial-specific fluorescent dye) revealed that the prolonged presence of C5b-9 complex on the basal surface of pRPE cells (dynasore studies) reduces mitochondria numbers and/or changes the component of mitochondrial proteins in pRPE cells. Tim23 staining was greatly reduced in pRPE cells in which C5b-9 endocytosis was arrested via dynasore but no changes in the Tim23 and the Mitotracker®-specific staining were observed in cells where C5b-9 was endocytosed. These observations are consistent with persistent exposure to C5b-9 leading to deleterious effects on mitochondria in pRPE cells. Significantly, dynasore alone did not induce these changes in mitochondria. We also showed using electron microscopy that both C5b-9-treated and C5b-9 + dynasore-treated pRPE cells, exhibited reduced numbers of mitochondria. Western blotting for Tim23 and cytochrome C (essential for the electron transport between the two mitochondrial membranes) did not reveal any alterations in expression of either protein in C5b-9-treated pRPE cells.

Incubation of pRPE cells with fluorescently-tagged POS allowed us to investigate whether the C5b-9 complex interferes with phagocytosis. In performing these experiments we were able to verify that pRPE cells retained their phagocytic activity several days after their extraction from porcine eyes. Interestingly, basal deposition of C5b-9 seemed to have an effect on the binding of POS on the apical surface of pRPE cells. Thus, the C5b-9 complex (and C5b-8 complex to a lesser extent) delayed the binding of POS, when compared to pRPE cells in serum-free medium. There are numerous potential explanations for this observation, for example it could be attributed to changes in the expression levels of $\alpha_v\beta_5$ receptor and/or to the high demand for actin remodelling. Phagocytosis of POS requires extensive actin re-organisation on the apical surface, and C5b-9 has been demonstrated in chapter 2 to alter the actin cytoskeleton by increasing the presence of stress fibers. The effects of the C5b-9 complex appeared to be specific to binding, as there was no impact on the internalisation of POS in pRPE cells.

6.2 Future perspectives

To obtain greater insight into the interplay between the complement system and the RPE, it would be of interest to examine C5b-9 complex formation on hfRPE and/or iPS-derived RPE cells. Although pRPE cells provide authentic polarised monolayers to investigate the effects of C5b-9, they have limitations. It is possible that the current *in vitro* conditions of C5b-9 complex formation might be more or less efficient in RPE cells of human origin, and the effects of C5b-9 may vary according to the AMD haplotype of the target cells. The immuno-gold labelling studies could be extended to learn more about the cellular localisation of C5b-9 complex once it becomes endocytosed. Using fluorescently-tagged C9 may also provide a strategy for following the assembly and internalisation of C5b-9 in live cell imaging.

Although the propidium iodide experiments did not provide any indication of pore formation by C5b-9, Ca^{2+} influx experiments might be a more physiological way of demonstrating the ability of the C5b-9 complex to increase the cytoplasmic concentration of Ca^{2+} ions. It should be kept in mind that C5b-9 complexes of different sizes ($C5b\text{-}9_{(1\text{-}12)}$) can be formed and therefore the ability to increase cell permeability can be variable. Additionally, microarray analysis, RT-PCR and western blotting could all be used to investigate whether C5b-9 alters the global

transcriptome of RPE cells, or more specifically, the expression levels of two of the most common ER stress related proteins: bip and grp94, as was reported in GEC cells (Cybulsky et al., 2002).

Performing RT-PCR analysis of a wider range of complement regulators could reveal specific responses to C5b-9 beyond just CD59 and DAF negative regulators and perhaps sensitising RPE cells, either with a mixture of pro-inflammatory cytokines and/or hydrogen peroxide could make cells more susceptible to the presence of C5b-9.

Finally, to further examine the effects of alternative pathway activation on mitochondria, immunofluorescence and western blotting of various mitochondrial proteins could be performed in conjunction with live cell measurements of mitochondrial function. Also, repetition of the electron microscopy analysis would be essential to further validate the finding that C5b-9 reduces mitochondrial numbers in pRPE cells.

List of References

AARTS, P. A., BOLHUIS, P. A., SAKARIASSEN, K. S., HEETHAAR, R. M. & SIXMA, J. J. 1983. Red blood cell size is important for adherence of blood platelets to artery subendothelium. *Blood,* 62**,** 214-7.

ABLONCZY, Z., DAHROUJ, M., TANG, P. H., LIU, Y., SAMBAMURTI, K., MARMORSTEIN, A. D. & CROSSON, C. E. 2011. Human retinal pigment epithelium cells as functional models for the RPE in vivo. *Invest Ophthalmol Vis Sci,* 52**,** 8614-20.

ABRERA-ABELEDA, M. A., NISHIMURA, C., SMITH, J. L., SETHI, S., MCRAE, J. L., MURPHY, B. F., SILVESTRI, G., SKERKA, C., JOZSI, M., ZIPFEL, P. F., HAGEMAN, G. S. & SMITH, R. J. 2006. Variations in the complement regulatory genes factor H (CFH) and factor H related 5 (CFHR5) are associated with membranoproliferative glomerulonephritis type II (dense deposit disease). *J Med Genet,* 43**,** 582-9.

ADIJANTO, J., CASTORINO, J. J., WANG, Z. X., MAMINISHKIS, A., GRUNWALD, G. B. & PHILP, N. J. 2012. Microphthalmia-associated transcription factor (MITF) promotes differentiation of human retinal pigment epithelium (RPE) by regulating microRNAs-204/211 expression. *J Biol Chem,* 287**,** 20491-503.

AHMADO, A., CARR, A. J., VUGLER, A. A., SEMO, M., GIAS, C., LAWRENCE, J. M., CHEN, L. L., CHEN, F. K., TUROWSKI, P., DA CRUZ, L. & COFFEY, P. J. 2011. Induction of differentiation by pyruvate and DMEM in the human retinal pigment epithelium cell line ARPE-19. *Invest Ophthalmol Vis Sci,* 52**,** 7148-59.

ANDERSON, D. H., MULLINS, R. F., HAGEMAN, G. S. & JOHNSON, L. V. 2002. A role for local inflammation in the formation of drusen in the aging eye. *Am J Ophthalmol,* 134**,** 411-31.

BAALASUBRAMANIAN, S., HARRIS, C. L., DONEV, R. M., MIZUNO, M., OMIDVAR, N., SONG, W. C. & MORGAN, B. P. 2004. CD59a is the primary regulator of membrane attack complex assembly in the mouse. *J Immunol,* 173**,** 3684-92.

BADEA, T. C., NICULESCU, F. I., SOANE, L., SHIN, M. L. & RUS, H. 1998. Molecular cloning and characterization of RGC-32, a novel gene induced by complement activation in oligodendrocytes. *J Biol Chem,* 273**,** 26977-81.

BAEHR, W., WU, S. M., BIRD, A. C. & PALCZEWSKI, K. 2003. The retinoid cycle and retina disease. *Vision Res,* 43**,** 2957-8.

BALDA, M. S., GARRETT, M. D. & MATTER, K. 2003. The ZO-1-associated Y-box factor ZONAB regulates epithelial cell proliferation and cell density. *J Cell Biol,* 160**,** 423-32.

BALDA, M. S. & MATTER, K. 2000. The tight junction protein ZO-1 and an interacting transcription factor regulate ErbB-2 expression. *EMBO J,* 19**,** 2024-33.

BALDA, M. S., WHITNEY, J. A., FLORES, C., GONZALEZ, S., CEREIJIDO, M. & MATTER, K. 1996. Functional dissociation of paracellular permeability and transepithelial electrical resistance and disruption of the apical-basolateral intramembrane diffusion barrier by expression of a mutant tight junction membrane protein. *J Cell Biol,* 134**,** 1031-49.

BAN, Y. & RIZZOLO, L. J. 2000. Regulation of glucose transporters during development of the retinal pigment epithelium. *Brain Res Dev Brain Res,* 121**,** 89-95.

BANDYOPADHYAY, M. & ROHRER, B. 2012. Matrix metalloproteinase activity creates pro-angiogenic environment in primary human retinal pigment epithelial cells exposed to complement. *Invest Ophthalmol Vis Sci,* 53**,** 1953-61.

BARREAU, E., BROSSAS, J. Y., COURTOIS, Y. & TRETON, J. A. 1996. Accumulation of mitochondrial DNA deletions in human retina during aging. *Invest Ophthalmol Vis Sci,* 37**,** 384-91.

BAUDOUIN, C., BRIGNOLE, F., FREDJ-REYGROBELLET, D., NEGRE, F., BAYLE, J. & GASTAUD, P. 1992. Transferrin receptor expression by retinal pigment epithelial cells in proliferative vitreoretinopathy. *Invest Ophthalmol Vis Sci,* 33**,** 2822-9.

BAUER, J. & VALET, G. 1983. Cell volume and osmotic properties of erythrocytes after complement lysis measured by flow cytometry. *J Immunol,* 130**,** 839-44.

BELLAGAMBA, C., HUBAISHY, I., BJORGE, J. D., FITZPATRICK, S. L., FUJITA, D. J. & WAISMAN, D. M. 1997. Tyrosine phosphorylation of annexin II tetramer is stimulated by membrane binding. *J Biol Chem,* 272**,** 3195-9.

BENES, P., VETVICKA, V. & FUSEK, M. 2008. Cathepsin D--many functions of one aspartic protease. *Crit Rev Oncol Hematol,* 68**,** 12-28.

BLACK, A., VASIREDDY, V., CHUNG, D. C., MAGUIRE, A. M., GADDAMEEDI, R., TOLMACHOVA, T., SEABRA, M. & BENNETT, J. 2014. AAV8-mediated gene therapy for Choroideremia: preclinical studies in in vitro and in vivo models. *J Gene Med*.

BLASIAK, J. & SZAFLIK, J. P. 2011. DNA damage and repair in age-related macular degeneration. *Front Biosci (Landmark Ed),* 16**,** 1291-301.

BONILHA, V. L. 2008. Age and disease-related structural changes in the retinal pigment epithelium. *Clin Ophthalmol,* 2**,** 413-24.

BRAND, M. D., AFFOURTIT, C., ESTEVES, T. C., GREEN, K., LAMBERT, A. J., MIWA, S., PAKAY, J. L. & PARKER, N. 2004. Mitochondrial superoxide: production, biological effects, and activation of uncoupling proteins. *Free Radic Biol Med,* 37**,** 755-67.

BRODBECK, W. G., KUTTNER-KONDO, L., MOLD, C. & MEDOF, M. E. 2000. Structure/function studies of human decay-accelerating factor. *Immunology,* 101**,** 104-11.

BURKE, J. M. 2008. Epithelial phenotype and the RPE: is the answer blowing in the Wnt? *Prog Retin Eye Res,* 27**,** 579-95.

CARAGINE, T. A., IMAI, M., FREY, A. B. & TOMLINSON, S. 2002. Expression of rat complement control protein Crry on tumor cells inhibits rat natural killer cell-mediated cytotoxicity. *Blood,* 100**,** 3304-10.

CARR, A. J., VUGLER, A., LAWRENCE, J., CHEN, L. L., AHMADO, A., CHEN, F. K., SEMO, M., GIAS, C., DA CRUZ, L., MOORE, H. D., WALSH, J. & COFFEY, P. J. 2009. Molecular characterization and functional analysis of phagocytosis by human embryonic stem cell-derived RPE cells using a novel human retinal assay. *Mol Vis,* 15**,** 283-95.

CARROLL, M. V. & SIM, R. B. 2011. Complement in health and disease. *Adv Drug Deliv Rev,* 63**,** 965-75.

CASTORINO, J. J., GALLAGHER-COLOMBO, S. M., LEVIN, A. V., FITZGERALD, P. G., POLISHOOK, J., KLOECKENER-GRUISSEM, B., OSTERTAG, E. & PHILP, N. J. 2011. Juvenile cataract-associated mutation of solute carrier SLC16A12

impairs trafficking of the protein to the plasma membrane. *Invest Ophthalmol Vis Sci,* 52**,** 6774-84.
CHAITIN, M. H. & HALL, M. O. 1983. Defective ingestion of rod outer segments by cultured dystrophic rat pigment epithelial cells. *Invest Ophthalmol Vis Sci,* 24**,** 812-20.
CHAZOTTE, B. 2011. Labeling mitochondria with MitoTracker dyes. *Cold Spring Harb Protoc,* 2011**,** 990-2.
CHOGLE, A., BU, H. F., WANG, X., BROWN, J. B., CHOU, P. M. & TAN, X. D. 2011. Milk fat globule-EGF factor 8 is a critical protein for healing of dextran sodium sulfate-induced acute colitis in mice. *Mol Med,* 17**,** 502-7.
CHOU, J. Y. 1989. Differentiated mammalian cell lines immortalized by temperature-sensitive tumor viruses. *Mol Endocrinol,* 3**,** 1511-4.
CUDRICI, C., NICULESCU, F., JENSEN, T., ZAFRANSKAIA, E., FOSBRINK, M., RUS, V., SHIN, M. L. & RUS, H. 2006. C5b-9 terminal complex protects oligodendrocytes from apoptotic cell death by inhibiting caspase-8 processing and up-regulating FLIP. *J Immunol,* 176**,** 3173-80.
CYBULSKY, A. V., SALANT, D. J., QUIGG, R. J., BADALAMENTI, J. & BONVENTRE, J. V. 1989. Complement C5b-9 complex activates phospholipases in glomerular epithelial cells. *Am J Physiol,* 257**,** F826-36.
CYBULSKY, A. V., TAKANO, T., PAPILLON, J., KHADIR, A., LIU, J. & PENG, H. 2002. Complement C5b-9 membrane attack complex increases expression of endoplasmic reticulum stress proteins in glomerular epithelial cells. *J Biol Chem,* 277**,** 41342-51.
D'CRUZ, P. M., YASUMURA, D., WEIR, J., MATTHES, M. T., ABDERRAHIM, H., LAVAIL, M. M. & VOLLRATH, D. 2000. Mutation of the receptor tyrosine kinase gene Mertk in the retinal dystrophic RCS rat. *Hum Mol Genet,* 9**,** 645-51.
DACEY, D. M., LIAO, H. W., PETERSON, B. B., ROBINSON, F. R., SMITH, V. C., POKORNY, J., YAU, K. W. & GAMLIN, P. D. 2005. Melanopsin-expressing ganglion cells in primate retina signal colour and irradiance and project to the LGN. *Nature,* 433**,** 749-54.
DASHIELL, S. M., RUS, H. & KOSKI, C. L. 2000. Terminal complement complexes concomitantly stimulate proliferation and rescue of Schwann cells from apoptosis. *Glia,* 30**,** 187-98.
DAVIES, A., SIMMONS, D. L., HALE, G., HARRISON, R. A., TIGHE, H., LACHMANN, P. J. & WALDMANN, H. 1989. CD59, an LY-6-like protein expressed in human lymphoid cells, regulates the action of the complement membrane attack complex on homologous cells. *J Exp Med,* 170**,** 637-54.
DAVIES, M. E., HORNER, A., LOVELAND, B. E. & MCKENZIE, I. F. 1994. Upregulation of complement regulators MCP (CD46), DAF (CD55) and protectin (CD59) in arthritic joint disease. *Scand J Rheumatol,* 23**,** 316-21.
DEGUCHI, J., YAMAMOTO, A., YOSHIMORI, T., SUGASAWA, K., MORIYAMA, Y., FUTAI, M., SUZUKI, T., KATO, K., UYAMA, M. & TASHIRO, Y. 1994. Acidification of phagosomes and degradation of rod outer segments in rat retinal pigment epithelium. *Invest Ophthalmol Vis Sci,* 35**,** 568-79.
DENKER, B. M. & NIGAM, S. K. 1998. Molecular structure and assembly of the tight junction. *Am J Physiol,* 274**,** F1-9.
DING, Q. J., COOK, A. C., DUMITRESCU, A. V. & KUEHN, M. H. 2012. Lack of immunoglobulins does not prevent C1q binding to RGC and does not

alter the progression of experimental glaucoma. *Invest Ophthalmol Vis Sci,* 53**,** 6370-7.

DODDS, A. W., SIM, R. B., PORTER, R. R. & KERR, M. A. 1978. Activation of the first component of human complement (C1) by antibody-antigen aggregates. *Biochem J,* 175**,** 383-90.

DONEV, R. M., COLE, D. S., SIVASANKAR, B., HUGHES, T. R. & MORGAN, B. P. 2006. p53 regulates cellular resistance to complement lysis through enhanced expression of CD59. *Cancer Res,* 66**,** 2451-8.

DONZEAU, M., KALDI, K., ADAM, A., PASCHEN, S., WANNER, G., GUIARD, B., BAUER, M. F., NEUPERT, W. & BRUNNER, M. 2000. Tim23 links the inner and outer mitochondrial membranes. *Cell,* 101**,** 401-12.

DUNN, K. C., AOTAKI-KEEN, A. E., PUTKEY, F. R. & HJELMELAND, L. M. 1996. ARPE-19, a human retinal pigment epithelial cell line with differentiated properties. *Exp Eye Res,* 62**,** 155-69.

ENDOH, M., YAMASHINA, M., OHI, H., FUNAHASHI, K., IKUNO, T., YASUGI, T., ATKINSON, J. P. & OKADA, H. 1993. Immunohistochemical demonstration of membrane cofactor protein (MCP) of complement in normal and diseased kidney tissues. *Clin Exp Immunol,* 94**,** 182-8.

ETIENNE-MANNEVILLE, S. & HALL, A. 2002. Rho GTPases in cell biology. *Nature,* 420**,** 629-35.

FANNING, A. S., VAN ITALLIE, C. M. & ANDERSON, J. M. 2012. Zonula occludens-1 and -2 regulate apical cell structure and the zonula adherens cytoskeleton in polarized epithelia. *Mol Biol Cell,* 23**,** 577-90.

FARRIES, T. C., LACHMANN, P. J. & HARRISON, R. A. 1988. Analysis of the interaction between properdin and factor B, components of the alternative-pathway C3 convertase of complement. *Biochem J,* 253**,** 667-75.

FEBBRAIO, M., HAJJAR, D. P. & SILVERSTEIN, R. L. 2001. CD36: a class B scavenger receptor involved in angiogenesis, atherosclerosis, inflammation, and lipid metabolism. *J Clin Invest,* 108**,** 785-91.

FEHER, J., KOVACS, I., ARTICO, M., CAVALLOTTI, C., PAPALE, A. & BALACCO GABRIELI, C. 2006. Mitochondrial alterations of retinal pigment epithelium in age-related macular degeneration. *Neurobiol Aging,* 27**,** 983-93.

FENG, W., YASUMURA, D., MATTHES, M. T., LAVAIL, M. M. & VOLLRATH, D. 2002. Mertk triggers uptake of photoreceptor outer segments during phagocytosis by cultured retinal pigment epithelial cells. *J Biol Chem,* 277**,** 17016-22.

FEUCHT, H. E., ZWIRNER, J., BEVEC, D., LANG, M., FELBER, E., RIETHMULLER, G. & WEISS, E. H. 1989. Biosynthesis of complement C4 messenger RNA in normal human kidney. *Nephron,* 53**,** 338-42.

FINNEMANN, S. C. 2003. Focal adhesion kinase signaling promotes phagocytosis of integrin-bound photoreceptors. *Embo J,* 22**,** 4143-54.

FINNEMANN, S. C., BONILHA, V. L., MARMORSTEIN, A. D. & RODRIGUEZ-BOULAN, E. 1997. Phagocytosis of rod outer segments by retinal pigment epithelial cells requires alpha(v)beta5 integrin for binding but not for internalization. *Proc Natl Acad Sci U S A,* 94**,** 12932-7.

FINNEMANN, S. C. & NANDROT, E. F. 2006. MerTK activation during RPE phagocytosis in vivo requires alphaVbeta5 integrin. *Adv Exp Med Biol,* 572**,** 499-503.

FINNEMANN, S. C. & RODRIGUEZ-BOULAN, E. 1999. Macrophage and retinal pigment epithelium phagocytosis: apoptotic cells and photoreceptors compete for alphavbeta3 and alphavbeta5 integrins, and protein kinase C regulates alphavbeta5 binding and cytoskeletal linkage. *J Exp Med,* 190**,** 861-74.

FINNEMANN, S. C. & SILVERSTEIN, R. L. 2001. Differential roles of CD36 and alphavbeta5 integrin in photoreceptor phagocytosis by the retinal pigment epithelium. *J Exp Med,* 194**,** 1289-98.

FLANNERY, J. G., O'DAY, W., PFEFFER, B. A., HORWITZ, J. & BOK, D. 1990. Uptake, processing and release of retinoids by cultured human retinal pigment epithelium. *Exp Eye Res,* 51**,** 717-28.

FOLMES, C. D., DZEJA, P. P., NELSON, T. J. & TERZIC, A. 2012. Mitochondria in control of cell fate. *Circ Res,* 110**,** 526-9.

FOSBRINK, M., CUDRICI, C., TEGLA, C. A., SOLOVIOVA, K., ITO, T., VLAICU, S., RUS, V., NICULESCU, F. & RUS, H. 2009. Response gene to complement 32 is required for C5b-9 induced cell cycle activation in endothelial cells. *Exp Mol Pathol,* 86**,** 87-94.

FURUSE, M., HIRASE, T., ITOH, M., NAGAFUCHI, A., YONEMURA, S., TSUKITA, S. & TSUKITA, S. 1993. Occludin: a novel integral membrane protein localizing at tight junctions. *J Cell Biol,* 123**,** 1777-88.

GAL, A., LI, Y., THOMPSON, D. A., WEIR, J., ORTH, U., JACOBSON, S. G., APFELSTEDT-SYLLA, E. & VOLLRATH, D. 2000. Mutations in MERTK, the human orthologue of the RCS rat retinal dystrophy gene, cause retinitis pigmentosa. *Nat Genet,* 26**,** 270-1.

GAMM, D. M. & MEYER, J. S. 2010. Directed differentiation of human induced pluripotent stem cells: a retina perspective. *Regen Med,* 5**,** 315-7.

GARCIA-DIAZ, J. F. & ESSIG, A. 1985. Capacitative transients in voltage-clamped epithelia. *Biophys J,* 48**,** 519-23.

GEORGIADIS, A., TSCHERNUTTER, M., BAINBRIDGE, J. W., BALAGGAN, K. S., MOWAT, F., WEST, E. L., MUNRO, P. M., THRASHER, A. J., MATTER, K., BALDA, M. S. & ALI, R. R. 2010. The tight junction associated signalling proteins ZO-1 and ZONAB regulate retinal pigment epithelium homeostasis in mice. *PLoS One,* 5**,** e15730.

GIBBS, D., KITAMOTO, J. & WILLIAMS, D. S. 2003. Abnormal phagocytosis by retinal pigmented epithelium that lacks myosin VIIa, the Usher syndrome 1B protein. *Proc Natl Acad Sci U S A,* 100**,** 6481-6.

GOEMANS, C. G., BOYA, P., SKIRROW, C. J. & TOLKOVSKY, A. M. 2008. Intra-mitochondrial degradation of Tim23 curtails the survival of cells rescued from apoptosis by caspase inhibitors. *Cell Death Differ,* 15**,** 545-54.

GOLD, B., MERRIAM, J. E., ZERNANT, J., HANCOX, L. S., TAIBER, A. J., GEHRS, K., CRAMER, K., NEEL, J., BERGERON, J., BARILE, G. R., SMITH, R. T., HAGEMAN, G. S., DEAN, M. & ALLIKMETS, R. 2006. Variation in factor B (BF) and complement component 2 (C2) genes is associated with age-related macular degeneration. *Nat Genet,* 38**,** 458-62.

GOLDMAN, A. I., TEIRSTEIN, P. S. & O'BRIEN, P. J. 1980. The role of ambient lighting in circadian disc shedding in the rod outer segment of the rat retina. *Invest Ophthalmol Vis Sci,* 19**,** 1257-67.

GONZALEZ-FERNANDEZ, F. 2003. Interphotoreceptor retinoid-binding protein--an old gene for new eyes. *Vision Res,* 43**,** 3021-36.

GONZALEZ-MARISCAL, L., BETANZOS, A., NAVA, P. & JARAMILLO, B. E. 2003. Tight junction proteins. *Prog Biophys Mol Biol,* 81**,** 1-44.

GOODSELL, D. S. 2004. The molecular perspective: cytochrome C and apoptosis. *Oncologist,* 9**,** 226-7.

GREEN, W. R. & ENGER, C. 2005. Age-related macular degeneration histopathologic studies: the 1992 Lorenz E. Zimmerman Lecture. 1992. *Retina,* 25**,** 1519-35.

GULCAN, H. G., ALVAREZ, R. A., MAUDE, M. B. & ANDERSON, R. E. 1993. Lipids of human retina, retinal pigment epithelium, and Bruch's membrane/choroid: comparison of macular and peripheral regions. *Invest Ophthalmol Vis Sci,* 34**,** 3187-93.

GUPTA, A. K. & SARIN, G. S. 1984. Serum complement component depression during acute adenovirus conjunctivitis. *Br J Ophthalmol,* 68**,** 350-2.

GUYER, D. R., FINE, S. L., MAGUIRE, M. G., HAWKINS, B. S., OWENS, S. L. & MURPHY, R. P. 1986. Subfoveal choroidal neovascular membranes in age-related macular degeneration. Visual prognosis in eyes with relatively good initial visual acuity. *Arch Ophthalmol,* 104**,** 702-5.

HAGEMAN, G. S., ANDERSON, D. H., JOHNSON, L. V., HANCOX, L. S., TAIBER, A. J., HARDISTY, L. I., HAGEMAN, J. L., STOCKMAN, H. A., BORCHARDT, J. D., GEHRS, K. M., SMITH, R. J., SILVESTRI, G., RUSSELL, S. R., KLAVER, C. C., BARBAZETTO, I., CHANG, S., YANNUZZI, L. A., BARILE, G. R., MERRIAM, J. C., SMITH, R. T., OLSH, A. K., BERGERON, J., ZERNANT, J., MERRIAM, J. E., GOLD, B., DEAN, M. & ALLIKMETS, R. 2005. A common haplotype in the complement regulatory gene factor H (HF1/CFH) predisposes individuals to age-related macular degeneration. *Proc Natl Acad Sci U S A,* 102**,** 7227-32.

HAGEMAN, G. S., HANCOX, L. S., TAIBER, A. J., GEHRS, K. M., ANDERSON, D. H., JOHNSON, L. V., RADEKE, M. J., KAVANAGH, D., RICHARDS, A., ATKINSON, J., MERI, S., BERGERON, J., ZERNANT, J., MERRIAM, J., GOLD, B., ALLIKMETS, R. & DEAN, M. 2006. Extended haplotypes in the complement factor H (CFH) and CFH-related (CFHR) family of genes protect against age-related macular degeneration: characterization, ethnic distribution and evolutionary implications. *Ann Med,* 38**,** 592-604.

HAINES, J. L., HAUSER, M. A., SCHMIDT, S., SCOTT, W. K., OLSON, L. M., GALLINS, P., SPENCER, K. L., KWAN, S. Y., NOUREDDINE, M., GILBERT, J. R., SCHNETZ-BOUTAUD, N., AGARWAL, A., POSTEL, E. A. & PERICAK-VANCE, M. A. 2005. Complement factor H variant increases the risk of age-related macular degeneration. *Science,* 308**,** 419-21.

HALL, M. O., ABRAMS, T. A. & MITTAG, T. W. 1991. ROS ingestion by RPE cells is turned off by increased protein kinase C activity and by increased calcium. *Exp Eye Res,* 52**,** 591-8.

HALL, M. O., OBIN, M. S., HEEB, M. J., BURGESS, B. L. & ABRAMS, T. A. 2005. Both protein S and Gas6 stimulate outer segment phagocytosis by cultured rat retinal pigment epithelial cells. *Exp Eye Res,* 81**,** 581-91.

HALL, M. O., PRIETO, A. L., OBIN, M. S., ABRAMS, T. A., BURGESS, B. L., HEEB, M. J. & AGNEW, B. J. 2001. Outer segment phagocytosis by cultured retinal pigment epithelial cells requires Gas6. *Exp Eye Res,* 73**,** 509-20.

HAMMER, C. H., WIRTZ, G. H., RENFER, L., GRESHAM, H. D. & TACK, B. F. 1981. Large scale isolation of functionally active components of the human complement system. *J Biol Chem,* 256**,** 3995-4006.

HANAYAMA, R., TANAKA, M., MIWA, K., SHINOHARA, A., IWAMATSU, A. & NAGATA, S. 2002. Identification of a factor that links apoptotic cells to phagocytes. *Nature,* 417**,** 182-7.

HAYES, M. J., SHAO, D. M., GRIEVE, A., LEVINE, T., BAILLY, M. & MOSS, S. E. 2009. Annexin A2 at the interface between F-actin and membranes enriched in phosphatidylinositol 4,5,-bisphosphate. *Biochim Biophys Acta,* 1793**,** 1086-95.

HE, Y., GE, J., BURKE, J. M., MYERS, R. L., DONG, Z. Z. & TOMBRAN-TINK, J. 2010. Mitochondria impairment correlates with increased sensitivity of aging RPE cells to oxidative stress. *J Ocul Biol Dis Infor,* 3**,** 92-108.

HE, Y. & TOMBRAN-TINK, J. 2010. Mitochondrial decay and impairment of antioxidant defenses in aging RPE cells. *Adv Exp Med Biol,* 664**,** 165-83.

HENLEY, J. R., KRUEGER, E. W., OSWALD, B. J. & MCNIVEN, M. A. 1998. Dynamin-mediated internalization of caveolae. *J Cell Biol,* 141**,** 85-99.

HERMAN, K. G. & STEINBERG, R. H. 1982a. Phagosome degradation in the tapetal retinal pigment epithelium of the opossum. *Invest Ophthalmol Vis Sci,* 23**,** 291-304.

HERMAN, K. G. & STEINBERG, R. H. 1982b. Phagosome movement and the diurnal pattern of phagocytosis in the tapetal retinal pigment epithelium of the opossum. *Invest Ophthalmol Vis Sci,* 23**,** 277-90.

HESTRIN, S. & KORENBROT, J. I. 1990. Activation kinetics of retinal cones and rods: response to intense flashes of light. *J Neurosci,* 10**,** 1967-73.

HETH, C. A. & MARESCALCHI, P. A. 1994. Inositol triphosphate generation in cultured rat retinal pigment epithelium. *Invest Ophthalmol Vis Sci,* 35**,** 409-16.

HILLMEN, P., HOWS, J. M. & LUZZATTO, L. 1992. Two distinct patterns of glycosylphosphatidylinositol (GPI) linked protein deficiency in the red cells of patients with paroxysmal nocturnal haemoglobinuria. *Br J Haematol,* 80**,** 399-405.

HOLT, D. S., BOTTO, M., BYGRAVE, A. E., HANNA, S. M., WALPORT, M. J. & MORGAN, B. P. 2001. Targeted deletion of the CD59 gene causes spontaneous intravascular hemolysis and hemoglobinuria. *Blood,* 98**,** 442-9.

HOLZ, F. G., SCHUTT, F., KOPITZ, J., ELDRED, G. E., KRUSE, F. E., VOLCKER, H. E. & CANTZ, M. 1999. Inhibition of lysosomal degradative functions in RPE cells by a retinoid component of lipofuscin. *Invest Ophthalmol Vis Sci,* 40**,** 737-43.

HORI, Y., YAMADA, K., HANAFUSA, N., OKUDA, T., OKADA, N., MIYATA, T., COUSER, W. G., KUROKAWA, K., FUJITA, T. & NANGAKU, M. 1999. Crry, a complement regulatory protein, modulates renal interstitial disease induced by proteinuria. *Kidney Int,* 56**,** 2096-106.

HOU, J. & GOODENOUGH, D. A. 2010. Claudin-16 and claudin-19 function in the thick ascending limb. *Curr Opin Nephrol Hypertens,* 19**,** 483-8.

HOWES, K. A., LIU, Y., DUNAIEF, J. L., MILAM, A., FREDERICK, J. M., MARKS, A. & BAEHR, W. 2004. Receptor for advanced glycation end products and age-related macular degeneration. *Invest Ophthalmol Vis Sci,* 45**,** 3713-20.

HU, V. W., ESSER, A. F., PODACK, E. R. & WISNIESKI, B. J. 1981. The membrane attack mechanism of complement: photolabeling reveals insertion of terminal proteins into target membrane. *J Immunol,* 127**,** 380-6.

HUBER-LANG, M., SARMA, J. V., ZETOUNE, F. S., RITTIRSCH, D., NEFF, T. A., MCGUIRE, S. R., LAMBRIS, J. D., WARNER, R. L., FLIERL, M. A., HOESEL, L. M., GEBHARD, F., YOUNGER, J. G., DROUIN, S. M., WETSEL, R. A. & WARD, P. A. 2006. Generation of C5a in the absence of C3: a new complement activation pathway. *Nat Med,* 12**,** 682-7.

HUMPHRIES, M. M., KENNA, P. F., CAMPBELL, M., TAM, L. C., NGUYEN, A. T., FARRAR, G. J., BOTTO, M., KIANG, A. S. & HUMPHRIES, P. 2012. C1q enhances cone photoreceptor survival in a mouse model of autosomal recessive retinitis pigmentosa. *Eur J Hum Genet,* 20**,** 64-8.

INDO, H. P., DAVIDSON, M., YEN, H. C., SUENAGA, S., TOMITA, K., NISHII, T., HIGUCHI, M., KOGA, Y., OZAWA, T. & MAJIMA, H. J. 2007. Evidence of ROS generation by mitochondria in cells with impaired electron transport chain and mitochondrial DNA damage. *Mitochondrion,* 7**,** 106-18.

ISHIBASHI, T., MURATA, T., HANGAI, M., NAGAI, R., HORIUCHI, S., LOPEZ, P. F., HINTON, D. R. & RYAN, S. J. 1998. Advanced glycation end products in age-related macular degeneration. *Arch Ophthalmol,* 116**,** 1629-32.

ITOH, M., FURUSE, M., MORITA, K., KUBOTA, K., SAITOU, M. & TSUKITA, S. 1999. Direct binding of three tight junction-associated MAGUKs, ZO-1, ZO-2, and ZO-3, with the COOH termini of claudins. *J Cell Biol,* 147**,** 1351-63.

ITOH, M., NAGAFUCHI, A., YONEMURA, S., KITANI-YASUDA, T., TSUKITA, S. & TSUKITA, S. 1993. The 220-kD protein colocalizing with cadherins in non-epithelial cells is identical to ZO-1, a tight junction-associated protein in epithelial cells: cDNA cloning and immunoelectron microscopy. *J Cell Biol,* 121**,** 491-502.

JANG, G. F., VAN HOOSER, J. P., KUKSA, V., MCBEE, J. K., HE, Y. G., JANSSEN, J. J., DRIESSEN, C. A. & PALCZEWSKI, K. 2001. Characterization of a dehydrogenase activity responsible for oxidation of 11-cis-retinol in the retinal pigment epithelium of mice with a disrupted RDH5 gene. A model for the human hereditary disease fundus albipunctatus. *J Biol Chem,* 276**,** 32456-65.

JARRETT, S. G., LIN, H., GODLEY, B. F. & BOULTON, M. E. 2008. Mitochondrial DNA damage and its potential role in retinal degeneration. *Prog Retin Eye Res,* 27**,** 596-607.

JAT, P. S. & SHARP, P. A. 1989. Cell lines established by a temperature-sensitive simian virus 40 large-T-antigen gene are growth restricted at the nonpermissive temperature. *Mol Cell Biol,* 9**,** 1672-81.

JIN, G. F., HURST, J. S. & GODLEY, B. F. 2001. Rod outer segments mediate mitochondrial DNA damage and apoptosis in human retinal pigment epithelium. *Curr Eye Res,* 23**,** 11-9.

JIN, M., BARRON, E., HE, S., RYAN, S. J. & HINTON, D. R. 2002. Regulation of RPE intercellular junction integrity and function by hepatocyte growth factor. *Invest Ophthalmol Vis Sci,* 43**,** 2782-90.

JIN, M., YAUNG, J., KANNAN, R., HE, S., RYAN, S. J. & HINTON, D. R. 2005. Hepatocyte growth factor protects RPE cells from apoptosis induced by glutathione depletion. *Invest Ophthalmol Vis Sci,* 46**,** 4311-9.

JOHNSON, L. V., FOREST, D. L., BANNA, C. D., RADEKE, C. M., MALONEY, M. A., HU, J., SPENCER, C. N., WALKER, A. M., TSIE, M. S., BOK, D., RADEKE, M. J. & ANDERSON, D. H. 2011. Cell culture model that mimics drusen formation and triggers complement activation associated with age-related macular degeneration. *Proc Natl Acad Sci U S A,* 108**,** 18277-82.

JOHNSON, L. V., OZAKI, S., STAPLES, M. K., ERICKSON, P. A. & ANDERSON, D. H. 2000. A potential role for immune complex pathogenesis in drusen formation. *Exp Eye Res,* 70**,** 441-9.

JOKIRANTA, T. S., ZIPFEL, P. F., HAKULINEN, J., KUHN, S., PANGBURN, M. K., TAMERIUS, J. D. & MERI, S. 1996. Analysis of the recognition mechanism of the alternative pathway of complement by monoclonal anti-factor H antibodies: evidence for multiple interactions between H and surface bound C3b. *FEBS Lett,* 393**,** 297-302.

JOSEPH, K., KULIK, L., COUGHLIN, B., KUNCHITHAPAUTHAM, K., BANDYOPADHYAY, M., THIEL, S., THIELENS, N. M., HOLERS, V. M. & ROHRER, B. 2013. Oxidative stress sensitizes retinal pigmented epithelial (RPE) cells to complement-mediated injury in a natural antibody-, lectin pathway-, and phospholipid epitope-dependent manner. *J Biol Chem,* 288**,** 12753-65.

KAARNIRANTA, K., SINHA, D., BLASIAK, J., KAUPPINEN, A., VEREB, Z., SALMINEN, A., BOULTON, M. E. & PETROVSKI, G. 2013. Autophagy and heterophagy dysregulation leads to retinal pigment epithelium dysfunction and development of age-related macular degeneration. *Autophagy,* 9**,** 973-84.

KAEMMERER, E., SCHUTT, F., KROHNE, T. U., HOLZ, F. G. & KOPITZ, J. 2007. Effects of lipid peroxidation-related protein modifications on RPE lysosomal functions and POS phagocytosis. *Invest Ophthalmol Vis Sci,* 48**,** 1342-7.

KARUNADHARMA, P. P., NORDGAARD, C. L., OLSEN, T. W. & FERRINGTON, D. A. 2010. Mitochondrial DNA damage as a potential mechanism for age-related macular degeneration. *Invest Ophthalmol Vis Sci,* 51**,** 5470-9.

KATOH, K., KANO, Y., MASUDA, M., ONISHI, H. & FUJIWARA, K. 1998. Isolation and contraction of the stress fiber. *Mol Biol Cell,* 9**,** 1919-38.

KAUPPINEN, A., NISKANEN, H., SUURONEN, T., KINNUNEN, K., SALMINEN, A. & KAARNIRANTA, K. 2012. Oxidative stress activates NLRP3 inflammasomes in ARPE-19 cells--implications for age-related macular degeneration (AMD). *Immunol Lett,* 147**,** 29-33.

KEMPER, C., MITCHELL, L. M., ZHANG, L. & HOURCADE, D. E. 2008. The complement protein properdin binds apoptotic T cells and promotes complement activation and phagocytosis. *Proc Natl Acad Sci U S A,* 105**,** 9023-8.

KENNEY, M. C., ATILANO, S. R., BOYER, D., CHWA, M., CHAK, G., CHINICHIAN, S., COSKUN, P., WALLACE, D. C., NESBURN, A. B. & UDAR, N. S. 2010. Characterization of retinal and blood mitochondrial DNA from age-related macular degeneration patients. *Invest Ophthalmol Vis Sci,* 51**,** 4289-97.

KHANDHADIA, S., HAKOBYAN, S., HENG, L. Z., GIBSON, J., ADAMS, D. H., ALEXANDER, G. J., GIBSON, J. M., MARTIN, K. R., MENON, G., NASH, K., SIVAPRASAD, S., ENNIS, S., CREE, A. J., MORGAN, B. P. & LOTERY, A. J. 2013. Age-related macular degeneration and modification of systemic complement factor H production through liver transplantation. *Ophthalmology,* 120**,** 1612-8.

KLEIN, M. L., FERRIS, F. L., 3RD, ARMSTRONG, J., HWANG, T. S., CHEW, E. Y., BRESSLER, S. B. & CHANDRA, S. R. 2008. Retinal precursors and the development of geographic atrophy in age-related macular degeneration. *Ophthalmology,* 115**,** 1026-31.

KLEIN, R., CRUICKSHANKS, K. J., NASH, S. D., KRANTZ, E. M., JAVIER NIETO, F., HUANG, G. H., PANKOW, J. S. & KLEIN, B. E. 2010. The prevalence of age-related macular degeneration and associated risk factors. *Arch Ophthalmol,* 128**,** 750-8.

KLETTNER, A., MOHLE, F., LUCIUS, R. & ROIDER, J. 2011. Quantifying FITC-labeled latex beads opsonized with photoreceptor outer segment fragments: an easy and inexpensive method of investigating phagocytosis in retinal pigment epithelium cells. *Ophthalmic Res,* 46**,** 88-91.

KO, G. Y., KO, M. L. & DRYER, S. E. 2001. Circadian regulation of cGMP-gated cationic channels of chick retinal cones. Erk MAP Kinase and Ca2+/calmodulin-dependent protein kinase II. *Neuron,* 29**,** 255-66.

KOBLINSKI, J. E., AHRAM, M. & SLOANE, B. F. 2000. Unraveling the role of proteases in cancer. *Clin Chim Acta,* 291**,** 113-35.

KOIRALA, A., MAKKIA, R. S., CONLEY, S. M., COOPER, M. J. & NAASH, M. I. 2013. S/MAR-containing DNA nanoparticles promote persistent RPE gene expression and improvement in RPE65-associated LCA. *Hum Mol Genet,* 22**,** 1632-42.

KOKKINAKI, M., SAHIBZADA, N. & GOLESTANEH, N. 2011. Human induced pluripotent stem-derived retinal pigment epithelium (RPE) cells exhibit ion transport, membrane potential, polarized vascular endothelial growth factor secretion, and gene expression pattern similar to native RPE. *Stem Cells,* 29**,** 825-35.

KONRAD, M., SCHALLER, A., SEELOW, D., PANDEY, A. V., WALDEGGER, S., LESSLAUER, A., VITZTHUM, H., SUZUKI, Y., LUK, J. M., BECKER, C., SCHLINGMANN, K. P., SCHMID, M., RODRIGUEZ-SORIANO, J., ARICETA, G., CANO, F., ENRIQUEZ, R., JUPPNER, H., BAKKALOGLU, S. A., HEDIGER, M. A., GALLATI, S., NEUHAUSS, S. C., NURNBERG, P. & WEBER, S. 2006. Mutations in the tight-junction gene claudin 19 (CLDN19) are associated with renal magnesium wasting, renal failure, and severe ocular involvement. *Am J Hum Genet,* 79**,** 949-57.

KORTY, P. E., BRANDO, C. & SHEVACH, E. M. 1991. CD59 functions as a signal-transducing molecule for human T cell activation. *J Immunol,* 146**,** 4092-8.

KOSKI, C. L., RAMM, L. E., HAMMER, C. H., MAYER, M. M. & SHIN, M. L. 1983. Cytolysis of nucleated cells by complement: cell death displays multi-hit characteristics. *Proc Natl Acad Sci U S A,* 80**,** 3816-20.

KRARUP, A., MITCHELL, D. A. & SIM, R. B. 2008. Recognition of acetylated oligosaccharides by human L-ficolin. *Immunol Lett,* 118**,** 152-6.

KROHNE, T. U., WESTENSKOW, P. D., KURIHARA, T., FRIEDLANDER, D. F., LEHMANN, M., DORSEY, A. L., LI, W., ZHU, S., SCHULTZ, A., WANG, J., SIUZDAK, G., DING, S. & FRIEDLANDER, M. 2012. Generation of retinal pigment epithelial cells from small molecules and OCT4 reprogrammed human induced pluripotent stem cells. *Stem Cells Transl Med,* 1**,** 96-109.

KUNCHITHAPAUTHAM, K., BANDYOPADHYAY, M., DAHROUJ, M., THURMAN, J. M. & ROHRER, B. 2012. Sublytic membrane-attack-complex activation and VEGF secretion in retinal pigment epithelial cells. *Adv Exp Med Biol,* 723**,** 23-30.

LAEMMLI, U. K. 1970. Cleavage of structural proteins during the assembly of the head of bacteriophage T4. *Nature,* 227**,** 680-5.

LAINE, R. O. & ESSER, A. F. 1989. Detection of refolding conformers of complement protein C9 during insertion into membranes. *Nature,* 341**,** 63-5.

LAKKARAJU, A., TOOPS, K. A. & XU, J. 2014. Should I Stay or Should I Go? Trafficking of Sub-Lytic MAC in the Retinal Pigment Epithelium. *Adv Exp Med Biol,* 801**,** 267-74.

LAMB, T. D. & PUGH, E. N., JR. 2004. Dark adaptation and the retinoid cycle of vision. *Prog Retin Eye Res,* 23**,** 307-80.

LAVAIL, M. M. 1976. Rod outer segment disc shedding in relation to cyclic lighting. *Exp Eye Res,* 23**,** 277-80.

LAW, A. L., LING, Q., HAJJAR, K. A., FUTTER, C. E., GREENWOOD, J., ADAMSON, P., WAVRE-SHAPTON, S. T., MOSS, S. E. & HAYES, M. J. 2009. Annexin A2 regulates phagocytosis of photoreceptor outer segments in the mouse retina. *Mol Biol Cell,* 20**,** 3896-904.

LI, B., LIN, H., FAN, J., LAN, J., ZHONG, Y., YANG, Y., LI, H. & WANG, Z. 2013. CD59 is overexpressed in human lung cancer and regulates apoptosis of human lung cancer cells. *Int J Oncol,* 43**,** 850-8.

LI, N., RAGHEB, K., LAWLER, G., STURGIS, J., RAJWA, B., MELENDEZ, J. A. & ROBINSON, J. P. 2003. Mitochondrial complex I inhibitor rotenone induces apoptosis through enhancing mitochondrial reactive oxygen species production. *J Biol Chem,* 278**,** 8516-25.

LIANG, F. Q. & GODLEY, B. F. 2003. Oxidative stress-induced mitochondrial DNA damage in human retinal pigment epithelial cells: a possible mechanism for RPE aging and age-related macular degeneration. *Exp Eye Res,* 76**,** 397-403.

LOPEZ, P. F., SIPPY, B. D., LAMBERT, H. M., THACH, A. B. & HINTON, D. R. 1996. Transdifferentiated retinal pigment epithelial cells are immunoreactive for vascular endothelial growth factor in surgically excised age-related macular degeneration-related choroidal neovascular membranes. *Invest Ophthalmol Vis Sci,* 37**,** 855-68.

LUECK, K., HENNIG, M., LOMMATZSCH, A., PAULEIKHOFF, D. & WASMUTH, S. 2012. Complement and UV-irradiated photoreceptor outer segments increase the cytokine secretion by retinal pigment epithelial cells. *Invest Ophthalmol Vis Sci,* 53**,** 1406-13.

LUECK, K., WASMUTH, S., WILLIAMS, J., HUGHES, T. R., MORGAN, B. P., LOMMATZSCH, A., GREENWOOD, J., MOSS, S. E. & PAULEIKHOFF, D. 2011. Sub-lytic C5b-9 induces functional changes in retinal pigment

epithelial cells consistent with age-related macular degeneration. *Eye (Lond),* 25**,** 1074-82.

LUO, C., CHEN, M. & XU, H. 2011. Complement gene expression and regulation in mouse retina and retinal pigment epithelium/choroid. *Mol Vis,* 17**,** 1588-97.

LUO, Y., ZHUO, Y., FUKUHARA, M. & RIZZOLO, L. J. 2006. Effects of culture conditions on heterogeneity and the apical junctional complex of the ARPE-19 cell line. *Invest Ophthalmol Vis Sci,* 47**,** 3644-55.

LYZOGUBOV, V. V., TYTARENKO, R. G., JHA, P., LIU, J., BORA, N. S. & BORA, P. S. 2010. Role of ocular complement factor H in a murine model of choroidal neovascularization. *Am J Pathol,* 177**,** 1870-80.

MA, K. N., CASHMAN, S. M., SWEIGARD, J. H. & KUMAR-SINGH, R. 2010. Decay accelerating factor (CD55)-mediated attenuation of complement: therapeutic implications for age-related macular degeneration. *Invest Ophthalmol Vis Sci,* 51**,** 6776-83.

MACIA, E., EHRLICH, M., MASSOL, R., BOUCROT, E., BRUNNER, C. & KIRCHHAUSEN, T. 2006. Dynasore, a cell-permeable inhibitor of dynamin. *Dev Cell,* 10**,** 839-50.

MAMINISHKIS, A., CHEN, S., JALICKEE, S., BANZON, T., SHI, G., WANG, F. E., EHALT, T., HAMMER, J. A. & MILLER, S. S. 2006. Confluent monolayers of cultured human fetal retinal pigment epithelium exhibit morphology and physiology of native tissue. *Invest Ophthalmol Vis Sci,* 47**,** 3612-24.

MANNI, J. A. & MULLER-EBERHARD, H. J. 1969. The eighth component of human complement (C8): isolation, characterization, and hemolytic efficiency. *J Exp Med,* 130**,** 1145-60.

MAO, Y. & FINNEMANN, S. C. 2013. Analysis of photoreceptor outer segment phagocytosis by RPE cells in culture. *Methods Mol Biol,* 935**,** 285-95.

MARCENARO, E., AUGUGLIARO, R., FALCO, M., CASTRICONI, R., PAROLINI, S., SIVORI, S., ROMEO, E., MILLO, R., MORETTA, L., BOTTINO, C. & MORETTA, A. 2003. CD59 is physically and functionally associated with natural cytotoxicity receptors and activates human NK cell-mediated cytotoxicity. *Eur J Immunol,* 33**,** 3367-76.

MARMORSTEIN, A. D. 2001. The polarity of the retinal pigment epithelium. *Traffic,* 2**,** 867-72.

MARMORSTEIN, A. D., GAN, Y. C., BONILHA, V. L., FINNEMANN, S. C., CSAKY, K. G. & RODRIGUEZ-BOULAN, E. 1998. Apical polarity of N-CAM and EMMPRIN in retinal pigment epithelium resulting from suppression of basolateral signal recognition. *J Cell Biol,* 142**,** 697-710.

MARNEROS, A. G., FAN, J., YOKOYAMA, Y., GERBER, H. P., FERRARA, N., CROUCH, R. K. & OLSEN, B. R. 2005. Vascular endothelial growth factor expression in the retinal pigment epithelium is essential for choriocapillaris development and visual function. *Am J Pathol,* 167**,** 1451-9.

MARTINEZ-HERVAS, S., CARMENA, R., ASCASO, J. F., REAL, J. T., MASANA, L., CATALA, M., VENDRELL, J., VAZQUEZ, J. A., VALDES, S., URRUTIA, I., SORIGUER, F., SERRANO-RIOS, M., ROJO-MARTINEZ, G., PASCUAL-MANICH, G., ORTEGA, E., MORA-PECES, I., MENENDEZ, E., MARTINEZ-LARRAD, M. T., LOPEZ-ALBA, A., GOMIS, R., GODAY, A., GIRBES, J., GAZTAMBIDE, S., FRANCH, J., DELGADO, E., CASTELL, C., CASTANO, L., CASAMITJANA, R., CALLE-PASCUAL, A. & BORDIU, E. 2014. Prevalence of

plasma lipid abnormalities and its association with glucose metabolism in Spain: the di@bet.es study. *Clin Investig Arterioscler,* 26**,** 107-14.

MASON, J. C., YARWOOD, H., SUGARS, K., MORGAN, B. P., DAVIES, K. A. & HASKARD, D. O. 1999. Induction of decay-accelerating factor by cytokines or the membrane-attack complex protects vascular endothelial cells against complement deposition. *Blood,* 94**,** 1673-82.

MATTER, K. & BALDA, M. S. 2003. Functional analysis of tight junctions. *Methods,* 30**,** 228-34.

MAY, R. C. & MACHESKY, L. M. 2001. Phagocytosis and the actin cytoskeleton. *J Cell Sci,* 114**,** 1061-77.

MCBEE, J. K., VAN HOOSER, J. P., JANG, G. F. & PALCZEWSKI, K. 2001. Isomerization of 11-cis-retinoids to all-trans-retinoids in vitro and in vivo. *J Biol Chem,* 276**,** 48483-93.

MEDOF, M. E., KINOSHITA, T. & NUSSENZWEIG, V. 1984. Inhibition of complement activation on the surface of cells after incorporation of decay-accelerating factor (DAF) into their membranes. *J Exp Med,* 160**,** 1558-78.

MERI, S., MORGAN, B. P., DAVIES, A., DANIELS, R. H., OLAVESEN, M. G., WALDMANN, H. & LACHMANN, P. J. 1990. Human protectin (CD59), an 18,000-20,000 MW complement lysis restricting factor, inhibits C5b-8 catalysed insertion of C9 into lipid bilayers. *Immunology,* 71**,** 1-9.

MERI, S., WALDMANN, H. & LACHMANN, P. J. 1991. Distribution of protectin (CD59), a complement membrane attack inhibitor, in normal human tissues. *Lab Invest,* 65**,** 532-7.

MEYER, T. N., SCHWESINGER, C. & DENKER, B. M. 2002. Zonula occludens-1 is a scaffolding protein for signaling molecules. Galpha(12) directly binds to the Src homology 3 domain and regulates paracellular permeability in epithelial cells. *J Biol Chem,* 277**,** 24855-8.

MIAO, J., LESHER, A. M., MIWA, T., SATO, S., GULLIPALLI, D. & SONG, W. C. 2014. Tissue-specific deletion of Crry from mouse proximal tubular epithelial cells increases susceptibility to renal ischemia-reperfusion injury. *Kidney Int*.

MICELI, M. V., LILES, M. R. & NEWSOME, D. A. 1994. Evaluation of oxidative processes in human pigment epithelial cells associated with retinal outer segment phagocytosis. *Exp Cell Res,* 214**,** 242-9.

MIQUEL, J., ECONOMOS, A. C., FLEMING, J. & JOHNSON, J. E., JR. 1980. Mitochondrial role in cell aging. *Exp Gerontol,* 15**,** 575-91.

MITIC, L. L. & ANDERSON, J. M. 1998. Molecular architecture of tight junctions. *Annu Rev Physiol,* 60**,** 121-42.

MIYAMOTO, T., MORITA, K., TAKEMOTO, D., TAKEUCHI, K., KITANO, Y., MIYAKAWA, T., NAKAYAMA, K., OKAMURA, Y., SASAKI, H., MIYACHI, Y., FURUSE, M. & TSUKITA, S. 2005. Tight junctions in Schwann cells of peripheral myelinated axons: a lesson from claudin-19-deficient mice. *J Cell Biol,* 169**,** 527-38.

MONTALVO, V., CAMPOS, M. M., CHAN, C. C., WAWROUSEK, E. F., BUSH, R. A., LAMBRIS, J. D. & GERY, I. 2007. Complement deposits on ocular tissues adjacent to sites of inflammation. *Curr Eye Res,* 32**,** 917-22.

MORGAN, B. P. 1999. Regulation of the complement membrane attack pathway. *Crit Rev Immunol,* 19**,** 173-98.

MORGAN, B. P. & GASQUE, P. 1997. Extrahepatic complement biosynthesis: where, when and why? *Clin Exp Immunol,* 107**,** 1-7.
MOSKOVICH, O. & FISHELSON, Z. 2007. Live cell imaging of outward and inward vesiculation induced by the complement c5b-9 complex. *J Biol Chem,* 282**,** 29977-86.
MOSKOVICH, O., HERZOG, L. O., EHRLICH, M. & FISHELSON, Z. 2012. Caveolin-1 and dynamin-2 are essential for removal of the complement C5b-9 complex via endocytosis. *J Biol Chem,* 287**,** 19904-15.
MOSMANN, T. 1983. Rapid colorimetric assay for cellular growth and survival: application to proliferation and cytotoxicity assays. *J Immunol Methods,* 65**,** 55-63.
MOTOYAMA, N., OKADA, N., YAMASHINA, M. & OKADA, H. 1992. Paroxysmal nocturnal hemoglobinuria due to hereditary nucleotide deletion in the HRF20 (CD59) gene. *Eur J Immunol,* 22**,** 2669-73.
MOUAWAD, F., AOUDJIT, L., JIANG, R., SZASZI, K. & TAKANO, T. 2014. Role of guanine nucleotide exchange factor-H1 in complement-mediated RhoA activation in glomerular epithelial cells. *J Biol Chem,* 289**,** 4206-18.
MULLINS, R. F., RUSSELL, S. R., ANDERSON, D. H. & HAGEMAN, G. S. 2000. Drusen associated with aging and age-related macular degeneration contain proteins common to extracellular deposits associated with atherosclerosis, elastosis, amyloidosis, and dense deposit disease. *Faseb J,* 14**,** 835-46.
MULLINS, R. F., SCHOO, D. P., SOHN, E. H., FLAMME-WIESE, M. J., WORKAMELAHU, G., JOHNSTON, R. M., WANG, K., TUCKER, B. A. & STONE, E. M. 2014. The Membrane Attack Complex in Aging Human Choriocapillaris: Relationship to Macular Degeneration and Choroidal Thinning. *Am J Pathol*.
MURINELLO, S., MULLINS, R. F., LOTERY, A. J., PERRY, V. H. & TEELING, J. L. 2014. Fcgamma receptor upregulation is associated with immune complex inflammation in the mouse retina and early age-related macular degeneration. *Invest Ophthalmol Vis Sci,* 55**,** 247-58.
MUSARELLA, M. A. & MACDONALD, I. M. 2011. Current concepts in the treatment of retinitis pigmentosa. *J Ophthalmol,* 2011**,** 753547.
NABI, I. R., MATHEWS, A. P., COHEN-GOULD, L., GUNDERSEN, D. & RODRIGUEZ-BOULAN, E. 1993. Immortalization of polarized rat retinal pigment epithelium. *J Cell Sci,* 104 (Pt 1)**,** 37-49.
NANDROT, E. F., ANAND, M., ALMEIDA, D., ATABAI, K., SHEPPARD, D. & FINNEMANN, S. C. 2007. Essential role for MFG-E8 as ligand for alphavbeta5 integrin in diurnal retinal phagocytosis. *Proc Natl Acad Sci U S A,* 104**,** 12005-10.
NANDROT, E. F., ANAND, M., SIRCAR, M. & FINNEMANN, S. C. 2006. Novel role for alphavbeta5-integrin in retinal adhesion and its diurnal peak. *Am J Physiol Cell Physiol,* 290**,** C1256-62.
NANDROT, E. F., KIM, Y., BRODIE, S. E., HUANG, X., SHEPPARD, D. & FINNEMANN, S. C. 2004. Loss of synchronized retinal phagocytosis and age-related blindness in mice lacking alphavbeta5 integrin. *J Exp Med,* 200**,** 1539-45.
NAUGHTON, M. A., WALPORT, M. J., WURZNER, R., CARTER, M. J., ALEXANDER, G. J., GOLDMAN, J. M. & BOTTO, M. 1996. Organ-specific contribution to

circulating C7 levels by the bone marrow and liver in humans. *Eur J Immunol,* 26**,** 2108-12.

NGUYEN-LEGROS, J. & HICKS, D. 2000. Renewal of photoreceptor outer segments and their phagocytosis by the retinal pigment epithelium. *Int Rev Cytol,* 196**,** 245-313.

NICULESCU, F., BADEA, T. & RUS, H. 1999. Sublytic C5b-9 induces proliferation of human aortic smooth muscle cells: role of mitogen activated protein kinase and phosphatidylinositol 3-kinase. *Atherosclerosis,* 142**,** 47-56.

NISHIKAWA, K., MATSUO, S., TAMAI, H., OKADA, N. & OKADA, H. 1998. Tissue distribution of the guinea-pig decay-accelerating factor. *Immunology,* 95**,** 302-7.

NORDGAARD, C. L., KARUNADHARMA, P. P., FENG, X., OLSEN, T. W. & FERRINGTON, D. A. 2008. Mitochondrial proteomics of the retinal pigment epithelium at progressive stages of age-related macular degeneration. *Invest Ophthalmol Vis Sci,* 49**,** 2848-55.

NOSE, M., KATOH, M., OKADA, N., KYOGOKU, M. & OKADA, H. 1990. Tissue distribution of HRF20, a novel factor preventing the membrane attack of homologous complement, and its predominant expression on endothelial cells in vivo. *Immunology,* 70**,** 145-9.

OSKOLKOVA, O. V., AFONYUSHKIN, T., LEITNER, A., VON SCHLIEFFEN, E., GARGALOVIC, P. S., LUSIS, A. J., BINDER, B. R. & BOCHKOV, V. N. 2008. ATF4-dependent transcription is a key mechanism in VEGF up-regulation by oxidized phospholipids: critical role of oxidized sn-2 residues in activation of unfolded protein response. *Blood,* 112**,** 330-9.

OTT, M., ROBERTSON, J. D., GOGVADZE, V., ZHIVOTOVSKY, B. & ORRENIUS, S. 2002. Cytochrome c release from mitochondria proceeds by a two-step process. *Proc Natl Acad Sci U S A,* 99**,** 1259-63.

PAIMELA, T., RYHANEN, T., MANNERMAA, E., OJALA, J., KALESNYKAS, G., SALMINEN, A. & KAARNIRANTA, K. 2007. The effect of 17beta-estradiol on IL-6 secretion and NF-kappaB DNA-binding activity in human retinal pigment epithelial cells. *Immunol Lett,* 110**,** 139-44.

PANGBURN, M. K., PANGBURN, K. L., KOISTINEN, V., MERI, S. & SHARMA, A. K. 2000. Molecular mechanisms of target recognition in an innate immune system: interactions among factor H, C3b, and target in the alternative pathway of human complement. *J Immunol,* 164**,** 4742-51.

PAPADIMITRIOU, J. C., PHELPS, P. C., SHIN, M. L., SMITH, M. W. & TRUMP, B. F. 1994. Effects of Ca2+ deregulation on mitochondrial membrane potential and cell viability in nucleated cells following lytic complement attack. *Cell Calcium,* 15**,** 217-27.

PAPADIMITRIOU, J. C., RAMM, L. E., DRACHENBERG, C. B., TRUMP, B. F. & SHIN, M. L. 1991. Quantitative analysis of adenine nucleotides during the prelytic phase of cell death mediated by C5b-9. *J Immunol,* 147**,** 212-7.

PAREEK, G., KRISHNAMOORTHY, V. & D'SILVA, P. 2013. Molecular insights revealing interaction of Tim23 and channel subunits of presequence translocase. *Mol Cell Biol,* 33**,** 4641-59.

PARK, I. H., LEROU, P. H., ZHAO, R., HUO, H. & DALEY, G. Q. 2008. Generation of human-induced pluripotent stem cells. *Nat Protoc,* 3**,** 1180-6.

PARTON, R. G. & SIMONS, K. 2007. The multiple faces of caveolae. *Nat Rev Mol Cell Biol,* 8**,** 185-94.

PENG, S., GAN, G., RAO, V. S., ADELMAN, R. A. & RIZZOLO, L. J. 2012. Effects of proinflammatory cytokines on the claudin-19 rich tight junctions of human retinal pigment epithelium. *Invest Ophthalmol Vis Sci,* 53**,** 5016-28.

PENG, S., RAO, V. S., ADELMAN, R. A. & RIZZOLO, L. J. 2011. Claudin-19 and the barrier properties of the human retinal pigment epithelium. *Invest Ophthalmol Vis Sci,* 52**,** 1392-403.

PHILLIPS, B. E., CANCEL, L., TARBELL, J. M. & ANTONETTI, D. A. 2008. Occludin independently regulates permeability under hydrostatic pressure and cell division in retinal pigment epithelial cells. *Invest Ophthalmol Vis Sci,* 49**,** 2568-76.

PHILP, N. J., YOON, H. & GROLLMAN, E. F. 1998. Monocarboxylate transporter MCT1 is located in the apical membrane and MCT3 in the basal membrane of rat RPE. *Am J Physiol,* 274**,** R1824-8.

PICARD, E., HOUSSIER, M., BUJOLD, K., SAPIEHA, P., LUBELL, W., DORFMAN, A., RACINE, J., HARDY, P., FEBBRAIO, M., LACHAPELLE, P., ONG, H., SENNLAUB, F. & CHEMTOB, S. 2010. CD36 plays an important role in the clearance of oxLDL and associated age-dependent sub-retinal deposits. *Aging (Albany NY),* 2**,** 981-9.

PILZER, D. & FISHELSON, Z. 2005b. Mortalin/GRP75 promotes release of membrane vesicles from immune attacked cells and protection from complement-mediated lysis. *Int Immunol,* 17**,** 1239-48.

PILZER, D., GASSER, O., MOSKOVICH, O., SCHIFFERLI, J. A. & FISHELSON, Z. 2005a. Emission of membrane vesicles: roles in complement resistance, immunity and cancer. *Springer Semin Immunopathol,* 27**,** 375-87.

PODACK, E. R. & MULLER-EBERHARD, H. J. 1979. Isolation of human S-protein, an inhibitor of the membrane attack complex of complement. *J Biol Chem,* 254**,** 9808-14.

PODACK, E. R. & MULLER-EBERHARD, H. J. 1980. SC5b-9 complex of complement: formation of the dimeric membrane attack complex by removal of S-protein. *J Immunol,* 124**,** 1779-83.

PODACK, E. R. & TSCHOPP, J. 1982. Polymerization of the ninth component of complement (C9): formation of poly(C9) with a tubular ultrastructure resembling the membrane attack complex of complement. *Proc Natl Acad Sci U S A,* 79**,** 574-8.

POST, T. W., ARCE, M. A., LISZEWSKI, M. K., THOMPSON, E. S., ATKINSON, J. P. & LUBLIN, D. M. 1990. Structure of the gene for human complement protein decay accelerating factor. *J Immunol,* 144**,** 740-4.

PRESLEY, A. D., FULLER, K. M. & ARRIAGA, E. A. 2003. MitoTracker Green labeling of mitochondrial proteins and their subsequent analysis by capillary electrophoresis with laser-induced fluorescence detection. *J Chromatogr B Analyt Technol Biomed Life Sci,* 793**,** 141-50.

QIN, S. & RODRIGUES, G. A. 2012. Roles of alphavbeta5, FAK and MerTK in oxidative stress inhibition of RPE cell phagocytosis. *Exp Eye Res,* 94**,** 63-70.

QIN, X., DOBARRO, M., BEDFORD, S. J., FERRIS, S., MIRANDA, P. V., SONG, W., BRONSON, R. T., VISCONTI, P. E. & HALPERIN, J. A. 2005. Further characterization of reproductive abnormalities in mCd59b knockout

mice: a potential new function of mCd59 in male reproduction. *J Immunol,* 175**,** 6294-302.
RAMM, L. E., WHITLOW, M. B. & MAYER, M. M. 1982. Size of the transmembrane channels produced by complement proteins C5b-8. *J Immunol,* 129**,** 1143-6.
RAMM, L. E., WHITLOW, M. B. & MAYER, M. M. 1985. The relationship between channel size and the number of C9 molecules in the C5b-9 complex. *J Immunol,* 134**,** 2594-9.
RATTNER, A., SMALLWOOD, P. M. & NATHANS, J. 2000. Identification and characterization of all-trans-retinol dehydrogenase from photoreceptor outer segments, the visual cycle enzyme that reduces all-trans-retinal to all-trans-retinol. *J Biol Chem,* 275**,** 11034-43.
RAWAL, N. & PANGBURN, M. K. 1998. C5 convertase of the alternative pathway of complement. Kinetic analysis of the free and surface-bound forms of the enzyme. *J Biol Chem,* 273**,** 16828-35.
REDMOND, T. M., YU, S., LEE, E., BOK, D., HAMASAKI, D., CHEN, N., GOLETZ, P., MA, J. X., CROUCH, R. K. & PFEIFER, K. 1998. Rpe65 is necessary for production of 11-cis-vitamin A in the retinal visual cycle. *Nat Genet,* 20**,** 344-51.
REMUZZI, G., RUGGENENTI, P., CODAZZI, D., NORIS, M., CAPRIOLI, J., LOCATELLI, G. & GRIDELLI, B. 2002. Combined kidney and liver transplantation for familial haemolytic uraemic syndrome. *Lancet,* 359**,** 1671-2.
RENNER, B., COLEMAN, K., GOLDBERG, R., AMURA, C., HOLLAND-NEIDERMYER, A., PIERCE, K., ORTH, H. N., MOLINA, H., FERREIRA, V. P., CORTES, C., PANGBURN, M. K., HOLERS, V. M. & THURMAN, J. M. 2010. The complement inhibitors Crry and factor H are critical for preventing autologous complement activation on renal tubular epithelial cells. *J Immunol,* 185**,** 3086-94.
RIZZOLO, L. J. 2014. Barrier properties of cultured retinal pigment epithelium. *Exp Eye Res*.
RIZZOLO, L. J. & ZHOU, S. 1995. The distribution of Na+,K(+)-ATPase and 5A11 antigen in apical microvilli of the retinal pigment epithelium is unrelated to alpha-spectrin. *J Cell Sci,* 108 (Pt 11)**,** 3623-33.
ROBERTS, W. G. & PALADE, G. E. 1995. Increased microvascular permeability and endothelial fenestration induced by vascular endothelial growth factor. *J Cell Sci,* 108 (Pt 6)**,** 2369-79.
RODIECK, R. W. & RUSHTON, W. A. 1976. Cancellation of rod signals by cones, and cone signals by rods in the cat retina. *J Physiol,* 254**,** 775-85.
ROHRER, B., KUNCHITHAPAUTHAM, K., GENEWSKY, A. & STRAUSS, O. 2014. Prolonged SRC kinase activation, a mechanism to turn transient, sublytic complement activation into a sustained pathological condition in retinal pigment epithelium cells. *Adv Exp Med Biol,* 801**,** 221-7.
ROLLINS, S. A. & SIMS, P. J. 1990. The complement-inhibitory activity of CD59 resides in its capacity to block incorporation of C9 into membrane C5b-9. *J Immunol,* 144**,** 3478-83.
ROMMEL, F. A. & MAYER, M. M. 1973. Studies of guinea pig complement component C9: reaction kinetics and evidence that lysis of EAC1-8

results from a single membrane lesion caused by one molecule of C9. *J Immunol,* 110**,** 637-47.

ROORDA, A., ZHANG, Y. & DUNCAN, J. L. 2007. High-resolution in vivo imaging of the RPE mosaic in eyes with retinal disease. *Invest Ophthalmol Vis Sci,* 48**,** 2297-303.

RUDD, P. M., MORGAN, B. P., WORMALD, M. R., HARVEY, D. J., VAN DEN BERG, C. W., DAVIS, S. J., FERGUSON, M. A. & DWEK, R. A. 1997. The glycosylation of the complement regulatory protein, human erythrocyte CD59. *J Biol Chem,* 272**,** 7229-44.

RUIZ, A., WINSTON, A., LIM, Y. H., GILBERT, B. A., RANDO, R. R. & BOK, D. 1999. Molecular and biochemical characterization of lecithin retinol acyltransferase. *J Biol Chem,* 274**,** 3834-41.

RUS, H. G., NICULESCU, F. & SHIN, M. L. 1996. Sublytic complement attack induces cell cycle in oligodendrocytes. *J Immunol,* 156**,** 4892-900.

RYEOM, S. W., SPARROW, J. R. & SILVERSTEIN, R. L. 1996. CD36 participates in the phagocytosis of rod outer segments by retinal pigment epithelium. *J Cell Sci,* 109 (Pt 2)**,** 387-95.

SAAR RAY, M., MOSKOVICH, O., IOSEFSON, O. & FISHELSON, Z. 2014. Mortalin/Grp75 Binds to Complement C9 and Plays a Role in Resistance to Complement-Dependent Cytotoxicity. *J Biol Chem*.

SAARI, J. C., NAWROT, M., GARWIN, G. G., KENNEDY, M. J., HURLEY, J. B., GHYSELINCK, N. B. & CHAMBON, P. 2002. Analysis of the visual cycle in cellular retinol-binding protein type I (CRBPI) knockout mice. *Invest Ophthalmol Vis Sci,* 43**,** 1730-5.

SAARI, J. C., NAWROT, M., KENNEDY, B. N., GARWIN, G. G., HURLEY, J. B., HUANG, J., POSSIN, D. E. & CRABB, J. W. 2001. Visual cycle impairment in cellular retinaldehyde binding protein (CRALBP) knockout mice results in delayed dark adaptation. *Neuron,* 29**,** 739-48.

SAHU, A. & PANGBURN, M. K. 1995. Tyrosine is a potential site for covalent attachment of activated complement component C3. *Mol Immunol,* 32**,** 711-6.

SANGHERA, N. & PINHEIRO, T. J. 2000. Unfolding and refolding of cytochrome c driven by the interaction with lipid micelles. *Protein Sci,* 9**,** 1194-202.

SCHAINUCK, L. I., STRIKER, G. E., CUTLER, R. E. & BENDITT, E. P. 1970. Structural-functional correlations in renal disease. II. The correlations. *Hum Pathol,* 1**,** 631-41.

SCHLAGER, S. I., OHANIAN, S. H. & BORSOS, T. 1978. Correlation between the ability of tumor cells to resist humoral immune attack and their ability to synthesize lipid. *J Immunol,* 120**,** 463-71.

SCHRECK, S. F., PLUMB, M. E., PLATTEBORZE, P. L., KAUFMAN, K. M., MICHELOTTI, G. A., LETSON, C. S. & SODETZ, J. M. 1998. Expression and characterization of recombinant subunits of human complement component C8: further analysis of the function of C8 alpha and C8 gamma. *J Immunol,* 161**,** 311-8.

SEDDON, J. M., YU, Y., MILLER, E. C., REYNOLDS, R., TAN, P. L., GOWRISANKAR, S., GOLDSTEIN, J. I., TRIEBWASSER, M., ANDERSON, H. E., ZERBIB, J., KAVANAGH, D., SOUIED, E., KATSANIS, N., DALY, M. J., ATKINSON, J. P. & RAYCHAUDHURI, S. 2013. Rare variants in CFI, C3 and C9 are associated

with high risk of advanced age-related macular degeneration. *Nat Genet,* 45**,** 1366-70.

SHARMA, A. K. & PANGBURN, M. K. 1996. Identification of three physically and functionally distinct binding sites for C3b in human complement factor H by deletion mutagenesis. *Proc Natl Acad Sci U S A,* 93**,** 10996-1001.

SILVERSMITH, R. E. & NELSESTUEN, G. L. 1986. Interaction of complement proteins C5b-6 and C5b-7 with phospholipid vesicles: effects of phospholipid structural features. *Biochemistry,* 25**,** 7717-25.

SINGHRAO, S. K., NEAL, J. W., MORGAN, B. P. & GASQUE, P. 1999. Increased complement biosynthesis by microglia and complement activation on neurons in Huntington's disease. *Exp Neurol,* 159**,** 362-76.

SIT, S. T. & MANSER, E. 2011. Rho GTPases and their role in organizing the actin cytoskeleton. *J Cell Sci,* 124**,** 679-83.

SIVASANKAR, B., DONEV, R. M., LONGHI, M. P., HUGHES, T. R., DAVIES, R., COLE, D. S., MORGAN, B. P. & MARCHBANK, K. J. 2007. CD59a deficient mice display reduced B cell activity and antibody production in response to T-dependent antigens. *Mol Immunol,* 44**,** 2978-87.

SJOHOLM, A. G. 1975. Complement components in normal serum and plasma quantitated by electroimmunoassay. *Scand J Immunol,* 4**,** 25-30.

SJOHOLM, A. G., BRACONIER, J. H. & SODERSTROM, C. 1982. Properdin deficiency in a family with fulminant meningococcal infections. *Clin Exp Immunol,* 50**,** 291-7.

SLOT, J. W., GEUZE, H. J., GIGENGACK, S., LIENHARD, G. E. & JAMES, D. E. 1991. Immuno-localization of the insulin regulatable glucose transporter in brown adipose tissue of the rat. *J Cell Biol,* 113**,** 123-35.

SMITH, W., ASSINK, J., KLEIN, R., MITCHELL, P., KLAVER, C. C., KLEIN, B. E., HOFMAN, A., JENSEN, S., WANG, J. J. & DE JONG, P. T. 2001. Risk factors for age-related macular degeneration: Pooled findings from three continents. *Ophthalmology,* 108**,** 697-704.

SONODA, S., SPEE, C., BARRON, E., RYAN, S. J., KANNAN, R. & HINTON, D. R. 2009. A protocol for the culture and differentiation of highly polarized human retinal pigment epithelial cells. *Nat Protoc,* 4**,** 662-73.

SONODA, S., SREEKUMAR, P. G., KASE, S., SPEE, C., RYAN, S. J., KANNAN, R. & HINTON, D. R. 2010. Attainment of polarity promotes growth factor secretion by retinal pigment epithelial cells: relevance to age-related macular degeneration. *Aging (Albany NY),* 2**,** 28-42.

SPARROW, J. R., KIM, S. R. & WU, Y. 2010. Experimental approaches to the study of A2E, a bisretinoid lipofuscin chromophore of retinal pigment epithelium. *Methods Mol Biol,* 652**,** 315-27.

SPILLER, O. B., CRIADO-GARCIA, O., RODRIGUEZ DE CORDOBA, S. & MORGAN, B. P. 2000. Cytokine-mediated up-regulation of CD55 and CD59 protects human hepatoma cells from complement attack. *Clin Exp Immunol,* 121**,** 234-41.

SPITZER, D., MITCHELL, L. M., ATKINSON, J. P. & HOURCADE, D. E. 2007. Properdin can initiate complement activation by binding specific target surfaces and providing a platform for de novo convertase assembly. *J Immunol,* 179**,** 2600-8.

SRIPATHI, S. R., HE, W., ATKINSON, C. L., SMITH, J. J., LIU, Z., ELLEDGE, B. M. & JAHNG, W. J. 2011. Mitochondrial-nuclear communication by prohibitin shuttling under oxidative stress. *Biochemistry,* 50**,** 8342-51.

STASI, K., NAGEL, D., YANG, X., WANG, R. F., REN, L., PODOS, S. M., MITTAG, T. & DANIAS, J. 2006. Complement component 1Q (C1Q) upregulation in retina of murine, primate, and human glaucomatous eyes. *Invest Ophthalmol Vis Sci,* 47**,** 1024-9.

STEVENSON, B. R., SILICIANO, J. D., MOOSEKER, M. S. & GOODENOUGH, D. A. 1986. Identification of ZO-1: a high molecular weight polypeptide associated with the tight junction (zonula occludens) in a variety of epithelia. *J Cell Biol,* 103**,** 755-66.

STEWART, J. L., KOLB, W. P. & SODETZ, J. M. 1987. Evidence that C5b recognizes and mediates C8 incorporation into the cytolytic complex of complement. *J Immunol,* 139**,** 1960-4.

STRAUSS, O. 2005. The retinal pigment epithelium in visual function. *Physiol Rev,* 85**,** 845-81.

STRUNK, R. C., EIDLEN, D. M. & MASON, R. J. 1988. Pulmonary alveolar type II epithelial cells synthesize and secrete proteins of the classical and alternative complement pathways. *J Clin Invest,* 81**,** 1419-26.

STRUNNIKOVA, N. V., MAMINISHKIS, A., BARB, J. J., WANG, F., ZHI, C., SERGEEV, Y., CHEN, W., EDWARDS, A. O., STAMBOLIAN, D., ABECASIS, G., SWAROOP, A., MUNSON, P. J. & MILLER, S. S. 2010. Transcriptome analysis and molecular signature of human retinal pigment epithelium. *Hum Mol Genet,* 19**,** 2468-86.

STUIVER, I., RUGGERI, Z. & SMITH, J. W. 1996. Divalent cations regulate the organization of integrins alpha v beta 3 and alpha v beta 5 on the cell surface. *J Cell Physiol,* 168**,** 521-31.

SUN, H. & NATHANS, J. 2001. Mechanistic studies of ABCR, the ABC transporter in photoreceptor outer segments responsible for autosomal recessive Stargardt disease. *J Bioenerg Biomembr,* 33**,** 523-30.

TATE, D. J., JR., MICELI, M. V. & NEWSOME, D. A. 1995. Phagocytosis and H2O2 induce catalase and metallothionein gene expression in human retinal pigment epithelial cells. *Invest Ophthalmol Vis Sci,* 36**,** 1271-9.

TEGLA, C. A., CUDRICI, C., PATEL, S., TRIPPE, R., 3RD, RUS, V., NICULESCU, F. & RUS, H. 2011. Membrane attack by complement: the assembly and biology of terminal complement complexes. *Immunol Res,* 51**,** 45-60.

THIEL, S., VORUP-JENSEN, T., STOVER, C. M., SCHWAEBLE, W., LAURSEN, S. B., POULSEN, K., WILLIS, A. C., EGGLETON, P., HANSEN, S., HOLMSKOV, U., REID, K. B. & JENSENIUS, J. C. 1997. A second serine protease associated with mannan-binding lectin that activates complement. *Nature,* 386**,** 506-10.

THURMAN, J. M. & HOLERS, V. M. 2006. The central role of the alternative complement pathway in human disease. *J Immunol,* 176**,** 1305-10.

THURMAN, J. M., RENNER, B., KUNCHITHAPAUTHAM, K., FERREIRA, V. P., PANGBURN, M. K., ABLONCZY, Z., TOMLINSON, S., HOLERS, V. M. & ROHRER, B. 2009. Oxidative stress renders retinal pigment epithelial cells susceptible to complement-mediated injury. *J Biol Chem,* 284**,** 16939-47.

TILLEUL, J., RICHARD, F., PUCHE, N., ZERBIB, J., LEVEZIEL, N., SAHEL, J. A., COHEN, S. Y., KOROBELNIK, J. F., FEINGOLD, J., MUNNICH, A., KAPLAN, J., ROZET, J. M. & SOUIED, E. H. 2013. Genetic association study of mitochondrial polymorphisms in neovascular age-related macular degeneration. *Mol Vis,* 19**,** 1132-40.

TOMBRAN-TINK, J., SHIVARAM, S. M., CHADER, G. J., JOHNSON, L. V. & BOK, D. 1995. Expression, secretion, and age-related downregulation of pigment epithelium-derived factor, a serpin with neurotrophic activity. *J Neurosci,* 15**,** 4992-5003.

TOMLINSON 2006. Defining the CD59-C9 binding interaction.

TOSINI, G. 2000. Melatonin circadian rhythm in the retina of mammals. *Chronobiol Int,* 17**,** 599-612.

TRIANTAFILOU, K., HUGHES, T. R., TRIANTAFILOU, M. & MORGAN, B. P. 2013. The complement membrane attack complex triggers intracellular Ca2+ fluxes leading to NLRP3 inflammasome activation. *J Cell Sci,* 126**,** 2903-13.

TRIANTAFYLLA, M., MASSA, H. F., DARDABOUNIS, D., GATZIOUFAS, Z., KOZOBOLIS, V., IOANNAKIS, K., PERENTE, I. & PANOS, G. D. 2014. Ranibizumab for the treatment of degenerative ocular conditions. *Clin Ophthalmol,* 8**,** 1187-98.

TUROWSKI, P., ADAMSON, P., SATHIA, J., ZHANG, J. J., MOSS, S. E., AYLWARD, G. W., HAYES, M. J., KANUGA, N. & GREENWOOD, J. 2004. Basement membrane-dependent modification of phenotype and gene expression in human retinal pigment epithelial ARPE-19 cells. *Invest Ophthalmol Vis Sci,* 45**,** 2786-94.

UDAR, N., ATILANO, S. R., MEMARZADEH, M., BOYER, D. S., CHWA, M., LU, S., MAGUEN, B., LANGBERG, J., COSKUN, P., WALLACE, D. C., NESBURN, A. B., KHATIBI, N., HERTZOG, D., LE, K., HWANG, D. & KENNEY, M. C. 2009. Mitochondrial DNA haplogroups associated with age-related macular degeneration. *Invest Ophthalmol Vis Sci,* 50**,** 2966-74.

UMEDA, K., MATSUI, T., NAKAYAMA, M., FURUSE, K., SASAKI, H., FURUSE, M. & TSUKITA, S. 2004. Establishment and characterization of cultured epithelial cells lacking expression of ZO-1. *J Biol Chem,* 279**,** 44785-94.

VAN DE VEN, J. P., NILSSON, S. C., TAN, P. L., BUITENDIJK, G. H., RISTAU, T., MOHLIN, F. C., NABUURS, S. B., SCHOENMAKER-KOLLER, F. E., SMAILHODZIC, D., CAMPOCHIARO, P. A., ZACK, D. J., DUVVARI, M. R., BAKKER, B., PAUN, C. C., BOON, C. J., UITTERLINDEN, A. G., LIAKOPOULOS, S., KLEVERING, B. J., FAUSER, S., DAHA, M. R., KATSANIS, N., KLAVER, C. C., BLOM, A. M., HOYNG, C. B. & DEN HOLLANDER, A. I. 2013. A functional variant in the CFI gene confers a high risk of age-related macular degeneration. *Nat Genet,* 45**,** 813-7.

VAN REMMEN, H. & RICHARDSON, A. 2001. Oxidative damage to mitochondria and aging. *Exp Gerontol,* 36**,** 957-68.

VETVICKA, V., VEKTVICKOVA, J. & FUSEK, M. 1994. Effect of human procathepsin D on proliferation of human cell lines. *Cancer Lett,* 79**,** 131-5.

VON SCHANTZ, M., LUCAS, R. J. & FOSTER, R. G. 1999. Circadian oscillation of photopigment transcript levels in the mouse retina. *Brain Res Mol Brain Res,* 72**,** 108-14.

WALLIS, R., MITCHELL, D. A., SCHMID, R., SCHWAEBLE, W. J. & KEEBLE, A. H. 2010. Paths reunited: Initiation of the classical and lectin pathways of complement activation. *Immunobiology,* 215**,** 1-11.

WANG, A. L., LUKAS, T. J., YUAN, M., DU, N., TSO, M. O. & NEUFELD, A. H. 2009. Autophagy and exosomes in the aged retinal pigment epithelium: possible relevance to drusen formation and age-related macular degeneration. *PLoS One,* 4**,** e4160.

WANG, S., LIU, S., MAO, J. & WEN, D. 2014. Effect of retinoic acid on the tight junctions of the retinal pigment epithelium-choroid complex of guinea pigs with lens-induced myopia in vivo. *Int J Mol Med,* 33**,** 825-32.

WANG, X., PEREZ, E., LIU, R., YAN, L. J., MALLET, R. T. & YANG, S. H. 2007. Pyruvate protects mitochondria from oxidative stress in human neuroblastoma SK-N-SH cells. *Brain Res,* 1132**,** 1-9.

WANG, Y. & BOGENHAGEN, D. F. 2006. Human mitochondrial DNA nucleoids are linked to protein folding machinery and metabolic enzymes at the mitochondrial inner membrane. *J Biol Chem,* 281**,** 25791-802.

WATSON, R., WEARMOUTH, E., MCLOUGHLIN, A. C., JACKSON, A., WARD, S., BERTRAM, P., BENNACEUR, K., BARKER, C. E., PAPPWORTH, I. Y., KAVANAGH, D., LEA, S. M., ATKINSON, J. P., GOODSHIP, T. H. & MARCHBANK, K. J. 2014. Autoantibodies to CD59, CD55, CD46 or CD35 are not associated with atypical haemolytic uraemic syndrome (aHUS). *Mol Immunol*.

WEI, Y. H. 1998. Oxidative stress and mitochondrial DNA mutations in human aging. *Proc Soc Exp Biol Med,* 217**,** 53-63.

WELCH, T. R., BEISCHEL, L. S., FRENZKE, M. & WITTE, D. 1996. Regulated expression of complement factor B in the human kidney. *Kidney Int,* 50**,** 521-5.

WELCH, T. R., BEISCHEL, L. S. & WITTE, D. P. 1993. Differential expression of complement C3 and C4 in the human kidney. *J Clin Invest,* 92**,** 1451-8.

WESTENSKOW, P. D., MORENO, S. K., KROHNE, T. U., KURIHARA, T., ZHU, S., ZHANG, Z. N., ZHAO, T., XU, Y., DING, S. & FRIEDLANDER, M. 2012. Using flow cytometry to compare the dynamics of photoreceptor outer segment phagocytosis in iPS-derived RPE cells. *Invest Ophthalmol Vis Sci,* 53**,** 6282-90.

WIEDMER, T. & SIMS, P. J. 1991. Participation of protein kinases in complement C5b-9-induced shedding of platelet plasma membrane vesicles. *Blood,* 78**,** 2880-6.

YAKES, F. M. & VAN HOUTEN, B. 1997. Mitochondrial DNA damage is more extensive and persists longer than nuclear DNA damage in human cells following oxidative stress. *Proc Natl Acad Sci U S A,* 94**,** 514-9.

YAMAMOTO, T., NAKANE, T., DOI, S. & OSAKI, T. 2003. Lipopolysaccharide signal transduction in oral keratinocytes--involvement of CD59 but not CD14. *Cell Signal,* 15**,** 861-9.

YAMASHINA, M., UEDA, E., KINOSHITA, T., TAKAMI, T., OJIMA, A., ONO, H., TANAKA, H., KONDO, N., ORII, T., OKADA, N. & ET AL. 1990. Inherited complete deficiency of 20-kilodalton homologous restriction factor (CD59) as a cause of paroxysmal nocturnal hemoglobinuria. *N Engl J Med,* 323**,** 1184-9.

YANG, P., TYRRELL, J., HAN, I. & JAFFE, G. J. 2009. Expression and modulation of RPE cell membrane complement regulatory proteins. *Invest Ophthalmol Vis Sci,* 50**,** 3473-81.

YASOJIMA, K., MCGEER, E. G. & MCGEER, P. L. 1999. Complement regulators C1 inhibitor and CD59 do not significantly inhibit complement activation in Alzheimer disease. *Brain Res,* 833**,** 297-301.

YOSHIKAWA, T., OGATA, N., IZUTA, H., SHIMAZAWA, M., HARA, H. & TAKAHASHI, K. 2011. Increased expression of tight junctions in ARPE-19 cells under endoplasmic reticulum stress. *Curr Eye Res,* 36**,** 1153-63.

YOUNG, R. W. & BOK, D. 1969. Participation of the retinal pigment epithelium in the rod outer segment renewal process. *J Cell Biol,* 42**,** 392-403.

YOUNG, R. W. & DROZ, B. 1968. The renewal of protein in retinal rods and cones. *J Cell Biol,* 39**,** 169-84.

ZALMAN, L. S. & MULLER-EBERHARD, H. J. 1990. Comparison of channels formed by poly C9, C5b-8 and the membrane attack complex of complement. *Mol Immunol,* 27**,** 533-7.

ZHANG, C., BAFFI, J., COUSINS, S. W. & CSAKY, K. G. 2003. Oxidant-induced cell death in retinal pigment epithelium cells mediated through the release of apoptosis-inducing factor. *J Cell Sci,* 116**,** 1915-23.

ZHANG, H., CYBULSKY, A. V., AOUDJIT, L., ZHU, J., LI, H., LAMARCHE-VANE, N. & TAKANO, T. 2007. Role of Rho-GTPases in complement-mediated glomerular epithelial cell injury. *Am J Physiol Renal Physiol,* 293**,** F148-56.

ZHOU, W., SCOTT, S. A., SHELTON, S. B. & CRUTCHER, K. A. 2006. Cathepsin D-mediated proteolysis of apolipoprotein E: possible role in Alzheimer's disease. *Neuroscience,* 143**,** 689-701.

ZIPFEL, P. F. & SKERKA, C. 2009. Complement regulators and inhibitory proteins. *Nat Rev Immunol,* 9**,** 729-40.

ZUNDEL, S., CSEH, S., LACROIX, M., DAHL, M. R., MATSUSHITA, M., ANDRIEU, J. P., SCHWAEBLE, W. J., JENSENIUS, J. C., FUJITA, T., ARLAUD, G. J. & THIELENS, N. M. 2004. Characterization of recombinant mannan-binding lectin-associated serine protease (MASP)-3 suggests an activation mechanism different from that of MASP-1 and MASP-2. *J Immunol,* 172**,** 4342-50.